



**HAL**  
open science

# Computer simulations of supercooled liquids near the experimental glass transition

Andrea Saverio Ninarello

► **To cite this version:**

Andrea Saverio Ninarello. Computer simulations of supercooled liquids near the experimental glass transition. Soft Condensed Matter [cond-mat.soft]. Université Montpellier, 2017. English. NNT : 2017MONT071 . tel-01938631

**HAL Id: tel-01938631**

**<https://theses.hal.science/tel-01938631>**

Submitted on 28 Nov 2018

**HAL** is a multi-disciplinary open access archive for the deposit and dissemination of scientific research documents, whether they are published or not. The documents may come from teaching and research institutions in France or abroad, or from public or private research centers.

L'archive ouverte pluridisciplinaire **HAL**, est destinée au dépôt et à la diffusion de documents scientifiques de niveau recherche, publiés ou non, émanant des établissements d'enseignement et de recherche français ou étrangers, des laboratoires publics ou privés.

# THÈSE POUR OBTENIR LE GRADE DE DOCTEUR DE L'UNIVERSITÉ DE MONTPELLIER

En Physique

École doctorale I2S

Unité de recherche Laboratoire Charles Coulomb

## Computer Simulations of Supercooled Liquids near the Experimental Glass Transition

Présentée par Andrea NINARELLO

Le 2 octobre 2017

Sous la direction de Ludovic BERTHIER

Devant le jury composé de

M. Ludovic BERTHIER, Directeur de recherche, Université de Montpellier et CNRS

M. Daniele COSLOVICH, Maître de conférences, Université de Montpellier

M. Jeppe DYRE, Professor, Roskilde University

M. Florent KRZAKALA, Professeur, ENS Paris

Mme. Chantal VALERIANI, Assistant Professor, Complutense University of Madrid

M. Matthieu WYART, Associate Professor, EPFL

Directeur de thèse

Co-encadrant

Président du jury

Rapporteur

Examineur

Rapporteur



UNIVERSITÉ  
DE MONTPELLIER



*A Giulia,  
alla mia famiglia*



## Abstract

Understanding the mechanisms that lead to glass formation is one of the open problems for the condensed matter research. Numerous questions remain unanswered, because the tremendous increase of relaxation times during the cooling process prevents the exploration of equilibrium properties of supercooled liquids at very low temperature. Computer simulations of glass-forming liquids are nowadays able to reach equilibrium at temperatures comparable to the Mode-Coupling crossover temperature, which is well above the experimental glass transition temperature. As a consequence, simulations lag eight orders of magnitude behind experiments in terms of equilibration times. Progress to close this gap has been slow, and stems mostly from hardware improvements.

In this thesis we make an important step to close this gap. We combine the use of a Monte Carlo algorithm, known as the swap algorithm, with the design of novel glass-forming models. We systematically test numerous models using both discrete mixtures and polydisperse systems. We discuss the role that polydispersity and particle softness play in avoiding crystallization and in efficiently reaching previously unexplored regimes. We study the dynamical processes taking place during swap Monte Carlo simulations. We demonstrate that in some cases our technique is able to produce thermalized configurations at temperatures inaccessible even by experiments.

In this newly accessible regime, we investigate some open questions concerning the glass transition. We show that a hard sphere fluid can be equilibrated at, and even beyond, the jamming packing fraction. We measure the configurational entropy in extremely supercooled liquid, finding a strong dimensional dependence that supports, on the one hand, the existence of an ideal glass transition at a finite temperature in three dimensions and, on the other hand, its absence in two dimensions. We detect the increase of amorphous order quantified through a static point-to-set length throughout the glass formation. We measure the critical exponents introduced in the mean-field theory of glasses much closer to the supposed ideal glass transition. Finally, we reveal the absence of a sharp geometric transition in the potential energy landscape across the Mode-Coupling crossover.

The models and the algorithms developed in this thesis shift the computational studies of glass-forming liquids to an entirely new territory, which should help to close the gap between theory and experiments, and get us closer to solve the long-standing problem of the glass transition.



## Résumé

La compréhension du mécanisme de la formation du verre est l'un des importants problèmes ouverts en recherche sur la matière condensée. De nombreuses questions restent sans réponse, en raison d'une énorme augmentation des temps de relaxation pendant le processus de refroidissement qui ne permet pas l'exploration des propriétés d'équilibre des liquides surfondus à très basses températures. Les simulations numériques des liquides surfondus sont actuellement en mesure d'atteindre l'équilibre à des températures comparables à la température du crossover de la théorie de couplages de modes, qui est bien supérieure à la température de transition vitreuse expérimentale. En conséquence, les simulations plus lentes que les expériences pour équilibrer un liquide surfondu par un facteur d'environ huit ordres de grandeur. Les progrès réalisés pour combler cet écart ont été lents et résultent essentiellement d'améliorations de l'architecture des ordinateurs.

Dans cette thèse, nous résolvons en partie le problème de la thermalisation à basse température de liquides surfondus dans des simulations numériques. Nous combinons l'utilisation d'un algorithme Monte Carlo, connu sous le nom d'algorithme de swap, avec la conception de nouveaux modèles de formateurs de verre. Nous examinons systématiquement des nombreux systèmes, à la fois des mélanges discrets de particules, ainsi que des systèmes à polydispersité continue. Nous discutons le rôle que la polydispersité et la forme du potentiel entre particules jouent pour éviter la cristallisation et parvenir efficacement à des régimes de température inexplorés. De plus, nous étudions les processus dynamiques à l'oeuvre pendant une simulation de swap Monte Carlo. Nous démontrons que, dans certains cas, notre technique permet de produire des configurations équilibrées à des températures inaccessibles même dans des expériences.

Dans ce régime de température complètement nouveau, nous examinons plusieurs questions ouvertes concernant la physique de la transition vitreuse. Nous montrons qu'un fluide de sphères dures peut être équilibré jusqu'à la densité critique du jamming, et même au-delà. Nous mesurons l'entropie configurationnelle dans un liquide refroidi à très basse température. Nous mettons en évidence une forte dépendance dimensionnelle, qui suggère l'existence d'une transition vitreuse idéale à une température finie en trois dimensions et à son absence en deux dimensions. Nous détectons l'augmentation de l'ordre amorphe quantifié par une longueur statique point-to-set pendant la formation du verre. Nous mesurons les exposants critiques introduits dans la théorie de champ moyen des verres beaucoup plus proche de la température critique prédite dans la théorie. Enfin, nous révélons l'absence de transition géométrique caractérisant le paysage d'énergie potentiel au travers de la température du crossover de la théorie de couplages de modes.

Les modèles et les algorithmes développés dans cette thèse déplacent les études des liquides surfondus vers un territoire entièrement nouveau, en réduisant l'écart entre la théorie et les expériences, ce qui nous amène plus proche de la solution du problème de la transition vitreuse.



# Contents

<b>1</b>	<b>Introduction</b>	<b>1</b>
1.1	Experimental facts . . . . .	1
1.2	Thermodynamic theories of the glass formation . . . . .	5
1.2.1	Potential Energy Landscape . . . . .	6
1.2.2	The Adam-Gibbs-Di Marzio theory . . . . .	7
1.2.3	Mode-Coupling theory . . . . .	8
1.2.4	Mean-Field theories and growing static lengths . . . . .	9
1.2.5	Franz-Parisi approach and the configurational entropy . . . . .	11
1.3	Simulations of glass-forming liquids . . . . .	13
1.3.1	The dynamical arrest in simulations . . . . .	13
1.3.2	Algorithms to speed up thermalization . . . . .	15
1.3.3	The swap Monte Carlo algorithm . . . . .	17
1.3.4	Potential Energy Landscape in simulations . . . . .	18
1.3.5	Glassy dynamics in two dimensions . . . . .	21
1.4	Motivation of the thesis . . . . .	22
<b>2</b>	<b>Structure and dynamics of coupled viscous liquids</b>	<b>25</b>
2.1	An introduction to coupled viscous liquids . . . . .	25
2.2	Model and methods . . . . .	26
2.3	Results . . . . .	28
2.3.1	Static properties . . . . .	28
2.3.2	Dynamical properties . . . . .	31
2.4	Discussion . . . . .	35
<b>3</b>	<b>Equilibrating supercooled liquids at low temperatures</b>	<b>37</b>
3.1	Introduction and main results . . . . .	37
3.2	Models . . . . .	39
3.3	Methods . . . . .	42
3.4	Equilibrium fluid . . . . .	45
3.5	Optimizing the algorithm . . . . .	49
3.6	Mixtures . . . . .	51
3.6.1	Binary mixture . . . . .	51

3.6.2	Ternary mixture . . . . .	52
3.6.3	Pentary mixtures . . . . .	56
3.7	Continuously polydisperse systems . . . . .	56
3.7.1	Phase behaviour . . . . .	56
3.7.2	Additive and Non additive soft spheres . . . . .	58
3.7.3	Closing the gap with experimental timescales . . . . .	63
3.7.4	Hard spheres . . . . .	64
3.8	Microscopic insight into the swap dynamics . . . . .	66
3.9	Designing new models for swap Monte Carlo simulations . . . . .	70
3.9.1	Binary mixtures, polydispersity and attractive forces . . . . .	70
3.9.2	Extending the Kob-Andersen Lennard-Jones model . . . . .	72
3.10	Swap Monte Carlo in 2D . . . . .	76
<b>4</b>	<b>Thermodynamic properties at deep supercooling</b>	<b>81</b>
4.1	Equilibration of a hard sphere fluid at and beyond the jamming density	82
4.2	Configurational entropy in extremely supercooled liquids: assessing the role of dimensionality . . . . .	84
4.2.1	Why measuring configurational entropy? . . . . .	84
4.2.2	Total entropy . . . . .	86
4.2.3	Mixing entropy . . . . .	87
4.2.4	Vibrational entropy . . . . .	88
4.2.5	Configurational entropy . . . . .	90
4.3	A static correlation length grows throughout the glass formation . . .	92
4.3.1	Counting metastable states: 4 different methods . . . . .	92
4.3.2	The two dimensional case . . . . .	94
4.3.3	The three dimensional case . . . . .	96
4.4	Critical exponents of RFOT theory close to the ideal glass transition . .	99
4.4.1	Relating relaxation times and configurational entropy . . . . .	99
4.4.2	Failure of the Adam-Gibbs equation . . . . .	100
4.4.3	A RFOT theory interpretation . . . . .	102
4.4.4	Measuring $\theta$ . . . . .	104
4.4.5	Agreement with experimental data . . . . .	105
4.5	Absence of a geometric transition across the Mode-Coupling crossover	107
4.5.1	Transition points in mean field and structural glasses . . . . .	107
4.5.2	Statistical properties of saddles in simulations . . . . .	109
4.5.3	The geometric crossover . . . . .	110
<b>5</b>	<b>Summary of the work</b>	<b>117</b>
<b>6</b>	<b>Discussion and Perspectives</b>	<b>123</b>
<b>7</b>	<b>Acknowledgements</b>	<b>127</b>

*CONTENTS*

<b>8</b>	<b>Résumé en français</b>	<b>129</b>
8.1	Motivations . . . . .	129
8.2	Résultats . . . . .	130
8.3	Discussion et Perspectives . . . . .	135
	<b>Bibliography</b>	<b>139</b>

*CONTENTS*

# Chapter 1

## Introduction

### 1.1 Experimental facts

Liquids are in a state of matter characterized by a high degree of structural disorder and short-ranged spatial correlations. Relaxations happen quickly as compared to observational timescales and the typical relaxation time is in the range of  $10^{-13} - 10^{-11}$  s. Their behaviour can be explained in terms of excluded volume forces that plays a major role in determining static and dynamic properties of the system. The liquid state can be studied with theoretical tools from thermodynamics and equilibrium statistical mechanics [1]. Since human observational timescales are orders of magnitude longer compared to relaxation times, theoretical predictions have a prompt experimental test, the only issue being the design and the implementation of the experiments. Now imagine to cool down a liquid below its melting temperature  $T_m$  by placing it in contact with a thermal reservoir. Using a slow cooling rate there will be some regions of the liquid that rearrange such that their free energy is lower than the rest. A crystalline phase is nucleating and it is characterized by a typical timescale. Because of local free energy fluctuations, crystal droplets are able to expand and invade the whole system which enters in the ordered crystalline phase. However, if the cooling is fast enough local free energy fluctuations are suppressed and small crystal droplets vanish in the liquid phase. The system enters a regime, called *supercooled*, for which its ground state is the crystal. Dynamic processes slow down by decreasing temperature although, contrary to crystals, relaxation processes are still present and correlations of the local density fluctuations decay to zero on experimental timescales. By further lowering the temperature, the relaxation processes become more and more sluggish until they are so slow that the experimental system falls out of equilibrium. This is called the experimental glass transition temperature  $T_g$ , below which the system is a disordered solid or a *glass*.

In the following we will discuss three major experimental properties that supercooled liquids share together. These are essential experimental properties that motivate this thesis and will be summarized in three figures.

Figure 1.1 shows the viscosity as a function of the inverse temperature for many

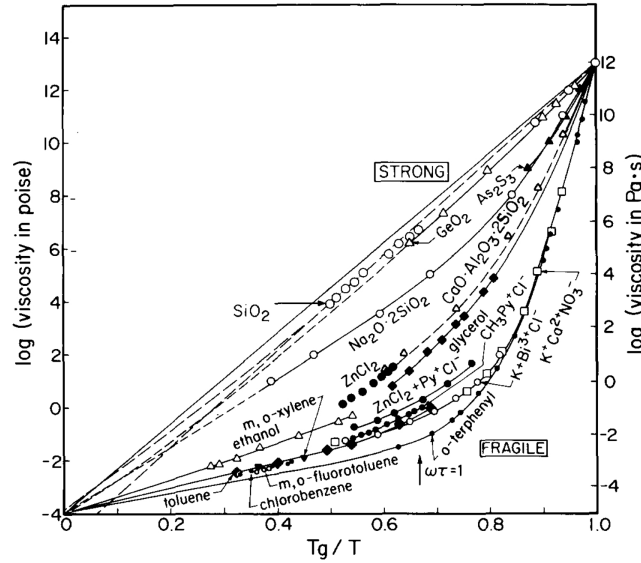


**Figure 1.1** – Viscosity  $\eta$  as a function of inverse temperature  $1/T$  for many glass forming liquids. The temperature is rescaled by the laboratory glass transition temperature  $T_g$  defined such as  $\eta(T_g) = 10^{13}$ poise. By a moderate change of the temperature the viscosity increases of numerous orders of magnitude. From this plot two classes of liquids can be defined. *Strong* liquids present an Arrhenius behaviour, *fragile* liquids are Super-Arrhenius. The image is taken from Ref. [2].

supercooled liquids. Temperature is rescaled by the glass transition temperature  $T_g$ . The onset temperature of the slow dynamics is called *onset temperature*  $T_0$ . The typical value of the viscosity at  $T_0$  is  $\eta \sim 1$  poise whereas the viscosity at the glass transition is set to be  $\eta \sim 10^{13}$  poise. One observes that the viscosity increases by around 15 orders of magnitude compared to the high temperature liquid and 13 orders compared to the onset of the supercooled regime  $T_0$ . We notice here that the experimental glass transition is an arbitrary limit given by human limitations on the typical observational time window. This plot suggests an exponential relation between the viscosity and the temperature of the form

$$\eta \propto \exp\left(\frac{\Delta(T)}{k_B T}\right), \quad (1.1)$$

where  $\Delta(T)$  is an effective activation energy.

From this figure one can recognize two extreme cases. A *strong* behaviour, characterized by an Arrhenius  $T$ -dependence of the viscosity, indicating that energy barriers are constant as a function of the temperature, and a *fragile* behaviour, showing a super-Arrhenius  $T$ -dependence of viscosity, indicating increasing energy barriers with decreasing temperature. The physical and theoretical reason behind this difference is not completely established and some explanations will be discussed in the following.

The second crucial experimental feature of glass-forming liquids is of thermodynamic nature. It is experimentally known that the entropy of a liquid is higher compared to the crystal due to a higher specific heat [4]. With the aim of comparing the entropy

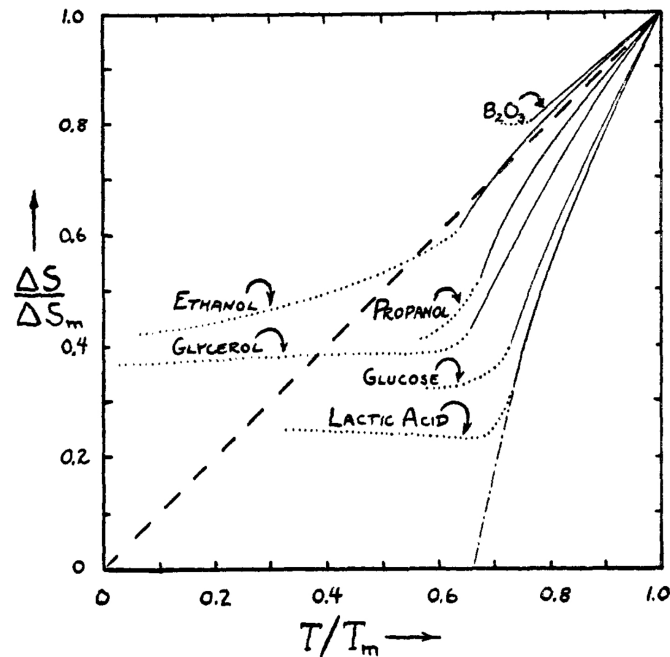


**Figure 1.2** – Excess entropy  $\Delta S$  normalized by its value at melting temperature  $T_m$  as a function of temperature  $T/T_m$  for many glass forming liquids (full lines). Excess entropy is defined as the liquid's entropy minus the crystal entropy and it decreases with lowering the temperature. Dotted lines are out of equilibrium extension of the full lines. Dashed lines are by eye extrapolation of the equilibrium behaviour of the entropy. Image is taken from Ref. [3].

of the metastable liquid and the crystal, in 1948 Kauzmann proposed the following argument [3]. He defined an *excess entropy* of a supercooled liquid by subtracting the entropy measured in the crystalline phase to the supercooled liquid entropy and then he plotted this quantity as a function of temperature. The result is shown in Fig. 1.2 for various materials. The excess entropy decreases as  $T$  drops, as it was expected from the calorimetric properties of liquids. By further lowering the temperature, the system undergoes the glass transition and falls out of equilibrium, which reflects in a bending of the excess entropy curve. Linear extrapolation of the excess entropy towards lower temperatures gives a vanishing value at a temperature called the Kauzmann transition temperature  $T_K$ . Whether a Kauzmann transition exists or not is being matter of debate since 1948. Its existence would mean that the entropy of a liquid could be equal than that of the corresponding crystal. A situation which is hard to imagine since the liquid is disordered, however this is theoretically possible and it is actually the case in the mean field theories of glasses that will be introduced later. Another theoretical possibility is that the entropy would bend and would always remain larger than the crystal one. This means that no Kauzmann transition would exist at a finite temperature. The main problem for the investigation of the existence of a Kauzmann transition is given from the experimental kinetic arrest which always prevents the exploration of temperatures lower than  $T_g$ , such that, experimentally, the Kauzmann transition is unattainable. In

the context of the search for a theory of the glass formation mechanism, the excess entropy is usually called *configurational entropy* and is related to the logarithm of the number of accessible glassy states. The definition of this quantity within some theoretical approaches will be discussed in the following.

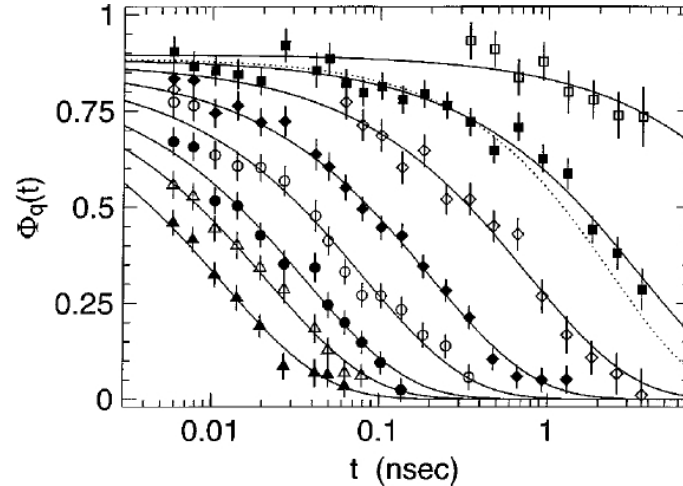


**Figure 1.3** – Intermediate scattering function as a function of time measured with neutron scattering experiments of glycerol. Particle positions are completely correlated (uncorrelated) when this quantity is equal to 1 (0). Lowering the temperature we observe a separation of timescales between short time ( $\beta$ -relaxations) and the long time ( $\alpha$ -relaxations) decays with the appearance of a plateau consequence of the *cage effect*. The figure is taken from Ref. [5].

The third fundamental piece of information for this dissertation concerns the static and dynamical properties of supercooled liquids. Interestingly, the structure of liquids not change significantly down to and across  $T_g$  does. In particular two point static correlation functions show very mild changes [6]. However, as we will discuss later, static quantities can be used to predict the dynamical arrest, which means that even small changes in the local arrangements may have considerable consequences for the dynamics. On the other hand, the dynamical properties of supercooled liquids do change remarkably with respect to the liquid phase. The most remarkable feature is the emergence of a separation of dynamical timescales. Namely, particles vibrate around their initial position exploring a limited portion of space at short timescales. These vibrations are localized in space by the presence of neighbouring particles. This phenomenon is often called *cage effect*, however the true nature of the *cage* is blurry since the effect is intrinsically collective, each particle being caged and taking part of cages for other particles. On longer timescales particles escape from the cage and are able to travel a long path from their initial position and the system completely loses memory of its initial configuration. These two processes are called respectively  $\beta$  and  $\alpha$  relaxations and are amongst the most relevant dynamical features of supercooled liquids. This behaviour is observed for instance experimentally through dielectric measurements of neutron scattering. Neutron experiments give access to the intermediate scattering function [7] that measures density

relaxations by quantifying the degree of correlation of particle positions between an initial time 0 and an observational time  $t$ . The intermediate scattering function assumes values between 1 for perfect correlation and 0 in case of completely uncorrelated situation with respect to the initial time. Fig. 1.3 presents the results for the collective part of the intermediate scattering function measured in glycerol. It can be seen that there is a first decorrelation at short time  $t < 0.003$  ns ( $\beta$ -relaxation) due to vibrations inside the cage. Then a plateau value is attained as a consequence of the cage effect. Finally, the function decays to zero at long time ( $\alpha$ -relaxation). One can define the self part of the intermediate scattering function (see Eq. 2.8),  $F_s(k, t)$ , and extract the typical decay time for  $\alpha$ -relaxation as  $\tau_\alpha$ . This quantity indicates the time needed for each particle in the system to travel on average a distance  $r \approx 2\pi/q$  where  $q$  is the wave vector at which correlations are tested.

The relaxation time can be directly related to the viscosity using shear properties within the Maxwell model [8] through the relation  $\eta \propto G_\infty \tau_M$ , where  $G_\infty$  is the high frequency shear modulus and  $\tau_M$  is a characteristic relaxation time which is defined within the model. This model allows to reconsider all the phenomenology shown in Fig. 1.1 for the viscosity in terms of relaxation times.

Finally, we notice that an analogous glass transition can be observed by increasing the density instead of reducing the temperature. This is the case, for instance, in experiments of colloidal systems [9] or in simulations of hard spheres [10]. In the following we will refer to glass formation either due to a decreasing temperature or to an increasing packing fraction interchangeably.

The glassy phenomenology presented here rises many theoretical questions, about the nature of the dynamical transition, the microscopic mechanism leading to the slowing down and the possible existence of a Kauzmann transition. In the next section we will introduce some theoretical approaches that deal with these problems formally and make predictions that can be tested in experiments and simulations.

## 1.2 Thermodynamic theories of the glass formation

Glass formation is characterized by a dramatic change in the viscosity leading to a kinetic arrest and to the formation of an amorphous solid. From an experimental point of view, a solid has a non-zero static shear modulus  $G_\infty$ . However, for the glass state, this is hard to justify from a theoretical point of view. As it was noticed by Anderson [11], indeed, the shear modulus can be computed as an equilibrium thermodynamic average and is zero on an ergodic ensemble. In the case of glasses, one could be tempted to compute it on the same ensemble as a high temperature equilibrium liquid (remember that the structure does not change significantly during glass formation) and would find no rigidity, contrary to any experimental observation. This fact makes the glass transition, using the word of Anderson *"the deepest and most interesting unsolved problem in solid state theory"*. A lot of theories have been proposed during the last seventy years to explain the nature

of supercooled liquids and the glass transition, among them: Adam-Gibbs-DiMarzio theory [12, 13, 14], Mode Coupling Theory [15], Potential Energy Landscape [16], Random First Order Transition theory [17, 18], Frustration-Limited Domains [19], Dynamical Facilitation [20]. Some of them present conflicting explanations, some of them are extension and refinements of others. In the next paragraphs we concentrate mainly on four of them. First we will introduce the Potential Energy Landscape framework, which gives a good and largely accepted thermodynamic description of supercooled liquid and glasses. Then we will briefly sketch the Adam-Gibbs-DiMarzio theory and the Mode-Coupling theory and finally discuss the Random First Order Transition and the mean field theory of hard spheres.

### 1.2.1 Potential Energy Landscape

The separation of dynamical timescales discussed in Fig. 1.3 inspired a thermodynamic construction able to describe the supercooled regime called the Potential Energy Landscape (PEL) formalism. Already Goldstein at the end of the 60s [21] observed that the two step relaxation in supercooled liquids can be explained by assuming that the liquid anharmonically vibrates around a minimum point of its potential energy (corresponding to the  $\beta$  relaxation) and very rarely it jumps between two different minima leading to large rearrangements of the particle positions (corresponding to  $\alpha$  relaxations).

A solid formulation of this argument was settled in the 80s with the work of Stillinger and Weber [22, 23, 24]. Their formalism is built on the notion of the Potential Energy Landscape that is a  $3N$  dimensional hypersurface in the configurational space, where  $N$  is the number of particles in the system and a specific configuration corresponds to a point on the hypersurface. Stillinger and Weber offered a description of the supercooled regime based on the partitioning of the configurational space into basins of attraction for equilibrium configurations and minima underlying each basin called *inherent structures*. This structure allows to separate the partition function in two contributions, one quantifies the portion of configurational space related to short time vibrations inside a basin of attraction and the other quantifies the multiplicity of the basins of attraction and concerns slow relaxation processes between different basins. The partition function in the  $(N, V, T)$  ensemble can be written as:

$$Z(T, V) = \sum_{e_{IS}} \Omega(e_{IS}) e^{-\beta f(e_{IS}, T, V)}. \quad (1.2)$$

The vibrational contribution to the partition function of a basin of attraction with corresponding inherent structures energy  $e_{IS}$  is given by  $f(e_{IS}, T, V)$ . Here it has to be noted the explicit dependence on the energy of the inherent structure, the volume and the temperature. This value needs to be multiplied by the number of inherent structures at that specific energy  $\Omega(e_{IS})$  and summed over different inherent structure energies. In the PEL framework one identifies inherent structures and thermodynamic glassy states, although this assumption is theoretically weak as it will be discussed later. However,

based on this assumption one can also define a configurational entropy as:

$$s_c(e_{IS}) = k_B \ln [\Omega(e_{IS})]. \quad (1.3)$$

The study of this quantity and, in general, of the properties of the PEL, were found to be successful in computational studies of the supercooled state as it will be discussed in the following.

The PEL framework is strongly justified by experimental and computational studies and it represents a fundamental construction to describe supercooled liquids. However, in this theory, some questions remain unanswered: How does the microscopic mechanism for relaxation look like? Which is the nature of energy barriers and how do they change with changing temperature? Is there a thermodynamic explanation for the dynamical slowing down? All these questions have been addressed by other theories that will be briefly reviewed in the next sections.

### 1.2.2 The Adam-Gibbs-Di Marzio theory

As anticipated in Sec. 1.1, the prominent increase of relaxation times can be expressed by:

$$\tau_\alpha = \tau_0 \exp \left[ \frac{\Delta(T)}{k_B T} \right], \quad (1.4)$$

where  $\Delta(T)$  indicates the activation energy, generically dependent on temperature. Strong glass-formers are well described by an Arrhenius law and the activation energy often corresponds to the energy to break an intermolecular bond. More generally it indicates a geometrical, system specific and temperature independent energetic price to be paid for relaxation. On the other hand, in the case of fragile glass formers, a super-Arrhenius behaviour of relaxation times indicates that energy barriers are changing with temperature. Explaining the microscopic reason why this is happening is one of the main purposes of the three theories that will be sketched in the following.

One of the first attempts to formulate a theory for rearrangements in supercooled liquids is due to Adam, Gibbs and Di Marzio [12, 13, 14]. This theory builds on the notion of Cooperatively Rearranging Region (CRR), namely independent and equivalent subsystems composed of a certain number of correlated particles  $n(T)$ . The presence of these regions intrinsically bears the notion of a spatial correlation

$$\xi(T) \propto n(T)^{\frac{1}{D}}, \quad (1.5)$$

where  $D$  is the spatial dimension. Each CRR can take a certain amount of different states  $\Omega$ . This is a finite number independent of the temperature and the CRRs size. Thermal fluctuations push the CRR to rearrange into a new locally stable state. Then one can define a configurational entropy  $s_c$  as the logarithmic density of the number of stable states

$$s_c(T) = \frac{1}{N} \ln [\Omega^{n(T)}], \quad (1.6)$$

where  $N$  is the number of particles in the system. Interestingly  $s_c$  is inversely proportional to the average size of a CRR. Supposing that the global energy barrier that the system has to overcome in order to perform a rearrangement  $\Delta(T)$  is proportional to  $n(T)$ , one can find a relation between the configurational entropy and  $\Delta(T)$  such that

$$\Delta(T) \propto \frac{1}{s_c(T)}. \quad (1.7)$$

Plugging this relation into Eq. 1.4 one finds a link between entropy and relaxation times expressed by the Adam Gibbs relation

$$\tau_\alpha = \tau_0 \exp \left[ \frac{A}{T S_c(T)} \right], \quad (1.8)$$

where  $A$  is a constant. This theory gives a simple explanation of the mechanism for relaxation in glass systems, but it relies on two weak assumptions. Namely, accessible states  $\Omega$  are independent on temperature and CRR size and different CRR do not interact, given the absence of a surface tension. We will see in the following how these issues can be solved without losing the thermodynamic foundation of the theory.

### 1.2.3 Mode-Coupling theory

Another theory dealing with the explanation of the dynamical arrest is the Mode Coupling Theory (MCT) [15]. The main idea in MCT is to use structural quantities as an input variable (namely the structure factor  $S(k)$  [1]) and, exploiting the Zwanzig-Mori formalism, to write self-consistent equations for the dynamics of density fluctuations [15]. The theory gives remarkably good quantitative predictions of the  $\beta$ -relaxation and the plateau of  $F_s(k, t)$  (see Fig. 1.3). On the other hand it predicts a dynamical arrest at a temperature  $T_{MCT}$  describing self density relaxation times  $\tau_\alpha$  with the following law:

$$\tau_\alpha \propto \frac{1}{(T - T_{MCT})^\gamma}, \quad (1.9)$$

where  $\gamma$  is a universal exponent that can be exactly computed in the theory. Below  $T_{MCT}$  ergodicity is broken and the plateau of  $F_s(k, t)$  does not decorrelate to zero, which corresponds to a glass transition. Yet in experimental and computational systems a power law fit of relaxation times is only possible in a mildly supercooled regime covering three or four orders of magnitude from the onset temperature. This is a much narrower range compared to the observed 13 orders of magnitude of glassy slowdown. The lack of a reliable description of the slowing down is the main failure of MCT. This failure has been usually explained by the absence of activation processes in the MCT formalism and the fact that the theoretical derivation itself relies on some uncontrolled approximations.

Overall, the theory gives good predictions of the dynamical slowing down and it inspired the search for a growing dynamical lengthscale characterizing the glassy slowdown [25]. However, MCT presents the drawback that good predictions are either

limited in a temperature region close and above  $T_{MCT}$ , such that  $\frac{T-T_{MCT}}{T_{MCT}} \ll 1$ , or they are limited to  $\beta$  relaxation. Moreover, the nature of energy barriers, the mechanism of relaxation lowering the temperature and the possible growing of static lengthscales are questions that remain unanswered within this theory.

#### 1.2.4 Mean-Field theories and growing static lengths

The quest for a theory that at the same time explains the dynamical and thermodynamic behaviour of supercooled liquids and glasses led to the introduction of the Random First Order Transition theory (RFOT) by Kirkpatrick, Thirumalai and Wolynes in the 80s [26, 27, 28]. At that time they noticed that a class of spin systems, namely p-spin models, undergo a similar dynamical transition as glass-forming liquids. These models can be theoretically defined by the following Hamiltonian

$$H = - \sum_{k_1, k_2, \dots, k_p}^N J_{k_1, k_2, \dots, k_p} \sigma_{k_1} \sigma_{k_2} \dots \sigma_{k_p}, \quad (1.10)$$

where  $\sigma$ s are spin values and  $J_{k_1, k_2, \dots, k_p}$  are random distributed coupling that enforce a quenched disorder in the system. The problem defined by this Hamiltonian was solved in the '80 using replica symmetry breaking techniques in which the free energy of the system is replicated and takes into account all the possible realizations of the disorder [29]. The interesting fact is that the solution of this problem has two features closely recalling the glass formation in systems of particles. By lowering the temperature first there is a transition at  $T_d$  from an ergodic liquid at high temperature and a non-ergodic liquid at low temperature characterized by an exponentially large number of (meta)stable states living for an infinite time. Remarkably the dynamical equation describing this behaviour has the same structure of the Mode-Coupling theory and in this context  $T_d$  can be identified with  $T_{MCT}$  [18]. At the same time it resembles the dynamical behaviour of experimental supercooled liquids even though in real systems metastable states have a finite lifetime, and they will at a certain point turn into stable crystalline states. Then at a lower temperature  $T_K$  there is a Kauzmann transition, with a sub-exponential number of glassy states and a vanishing configurational entropy. These deep analogies pushed some theoreticians to explain the structural glass formation mechanism using mean-field systems. However one has to notice that the spin system introduced previously is quite different from structural glasses both because it has a quenched disorder, not present in the liquid case, and because there is no reference to particles in real space. These two drawbacks have been solved recently with the formulation of mean-field theory for hard spheres valid in infinite dimensions [30, 31, 32, 18]. First the theory deals with particles, namely hard spheres, which represent the simplest description of a liquid [1]. Secondly, quenched disorder is replaced by imposing an external field that selects an amorphous state, solving the problem by means of replica methods and continuing the solution in the case at zero field. Thus, the unphysical

presence of quenched disorder is removed. Interestingly the results concerning the dynamical arrest and the Kauzmann transition are equivalent to the ones of the spin models. The main problem left in this theory is its infinite dimensions formulation, which entails the absence of relaxation mechanisms and estimations of finite energy barriers for rearrangements. To solve this problem one has to introduce a nucleation argument readjusted in the language of glassy physics. Before doing this, let us first take a step back and introduce a theorem which helps in understanding the following discussion. At the basis of any modern theoretical introduction of the glass-transition problem, it is important to recall a theorem formulated by Montanari and Semerjian in 2006 which states that any increase of relaxation timescales in glassy systems  $\tau$  has to be accompanied by an increasing static correlation length  $\xi$  [33]. In particular, they were able to find an upper and a lower bound for the relaxation times:

$$C_1\xi \leq \tau \leq \exp(C_2\xi^D) \quad (1.11)$$

Here  $C_{1,2}$  are constant and  $D$  is the spatial dimension. The physical reasoning behind these two equalities is the following. The relaxation time is bounded from below from the fact that the propagation of the relaxation cannot be faster than ballistic in the system. It is also bounded from above because the system could be divided into boxes of size  $\xi$  and within each box the relaxation time cannot be larger than an exponential of the volume. The nature of the length  $\xi$  has been clarified in the context of the nucleation argument for the RFOT theory [17], which relies on entropic considerations and is analogous to the one used in first order transitions, such as crystallization. Let us take a supercooled liquid in a metastable state and a dynamical process causing a local rearrangement of a sub-system of size  $R$ . Since the number of states is exponentially large, no specific local arrangement is preferred and local energy fluctuations can bring the sub-system in a new state with a total gain in free-energy proportional to configurational entropy:  $\Delta F_{bulk} = -TS_c(T)R^D$  where  $D$  is the system dimensionality. On the other hand the rearrangement would cause a mismatch at the interface between the subsystem and the rest of the system quantified as  $\Delta F_{surface} = \Upsilon(T)R^\theta$  where  $\Upsilon(T)$  is a surface tension which has an entropic nature and  $\theta$  is an exponent satisfying  $\theta \leq D - 1$ . The critical size at which the rearrangement is energetically favourable and above which the new state would invade the whole system is given by:

$$\xi = \left( \frac{\Upsilon(T)}{TS_c(T)} \right)^{\frac{1}{D-\theta}} \quad (1.12)$$

From these considerations one can extract an energetic barrier height to insert into Eq. 1.4 for the relaxation times, finding:

$$\tau_\alpha = \tau_0 \exp\left(\frac{\Delta_0(T)\xi^\psi}{T}\right) = \tau_0 \exp\left[\frac{\Delta_0(T)}{T} \left(\frac{\Upsilon(T)}{TS_c(T)}\right)^{\frac{\psi}{D-\theta}}\right] \quad (1.13)$$

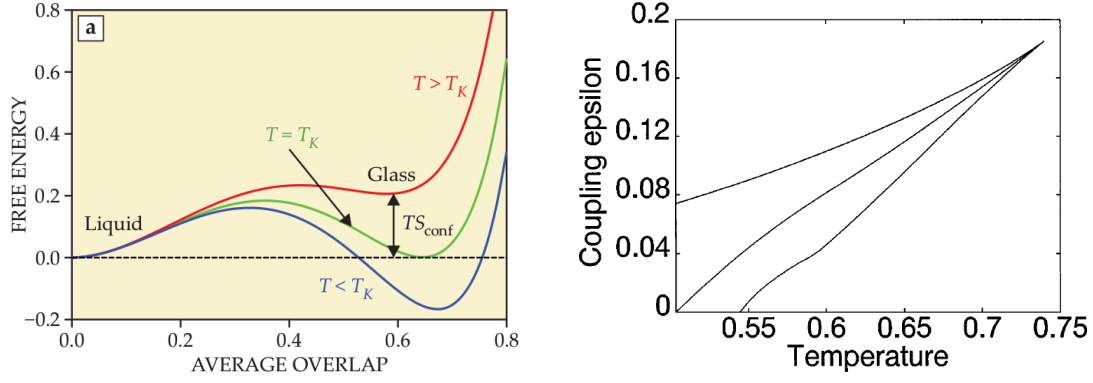
As one can see, here we regain an Adam-Gibbs like relation between configurational entropy (thermodynamics) and relaxation times (dynamics). The dependence of relaxation times on the static correlation length is accounted for by the exponent  $\psi$ . The length  $\xi$  is one of the key ingredients of the RFOT theory. It is a *point-to-set* correlation, which brings about the notion of *amorphous order*. Its definition and estimation was defined in Ref. [34]. The idea is the following: imagine taking a configuration at a given temperature and to freeze all the particles except the ones in a cavity of radius  $R$ . If a static correlation  $\xi$  is present in the system then particles inside the cavity will feel an amorphous order which pins them from outside in their initial position, and they will not decorrelate in a shell of radius  $\xi$  from the cavity edge. Then if the cavity is small enough  $R < \xi$  particles inside will be frozen otherwise if  $R > \xi$  the center of the cavity is free to find another local arrangement. The growth of  $\xi$  is accompanied by a rarefaction of accessible thermodynamic states. If we image the cavity to be in one of the available states, in a finite dimensional system, it will escape in a finite time depending on fluctuation driven by entropy. At this point it is important to discuss more clearly the notion of configurational entropy within the replica approach, this will be done in the next subsection.

### 1.2.5 Franz-Parisi approach and the configurational entropy

One relevant aspect of the mean field theory of glasses concerns a better characterization of the thermodynamic states and the notion of configurational entropy. A big step forward was done within an approach first introduced by Franz and Parisi [36, 37]. The idea is to extend the p-spin model to a framework presenting a coupling field  $\epsilon$  between pairs of replicas  $(x, y)$  of the system. It was found that from this procedure a first-order transition line emerges at equilibrium in the phase diagram  $(\epsilon, T)$ , terminating in a second order critical point. There are two possible approaches for the theoretical construction. In one case the two coupled replicas are both free to explore the phase space. This is usually called *annealed* coupling. On the other hand, it is also possible that one of the two replicas is frozen at a temperature  $T'$  and the other explores the phase space at temperature  $T$  in presence of the coupling field  $\epsilon$ . This last setting goes under the name of *quenched* coupling. In the following we will be dealing with the quenched case since it will be employed later in our simulations. Here we also set  $T = T'$  although other choices are possible [37]. The starting point of the construction is to define a coupled Hamiltonian between two replicas

$$H_\epsilon(x, y) = H(x) - \epsilon Q(x, y), \quad (1.14)$$

where  $\epsilon$  is the coupling field and  $H(x)$  is the bare Hamiltonian of the replica  $x$ .  $Q(x, y)$  is called the *overlap* and it is a conjugate variable to the field  $\epsilon$  accounting for the degree of similarity between the two replicas which is defined to be 1 if the two replicas coincides and 0 if they completely differ. Here the presence of the coupling term forces



(a) Free energy as a function of the overlap for different temperature. The overlap is the order parameter of the phase transition and quantifies the similarity between replicas. Within the glass phase  $T < T_d$ , the free energy present a secondary minimum which gives an estimation of the configurational entropy. At the Kauzmann transition the two minima are at the same free energy level. For lower temperature the high overlap phase is thermodynamically preferred. Figure is taken from Ref. [35].

(b) The phase diagram in the  $(\epsilon, Q)$  plane. The central line indicates a first order transition between a low- $Q$  and a high- $Q$  state. The upper and the lower lines indicates spinodal curve for the transition. The three lines culminates in a second order critical point. Figure is taken from Ref. [36].

Figure 1.4 –

the configuration of the replica  $x$  to be similar to the one of replica  $y$ . The free energy of the replica  $x$  in presence of a specific replica  $y$  can be defined as [37]:

$$F(T, \epsilon, y) = \frac{1}{N\beta} \ln \left[ \int dx \exp(-\beta H(x) + \beta \epsilon Q(x, y)) \right]. \quad (1.15)$$

Taking the average over the probability distribution of the  $y$  configuration

$$F(T, \epsilon) = \frac{\int dy \exp(-\beta H(y)) F(T, \epsilon, y)}{\int dy \exp(-\beta H(y))}. \quad (1.16)$$

The Legendre transform of this function is called the *Franz-Parisi potential*

$$V_\epsilon(Q, T) = \min_\epsilon F(T, \epsilon) + \epsilon Q, \quad (1.17)$$

which shows interesting properties when varying the temperature for  $\epsilon > 0$ . At temperature higher than a transition temperature  $T_c^\epsilon$  the probability to have a non zero overlap is exponentially small and  $V_\epsilon(Q, T)$  has a unique global minimum for  $Q = 0$ . By reducing the temperature below the transition temperature  $T < T_c^\epsilon$ ,  $V_\epsilon(Q, T)$  develops a secondary local minimum for a finite value of the overlap  $Q^*$  indicating an increasing probability to find the two replicas in the same thermodynamic state. This is a first order

transition characterized by a discontinuous jump of the overlap between a low- $Q$  regime to a high- $Q$  regime. The situation is illustrated in Fig. 1.4a where a sketch of the free energy  $V_\epsilon(Q, T)$  is plotted as a function of  $Q$  for various temperatures. By varying  $\epsilon$ , a first-order transition line is revealed in the  $(\epsilon, T)$  phase diagram as shown in Fig. 1.4b. At high field it terminates in a second order critical point  $(T_c, \epsilon_c)$  whereas, by extension to zero field, it reveals a Kauzmann transition at finite temperature  $T_K$ .

In this framework one can give a robust definition of the configurational entropy. Given that the secondary minimum at  $Q^*$  is a local one, the system has to spend a certain amount of free energy to remain confined in the same state as the reference replica. The amount of free energy is quantified by the height of this secondary minimum with respect to the global minimum  $V_{\epsilon=0}(Q^*)$  and it is related to the number of available states. For this reason an explicit relation exists between the Franz-Parisi potential computed at  $Q^*$  and the configurational entropy [38]:

$$V_{\epsilon=0}(Q^*) \approx T s_c(T). \quad (1.18)$$

By further lowering the temperature below  $T_K$  a Kauzmann transition is reached at which the two minima have the same height and the configurational entropy becomes zero.

Although initially developed in the context of the in mean-field glassy models, the Franz-Parisi construction turned out to be very useful in simulations of glass-forming liquids both in giving a mean field like definition of the configurational entropy and in helping the investigation of the Kauzmann transition using higher temperature regimes. This has been done in a series of articles [39, 38] as it will be further discussed in following chapters.

## 1.3 Simulations of glass-forming liquids

### 1.3.1 The dynamical arrest in simulations

Computer simulations of liquids have existed for more than half a century [43, 44]. The main advantage of this approach is that one can compute physical properties of systems for which an analytical approach can be highly nontrivial and, on the other hand, one can easily access single particle positions and velocities which could be difficult to retrieve in an experiment involving more than few particles. In their book on molecular dynamics simulations [44], Frenkel and Smit discuss the notion of *computer experiments*. This must be understood as a framework that allows to define a computer model and calculate some physical properties, to later compare the result both with experiments and with analytic theories. The former comparison is done to test the ability of the computer model to reproduce experimental findings. The latter one is a theory testing procedure which can help to validate or falsify them.

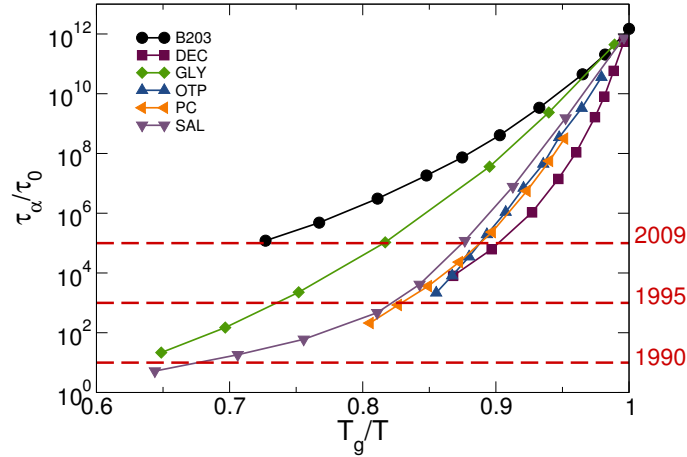


**Figure 1.5** – Self density relaxation times as a function of the inverse temperature for many different experimental glass forming liquids. The  $x$ -axis is rescaled by the glass transition temperature  $T_g$ , the  $y$ -axis is rescaled by the onset value of relaxation times. Data are taken from Ref. [6]. The three vertical lines give an estimation of the upper limit for the accessible regime in simulations in Ref. [40, 41, 42] from bottom to top. Nowadays, computer simulations cover at maximum five orders of magnitude of relaxation times at equilibrium, that is, they are eight orders of magnitude slower than experiments in equilibrating.

Computer simulations of supercooled liquids and glasses have been employed since a long time [43, 45]. We will focus here on the cases in which the system is treated as classical, where two particle interactions in most of the cases depend only on the distance between two particles. All three or many body interactions are neglected and the potential has a very simple form, such as inverse power law or Lennard-Jones. Once the model is set up, a dynamical rule must be chosen either for the evolution in time or in the phase space. There are two main possibilities to study the statistical mechanics of the system: Molecular Dynamics (MD) simulations or Monte Carlo (MC) simulations. In the first case a system of differential equations for particle positions and velocities is assigned (e.g. Newtonian or Langevin) and solved controlling the system thermodynamic state from outside via external thermostats or barostats. Positions and velocities are updated at each time step given by the shortest typical timescale of the system, which in a liquid is around 1 fs. Another possibility is to perform Monte Carlo simulations. In this case the main aim is to set up a stochastic method to sample the phase space. The general strategy in this case is to assign a transition probability to move from a configuration  $C$  to another  $C'$  and an updating rule to generate the new configuration. One of the most common transition probability is given by the Metropolis Monte Carlo algorithm [46] where the transition probability is given by the ratio of the Boltzmann factor of the two configurations. Within this approach the standard updating rule consists in displacing the particle in a random direction to create a new configuration. The algorithm will be discussed in details in the following chapters. The interesting aspect of Monte Carlo simulations of supercooled liquids is that their dynamics, even

though unphysical, behaves in a very similar way to a Brownian motion and it can also be used to give a dynamical description of the supercooled state [47].

The main problems in simulations of glass-forming liquids are the number of particles that can be simulated and the accessible timescales. Thirty years ago, simulations were able to probe a supercooled liquid at equilibrium in a very narrow regime of relaxation times. In Ref. [40] for instance a binary mixture of repulsive spheres was simulated for around one order of magnitude of relaxation times in the supercooled regime. In 1994, Kob and Andersen introduced one of the most employed models of glass-forming liquids, the Kob-Andersen Lennard-Jones binary mixture [48]. At that time, they were able to simulate 3 orders of magnitude of relaxation times in the supercooled regime. More recently, very long simulations of glass-forming liquids were performed in 2009 [42]. In this case a binary mixture of hard sphere was simulated over roughly 5 orders of magnitude of relaxation times. These improvements throughout the years are mainly due to hardware performance advancement and the speed of this process has been quite slow with a rate of one or two order of magnitudes gained every 10 years. Recently introduced hardware tools to push the computation to higher efficiency consist in the use of graphic cards or large scale parallelization [49]. This strategy can be very effective for increasing the system size, although it does not allow a huge increase of accessible timescales. Nowadays, a typical single core simulation of a system of  $O(1000)$  particles lasts for around  $10^9$  steps, which correspond to  $1 \mu\text{s}$ . This value is eight orders of magnitude smaller than the experimental glass transition, which takes place for relaxation times of  $10^2$  s. The situation is shown in Fig. 1.5, where relaxation times of experimental glass-formers are shown as a function of the inverse temperature. The  $x$ -axis is rescaled by  $T_g$  and the figure is the equivalent to Fig. 3.3 where relaxation times are used instead of viscosities. Experiments of glass-forming liquids fall out of equilibrium at  $T_g$ . The horizontal lines give an indication of the evolution of accessible timescale in simulations during the last thirty years taken from Ref. [40, 41, 42]. We observe that computer simulations of glass-forming liquids still lag eight orders of magnitude behind experiments. Assuming a constant progress rate for hardware performances, this gap will be closed in about a century by standard simulations.

### 1.3.2 Algorithms to speed up thermalization

Since a brute force approach to increase simulation timescales will not achieve a remarkable improvement, during the last decades some alternative algorithmic solutions were proposed. They mainly consist in clever methods to explore the phase space at lower temperatures at a faster pace.

A class of algorithms was inspired by successful spin algorithms first introduced in [50, 51], which consist in performing collective moves of clusters of spins to facilitate the study of phase transitions. The idea was generalized to off-lattice systems by performing rotations or displacements of chain or clusters of particles [52]. Thanks to this method it

was found that polydisperse hard disks can be equilibrated across the Mode-Coupling packing fraction  $\phi_{MCT}$  showing that no Mode-Coupling like divergence of relaxation times is present [53]. The algorithm used at that time was based on the reflection of the position of particles inside clusters of particle with respect to a randomly chosen *pivot* point. More recently, another algorithm belonging to the same class was introduced for hard spheres and hard disks [54] and generalized to the case of continuous potential interactions [55]. This goes under the name of Event-Chain Monte Carlo algorithm and the basic move consists in displacements of chain of particles in a given direction. This algorithm does not satisfy detailed balance, although it satisfies a maximal global balance condition sufficient to converge to the stationary distribution. Some important results have been obtained thanks to this technique, for instance the existence of a first-order liquid-hexatic transition in two dimensional hard spheres [56]. Also, the three dimensional hard-sphere equation of state has been computed with higher precision [57]. In a dense hard spheres fluid the dynamical speedup given by this algorithm has been estimated of about a factor 40.

Another technique to accelerate thermalization employs the notion of parallel tempering. Inspired by algorithms previously employed by the spin glass community [58, 59], Yamamoto and Kob [60] introduced a *replica exchange* method. This consists in performing several parallel simulations of independent replicas of the system at different temperatures and then try to swap two configurations at contiguous temperatures based on a Metropolis acceptance rule. This method enhances the sampling of low temperature distributions by performing a more efficient exploration of the free energy landscape and it speeds up the equilibration of about two orders of magnitude [60, 61]. However, it presents two drawbacks: first, the method mainly works with systems of small sizes (few hundreds of particles) [61] and second, because of the exchange of different configurations, single particle dynamics cannot be followed anymore in time. Nonetheless, the technique found many successful applications for the glass science, especially in studies of equilibrium phase transition in small systems [62, 63, 64, 39]

A sequential Monte Carlo scheme, the Population Annealing, was also recently applied in simulations of supercooled liquids [65]. The method is particularly suitable for simulations of systems with rough free energy landscape and it was employed to simulate a binary hard sphere mixture. The idea is to exploit rare fluctuations at temperatures where the system can be equilibrated with standard molecular dynamics to reconstruct the Gibbs measure at lower temperatures. The method consists in a single annealing that populates the free energy landscape using configurations produced at a higher temperature. Also in this case the dynamical gain with respect to standard simulations can be quantified in around 2 orders of magnitude.

Interestingly, despite the numerous techniques introduced to accelerate the dynamics of dense supercooled systems, the maximal obtained dynamical gain is globally of a couple of orders of magnitude and none of the algorithms discussed before is particularly preferable to the others. In the following paragraph we will give a historical review of

one further simulation strategy that will be used largely in this thesis.

### 1.3.3 The swap Monte Carlo algorithm

The idea of swapping particles between two systems or insert particles taken from a thermal bath has been widely employed in computational physics of polymers and colloids [44], with the main aim of efficiently sample the phase space or compute thermodynamic potentials. A particle-swapping Monte Carlo method was first introduced in Ref. [66, 67]. In that case the aim was to compute partial molar quantities by performing exchanges of particles with different identities between two boxes.

Some years later, a Monte Carlo method employing particle swap moves of particle within the simulations box was implemented by Gazzillo and Pastore [68] to determine the equation of state of a non-additive hard sphere fluid and compare with analytical findings. This method consists in combining two different kinds of Monte Carlo updating rules. During the simulation one performs both standard Monte Carlo moves, in which particles are displaced randomly, and some additional moves, which consisting in taking two particles at random and try to exchange their positions. The algorithm will be explicitly explained in Sec. 3.4.

Parisi and Grigera [69] first applied the swap technique to a glass-forming mixture. They first named it swap Monte Carlo algorithm as we also do. The system was a binary mixture of particles interacting via an inverse power law potential [40]. The authors observed a peak in the specific heat that was interpreted with the presence of a thermodynamic transition to an ideal glass phase. The result was questioned by Brumer and Reichman [70] who performed new swap Monte Carlo simulations of the same system and observed that the system easily crystallizes at low temperatures. Even though prone to crystallize, this system was largely employed in swap simulations and many results concerning glass physics were claimed to be realized below the Mode-Coupling transition temperature. Namely, a phononic interpretation of the boson peak was given in [71]. The presence of amorphous order was detected both in cavity geometry [72, 73] and in sandwich geometry [74]. A specific heat behaviour was found to be consistent with an entropy crisis in [75] and anomalous across the Mode-Coupling crossover in a cavity geometry in [76]. Finally, confirmation for a geometric transition in the Potential Energy Landscape in supercooled liquids was found [77].

In 2001 swap simulations were employed also in systems made of continuously polydisperse particles [78]. In this case hard disks were used to confirm the absence of a thermodynamic transition crossing the Mode-Coupling transition density  $\rho_{MCT}$ , a result already found by means of a cluster move algorithm [53] as discussed previously. They were also able to sketch the phase diagram of the system as a function of polydispersity and density. The use of swap Monte Carlo in polydisperse systems was later revisited in Ref. [70]. First the authors tested the 2D system of Refs. [53, 78], finding similar results regarding the absence of a thermodynamic transition across  $\rho_{MCT}$ . The idea of

using swap MC simulations to enhance sampling of the phase space for polydisperse soft spheres was used systematically in Ref. [79]. The authors were able to find three different phases at varying density and polydispersity consisting in a disorder fluid, a crystal, and a demixed phase.

More recently swap simulations were used by the group of Procaccia [80]. They had the idea of introducing a ternary mixture to facilitate the swap moves. They claimed to be able to equilibrate at very low temperature compared to standard simulations, achieving a maximum speed up of relaxation times of 15 orders of magnitude. Using this method they observed the growth of a static lengthscale in low temperature supercooled liquids. This static lengthscale was first introduced in Ref [81] and it was predicted to increase at low temperatures and to be related to the point-to-set static order measured by  $\xi_{PTS}$  [82].

All these previous results on swap Monte Carlo simulations have been inspiring for our research and some of them will be reproduced, discussed or revisited in the following chapters.

### 1.3.4 Potential Energy Landscape in simulations

In Sec. 1.2.1 we briefly discussed the notion of the Potential Energy Landscape (PEL), a theoretical construction able to describe the thermodynamic properties of glass-forming liquids. The PEL has been widely employed in simulations, where some specific features can be directly measured and were used to validate and expand the theory. The literature concerning the subject is huge (see for instance [16]). The goal of the computational study of the PEL is the observation of its statistical properties, such as the number of inherent structures visited at a certain temperature or the height of the energy barrier for rearrangements using PEL topology.

We recall that in the PEL framework an inherent structure is defined as the minimum of the basin of attraction of many equilibrium configurations. Starting from an equilibrium configuration at a given temperature  $T$ , to find the corresponding inherent structure one has to perform a minimization of the potential energy. This can be done using common minimization algorithms, such as steepest descent or conjugate gradient. After the minimization one can extract the energy of the configuration, namely the inherent structure energy  $e_{IS}$  and study the properties of the minima of the PEL.

It was found that, depending on the temperature of the starting configuration, two regimes can be distinguished in relation to the dynamical properties of the system [83, 84]. At high temperature the liquid visit basins with similar properties and average inherent structure energy  $\langle e_{IS} \rangle$  is only mildly dependent on the sampling temperature. With cooling, the system enters a *landscape-influenced* regime at a temperature corresponding to the onset of the supercooled dynamics  $T_0$ . In this regime the energy of inherent structure decreases considerably by decreasing  $T$  since the system explores zone of the landscape corresponding to deeper and deeper basins. Time correlation functions for

density degrees of freedom present a two step decay in time and the permanence in a given basin increases by reducing the temperature. At even lower temperature the system enters the so-called *landscape-dominated* regime, where dynamics starts to be extremely slow, rearrangements are rare and the system remains confined in a basin. This roughly coincides with the computational kinetic transition and with  $T_{MCT}$ . Based on these properties of the PEL, the relation between  $\langle e_{IS} \rangle$  and  $T$  it was shown to hold and to be bijective [83, 85] already at moderate supercooling.

This allowed to retrieve the temperature dependence of the configurational entropy introduced in Eq. 1.3 using a standard thermodynamic relation [86]

$$\frac{ds_c(T)}{d\langle e_{IS} \rangle} = \frac{1}{T}, \quad (1.19)$$

and integrating the  $T$  dependence of  $d\langle e_{IS} \rangle/T$ . This can be achieved by separately computing the  $T$  dependence of the total entropy and the vibrational entropy in the *PEL* formalism. Then,  $s_c(T)$  is obtained by subtraction of the vibrational entropy to the total entropy, using an analogous procedure to the one followed in experiments. This procedure will be employed and discussed in details in Ch. 4. The configurational entropy obtained within the PEL formalism was measured in many glass-forming liquids as a function of temperature [86, 87, 84, 88, 89]. In many cases, a continuously decreasing value with lowering the temperature was found. However, all these results were obtained for mildly supercooled liquids since the dynamic arrest prevents equilibration at low temperature. Moreover, the configurational entropy measured using the PEL framework is a quantity that relies on the identification between thermodynamic states and inherent structures. This identification does not hold theoretically [38] as it will be discussed later in Ch. 4.

Another information that can be obtained by computational studies of the PEL concerns its topological properties and the connection with the relaxation dynamics. So far we have been discussing short time vibrations as periods of permanence in the basin of attraction and long time relaxations as jumps between one basin to another. How this relaxation happens, however, is unclear. It was suggested that the knowledge of saddles of the PEL could clarify this point [90]. Minima are stationary points characterized by a positive curvature of the  $3N$ -dimensional manifold in all the possible directions. Saddles are also stationary points, but they are distinguished by a negative curvature of the landscape in some directions and positive in the remaining ones. Consequently, the system is in unstable equilibrium if perturbed in one of the directions with negative curvature.

To explain the role of saddles in structural glass-formers, let us step back on the analogy between the p-spin models and the structural glasses introduced in Sec. 1.2.4. Interestingly, it was found in mean-field models that the exploration of stationary points of their energy landscape has a remarkable evolution with temperature [91, 92, 90, 93, 94]. Namely, for temperatures above the ergodic/non-ergodic transition temperature  $T_d$  the systems explores both minima and saddles of the landscape. By further reducing the

temperature, saddle points cannot be visited by the system below the ergodic/non-ergodic transition temperature  $T_d$  and the behaviour of the system for  $T_K < T < T_d$  is completely determined by the minima of the landscape. The transition from a saddle-dominated regime to a minima-dominated regime was named *geometric transition* and in case of mean field models its existence was confirmed by analytic calculations.

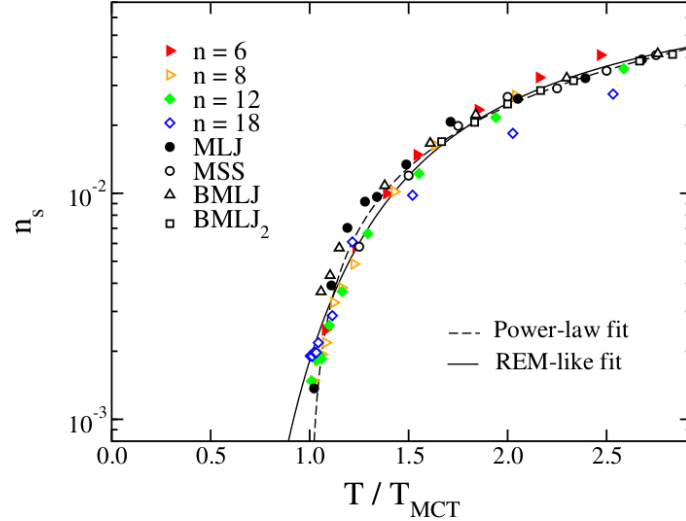


**Figure 1.6** – Saddle order  $n_s$ , that quantifies the number of unstable directions of the stationary point, as a function of the temperature for many glass-forming liquids. The extrapolations are based on a power law fit and a Random Energy model fit. Temperature is rescaled by Mode-Coupling temperature  $T_{MCT}$ . Image is taken from Ref. [95].

Following the analogy between mean-field models and structural glasses it was suggested [90] that saddles could also explain relaxations in realistic glass-forming models. Computational studies of the landscape were performed to analyze the statistics of saddle points with changing temperatures [96, 97, 98, 99, 100, 101, 95]. The main finding was that the exploration of saddle points depends on the temperature of the system.

By employing numerous glass forming liquids saddles order  $n_s$  (that quantifies the number of unstable directions) and saddle energy were measured for different sampling temperatures and it was claimed that the system does not visit saddles for temperature below  $T_{MCT}$ .

The situation is shown in Fig. 1.6 where  $n_s$  is plotted as a function of the temperature rescaled by  $T_{MCT}$  for different glass-forming liquids. We observe that the number of negative directions of the stationary points decreases with decreasing temperature. A power law extrapolation suggests that  $n_s$  vanishes at  $T = T_{MCT}$ . This result is in agreement with the presence of a geometric transition and also with the identification  $T_c \sim T_{MCT}$ . However, it is based on extrapolation from higher temperatures as compared to  $T_{MCT}$ , and not by studying the systems exactly at the putative transition temperature.

### 1.3.5 Glassy dynamics in two dimensions

Until now we dealt with results of experiments and simulations for the three dimensional systems. For a long time, the traditional assumption has been that the glass transition has similar characteristics in two or three dimensions. Quoting a sentence by P. Harrowell "In Flatland, glasses reproduce all the behaviour of their three-dimensional relatives" [102]. This is also reflected by the fact that most of the glass transition theories do not predict changes in two or three dimensions [6].

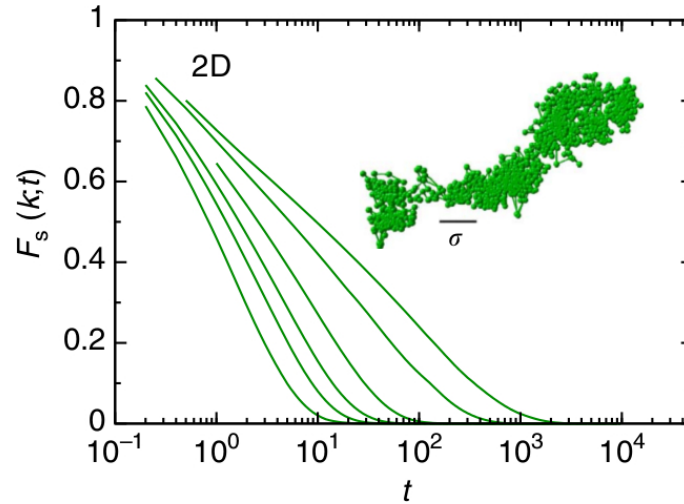


**Figure 1.7** – Self-intermediate scattering function  $F_s(q, t)$  in a two dimensional model of glass-forming liquids. As in Fig.1.3, particle positions are completely correlated (uncorrelated) when this quantity is equal to 1 (0). Lowering the temperature we observe a slowing down characterized by a single stretched exponential decay. The inset shows the single particle trajectory where sudden jumps are absent and replaced by a continuous displacement. The figure is taken from Ref. [103].

In recent years, however, the situation has changed and there is increasing evidence that glasses in  $2D$  are very different from their  $3D$  version. The situation started to change in 2015, when Flenner and Szamel published a paper [103], in which they simulated two dimensional systems with sizes ranging from few hundreds up to millions of particles. They found a remarkable system size dependence in the dynamics as compared to the three dimensional case, namely, increasing the system size, relaxation times decrease and the transient localization (cage effect) disappears. This is shown in Fig. 1.7, where the self-intermediate scattering function is measured for a system made of millions of particles in two dimensions. The behaviour is qualitatively different from the one observed in Fig. 1.3 for  $3D$  systems. In that case the presence of a plateau was evident and the idea of particles being caged by the neighbours could find an observational validation. On the contrary, in the two-dimensional system the plateau disappears and the slowing down of the dynamics is indicated by the presence of a stretched exponential. A better analysis reveals that particles move long distances together with their neighbours and do not change the local environment on the timescale of single particle displacements.

Measuring two time correlation functions that account for the orientational changes of neighbouring particles, such as the bond orientational correlation function [104], one finds that the relaxation happens at longer timescales, the plateau in the shape of the correlation function is reestablished and the cage effect reemerges. Similar findings were confirmed in simulations by another group [105], where also a phononic interpretation to the two dimensional behaviour was given. The absence of caging was ascribed to the presence of long wavelength fluctuations, which are present in two dimensional solids [106].

Recently, two experimental papers were also able to give a dynamical investigation of glassy behaviour in two dimensions [107, 108]. This was possible by using colloidal systems, where particles are orders of magnitude larger compared with molecular glass formers and the single particle dynamics can be directly observed using confocal microscopy. Interestingly, the authors confirmed all the simulation results about the absence of transitional localization and, on the other hand, they observed a glassy slowing down in the dynamical quantities that take into account the local environment.

This recent progress in understanding the supercooled behaviour in two dimensions systems started a discussion in the glass community about the difference of the glass transition varying the dimensionality.

While some researchers agree to consider the nature of the glass transition fundamentally different in two and three dimensions [103], some others try to reconcile the dimensionality dependence by considering neighbour relative observables [107, 108, 109]. This recent debate, however, is still far to be settled and it lacks coherent theoretical predictions.

## 1.4 Motivation of the thesis

In this introduction chapter, we deal with several topics related to the glass formation that provide the research context of this thesis. In this section we briefly focus on some of them that have been the main source of motivation for this work.

In Sec. 1.2.5 we have been discussing coupled systems in mean field theory. We saw that the introduction of a coupling field between two replicas of the system lead to the emergence of a first order transition whose order parameter is given by an overlap which measures the similarity between the two replicas. The probability distribution of this quantity is directly related to the Franz-Parisi potential and to the configurational entropy. In the first few months of this thesis we have been used computer simulations to investigate the static and dynamic properties of coupled liquids, in particular concerning the overlap behaviour with reducing the temperature, in the attempt to reveal the presence of the transition in a structural glass formers.

We anticipated in Sec. 1.3.1 that a fundamental issue in computational studies of supercooled liquids comes from the fact that only four or five orders of magnitude of relaxation times are accessible in equilibrium, compared with the 13 orders of magnitude

that experiment can probe at equilibrium. Some techniques have been introduced to equilibrate supercooled liquids at lower temperature. Overall they were proved to accelerate the equilibration of around two orders of magnitude (Sec. 1.3.2). Only in the case of Ref. [80] it was claimed that speed up of more than ten orders of magnitude is possible using the swap Monte Carlo algorithm (Sec. 1.3.3). One of the main purposes of this thesis is to design and implement models and methods to accelerate thermalization and extend the simulation regime to timescales comparable with the experimental accessible ones. We are particular careful to ensure that our systems reach a proper equilibration and that remain disordered fluids. Having succeeding in our purpose, we are able to study supercooled liquids and glasses in an unexplored regime.

The third part of the thesis is dedicated to the investigation of supercooled liquids in this novel regime. Among the open questions discussed previously, we will address the followings.

Measurements of the configurational entropy using the Potential Energy Landscape framework, discussed in Secs. 1.2.1 and 1.3.4, revealed a decrease of this quantity with decreasing temperature in numerous supercooled liquids. However, these results were always obtained for temperature higher than the dynamic slowdown of simulations. The large majority of the results were obtained in three dimensions and a little is known about the thermodynamic behaviour of two dimensional system, although from a dynamical point of view the glass transition was found to be different in two and three dimensions (Sec. 1.3.5). In this thesis we address two problems at the same time. On the one hand, we measure configurational entropy in a completely unexplored regime and, on the other hand, we directly compare between a two dimensional and a three dimensional realization of a system. This study will give us a better insight on the presence of a finite  $T$  Kauzmann transition and the role of thermodynamics in the glass formation.

In supercooled liquids, it is still unclear what is the relation between thermodynamic and dynamic, namely between relaxation times and configurational entropy. Some theoretical approach, such as the Adam-Gibbs-DiMarzio (Sec. 1.2.2) or RFOT (Sec. 1.2.4), support a direct relation between these two quantity. Testing these theories is a difficult task both for experiments and simulations. In the former case, static quantities characteristic of theoretical frameworks are inaccessible to experimental measurements. In the latter case, accessible temperature regime is bounded by the presence of a computational dynamical slowdown. We address the two problems at once by employing simulation results obtained at extremely low temperature, both for the configurational entropy and for a static point-to-set length, to directly test these theories and measure critical exponent of the RFOT.

Some years ago, it was claimed the existence of a geometric transition in the landscape of glass-forming liquids previously found in mean field models (Sec. 1.3.4). The computational result, however, was obtained for temperature above the putative transition. We investigate the presence of this transition performing studies of the energy landscape in the novel regime accessible with swap simulations, this gives us a privileged

viewpoint on its existence.

The work of the thesis lead to four publications [110, 111, 112, 113]. Two of them are a direct output of this thesis [110, 112]. The other two result from broad collaboration and include some results and analysis developed in this thesis [111, 113]. Three other publications are in preparation. One concerns the results on configurational entropy and point-to-set length in a two dimensional system and the possible absence of a finite temperature ideal glass transition. One deals with the relation between relaxation times and the configurational entropy and the measurement of critical exponent of the RFOT close to the transition. The last regards the absence of a geometric transition in computational models of glass-forming liquids.

# Chapter 2

## Structure and dynamics of coupled viscous liquids

This chapter includes results from Ref. [110]

### 2.1 An introduction to coupled viscous liquids

The concept of replicating systems to study their phase properties had a great success in the study of disordered systems since the first introduction of the Replica theory in the late '70 and the Replica Symmetry Breaking solution in the '80 [114, 115]. The theory had first been developed in the context of spin systems and since then theoretical, computational and experimental applications have been developed for a huge number of systems ranging from neural networks, agent based models, random lasers, Bose glasses, noise analysis and information theory [29]. The general idea at the basis of this approach is the fact that due to the implicit disorder of the system, thermodynamic phase transition cannot be easily revealed using traditional order parameter and an additional order parameter accounting for the similarity between statistically independent realizations of the quenched disorder must be introduced to reveal a finite temperature thermodynamic transition. Approaches based or inspired by replica theory have been employed in theory and simulations of structural glasses as well [6]. The origin of these studies has its root already in the first formulation of the Random First Order Transition theory (RFOT) [27]. From that moment, the idea of considering molecular glass-formers in the same universality class of some spin glasses found deeper foundations both in the modern version of RFOT [17] and in the mean field theory of hard spheres [18]. Predictions of these theories for the behaviour of structural glass-forming liquids have been only partially confirmed so far and they need better clarification from a computational and experimental point of view. In computations it is possible to probe the RFOT scheme for

the thermodynamic glass transition in a temperature regime more easily accessible by using *extended* phase diagrams. In these cases a thermodynamic glass-liquid transition at equilibrium can be directly induced by the introduction of additional fields constraining the system. Some of these external constraints are based on the idea of pinning some of the particles of the system [34, 33], in various geometries as cavity [72, 73, 116], walls [117, 118] or random pinning [119, 64, 120].

Another possibility is to duplicate the system and introduce a coupling field  $\epsilon$  between the two copies as a conjugate variable of the degree of similarity between them, the overlap  $Q$ . This scenario has been carefully studied in mean field models and two different possible realizations were proposed [36, 37]. An *annealed* case and a *quenched* case. In this chapter we will be dealing with simulations in the quenched framework, for which the phase diagram in  $(\epsilon, T)$  has been carefully studied in mean field and partially confirmed using numerical simulations. This point was discussed in the introduction and the result is reported in Fig. 1.4b. A first-order transition line has been found at varying the coupling field  $\epsilon$  that separates a low- $Q$  phase at low field, in which particles in the two replicas of the system are uncorrelated, with a high- $Q$  phase at high field, in which particles are localized in space by the presence of the coupling replica. The first-order line culminates in a second order critical point which is in the same universality class as the Random Field Ising model [121, 122].

In this section we simulate coupled replicas of a known glass forming liquid in the quenched framework. The main aim is to study the statics and dynamics of the system in detail, at temperature regimes accessible by standard equilibrium simulations. We observe that directly testing the first order transition line in standard simulations is unachievable, therefore we concentrate in a temperature region above the second order critical point to reveal the existence of what in standard phase transition is called a Widom line, across which some observables, and particularly susceptibilities, present vestiges of the existence of the transition. Our observations are not entirely conclusive, but they strongly support the presence of a transition at lower temperature.

In the following, first we introduce the model and the methods employed (Sec. 2.2). Then we go through our results both concerning the static (Sec. 2.3.1) and the dynamics (Sec. 2.3.2) of the coupled systems. Finally we discuss our results and compare with literature findings (Sec. 2.4).

## 2.2 Model and methods

We perform Monte Carlo simulations of a three dimensional 80:20 mixture of soft spheres which has a well known glass-forming behaviour, first introduced by Kob and Andersen in Ref. [48]. The two particle interaction is described by

$$v(r_{ij}) = 4\epsilon_{ij} \left[ \left( \frac{\sigma_{ij}}{r_{ij}} \right)^{12} - \left( \frac{\sigma_{ij}}{r_{ij}} \right)^6 \right] + c_{LJ}, \quad (2.1)$$

where  $\epsilon_{AA} = 1.0$ ,  $\epsilon_{AB} = 1.5$ ,  $\epsilon_{BB} = 0.5$ ,  $\sigma_{AA} = 1.0$ ,  $\sigma_{AB} = 0.8$ ,  $\sigma_{BB} = 0.88$ . Here we cut off and shift the pair potential at the cutoff distance  $r_{cut} = 2.5\sigma_{ij}$ . We use  $\epsilon_{AA}$  and  $\sigma_{AA}$  as energy and length unit respectively and the Boltzmann constant is set to one  $k_B = 1$ . We study a system of  $N = 1000$  particles at a number density  $\rho = 1.2$ . The Monte Carlo dynamics consists in drawing a random displacement between zero and  $\Delta r_{MAX} = 0.06$  in the three spatial direction and attempt to perform a move based on a Metropolis acceptance rule. The time unit consists in  $N$  Monte Carlo attempts.

The degree of similarity between two coupled configuration  $\{r_1\}$ ,  $\{r_2\}$  is given by the overlap

$$Q_{12} = \frac{1}{N} \sum_{i,j} \theta(a - |\mathbf{r}_{1,i} - \mathbf{r}_{2,j}|). \quad (2.2)$$

Here  $\theta(x)$  is the Heavyside function,  $a = 0.3$  is a cut-off distance which is comparable with the size of the cage in the unconstrained system and  $r_{\alpha,i}$  denotes the position of particle  $i$  in the configuration  $\alpha$ .

We produce a set of equilibrium configurations  $\{r_1\}$  at a certain temperature  $T_1$  and  $\{r_2\}$  at  $T_2$ . The first ones are used as reference configurations and the second are let to evolve with a biased Hamiltonian

$$H_{\{r_1\}}(\{r_2\}) = H_{LJ}(\{r_2\}) - \epsilon Q_{12}, \quad (2.3)$$

where

$$H_{LJ}(\{r_2\}) = \frac{1}{2} \sum_{i,j}^N v(r_{ij}) \quad (2.4)$$

is the bare Hamiltonian of a single copy  $\{r_2\}$ . Here the field  $\epsilon > 0$  is the coupling field and favours high values of overlap. We study systems such that  $T_1 = T_2 = T$ . This is due to the quenched disorder present in the Hamiltonian  $H_{\{r_1\}}$  given from a specific configuration  $\{r_1\}$ . In order to obtain meaningful result one has to perform two different averages in this system. First, given a single configuration  $\{r_1\}$  an average for independent realizations of the mobile system  $\{r_2\}$  is needed. Then a disorder average has to be done for independent disorder realizations of  $\{r_1\}$ . The number of configurations needed to average using systems of this size is restricted to a small value (around ten) for a system of our size.

For this system the onset temperature is  $T_0 = 1$  and the Mode-Coupling temperature is  $T_{MCT} \approx 0.435$ . This is roughly the temperature interval that can be accessed at equilibrium with standard simulations. In the context of coupled replicas, the situation becomes more difficult and the exploration of the  $(\epsilon, T)$  diagram is not easy at low temperature or high values of the coupling field. We are able to equilibrate easily the system at temperature around  $T = 0.7$  and we include the point at  $T = 0.6$  in the analysis which also reached stationarity, although being more difficult to simulate using our protocols. As a test of equilibration we look at the absence of drift in the instantaneous value of the overlap over a time period of  $10^5$  steps. Moreover we require

that particles have travelled for a distance of around 3 particle diameters. These somehow empirical tests are enough for our analysis here. However we believe that strong tests of equilibration are essential in Monte Carlo simulations of supercooled liquids and we will discuss largely this point in the next chapter. Overall we have not been able to get very close to the meaningful portion of the phase diagram due to the limitation of the standard simulations.

## 2.3 Results

### 2.3.1 Static properties

In this section we report both static and dynamic results of our simulations at varying the values of  $(\epsilon, T)$ .

It is reasonable to expect that at a given temperature, bigger values of the coupling field give rise to higher values of the overlap. This is actually the case as is shown in Fig. 2.1 where the distribution probabilities of the overlap are shown for different values of  $\epsilon$  at temperature  $T = 0.8$ , which is slightly below the onset temperature  $T_0 = 1$ . As

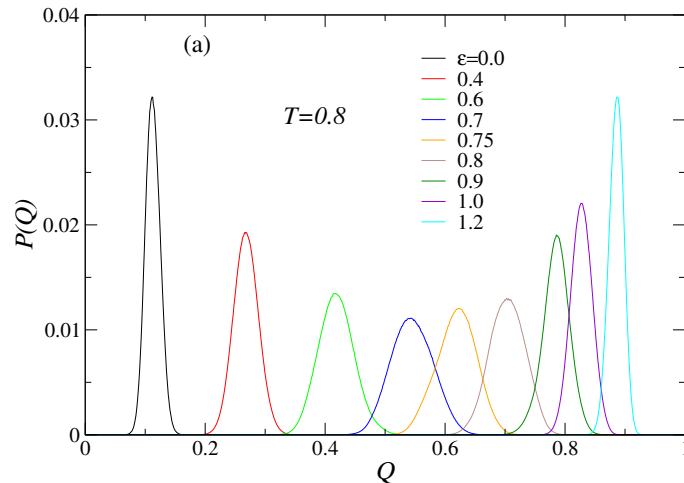


**Figure 2.1** – Probability distribution of the overlap  $P(Q)$  at several  $\epsilon$  vales along the isotherm  $T = 0.8$ . The shape is broader near  $\epsilon^* \approx 0.7$

expected, probability distributions are narrow for high and low values of the field and centered respectively at high and low values of the overlap. Interestingly they become broader for intermediate values of the field ( $\epsilon \approx 0.7$ ). This corresponds to large amplitude fluctuations of the overlap. We observe this feature in the time series of the overlap (not reported) together with the fact that exploration of the equilibrium properties of the system is more difficult in this regimes where long simulations are needed. On the other hand at low and high values of the field, overlap fluctuations and long time correlation are suppressed and the system is either uncorrelated from its pinning replica or strongly coupled. This situation is in agreement with the presence of critical slowing

down due to the vicinity of a second order critical point at a lower temperature. At even lower temperatures a first order phase transition would manifest itself with a bimodal probability distribution. All these thermodynamic features are not directly observable in our simulations which last for about  $10^7$  steps, a time period four orders of magnitude longer than the relaxation time of the unconstrained system  $\tau \approx 2 \times 10^3$ . This also shows the computational difficulty introduced by the presence of the coupling and quenched disorder.

To better study the properties of the transition, let us now introduce the moments of the distribution of the overlap

$$\langle Q^n \rangle = \int_0^1 dQ P(Q) Q^n. \quad (2.5)$$

In Fig. 2.2a we show the average of the overlap  $\langle Q \rangle$  as a function of  $\epsilon$  for the different studied temperatures. We find that the overlap value increases continuously with increasing field. The steepness of the curve increases with reducing temperature and the field values necessary to obtain the same degree of localization are smaller by cooling. These two features imply that the thermodynamic driving force to escape from a randomly chosen configuration is smaller with decreasing temperature and the crossover becomes more sharply pronounced and similar to a real thermodynamic transition, in agreement with a prediction made in the RFOT theory framework [27].

In order to detect the crossover value from a low- $Q$  to a high- $Q$  regime we define the overlap susceptibility

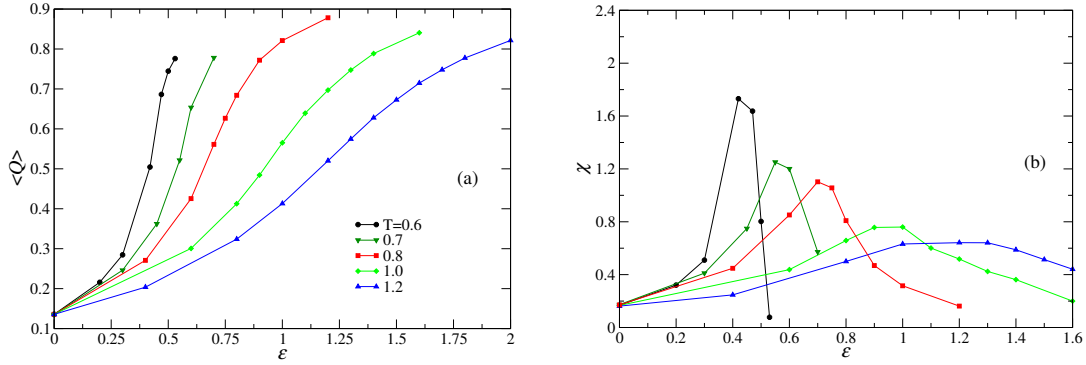
$$\chi = N [\langle Q^2 \rangle - \langle Q \rangle^2]. \quad (2.6)$$

We report the results in Fig. 2.2b for each studied temperature. This quantity has a peak at a given value of the field corresponding to the crossover observed in the overlap average. The peak increases in intensity, becomes sharper at lower temperature and is expected to diverge at a second order critical point.

All these evidences support a RFOT description of the problem, although an alternative view is also possible in which the observed features remains a crossover lowering the temperature and it do not become a real thermodynamic transition even going at  $T = 0$  [123, 124]. The accessed temperature range in this work, however, does not allow to tell which of the two scenarios is correct.

Increasing values of the coupling field  $\epsilon$  provokes increasing overlap between copies of the system. At a single particle level this means that particles in the mobile replica tend to be in similar position as the particle in the frozen replica. More specifically situations in which a particle in  $\{r_2\}$  is within a range of  $a = 0.3$  from the position of the center of a particle in  $\{r_1\}$  are energetically preferred. We call this geometry a *dimer*. To quantitatively evaluate the presence of dimers in our system we define a radial distribution function between the quenched and the liquid replica

$$g_{\alpha\beta}(r) = \frac{1}{VN_{\alpha}N_{\beta}} \sum_{i=1}^{N_{\alpha}} \sum_{j=1}^{N_{\beta}} \delta(r - |\mathbf{r}_{2,i} - \mathbf{r}_{1,j}|) \quad (2.7)$$



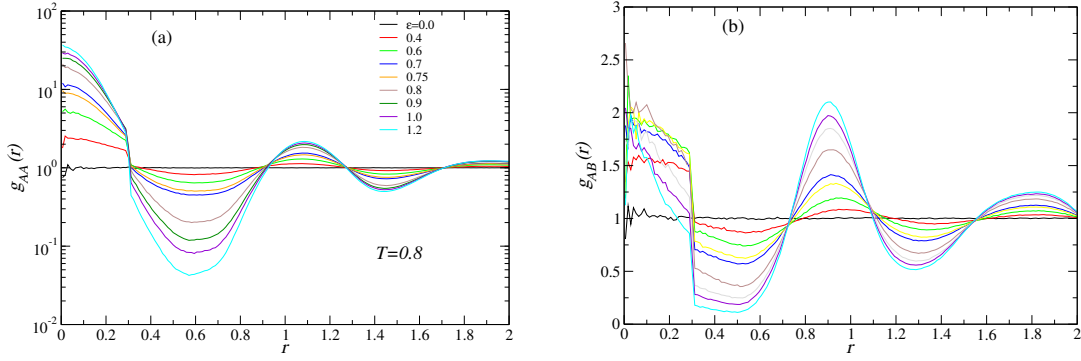
(a) Average overlap  $\langle Q \rangle$  as a function of the coupling field  $\epsilon$  and for various temperatures. The crossover between low- $Q$  regime and high- $Q$  regime becomes sharper at lower  $T$ .

(b) Overlap susceptibility  $\chi$  as a function of the coupling field  $\epsilon$  and for various temperatures. The crossover between low- $Q$  regime and high- $Q$  occurs at smaller  $\epsilon$  for lower  $T$ .

Figure 2.2 –

Here  $\alpha, \beta$  are species indices. The behaviour of this function varies with  $\epsilon$  and  $T$ . We show the result for dimers between particles of species  $A$  in Fig. 2.3a for a reference temperature  $T = 0.8$ . It shows a peak for values  $r \approx 0$  that increases with higher values of the field  $\epsilon$ . This means that a localization of particles and dimers formation increases going at stronger couplings. The effect could have been guessed by the increasing value of the overlap  $\langle Q \rangle$  since this can be directly related to the area below the curve of the radial distribution function between  $r = 0$  and  $r = a$ . The abrupt drop at  $r = a$  is connected to the choice of a step function in the definition of the overlap. The use of a smoother function would result in a continuously decreasing behaviour of the radial distribution.

We also measure  $g_{AB}(r)$  and  $g_{BB}(r)$ . The case of  $g_{BB}(r)$  (not shown) is very similar to the one of  $g_{AA}(r)$  with an increasing number of dimers of  $B$  particles at increasing coupling field. The case of  $g_{AB}(r)$  between particles of different species, however, is different. As shown in Fig. 2.3b the overall values of the peak at  $r = 0$  in this case are smaller and they always remains below 3. Interestingly in this case the peak shows a non monotonic behaviour going at higher values of the coupling. The maximum value of the peak is reached close to  $\epsilon^* = 0.7$  which coincides with the maximum of the overlap susceptibility for this temperature (see Fig. 2.2b). This means that the system, close to the Widom line, tends to develop dimers made of particles of different species, such that the geometrical heterogeneity in the coupling has a non monotonic behaviour as well. By increasing the field beyond  $\epsilon^*$ , the  $AB$  dimers are suppressed and the systems shows mostly dimers composed of particles of the same species. This geometrical and static behaviour must be better analyzed using dynamical observables as we do in the following.



(a) Radial distribution function between quenched and fluid replicas  $g_{AA}(r)$ , see Eq. 2.7. It develops a maximum near  $r = 0$  that increases monotonically as  $\epsilon$  increases. This reflects the increase of the overlap and the formation of *dimers*.

(b) Radial distribution function between quenched and fluid replicas  $g_{AB}(r)$ , see Eq. 2.7. It develops a maximum near  $r = 0$  as  $\epsilon$  increases. For high values of  $\epsilon$  this maximum decreases and the formation of  $AB$  dimers is suppressed.

Figure 2.3 –

### 2.3.2 Dynamical properties

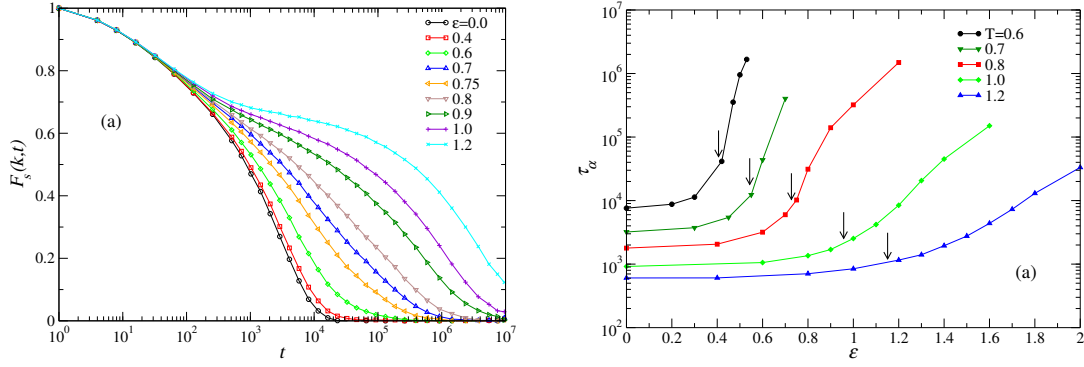
From a structural point of view we saw that increasing the field  $\epsilon$  the amplitude of overlap fluctuations first increases, reaches a maximum for intermediate values of the coupling and finally decreases again. We attributed this behaviour to the presence of a Widom line, adding different static supporting evidences. How does this crossover reflect in the dynamical behaviour of the system? How does localization affect the available relaxation pathways for the system?

Let us first concentrate on local density relaxation. To this aim we study the self intermediate scattering function

$$F_s(k, t) = \frac{1}{N} \left\langle \sum_i \exp[i\mathbf{k} \cdot (\mathbf{r}_i(t) - \mathbf{r}_i(0))] \right\rangle. \quad (2.8)$$

The value of  $k$  corresponds to the wave vector of the first peak of the structure factor. The results for big  $A$  particles is shown in Fig. 2.3a for a reference temperature  $T = 0.8$ . For  $\epsilon = 0$  relaxation is exponential and very fast. With increasing value of the coupling the system slows down and the exponential becomes stretched. For very high values of the field  $F_s(k, t)$  shows a two step relaxation with the presence of plateau. This is in agreement with the localization effect that we revealed in the static properties. A comparison between quantities for  $A$  and  $B$  particles (not shown here) indicates that the slowing down effect is less pronounced for small particles. A similar decoupling in the dynamic properties is also observed in the bulk system at low temperature [125].

We extract the structural relaxation times using the common definition  $F(k, \tau_\alpha) = e^{-1}$ . The result is reported in Fig. 2.4b. We observe that at a given temperature the dynamics has a dramatic slowing down for values of the coupling field comparable with



(a) Self intermediate scattering function  $F_s(k, t)$  evaluated at  $k = 7.4$  along the isotherm  $T = 0.8$  varying the coupling  $\epsilon$ . The single particle dynamics slows down monotonically by increasing  $\epsilon$ , a clear indication of the particle localization effect.

(b) Evolution of the structural relaxation times  $\tau_\alpha$  as a function of  $\epsilon$  at various temperatures. The dynamics slows down abruptly when the crossover field  $\epsilon^*(T)$  is crossed.  $\epsilon^*$  is defined through overlap susceptibility and indicated with a black arrow.

Figure 2.4 –

$\epsilon^*$ , the crossover field defined using the overlap susceptibility (see Eq. (2.6) and Fig. 2.2b). Going at lower temperature the curve develops a kink that becomes more and more pronounced.

We also compute the diffusion coefficient using the mean-squared displacement  $\delta r^2(t) = \frac{1}{N} \langle \sum_i |\mathbf{r}_i(t) - \mathbf{r}_i(0)|^2 \rangle$  and the diffusion coefficient  $D$  using the Einstein relation  $\lim_{t \rightarrow \infty} \delta r^2(t) = 6Dt$ . For this quantity we observe a qualitative similar behaviour as for the relaxation times. However the change with coupling  $\epsilon$  is quantitatively smaller in the case of diffusion properties. This is shown in Fig. 2.5. Here we plot the product

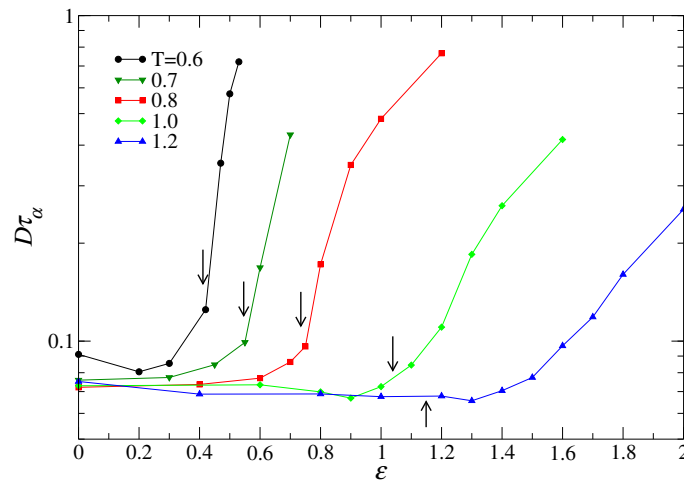


Figure 2.5 – Product  $D\tau_\alpha$  of the diffusion constant with the structural relaxation time. A decoupling of the two quantities by increasing the field  $\epsilon$  arises at the crossover  $\epsilon^*(T)$ , indicated with a black arrow.

$D\tau_\alpha$  between the diffusion constant and the structural relaxation time. This quantity is constant for small values of the coupling field  $\epsilon$  and undergoes a sudden change, increasing remarkably at the crossover between a low- $Q$  regime and a high- $Q$  regime, for corresponding values of the field  $\epsilon^*(T)$ . We remember that the Stokes-Einstein relation can be written in term of relaxation times  $D\tau_\alpha \approx D\eta \sim cst$  [7]. Deviations from this relation have been found in supercooled liquids at low temperature and are usually ascribed to the presence of dynamical heterogeneities [126] although other sources of the decoupling were also found in liquids [127]. The usual reasoning for this to happen in supercooled liquids is given by the fact that relaxation times are mostly dominated by slow particles of the system, whereas diffusion coefficients are dominated by the fast ones. However, here we detect a deviation of the Stokes-Einstein relation which is suddenly happening at the crossover and that is quantitatively bigger than the one noted in the unconstrained system. This suggests that the reason for the decoupling could be different for bulk or coupled supercooled liquids. To elucidate the origin of this decoupling, as a first test, we quantify the degrees of spatial dynamical correlation present in the system. In order to do that we evaluate a four-point dynamic susceptibility [128]

$$\chi_4(t) = N [\langle f_s(k, t)^2 \rangle - \langle f_s(k, t) \rangle^2], \quad (2.9)$$

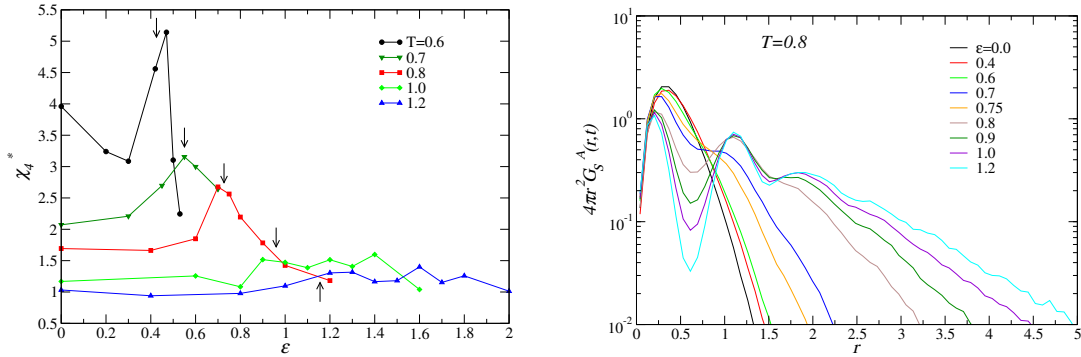
where  $f_s(k, t) = \frac{1}{N} \sum_i \exp[i\mathbf{k} \cdot (\mathbf{r}_i(t) - \mathbf{r}_i(0))]$  represents the non averaged value of the self-intermediate scattering function. In unconstrained supercooled liquids the behaviour of this quantity as a function of time is well known [129, 130]. It has a single peak located around  $t = \tau_\alpha$ , whose height  $\chi_4^*$  gives a rough measure of the volume of the dynamically correlated region in the system [25]. We found similar peaks for  $\chi_4(t)$  measured in the constrained system and we report the value of the peaks with varying  $\epsilon$  for various temperatures in Fig. 2.6a

First we notice that at high temperature this quantity remains flat even for high values of the field  $\epsilon$ . However when the temperature is reduced below the onset temperature  $T < 1.0$  its behaviour changes and it varies non-monotonically starting for low values in the low- $Q$  regime, reaching a maximum corresponding to the crossover  $\epsilon^*$  and then decreasing again in the localization regime. This gives two pieces of information. First, the spatial correlation of the dynamics are a consequence of the spatial fluctuations of the overlap already observed in the statics. Secondly, in the high field regime, dynamic correlation decrease again and this can be interpreted as a consequence of a localization. However the violation of the Stokes Einstein equation, which keeps increasing with  $\epsilon$ , cannot be explained in term of spatial correlations in the dynamics in this regime. It has also to be noticed that the value of  $\chi_4^*(\epsilon \rightarrow 0)$  increases with decreasing temperature, revealing the existence of correlated regions already in the bulk system, as already observed numerous times in the previous literature [129]. This is different from the situation for static overlap fluctuations that remain always small in the unconstrained system. A distinct temperature dependence for static and dynamic fluctuations has already noted before in moderately supercooled liquids [127, 117]. As

concluded previously, the decoupling between diffusivity and structural relaxation in the system at high coupling  $\epsilon$  noted in Fig. 2.5 cannot be explained using spatial correlation in the dynamics, consequently the single particle dynamics must be resolved and inspected. To this aim we introduce the self-part of the Van-Hove correlation function

$$G_s(r, t) = \left\langle \sum_i \delta(r - |\mathbf{r}_i(t) - \mathbf{r}_i(0)|) \right\rangle. \quad (2.10)$$

In an isotropic system, one can consider only the dependence on the modulus of  $r$  and thus an integration on the angular degrees of freedom can be carried out. Doing so this observable can be renormalized with its value for the ideal gas case  $G_s(r, t) = 4\pi r^2 G_s(r, t)$ , obtaining the probability distribution of single particle displacements.



(a) Maximum of the four-point dynamic susceptibility  $\chi_4^*$  as a function of  $\epsilon$  for various temperatures. Dynamical spatial correlations have a maximum close to the static crossover  $\epsilon^*(T)$  indicated by black arrows.

(b) Self-part of the Van-Hove correlation function  $4\pi r^2 G_s^A(r, t)$  for particles of the species  $A$  with varying the value of  $\epsilon$ . Here  $T = 0.8$  and the quantity is evaluated at a time  $t$  such that  $F_s(k, t) = 0.2$ . By increasing the coupling  $\epsilon$  the distributions broaden and the tails develop a multi-peak structure due to a discrete particle hopping.

Figure 2.6 –

In Fig. 2.6b we show the result for particles in the  $A$  species at different coupling fields. The time  $t$  for the measurement have been chosen such that  $F_s(k, t) = 0.2$ , meaning that particles have travelled enough to better reveal the structure of the Van-Hove function. We notice that for zero or small values of the coupling, the distribution has a Gaussian shape. This indicates homogeneous and diffusive behaviour of particles. Increasing the coupling field above a certain threshold given by  $\epsilon^*(T)$ , the distribution broadens considerably suggesting the presence of slow and fast particles in the system. This feature alone is enough to explain the decoupling between relaxation time and diffusion coefficient [131]. Interestingly, here a dynamical heterogeneity arises in absence of increasing dynamical correlation length, being a purely local phenomena. Looking more carefully at Fig. 2.6b we observe that for high values of the coupling field distributions

not only are broader but they also present a very non-Gaussian shape, characterized by the emergence of one or two secondary peaks. This indicates that particles perform slow and intermittent jump dynamics, hopping from one site to another, where the sites are given by the underlining quenched replica. This is consistent with the localization already observed in static quantities before.

## 2.4 Discussion

The work presented in this chapter was performed at the beginning of this thesis. We used it as a preparation for the bulk of the thesis that will be presented in the next chapters. Here we studied the static and dynamic properties of a coupled supercooled liquid. We were able to find evidences of the presence of a Widom line [132] that could indicate an underlining second order critical point. However, strictly speaking, we are far from the transition. This is due to the marked slowing down appearing in coupled systems, which has two main sources. On the one hand, by reducing the temperature, the system presents the usual slowing down of supercooled liquids that has been discussed in the introduction (Sec. 1.3.1). On the other hand, the coupling with a quenched configuration further slows down the dynamics, especially in the high field region where individual particles show high overlaps with the pinned particle of the coupled configuration. Some techniques can be employed to solve these drawbacks. In Ref. [63] umbrella sampling and replica exchange methods were employed in the same model glass forming, although in that case the maximum system size was  $N = 256$ . Thanks to those advanced methods stronger evidences of a critical point were observed, involving, for instance, bimodal distributions of the overlap probability or system size dependencies in the overlap susceptibility. Strong support to the existence of a coupling driven phase transition was also found for plaquette models [124]. Interestingly these models do not present any Kauzmann phase transition at finite temperature. Consequently this work has shown that the two transitions may be independent from one another, contrary to what has been predicted in the mean-field theory [37]. The main limitation of the results presented in this chapter concerns the inability to equilibrate at significantly low temperatures. For this reason the next chapter will be dedicated to solve this issue by implementing models and algorithms to reach equilibrium at extreme supercooling.



# Chapter 3

## Equilibrating supercooled liquids at low temperatures

### 3.1 Introduction and main results

In Sec. 1.3.1 we discussed the state of art of computer simulations of glass-forming liquids. Similarly to experiments, simulations need to overcome two main problems at once: the possible formation of ordered regions in the system and the remarkable increase of relaxation times leading to the dynamical arrest. However, experiments seem to stand in a better place on the two fronts. Good experimental molecular glass formers, not presenting evidence of crystalline droplets, are known since decades [2, 133] and their statics and dynamics can be studied at equilibrium over 12 – 13 orders of magnitude of relaxation times in the supercooled regime. In the case of colloids the range decreases to 4 – 5 orders of magnitude, with the advantage that nowadays microscopy is able to resolve colloidal particles in real space [9]. Simulation performances are worse than molecular experiments. Even though the single particle motion can be followed in time and any physically relevant observable can be computed using *in silico* models, ordering and dynamical slowdown are unresolved issues [6]. Computational models of glass-forming liquids usually fall out of equilibrium at temperatures comparable with the Mode Coupling temperature. From a dynamical viewpoint this means that the range of relaxation times currently accessible at equilibrium is around 4 – 5 orders of magnitude [42], similar to what can be achieved with colloidal glass formers and around 8 orders of magnitude less than molecular systems. On the other hand, with the increase of hardware performance, simulations become faster, even though at a mild pace. As discussed in the introduction, this results in around one new accessible order of magnitude of relaxation time every 10 years. At this rate, simulations will be able to reach experimental studies in about a century. This also entails a new problem: by accessing lower temperature and longer relaxation times many historical model of glass-forming liquids, which have been considered very robust with respect to crystallization for a long time, are progressively experiencing ordering effect [70, 134, 135] and they must

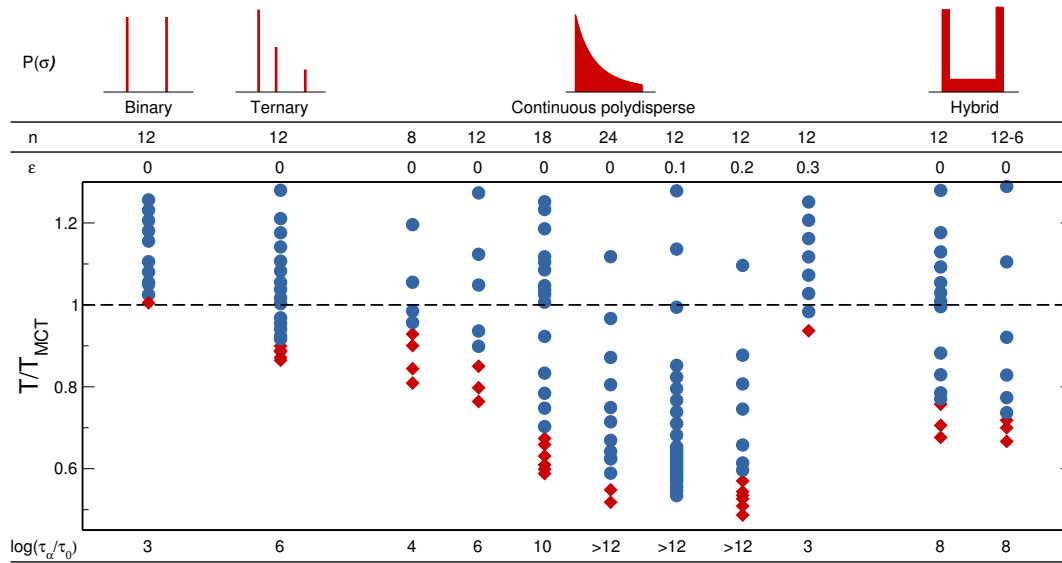


**Figure 3.1** – Summary of the results obtained for some models considered in this chapter. The top row is a sketch of the particle size distribution. The second and the third line specifies the pair potential and its additivity. In the main figure we use blue points to indicate equilibrium disorder fluid regime and red points to indicate instability towards crystalline or demixed states. The vertical axis report the temperature rescaled by the location of the mode-coupling crossover. The bottom line indicates the estimated range of equilibrium relaxation  $\tau_\alpha$  that can be studied in stable equilibrium condition for each model. Here  $\tau_0$  is the relaxation time at the onset temperature. Many of the implemented models can be equilibrated below  $T_{MCT}$  and some of allow to penetrate at temperatures below the experimental glass transition, conventionally defined as  $\tau_\alpha/\tau_0 = 10^{12}$ .

be replaced with more robust versions or new models.

In this chapter we tackle the two problems at once. First, to address the dynamical slowdown we employ a non local Monte Carlo algorithm [68, 69]. In the introduction we sketched many different approaches to bypass the huge increase of relaxation times: cluster algorithms, replica-exchange, population annealing, and the swap algorithm. We decide to employ the latter one encouraged by the strong claim of Ref. [80]. Our final aim is to bring Monte Carlo swap simulation to a new level by both carefully studying its dynamics and optimization and by testing its performances on numerous glass-forming liquids. At the same time, we carefully check for ordering effects by computing several different observables to exactly distinguish between a stable supercooled fluid and a system undergoing a change of phase and to understand which specific properties enhance glass-forming ability. We both study mixtures of different species and continuous polydisperse models. We vary polydispersity, softness and introduce non-additive interactions in order to understand which is the best combination of parameter that helps resolving the two puzzles by giving at the same time a considerable speed up in equilibration and remaining stable in the supercooled regime.

In Fig. 3.1 we quantified both the speed up as compared to standard simulations and the stability for some glass forming liquids under investigation. Blue points indicate

temperatures for which the system remains a fluid, whereas red diamonds correspond to temperatures where the system presents ordering during the simulations. The exact protocol as well as the methods employed to distinguish between the two conditions will be introduced later in this chapter. All temperatures are rescaled by  $T_{MCT}$  of the specific model. We observe that many systems can be equilibrated below  $T_{MCT}$ , some of them at extremely low values of the temperature. The last line of the figure reports an estimation of the accessible dynamical regime at which swap simulations can equilibrate in terms of orders of magnitude of relaxation times for each system. It can be seen that for some systems the accessible range is even larger than 12 orders of magnitude. This means that for some models we have been able to create *in silico* configurations in a regime never achieved before, which was exactly our aim: at the same time, we close the gap between experiments and simulations and we identify properties that suppress stability. We notice that swap Monte Carlo simulations do not provide information on the physical dynamics of the system. However, the statics is accessible now in a completely new regime. Moreover by using configurations prepared with swap dynamics as starting points for standard dynamics simulations, one can also investigate the short time equilibrium dynamics of glass-formers.

This chapter is organized as follows. In Sec. 3.2 we introduce all the characteristics of our models. Sec. 3.3 is dedicated to the methods and the physical observables employed. The details of the algorithm and its optimization are discussed respectively in Sec. 3.4 and 3.5. The following six sections report the results for the various models at test and for the physics behind the algorithm. First we perform new simulations of a well-studied binary mixture (Sec. 3.6.1) and ternary mixture (Sec. 3.6.2). Then we introduce continuous polydisperse models in Sec. 3.7: we discuss their phase behaviour (Sec. 3.7.1) and the results in the soft (Sec. 3.7.2) and in the hard sphere cases (Sec. 3.7.4). In Sec. 3.7.3 an estimation of the dynamical acceleration is given. Sec. 3.8 gives some physical insights on the dynamics during swap simulations. In Sec. 3.9 we introduce two models designed to be efficient in swap Monte Carlo simulations. The first combines properties of mixtures and continuous polydisperse models (Sec. 3.9.1). The second is an extension of a well known historical model, the Kob-Andersen Lennard Jones (Sec. 3.9.2). In Sec. 3.10 we study the implementation of our method in a two dimensional system.

## 3.2 Models

Performing computer simulations to investigate the physical nature of a system is a delicate matter when it comes to comparison with experimental results. Although there is a infinite amount of possibilities to design a computer simulation, on very general basis, two different guidelines can be followed, depending on the ultimate aim of the study. Either one wants to validate or falsify theoretical results or one wants to quantitatively predict experimental results. In this thesis we mostly concentrate on the first strategy, specifically we do not try to perform computations that have an exact

quantitative comparison with experiments. Instead, we set up and simulate models that have a glass-forming behaviour and then we compute physical quantities, inspired by mean field theories of the dynamical arrest. Our purpose is to find general properties of the behaviour of glass-forming liquids testing theories directly. At the same time we produce results comparable from a qualitative and roughly quantitative point of view with experiments.

In the following we introduce three main classes of systems and we justify some of our choices on the basis of experimental grounds. The three classes of systems can be distinguished by the form of their size dispersion. The first class is given by mixtures of species made of particles with different diameter. This is reminiscent of metallic glasses, that is, alloys of different metallic chemical components [136]. In recent years the study of glassy behaviour has also been achieved in colloids: systems made of suspensions, emulsions, foams and aerosol that are polydisperse in nature [9]. The colloidal glass transition has the big advantage that particles can be followed with single particle tracking in real space through microscopy techniques. The second class of systems that we introduce are made of particles continuously polydisperse and find an experimental equivalent of colloids. The third class of systems is a combination of the previous two, namely, it is made of systems having the structure of a mixture and presenting some degree of continuous polydispersity. These last have no direct experimental analog, at least up to now.

In case of mixtures of particles, the size dispersion can be written as

$$P(\sigma) = \sum_{\alpha} \gamma_{\alpha} \delta(\sigma - \sigma_{\alpha}), \quad (3.1)$$

where  $\alpha \in A, B, \dots, Z$  and  $\gamma_{\alpha}$  indicates the fractional composition of each species with a corresponding diameter  $\sigma_{\alpha}$ .

For continuous polydisperse systems the size dispersion scales as:

$$P(\sigma) = \frac{A}{\sigma^3}, \quad \text{with } \sigma \in [\sigma_{\min}, \sigma_{\max}]. \quad (3.2)$$

Here  $A$  is a normalizing constant,  $\sigma_{\min}$  and  $\sigma_{\max}$  are the minimum and the maximum values that the diameter can assume respectively. We employ this functional form because it ensures that the volume fraction occupied by particles with diameter in a interval  $\delta\sigma$  is similar. Recently, this scaling property was found to enhance glass-forming ability in discrete mixtures [137], however we do not systematically test this hypothesis for these continuously polydisperse systems. We avoid sample-to-sample fluctuations by assigning particle diameters with the following rule:

$$\sigma_i = \frac{\sigma_{\min}}{\sqrt{1 - \frac{1}{N} \left[ 1 - \left( \frac{\sigma_{\min}}{\sigma_{\max}} \right)^2 \right]}}, \quad \text{with } i \in (0, N) \quad (3.3)$$

for a  $N$  particles system.

The third class is made of systems that are a combination of the two previously introduced classes. In this case, the size dispersion can be written as:

$$P(\sigma) = \sum_{\alpha} \gamma_{\alpha} \theta(b_{\alpha} - |\sigma - \sigma_{\alpha}|). \quad (3.4)$$

Here  $\gamma_{\alpha}$  is as before and  $\theta(x)$  is a step function. Note that, in contrast to discrete mixtures, the presence of a step function gives a finite width  $b_{\alpha}$  of the diameter probability density associated to species  $\alpha$ .

The degree of polydispersity in all the systems employed is quantified by the normalized root mean square deviation of the diameter:

$$\delta = \frac{\sqrt{\langle \sigma^2 \rangle - \langle \sigma \rangle^2}}{\langle \sigma \rangle}. \quad (3.5)$$

We use  $\langle \sigma \rangle = \int P(\sigma) \sigma d\sigma$  as unit length everywhere, where the integral is over the value assumed by  $\sigma$ .

The two particle interaction potential of the majority of the systems we studied with swap simulations can be expressed via an inverse power law of the form:

$$v(r_{ij}) = \left( \frac{\sigma_{ij}}{r_{ij}} \right)^n + F(r_{ij}), \quad (3.6)$$

Where the coefficient  $n$  indicates the softness of the model and the function  $F(r_{ij})$  smooths the potential at a cut off distance  $r_c = r_{ij}/\sigma_{ij}$  beyond which the potential is set to zero. We employ this form to mimic soft interacting particles for which we are able to change the steepness of the interaction, namely the particle softness. Unless otherwise specified we use

$$F(r_{ij}) = c_0 + c_2 \left( \frac{r_{ij}}{\sigma_{ij}} \right)^2 + c_4 \left( \frac{r_{ij}}{\sigma_{ij}} \right)^4. \quad (3.7)$$

Where the coefficient  $c_0, c_2, c_4$  ensure the continuity of the potential up to the second derivative at the cut off distance  $r_c = r_{ij}/\sigma_{ij} = 1.25$ . This functional form is preferred since it allows easy minimization of the total potential in studies of landscape [16], vibrational modes [138, 80] and athermal shearing [139]. We also studied models with particles interacting through a Lennard Jones potential

$$v(r_{ij}) = 4\epsilon_{ij} \left[ \left( \frac{\sigma_{ij}}{r_{ij}} \right)^{12} - \left( \frac{\sigma_{ij}}{r_{ij}} \right)^6 \right] + c_{LJ}. \quad (3.8)$$

In this case, we cut off and shift the pair potential at the cutoff distance  $r_{cut} = 2.5\sigma_{ij}$  and  $\epsilon_{ij}$  represents the energy scale of interactions. We use this interaction in two cases. In the first model the size dispersion is given by Eq. (3.4). The second case represents an extension of the historical Kob-Andersen Lennard Jones mixture (See Ref. [48] and Ch. 2) to which we add some additional particles as explained below.

Finally, we also employ a hard sphere system presenting the usual two particle interaction

$$v(r_{ij}) \begin{cases} \infty & \text{if } r_{ij} \leq \sigma_{ij} \\ 0 & \text{if } r_{ij} > \sigma_{ij}. \end{cases} \quad (3.9)$$

Most of our systems present an interaction rule for the cross-diameter  $\sigma_{ij}$  given by

$$\sigma_{ij} = \frac{\sigma_i + \sigma_j}{2}(1 - \epsilon|\sigma_i - \sigma_j|). \quad (3.10)$$

Models characterized by  $\epsilon = 0$  are additive, whereas models using a  $\epsilon \neq 0$  are named non-additive. Besides, we introduce an extension of the historical Kob Andersen mixture where some particles are added to the original two component systems. These particles have both non-additivity in size and in energy which can be generally described by

$$\begin{aligned} x_{Ai} &= \omega_i x_{AA} + (1 - \omega_i) x_{AB} \\ x_{Bi} &= \omega_i x_{AB} + (1 - \omega_i) x_{BB} \\ x_{ij} &= \omega_{ij} x_{AA} + (1 - \omega_{ij}) x_{BB}. \end{aligned} \quad (3.11)$$

Here  $x_{ij} = \sigma_{ij}, \epsilon_{ij}$  indicate diameter and energy scale respectively,  $(A, B)$  are the species of the starting binary mixture,  $(i, j)$  are indices of the additional particles and  $\omega \in (0, 1)$ . Note that when  $\omega = 1$  we obtain an  $A$  particle, whereas for  $\omega = 0$  we regain a particle of the  $B$  species. These additional particles are introduced to enhance the efficiency of the swap Monte Carlo algorithm. The reason for this to work, the concentration of additional particles and the other details will be given in Sec. 3.9.2.

### 3.3 Methods

In this section we introduce the most frequently used physical observables and the methods in this chapter. Dealing with the supercooled regime we always want to carefully check the absence of crystalline local order in the system. As a very simple test we look at the radial distribution function [1]

$$g(r) = \sum_{i,j;i \neq j}^N \delta(r - |r_i - r_j|). \quad (3.12)$$

We recall that in an isotropic system the quantity  $\rho g(r) dr$  gives the density probability to find a particle in a spherical shell of thickness  $dr$  at a distance  $r$  from the origin, given the presence of a particle in the origin. We also monitor density fluctuations using the structure factor [1]

$$S(k) = \frac{1}{N} \langle \rho_k \rho_{-k} \rangle = \frac{1}{N} \left\langle \sum_i^N e^{-i\mathbf{k}\mathbf{r}_i} \sum_i^N e^{i\mathbf{k}\mathbf{r}_i} \right\rangle, \quad (3.13)$$

where the quantity  $\rho_k$  is the  $k$  component of the Fourier transform of the density of the system. Both for radial distributions and for structure factors one can define species-specific versions in which only particles in given species of the system are taken into account in the sum, i.e.  $g_{\alpha\beta}(r)$ ,  $S_{\alpha\beta}(r)$ . Here  $\alpha$  and  $\beta$  represent a species of the mixtures or a subset of particles in the continuously polydisperse systems. The behaviour of the structure factor gives information about density fluctuations at different wavelength  $\lambda = 2\pi/k$ . This means that the low  $k$  values give information about long wavelength fluctuations in the system. In a totally monodisperse system, this can be directly related to the system compressibility using Fluctuation-Dissipation relations [1]. In the multicomponent or polydisperse system, employed in this thesis, however one should invert a  $M \times M$  matrix, where  $M$  is the number of components [140]. We decided not to perform this further analysis and to simply focus on changes of the low  $k$  values with temperature. In supercooled liquids two point static correlation functions such as the radial distribution or the structure factor do not vary significantly with lowering the temperature [6]. The presence of crystalline or disordered states can be observed by detecting abrupt changes in this quantity as compared to the high temperature liquid phase. Particularly useful to this aim is the low- $k$  behaviour of the species-specific structure factor  $S_{\alpha\alpha}$  that gives information on phase separation or demixing, showing a pathological increase at low- $k$  when particles of the same species cluster together.

Another observable that detects crystalline order is the 6-fold bond-orientational order [104, 141]

$$Q_6 = \left\langle \frac{1}{N} \sum_{i=1}^N \sqrt{\frac{4\pi}{13} \sum_{m=-6}^6 \left| \frac{1}{N_b(i)} \sum_{j=1}^{N_b(i)} Y_{6m}(r_{ij}) \right|^2} \right\rangle, \quad (3.14)$$

where  $Y_{6m}(r_{ij})$  are spherical harmonics of degree  $n = 6$ . This observable measures the concentration of icosahedral order in the system, being one when all the particles belong to icosahedra and zero in the opposite case. The inner sum  $N_b(i)$  runs over the number of neighbours defined as particle closer than a cut-off value corresponding to the minimum of the rescaled radial-distribution function  $g(r_{ij}/\sigma_{ij})$ . Usually orientational correlators are computed using neighbours defined through Voronoi tessellation, however there is increasing evidence that the results remain unchanged if the neighbours are defined instead as particles within a distance less than a cut-off value corresponding to the first minimum of the radial distribution function [103]. Since we use polydisperse mixture both in the computation of this radial distribution and in the evaluation of the distances we always normalize by the two particle cross-diameter  $\sigma_{ij}$ . The two dimensional 6-fold bond orientational order can be analogously defined as [104, 141]

$$\psi_6 = \left\langle \frac{1}{N} \sum_{i=1}^N \frac{1}{N_b(i)} \sum_{j=1}^{N_b(i)} \left| \exp(i6\theta^{ij}) \right| \right\rangle. \quad (3.15)$$

Here  $\theta_m^i$  is the angle formed between particle  $m$  and  $i$ . This quantity measures the degree of orientational hexagonal order in the system, since local order in two dimensions is

usually hexagonal, and it is one for perfect triangular lattice [56]. In standard Monte-Carlo simulations we can monitor the self and collective dynamics by measuring particle displacements or time dependent density correlation functions [47]

$$F_s(k, t) = \langle f_s(k, t) \rangle = \left\langle \frac{1}{N} \sum_j e^{i\mathbf{k} \cdot [\mathbf{r}_j(t) - \mathbf{r}_j(0)]} \right\rangle. \quad (3.16)$$

Here we chose the wavenumber  $k$  as the value corresponding to the maximum of the total structure factor  $S(k)$ . The structural relaxation time can be defined as the time at which this function assume the value  $F_s(k, t) = e^{-1}$ . The same functional form can be also employed in swap simulations provided that one considers that the exchanges involve diameters of particles instead of their positions, such that a meaningful single particle dynamics is preserved. In mixtures and continuous polydisperse systems the dynamical properties may vary in a non trivial way depending on the diameter of the particles. In standard simulations one can divide the system into subsets and evaluate the dynamics for particles of different sizes. In swap simulations this is not possible, since particles change their sizes over time and consequently we always compute dynamical observables over all the particles in the system. Moreover we are forced to make the same choice for standard dynamics, since our final aim is to compare between the two dynamics.

We also compute collective relaxation of density degrees of freedom by using the time-dependent collective overlap function which has the form:

$$F_o(t) = \left\langle \frac{1}{N} \sum_{i,j} \theta(a - |\mathbf{r}_i(t) - \mathbf{r}_j(0)|) \right\rangle, \quad (3.17)$$

using a cutoff distance  $a = 0.3$  which is comparable with the size of the typical cage. This quantity gives similar information as the coherent intermediate scattering function at wavevector  $k = 2\pi/a$  [142], on the other hand it is computationally more advantageous since it presents much smaller statistical fluctuations. From this function, one can define a relaxation time  $\tau_o$  for the decorrelation of collective density fluctuations, at the time at which  $F_o(\tau_o) = e^{-1}$ .

Since we are interested in accelerating equilibration, we want to compare the standard dynamics and the swap dynamics. In order to do this we start from studying the dynamical arrest present in the standard dynamics using  $\alpha$ -relaxation. For each system we fit standard dynamics using an MCT like equation introduced in Eq. (1.9) form which we extract  $T_{MCT}$ . As discussed in Sec. 1.3.1 this temperature roughly coincides with the *in silico* dynamical arrest. We also employ three other functional forms. One is the famous Vogel-Fulcher-Talmann (VFT) law which has been extensively used in glass science [133]

$$\tau_\alpha \propto \exp\left(\frac{A}{T - T_0}\right), \quad (3.18)$$

here  $T_0$  is a fitting parameter and indicates the temperature of the divergence of relaxation times, in agreement with a Kauzmann scenario. This function, although widely employed to fit relaxation times, was questioned using experimental results in Ref. [143], where it was shown that other functional forms, not predicting a divergence of relaxation times at finite temperature are better estimator for dynamical data over the whole accessible experimental dynamical range. Another article questioning the VFT functional form was published in 2009 by Elmatad, Chandler and Garrahan [144]. They agree on the absence of a divergence of relaxation times at finite temperature and introduce a functional form to describe relaxation times with an increase proportional to an exponential of the inverse squared temperature

$$\tau_\alpha \propto \exp \left[ A' \left( \frac{1}{T} - \frac{1}{T_1} \right)^2 \right]. \quad (3.19)$$

here  $A'$  and  $T_1$  are fitting parameters that control respectively the speed and the location of the dynamical arrest. Finally, we also employ an Arrhenius law

$$\tau_\alpha \propto \exp \left( \frac{A''}{T} \right), \quad (3.20)$$

This typically describes relaxation times in a strong glass former [2]. Even though in this chapter we only deal with glass-forming liquids presenting a fragile behaviour we will employ this law, along with the others, to extrapolate relaxation times at lower temperatures, where the real dynamics cannot be followed up to the  $\alpha$ -relaxation time. The procedure will be better explained in Sec. 3.7.3. In general, in the following, we will refer to *dynamical gain* performing the following procedure: first we fit the standard dynamics with the parabolic law (Eq. 3.19). Then we plug in this equation the lowest temperature  $T^*$  at which swap simulation are able to equilibrate. Doing so we are able to estimate the corresponding relaxation times of standard simulations  $\tau_\alpha(T^*)$ . The dynamical gain is the number of orders of magnitude gained performing swap simulations as compared to standard simulations:

$$\text{dynamical gain} = \log_{10} \frac{\tau_\alpha^{\text{standard}}(T^*)}{\tau_\alpha^{\text{standard}}(T_{\text{MCT}})}. \quad (3.21)$$

We also define the *speed up* as the number of order of magnitude gained in equilibration at the kinetic slowing down in simulations:

$$\text{speed up} = \log_{10} \frac{\tau_\alpha^{\text{standard}}(T_{\text{MCT}})}{\tau_\alpha^{\text{swap}}(T_{\text{MCT}})}. \quad (3.22)$$

## 3.4 Equilibrium fluid

Equilibrium is a necessary condition to ensure a correct sampling in a Monte Carlo simulation [52]. Therefore this section will be dedicated to the introduction of the

simulation method and to all the criteria we followed to guarantee that the system is truly at equilibrium. Let us start by introducing the algorithm and deal with its optimization. Our simulations are based on Metropolis Monte Carlo [46, 44]. The time evolution consists in considering a configuration  $C$  at step  $t$  and attempt to generate a new configuration  $C'$  at step  $t + \Delta t$ . The probability for the new configuration to be accepted is given by a Metropolis acceptance rule

$$p(C \rightarrow C') = \min\{1, \exp[\beta(E_{C'} - E_C)]\}, \quad (3.23)$$

where  $E_{C'}$ ,  $E_C$  are the total potential energy of the system in configurations  $C'$ ,  $C$ . This algorithm respects detailed balance and from a mathematical point of view it is a Markov chain that, once stationarity has been reached, gives the correct sampling of the Gibbs distribution [52]. Any rule to generate the new configuration is theoretically accepted and in general Metropolis Monte Carlo methods are widely employed to study statistical properties of systems presenting rough free energy landscapes and they can efficiently sample distributions and find critical points.

In the last 10 years, Metropolis Monte Carlo was also used to obtain dynamical quantities in supercooled liquids after the technique was first employed in Ref [47]. The technique consists in using what we call *standard* Monte Carlo dynamics, a well known simulation technique [44], in which the rule to create the new configuration consists in randomly choosing a particle in the system and performing a displacement of  $\Delta r$ . The direction and the length are chosen at random: the first on the entire solid angle and the second in an interval between 0 and  $\Delta r_{max}$ . If this last value is too large, large jumps are attempted and the new configurations are very rarely accepted. If it is too small moves are almost always accepted but the timescale of the simulations increases uselessly. In our work, we always set a  $\Delta r_{MAX}$  which corresponds to acceptance rates of the order of 30 – 50%. Unless otherwise indicated, we will work in the canonical ensemble such that the number of particle  $N$ , the volume  $V$  and the temperature  $T$  are fixed. Even though from a strict theoretical point of view a Monte Carlo dynamics cannot be related to a physical dynamics, there are computational evidences [47] that the Monte Carlo dynamics presents the same relaxation behaviour as Stochastic and Brownian dynamics, where with Stochastic dynamics we mean a dynamics in which a friction term and a random noise are added to the Newton's equations of motion and with Brownian dynamics we mean that the evolution of the particle position is described using a Langevin equation. Moreover, as far as supercooled liquids are concerned, even though the vibrational behaviour on short timescales differs, all the dynamics mentioned so far have comparable long timescales behaviour and the same form for  $\alpha$ -relaxation as Newtonian dynamics.

On top of these standard moves, during the simulation we introduce some additional moves consisting in taking two particles at random and trying to exchange their diameters based on the same Metropolis acceptance method of Eq. (3.23). This means that the method directly inherits all the properties of the standard Monte Carlo method, that is,

it is able to reconstruct the Gibbs distribution at equilibrium. We refer to this dynamics presenting both standard displacements and diameter exchanges as *swap* Monte Carlo dynamics.

What is exactly equilibrium in a simulation of supercooled liquids? One could see that using time correlation in the system: imagine to introduce a general two time correlation function  $C(t, t')$ , which depends implicitly on the two time  $t$  and  $t'$  and on the state point of the system at two different times  $\mathbf{r}(t)$  and  $\mathbf{r}(t')$ , then the following condition is necessary and sufficient for stationarity:

$$C(t, t') = C(|t - t'|). \quad (3.24)$$

This means that correlation function depend only on the absolute value of difference of time and not on the single time values. In others words, this tells us that the system does not present aging. Once we are sure that the system is at equilibrium by computing correlation functions we can prepare a set of configuration sampling the Boltzmann distribution with the final aim to compute averages of mechanical statistical quantities.

Now, the second question that could be asked is: how many configurations do we need and how do we choose them? The first part of the question is easy to answer, one can estimate statistical error from fundamental statistics such as standard deviations or using well known techniques for computational studies as Jackknife or Bootstrap methods, depending on the observable at test [145]. The second part of the question is subtle. The answer being that there is not a unique solution and the right choices must be evaluated from case to case. For instance in order to observe logarithmic decays, one should store configurations logarithmically in time. On the other hand if only static properties are at test one could just employ a set of independent configurations. Overall the only essential piece of information which one has to be able to retrieve is to distinguish between configurations that are statistically independent or not. Defining independency in swap simulations is a tricky point. If we exchange two particles far enough and we exchange their position, the new configuration will be statistically independent on the starting one or not? We firmly believe that this is not always the case for reasons that have mainly to do with the roughness of the free energy in a glassy system.

Let us take two different configurations  $\{\mathbf{r}(t)\}$ ,  $\{\mathbf{r}'(t)\}$ . Even though the particle positions are not the same, it has been understood [38, 146] that they could belong to the same free energy basin and consequently to the same thermodynamic state if they are not different *enough*. This could be for instance the case of continuously polydisperse systems in which only the diameter of two particles with similar sizes has been exchanged, as clarified in Ref [146]. For these reasons, in order to define statistically independent configurations, we rely on density decorrelations. As said before, if we think of a swap move as an exchange of two particle diameters and not as an exchange of position, we are able to follow the single particle dynamics. We can compute the self-intermediate scattering function of Eq. 3.16 and define a  $\tau_\alpha$  relaxation time for swap simulations. We use the  $\alpha$ -relaxation time as the time period to create a configuration statistical

independent from the starting one. We notice here that the swap dynamics has no physical equivalent and consequently we mainly use dynamical observables in a totally technical way.

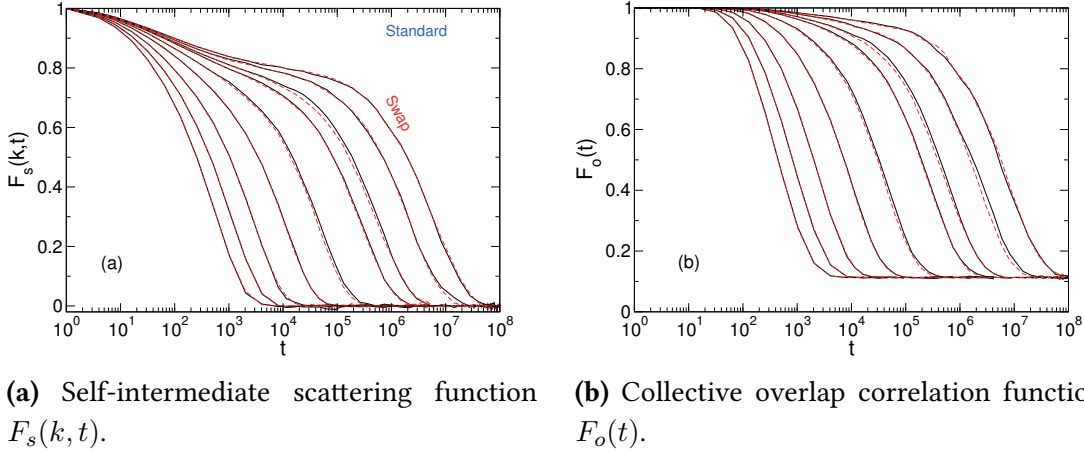


**Figure 3.2** – Results for swap dynamics computed respectively on the first (full black line) and the second (dashed red line) half of the simulation run. In both panels temperatures are  $T = 0.25, 0.175, 0.0.125, 0.092, 0.075, 0.065, 0.062, 0.058, 0.0555$ . Results for standard dynamics at the lowest temperature are shown with a blue dotted line. The system is studied in Sec. 3.7.2 and is made of non-additive soft repulsive particles with  $\epsilon = 0.2$ .

At the basis of our equilibration techniques we use long time relaxations in particle dynamics. We illustrate this point in Fig. 3.2. First we computed the self-intermediate scattering function during swap simulations over the first half and the second half of the simulation. This are shown in Fig. 3.2a respectively with black continuous curves and red dotted curves. As one could observe there is no mismatch between the two measurements beyond the statistical error and the two families of curves decorrelate to zero. This is showing clearly that there is no aging in the system and the equilibrium condition holds strongly. In the same plot we also show with a blue dotted line the same quantity computed on a standard simulation performed by starting from a configuration equilibrated with swap dynamics at the lowest accessible temperature. In this case the curve attains a plateau value and it does not relax to zero in standard simulation timescales. This means that this dynamics can only explore vibrations in the system and the temperature is so low that the system remains confined in visiting the same potential energy basin. Fig. 3.2b shows a similar analysis. Here we plot the overlap function (see Eq. (3.17)). Also in this case we observe the absence of aging in the system and the quantities computed in the first half and in the second half of the simulation decorrelate together to the same value for long times. This value depends on the system density and it is equal to  $\rho V_0$  where  $V_0 = 4/3\pi a^3$  is the spherical volume over which the overlap is computed. This result ensures that all the centers of mass of the particles decorrelate with respect to their initial positions. Moreover we also compute correlation functions for standard dynamics using as starting point both a configurations obtained

using only standard simulations and a configuration equilibrated with swap simulations at the same temperature. The results (not shown) perfectly match, confirming that swap simulations are trustfully reproducing the Boltzmann distribution. As further checks we also monitored the instantaneous value  $e(t)$  and the average value  $\langle e \rangle$  of the potential energy in order to detect the absence of aging in time and the departure from the equation of state, evaluated with standard simulations. However we will later see how the potential energy could be a misleading observable to look at in swap simulations.

### 3.5 Optimizing the algorithm

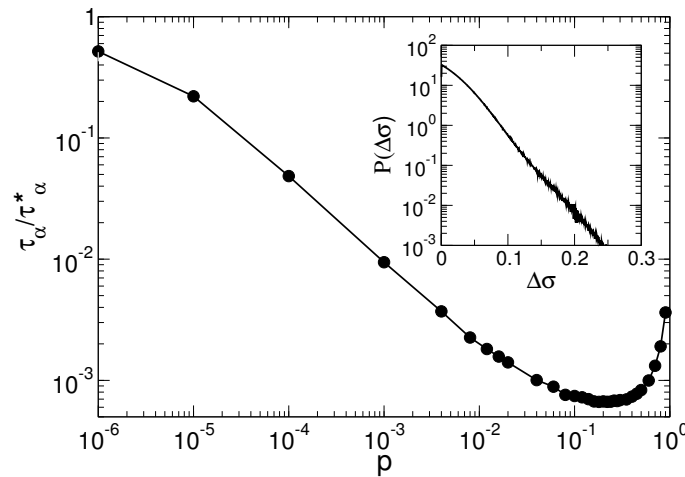


**Figure 3.3** – The relaxation time  $\tau_\alpha$  as a function of the swap attempt probability  $p$ , normalized by  $\tau_\alpha^*$ , its value for standard Monte Carlo simulations when  $p = 0$ . A broad minimum is present around  $p \approx 0.2$  indicating that this value optimizes the efficiency of the swap algorithm. The inset shows the probability distribution of the swap acceptance as a function of the diameter difference  $\Delta\sigma = |\sigma_1 - \sigma_2|$  between the particles for which the swap move is attempted. The system is studied in Sec. 3.7.2 and is made of non-additive soft repulsive particles with  $\epsilon = 0.2$ .

There are two possible optimizations of swap moves. First, one can adjust the probability  $p$  that a Monte Carlo move is a swap attempt to maximize the speed up. The complementary  $1 - p$  indicates the probability that a move is a standard displacement attempt. The optimal value of  $p$  can be found by performing standard simulations at one of the lowest temperatures where it is possible to equilibrate and measure the relaxation times and then switch on swap moves progressively, performing independent simulations at different values of  $p$ . In Fig. 3.3 we show the value of the relaxation time  $\tau_\alpha$  divided by the relaxation time of the standard simulations as a function of  $p$ . This figure shows that even for small  $p$  the relaxation time has a huge drop (axes are in logarithmic scale) and it reaches a minimum for values of  $p \approx 0.2$ . This minimum is broad enough to assume that this optimization holds also at different (and lower) temperatures. Another optimization that can be performed deals with particle diameters. As anticipated, we simulate both

mixtures and systems that are continuously polydisperse, namely characterized by a size dispersion described by a continuous function. Naively, one could expect that trying to exchange the position of two particles can be energetically very unfavourable if the particles have very different sizes. If we imagine a swap move as one particle that swells in one place and at the same time a particle that deflates independently elsewhere, we end up in a totally *local* description. This means that, locally, a particle will easily deflate while, on the contrary, the swelling could be very expensive energetically. This is what causes swap Monte Carlo moves between particles with a very different sizes to be almost never accepted. This hand-waving argument can be quantified by measuring the number of accepted swaps as a function of particle diameter difference  $\Delta\sigma$ . As one observes in the inset of Fig. 3.3, the acceptance decreases considerably as a function of  $\Delta\sigma$  and consequently we decide not to try swaps between particles having diameters that differ more than a cut-off value of  $\Delta\sigma_{MAX} = 0.2$  (this value being somehow arbitrarily chosen). The case of mixtures is easier. There, we do allow swap attempts only between species that have contiguous values of the diameter. The complete MC sweep in a system of  $N$  particles in pseudo code is the following:

```

1) extract a random number  $r_1 \in [0, 1]$ 
2) if  $r_1 > p$ 
    attempt a standard MC displacement
  else if  $r_1 < p$ 
    draw  $r_2, r_3 \in [0, N]$  while  $|\sigma_{r_2} - \sigma_{r_3}| < \Delta\sigma_{MAX}$ 
    attempt a swap between particles  $r_2$  and  $r_3$ 
3) repeat  $N$  times from 1).

```

Here, one has to be careful with two details. The first is that we extract  $r_2$  and  $r_3$  and if their diameters do not respect the cut-off condition we extract both of them again. This is done so that the configuration is not counted twice in the sampling of the Boltzmann distribution and the cut-off condition on the diameter difference does not explicitly enter the Metropolis acceptance rule. Moreover we extract again both of them. This is done so that any particle will have the same probability to be selected for a swap attempt and detailed balance condition is respected.

For all the models reported in Fig 3.1, we have studied crystallization and ordering extensively, using always the same protocol. We perform five independent simulations running for at least  $200\tau_\alpha$  at each different temperatures. If at least one of these simulations presented instability, we classify the system as a bad glass-forming liquid at that temperature. For the remaining systems we mainly equilibrated the system and explore equilibrium in simulations lasting for hundreds of relaxation times, although we have not carried out a strict protocol for each temperature. Overall our simulations are even longer than what is strictly necessary to produce equilibrium configurations. Anyway we think that computer simulations of supercooled liquids must respect stringent rules of equilibration and persistence in the metastable state before anything can be said about their physical properties.

## 3.6 Mixtures

### 3.6.1 Binary mixture

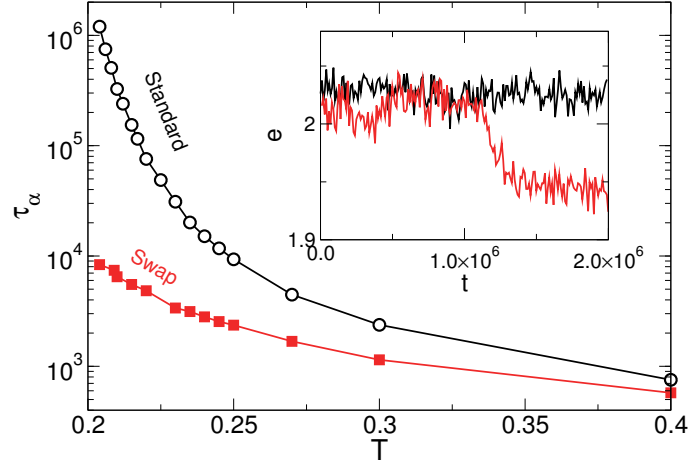


**Figure 3.4** – Relaxation times  $\tau_\alpha$  of standard (black empty points) and swap (red full squares) simulations for the binary mixture of soft repulsive spheres. The speedup given by swap simulations in equilibrating is obvious, but the system is unstable towards crystallization at  $T = 0.202$ . Temperature below Mode Coupling temperature  $T_{MCT} = 0.199$  cannot be studied. The inset shows a time series of the potential energy for standard (black) and swap (red) simulations at  $T = 0.2$ . Crystallization is easily observed when swap moves are introduced.

The aim of this section is to revise and reassess some previous literature results on swap simulations. This has both an pedagogical aim and it will also give new results to be compared to the previous literature findings. The first system we study is the historical 50:50 binary mixture of soft particles interacting via an inverse power law. The two particle interaction is defined by Eq (3.6) and (3.10), with  $\epsilon = 0$  and  $F(r_{ij}) = c_{\alpha\beta}$  where  $\alpha, \beta = A, B$  are species indices. The size ratio is  $\sigma_A/\sigma_B = 1.2$  and the polydispersity is  $\delta = 9.1\%$ . We perform simulation of  $N = 1024$  at density  $\rho = 1$ . This system was employed in many articles using swap simulations [69, 70, 71, 75, 147, 76]. First it was claimed that swap simulations could equilibrate the system below  $T_{MCT}$  and that it showed a peak in the constant volume specific heat indicating the presence of a Kauzmann transition [69]. Two years later, the Reichman group repeated the simulations [70], discovering that the system crystallizes using swap simulations already for moderately low temperatures. This allowed to reinterpret the findings of the previous paper and also it indicates that in using this system one has to beware of ordering and indeed sometimes a particular attention to crystallization was used [76]. Here we perform swap simulations of the system again. We found the acceptance of swap moves to be around  $a \sim 10^{-2}$ , as was previously found in literature. We confirm that the system presents crystallization and this is indicated both by a drop in the potential energy time series and by bond-orientational order analysis. Moreover, because of crystallization, the lowest

temperature at which the system can be equilibrated is around  $T_{MCT}$  and the system presents ordering already in standard simulations. Fig. 3.4 shows  $\alpha$ -relaxation times for standard simulations in black and swap simulations in red. The speed up (Eq. 3.22) reaches a maximum of two orders of magnitude at the lowest temperature and it increases lowering the temperature, contrary to old simulations where it was claimed a constant gain of a factor 180 [75]. We fit relaxation times of standard simulation to Eq. (1.9) to extract  $T_{MCT} \approx 0.199$ . There was an old and higher estimation of this value relying on the Van-Hove self correlation function  $T_{MCT} \approx 0.226$  [99]. We believe that our fitting of dynamical data gives a better estimation of this value. Overall swap simulations for this system do not give a huge improvement since crystallization intervenes at a rather high temperature and the Mode Coupling crossover cannot be crossed.

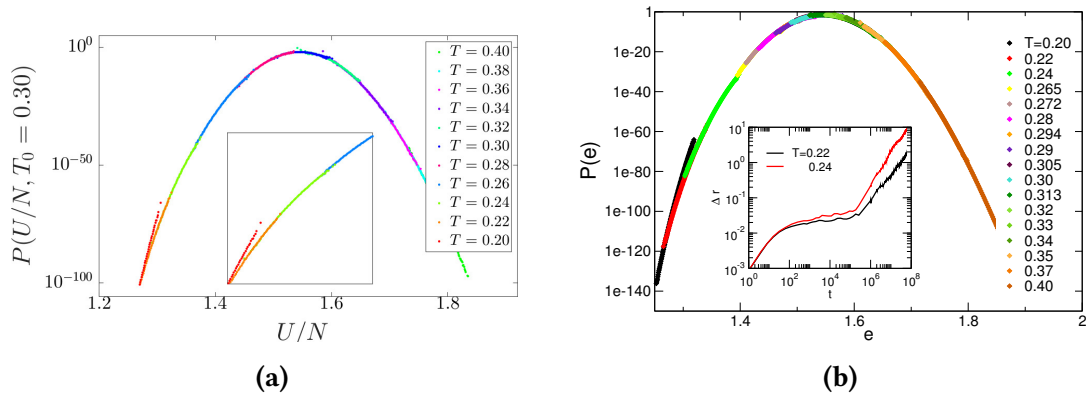


**Figure 3.5** – Potential energy distribution  $P(U/N, T_0 = 0.30)$ . The curve is obtained by histogram reweighting of the data for  $T=0.20, \dots, 0.40$  as shown in the legend. (a) is taken from Ref. [80] for a system of  $N = 1474$  particles. The inset shows a zoom on low temperature values. (b) the equivalent results obtained in our simulations. Here the system has  $N = 1500$  particles. The temperature range is the same as in previous literature and the agreement to the Boltzmann distribution seems to hold down to  $T \geq 0.20$ . The inset shows the mean squared displacement  $\Delta r$  for  $T = 0.22, 0.24$  where it can be observed that particles have globally travel of distance  $\sim 10$  for  $T = 0.24$  and  $\sim 2$  for  $T = 0.22$  respectively. This values are small for a correct exploration of equilibrium.

### 3.6.2 Ternary mixture

The second literature model under investigation was recently introduced by the Procaccia group [80]. This is a ternary mixture of soft particles interacting via potential of Eq. (3.6) and (3.10), where  $n = 12$ ,  $\epsilon = 0$ . and  $F(r_{ij})$  is defined by Eq. (3.7). Following Ref. [80] we perform simulations of  $N = 1500$  particles at a density  $\rho = 1.1$ . The size ratio between species is  $\frac{\sigma_A}{\sigma_B} = \frac{\sigma_B}{\sigma_C} = 1.25$  and the size dispersion is described by Eq. (3.1) where the fractional compositions are  $x_A = 0.15$ ,  $x_B = 0.30$  and  $x_C = 0.55$  respectively for species  $A, B, C$ , this results in a polydispersity of  $\delta \approx 17\%$  and in the fact that each species occupies roughly the same volume. For this system we attempt swap moves only

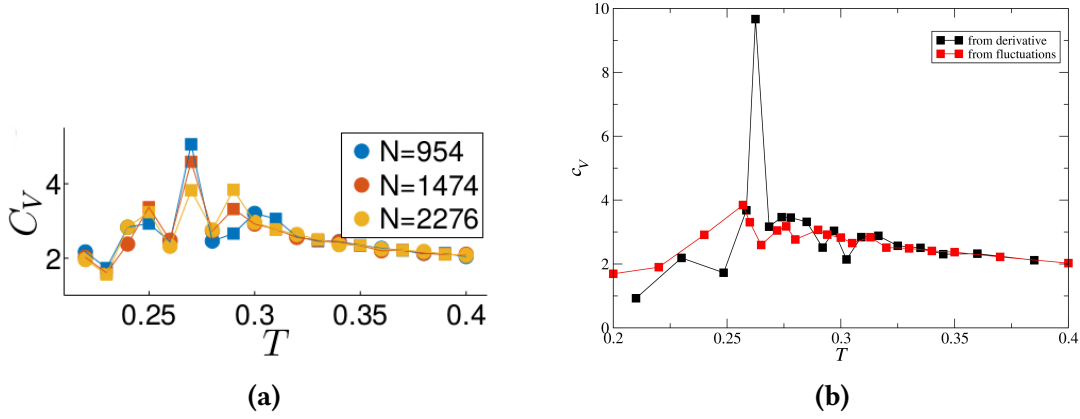


**Figure 3.6** – Specific heat of swap simulations computed both using derivatives  $c_V = \partial\langle U \rangle / \partial T$  (squares) and standard deviations  $c_V = (\langle U^2 \rangle - \langle U \rangle^2) / kT^2$  (circles) of the potential energy. (a) results are reproduced from Ref. [80]. (b) equivalent results obtained in our simulations. The peak in our case is more evident and coincide with phase separation in the system.

for particles in contiguous species and we found an acceptance of  $a \sim 10^{-5}$ , which is consistent with previous literature results. The acceptance is lower than in the binary system, due to the higher size ratio. We repeated the simulations of the previous paper adding more state points.

The first issue we concentrate on is equilibration. In Ref. [80] it was claimed that equilibration was achieved at extremely low temperatures as compared to  $T_{MCT} = 0.28$  showing two tests. The first test is a histogram reweighting [145] to collapse the probability distribution of the potential energy  $P(U, T)$  for different temperatures on the probability distribution at a high temperature  $T_0 = 0.30$  following [60]:

$$P_{T_0}(U, T) = \frac{P(U, T) \exp \left[ \left( \frac{1}{T} - \frac{1}{T_0} \right) U \right]}{\int dU' P(U', T) \exp \left[ \left( \frac{1}{T} - \frac{1}{T_0} \right) U' \right]}. \quad (3.25)$$

Here  $T_0$  has not to be confused with the onset temperature and  $U$  indicates the total potential energy. The result is shown in Fig. 3.5a. As one sees, apart from data computed at  $T = 0.20$ , all the other data lie on a Boltzmann shaped distribution. The authors claimed that they were able to equilibrate at  $T = 0.22$  and that only the lowest temperature is out of equilibrium. As a further proof of equilibrium they plot the specific heat computed from derivatives ( $c_V = \partial\langle U \rangle / \partial T$ ) and from standard deviation of the potential energy ( $c_V = (\langle U^2 \rangle - \langle U \rangle^2) / kT^2$ ). These estimations coincide when the system is at equilibrium. The result is shown in Fig. 3.6a. The two sets of values coincide down to  $T = 0.30$ , then deviations are present and one also can observe a peak at  $T = 0.26$ .

We repeat the two equilibration tests and the results are shown in Figs. 3.5b and 3.6b. Regarding the potential energy histogram reweighting we were able to obtain the canonical distribution as in the literature. However for temperatures  $T \leq 0.24$  we use, on purpose, simulations runs short enough that particles have barely moved. This is shown in

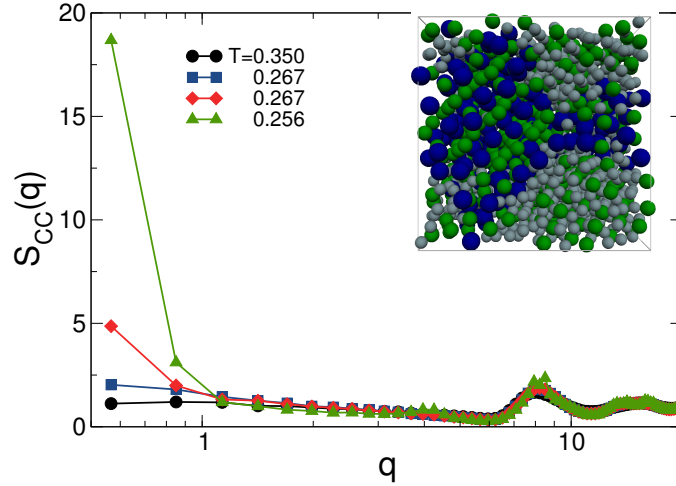


**Figure 3.7** – Partial structure factor  $S_{CC}(q)$  for small particles in the ternary mixture. It is featureless at high enough temperatures,  $T = 0.350$ , displays strong composition fluctuations at low  $q$  in the fluid at  $T = 0.267$ , that may eventually lead to a demixed state at long times. For  $T \leq 0.26$ , the system is demixed, as shown for  $T = 0.256$ . The inset shows a representative snapshot of a demixed and partially crystallized system at  $T = 0.256$ .

the inset of Fig. 3.5b where the mean squared displacement is reported for  $T = 0.22, 0.24$ . We believe that this histogram reweighting technique is a poor test of equilibration due to the extremely wide scale on the  $y$ -axis, where are reported more than 100 orders of magnitude. This easily hides defects of the shape of the distribution, which are only evident for  $T = 0.20$ . The second test concerns the specific heat, in this case, repeating the analysis of Ref. [80] we found similar results. The consistency seems to hold down to  $T = 0.30$ , then some fluctuations are presents which become bigger lowering the temperature and also we found a bigger peak at  $T = 0.26$ . Also in this case we believe that the test is not strong enough to certify that equilibrium is properly explored and clear results for  $T < 0.30$  are difficult to obtain unless one performs very long simulations and achieves very high statistics. Moreover there is another danger in the system which comes from ordering. Indeed we will show that the presence of a peak in the specific heat for  $T = 0.26$  is due to strong compositional fluctuations in the system.

Let us first concentrate on this last point and later discuss equilibration in the system. In our simulations of this model we experienced that the monitoring of energy and specific heat is not enough to detect ordering. To this aim, one of the best observables is the species-specific structure factor  $S_{\alpha\alpha}$  defined in Sec. 3.3. We report the results for the species C of the smallest particles in Fig.3.7. This figure shows that at high temperature the shape is the standard one for a liquid, with oscillations that account for density fluctuations at finite wevelength and a fixed and non vanishing low- $q$ . At a lower temperature ( $T = 0.267 \leq T_{MCT}$ ) this low- $q$  value remains small in short simulations, whereas it increases at longer times. Finally at very low temperature it assumes large values clearly indicating the presence of huge compositional fluctuations

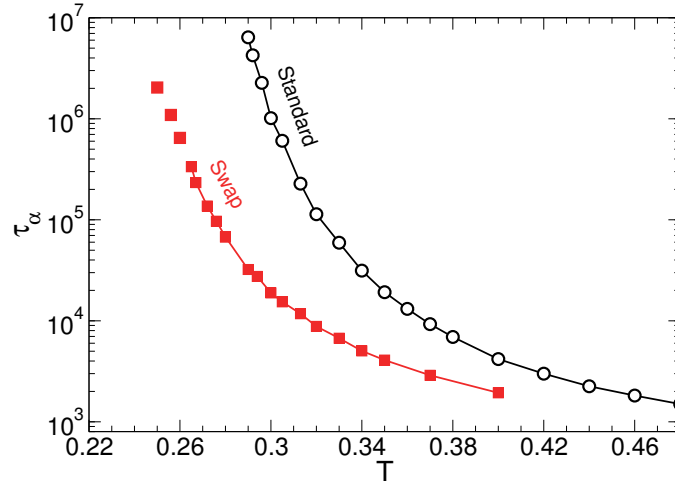


**Figure 3.8** – Relaxation times  $\tau_\alpha$  of standard (black empty points) and swap (red full squares) simulations for the ternary mixture of soft repulsive spheres. The speedup offered by the swap moves is obvious, but the system is unstable below  $T = 0.26 \approx 0.9T_{MCT}$  where it demixes and crystallizes. Disconnected squares are a rough estimate of  $\tau_\alpha$  obtained using short simulations in the unstable region. Stable and equilibrated states can be accessed down to  $T \approx 0.26 < T_{MCT} = 0.288$ , extending the dynamic range by about 2 orders of magnitude as compared to standard simulations.

in the system. This has also been confirmed by the observation of some screenshots where both demixing and crystallization can be observed by eyes (see inset of Fig. 3.7).

Beware of ordering effects, we can now evaluate the acceleration given by swap simulations. We do this as previously using  $\alpha$ -relaxation times. We report  $\tau_\alpha$  as a function of temperature for standard and swap simulations in Fig. 3.8. Despite the low acceptance rate, we notice that the acceleration given by swap simulations can be remarkable. At the lowest temperature at which we perform standard relaxation  $T = 0.29$ , the relaxation time is reduced of more than two orders of magnitude. We found that the lowest temperature for which the system is firmly an equilibrium fluid is  $T = 0.267$ . Beyond this point we were able to measure relaxation times (disconnected red points) by performing simulations shorter than  $200\tau_\alpha$ . Extrapolating the relaxation times for swap simulations, one finds that  $\tau_\alpha$  becomes too large at  $T \leq 0.24$  to be accurately measured and in our simulations at  $T = 0.22$ , lasting more than  $10^8$  Monte Carlo steps particles barely moved. In view of this result we believe that previous claims were too optimistic about the equilibration range. In Ref. [80] based on dynamical scaling arguments the authors quantified the relaxation time at  $T = 0.22$  of the order of  $\tau_\alpha/\tau_o = 10^{15}$  where  $\tau_o$  is the value of the relaxation time at the onset temperature  $T_o$ . They quantify the additional equilibration range corresponding to a dynamical gain of around 10 orders of magnitude beyond  $T_{MCT}$ . We performed this analysis again and we found that the lowest stable temperature  $T = 0.267$  correspond to a dynamical gain of two orders of magnitude. Overall this system represents a progress compared to the binary mixture, since it can be equilibrated easily below  $T_{MCT}$ . However it presents

serious issues concerning ordering and the actual accessible temperature regime. For this reason we decided to introduce new classes of models that can improve the swap performance.

### 3.6.3 Pentary mixtures

The main message of the previous subsections is that efficiency of swap simulations strongly depend on the glass-former under investigation. We already saw that the introduction of a third species increases the swap performances allowing equilibration below  $T_{MCT}$ . To push this idea even further, we introduce two different five-component mixtures. We adjust the concentrations such that each species occupy roughly the same volume and we choose a size ratio small enough to enhance swap acceptance. The first system has diameters linearly spaced between  $\sigma_{min} = 0.847$  and  $\sigma_{max} = 1.333$  for a polydispersity  $\delta = 16\%$ , the second between  $\sigma_{min} = 0.826$  and  $\sigma_{max} = 1.771$  for a polydispersity  $\delta = 23\%$ . Interaction potential is the same as the ternary mixture one. Swap Monte Carlo acceptance in these models increases considerably in comparison to the previously studied binary and ternary mixture to values around  $a \approx 10 - 20\%$  depending on the temperature. The main drawback of these models is the presence of phase separation, which prevents equilibration below  $T_{MCT}$ . Clearly these two attempts do not exhaust all the possible multi-component models that could be designed and a more careful exploration of the parameter space would be needed.

## 3.7 Continuously polydisperse systems

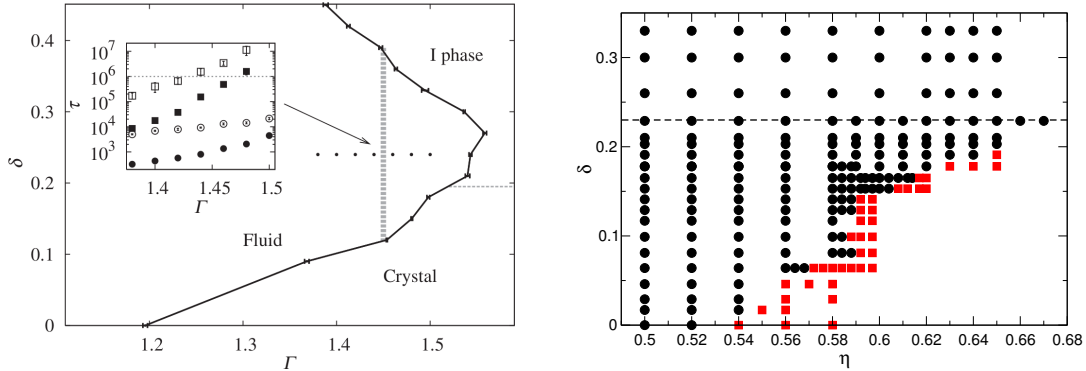
### 3.7.1 Phase behaviour

To maximize the dynamical gain of swap Monte Carlo simulations, we consider systems having a continuous polydispersity, that is, the diameter of the particles continuously interpolate between a lower and a higher bound.

We have been inspired by the work done in Ref [79], where particles with continuous polydispersity were simulated using swap Monte Carlo dynamics. In that case, the aim of the authors was to compute the phase diagram of a system presenting a flat size-dispersion using the enhanced exploration of the energy landscape enhanced by swap simulations. In the model of Ref. [79] particles interact via an inverse power law potential with exponent  $n = 12$  and the phase diagram was computed as a function of the control parameter  $\Gamma = \rho T^{-1/4}$  and polydispersity  $\delta$ . We recall that, in systems of soft-spheres,  $\Gamma$  is the only independent thermodynamic parameter [1] and  $\delta$  is the polydispersity defined as in Eq. 3.5.  $\Gamma$  is the also the only control parameter that drives the glass transition. The literature result is reproduced in Fig. 3.9a, taken from Ref. [79]. The authors identified three different regimes. The fluid regime, the crystal and the  $I$ -phase. At low polydispersity,  $0 \leq \delta \leq 0.2$ , the system is either a liquid, at low  $\Gamma$ , or a

single crystal, at high  $\Gamma$ . Increasing the polydispersity the system can attain a regime that the authors called *I*-phase, characterized by large density fluctuations. This corresponds to an ordered phase where particles with similar sizes phase separate and later crystallize. This effect in polydisperse soft-spheres, is known as fractionation and was widely studied by the Sollich group [148, 149, 150], by means of *semi-grand canonical* simulations and perturbative expansion theory.

Our main aim here is to reassess the validity of the phase diagram discussed before and to understand its relevance beyond the model simulated in Ref. [79]. We perform simulations of particles interacting via the two particle potential of Eqs. (3.6) and (3.10) where  $n = 36$ ,  $\epsilon = 0$  and  $F(ij)$  is set to a constant. The size dispersion is described by Eq. 3.2. We test many different realizations of the system varying the polydispersity in the interval  $\delta \in (0, 0.33)$ . This model presents two differences compared to the one simulated in Ref. [79]. First, in that case, the interaction parameter was softer ( $n = 12$ ). Moreover the size dispersion was flat, whereas in this case we opted for a size dispersion that goes as the inverse of the volume of the particle, chosen in order to enhance glass-forming ability [137]. In our system, since the interaction is very steep, the particle interpenetration at low temperature/high density is small and therefore we can define a packing fraction through the equation  $\phi = \frac{\pi}{6L} \langle \sigma^3 \rangle$ . We report the phase diagram as a function of density and polydispersity in Fig. 3.9b where, with black circles, we indicate state points at which the system remains a stable fluid during simulations and with red squares state point at which it present ordering. All simulations last for  $t \sim 10^7$  MC steps.



(a) Phase diagram of polydisperse soft-spheres obtained with swap simulations taken from Ref. [79]. The softness parameter is  $n = 12$ . On  $x$ -axis the thermodynamic parameter  $\Gamma = \rho T^{-1/4}$ . On the  $y$ -axis the particle polydispersity  $\delta$ . Authors identified three phases: a high temperature fluid, a crystal, and a inhomogeneous solid I. The vertical line in the fluid phase represent the kinetic glass transition.

(b) Phase diagram of polydisperse soft-sphere in our swap simulations. The softness parameter is  $n = 36$  which makes the system close to a hard sphere system. On the  $x$ -axis we plot the packing fraction and on the  $y$ -axis the polydispersity. Black circles indicate stable fluid phase and red squares indicate presence of order and long-range density fluctuations.

Even though the two systems have different softness exponents and different shapes of the size dispersion, their phase diagram look similar. They both show increasing resistance to ordering by increasing polydispersity and the literature result also presents a reentrant behaviour for polydispersity  $\delta \geq 0.3$ , where the fractionated phase can be reached for smaller values of  $\Gamma$ .

We note in passing that the two phase diagrams have been derived with very different purposes. In our case, we want to simulate supercooled liquids and we would like to enhance sampling of the metastable state and at the same time to suppress ordering effect. In Ref. [79], instead, swap simulations were intentionally used to faster explore the phase diagram and induce thermodynamic transitions. Thanks to this promising preliminary study, we were able to start studying continuous polydisperse models in depth. In the following we set  $\delta = 23\%$  for every system realization, given that lower and higher value imply easier demixing or fractionation.

### 3.7.2 Additive and Non additive soft spheres

In this section we study two classes of polydisperse systems of soft spheres, characterized by the value of the non-additivity parameter  $\epsilon$  in the interaction rule for the cross-diameter (Eq.(3.10)). The main aim is to explore the space of parameters in order to find the best combination that improves resistance to ordering in the system. The size dispersion is described in Eq. (3.2) with  $\sigma_{max}/\sigma_{min} = 2.219$  giving a polydispersity of  $\delta \approx 23\%$ . Particles interact through Eqs. (3.6),(3.7) and (3.10) where  $n$  and  $\epsilon$  assume different values. We perform simulations of  $N = 1500$  at  $\rho = 1.0186$ . The acceptance of swap moves in this model is  $a \sim 20\% - 30\%$  and it does not depend considerably on temperature. Also the acceptance of the standard displacement is  $a \sim 30\% - 50\%$  and it depends only mildly on particle diameter. Without even considering the real dynamical speed up, this high value of the acceptance already indicates that swap moves are much more efficient compared to the mixture case. This is explained by the fact that for each particle one can find numerous other particles in the system with a similar diameter, such that swap moves will be easier to be performed. This does not mean that the system would necessarily relax in time, indeed one could imagine swaps that always exchange the same particles between them and these particles would always vibrate around their initial positions. A high value of the acceptance could be misleading and not having big implication of the dynamics. We will better discuss about the physical mechanism behind swap simulations in Sec. 3.8. For this class of systems we show in the following that swap Monte Carlo simulations accelerate the dynamics tremendously.

Since this system is highly polydisperse there might be a dynamical decoupling between small and big particles already in the standard dynamics, especially at low temperature and close to the dynamical slowdown. To clarify this point, we performed two checks using standard simulations. First we measured the Van Hove function (defined in Eq.(2.10)) to detect the presence of particles whose positions do not relax with respect to

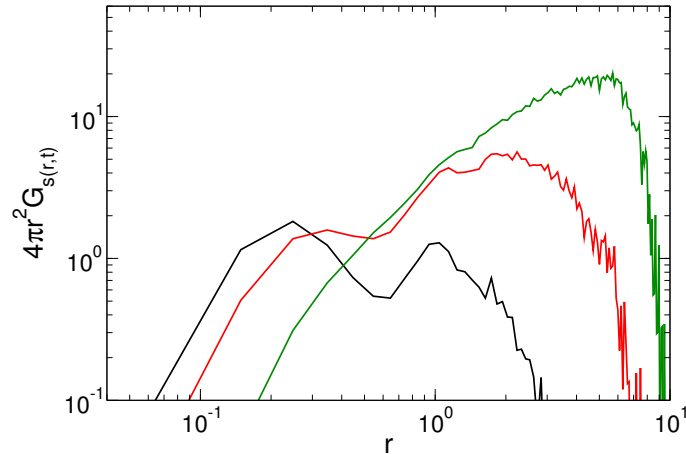


**Figure 3.10** – Self part of the Van-Hove correlation function  $4\pi r^2 G_s(r, t)$  for standard simulations (see Eq. (2.10) for a definition). The quantity is computed over all the particles at three different times  $\tau_\alpha/2$  (black),  $\tau_\alpha$  (red),  $2\tau_\alpha$  (green). The temperature is one of the lowest accessible one,  $T = 0.100$ . The system is the non-additive system with  $n = 12$  and  $\epsilon = 0.2$ . At short time the cage effect is remarkable, however for longer times all the particles decorrelate completely.

the initial positions. We show the result in Fig.3.10 for three different times, respectively  $\tau_\alpha/2, \tau_\alpha, 2\tau_\alpha$  at one of the lowest accessible temperature with standard simulations. As one can observe, after a period of time shorter or equal than the total relaxation time  $\tau_\alpha$  there is a fraction of particles that have not completely decorrelated with respect to their initial position. However, at longer times all the particles completely decorrelate. Then we also measured the relaxation time over the  $N/5$  smaller  $\tau_\alpha^S$  and bigger  $\tau_\alpha^B$  particles of the system as a function of temperature. We found that this quantity is almost constant on five orders of magnitude of slowing down its value being  $\tau_\alpha^S/\tau_\alpha^B \sim 10$ . The fact that it is constant in temperature guarantees that the dynamical slowdown for the two groups of particle does not change in nature. These two observations allow us to assert that even though there is a difference in timescales depending on particle size, we do not observe a real decoupling and the dynamics follow a similar arrest both for small and big particles.

Mindful of the analysis already carried on for the ternary system (Sec. 3.6.2), here we also carefully inspect ordering in the system, and we found that this system presents phase separation at lower temperature in swap simulations. This can be observed by looking at the structure factor at low- $q$ . In this system there is no precise distinction between different species, anyway we can look to statical properties of particles with similar diameters. To do so we group the particles with similar diameters in five different species, each containing  $N/5$  particles. Then we compute the species-specific structure factor and we use this to detect compositional fluctuations in the system. We observe a tendency, in many different system realizations, to phase separate. In the typical phase separated sample, the small particles present large fluctuations on shorter timescales as compared to the big ones.

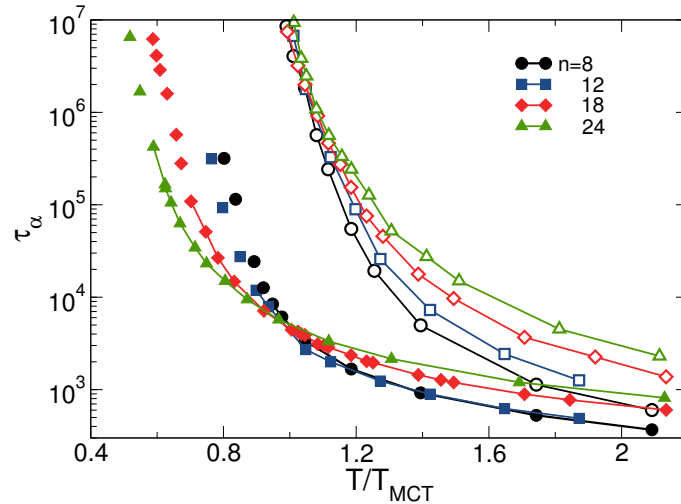


**Figure 3.11** – Relaxation times  $\tau_\alpha$  for continuously polydisperse systems of repulsive soft spheres with different softness exponents  $n = 8, 12, 18, 24$ . Temperatures are rescaled by  $T_{MCT} = 0.143, 0.267, 0.468, 0.662$ , respectively. Open symbols represent the standard Monte Carlo dynamics, closed symbols the swap dynamics, for which unconnected symbols represent structurally unstable points where only a rough estimate of  $\tau_\alpha$  is obtained in short simulations. A larger  $n$  yields better efficiency and structural stability.

So far, we have clarified different aspects which are common to all these continuously polydisperse models and we can therefore start to test their behaviour in swap simulations. The first class of tested models is the additive one, where we fix  $\epsilon = 0$  and use different values for the softness of the potential  $n = 8, 12, 18, 24$ . As before, to distinguish between temperatures where the system is stable or not, we used the protocol introduced in Sec. 3.4, and for this class of systems we distinguish between the two phases based on low- $q$  values of the structure factor. Relaxation times for swap and standard simulations are reported in Fig.3.11 as a function of the temperature. Temperature is rescaled by  $T_{MCT}$  of each model in order to compare them.

Looking at the standard dynamics, we first notice that a change in the softness of the potential causes a change in fragility, this being higher for smaller softness. This contradicts previous results [151] obtained for a soft binary mixture where the fragility was found to be invariant with changing softness. Even an opposite behaviour was found experimentally in Ref. [152], even though the microgel nature of the system employed in that case makes unclear the relation with our findings, which could be more easily related to colloids.

For this class of systems swap gives a huge speed up and the relaxation times are around three orders of magnitude smaller as compared to standard simulations at the Mode Coupling crossover. At very low temperatures the system presents phase separation and the disconnected points stand for temperatures at which the system leave the metastable equilibrium during the simulations and relaxation times can be measured on short simulations as it was done previously for the ternary system. We notice that

resistance to phase separation increases with increasing  $n$ , that is, by reducing softness. This result also suggests that the system with  $n \rightarrow \infty$  (i.e. hard spheres) represents the best glass former in this class of systems with respect to ordering issues. Overall this class of systems allows thermalization below  $T_{MCT}$ . For the system with  $n = 24$  we achieve equilibrium and stability for temperatures  $T \approx 0.5T_{MCT}$ . However we still observe huge density fluctuations at very low temperature in swap simulations, similarly to the results obtained for the ternary mixture.

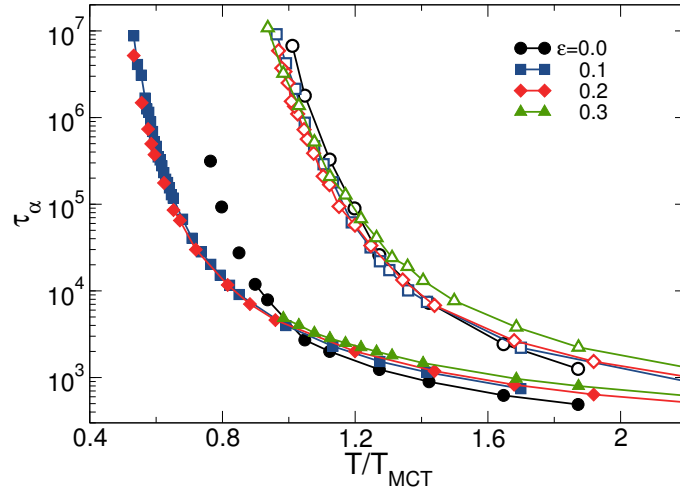


**Figure 3.12** – Relaxation times for systems with continuously polydispersity,  $n = 12$  and different non-additivity parameter  $\epsilon$ . Temperatures are scaled by  $T_{MCT}$  to allow direct comparison between models, with  $T_{MCT} = 0.267, 0.176, 0.104,$  and  $0.0534$ , respectively. Open symbols represent the standard Monte Carlo dynamics, closed symbols the swap algorithm, for which unconnected symbols represent structurally unstable state points where only a rough estimate of  $\tau_\alpha$  is obtained in short simulations. A well-chosen amount of non-additivity,  $\epsilon \approx 0.1-0.2$ , considerably improves the efficiency of thermalization and the structural stability.

To solve phase separation issues we decide to test another class of model, setting  $n = 12$  constant and varying the non-additive parameter  $\epsilon = 0.1, 0.2, 0.3$ . This was done in order to reduce the excluded volume between particles with large diameter differences with the aim to suppress phase separation. This effect is known to stabilize the metallic alloys [137, 48] and the opposite effect (i.e. enhancing phase separation) was exploited already for a hard sphere fluid [153, 154]. We already presented some result for the  $\epsilon = 0.2$  system previously. We report our result for relaxation times at different  $\epsilon$  in Fig. 3.12. We plot again the results for  $\epsilon = 0.0$  in order to compare with the non-additive case. Standard dynamics is rescaled by  $T_{MCT}$  and in this case we observe no change in the fragility of the system. From a dynamical point of view, the introduction of non-additivity yields a large speed up of the swap relaxation times compared to the additive case (in black), which seems to be constant at different non-additivity. The physical reason for this behaviour is unclear at this point.

The non-additivity improves remarkably the glass-forming ability of this system as



### 3.7.3 Closing the gap with experimental timescales

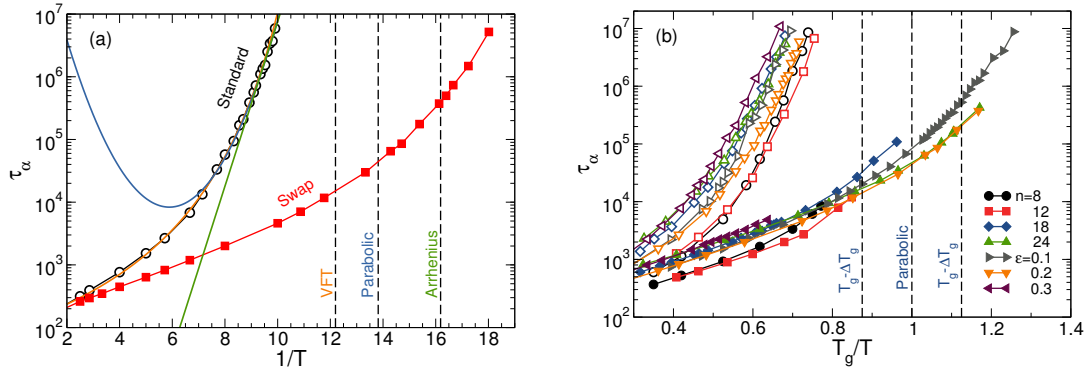
In this section we discuss in detail how to quantify the dynamical gain of swap simulations with respect to standard simulations. As anticipated in Sec. 3.3, this can be done by fitting relaxation times of standard simulations and extrapolate them at lower temperatures. This procedure is particularly reliable when the new accessible regime is not very deep compared to standard simulations and the extrapolation is performed over few orders of magnitude. In our case, extrapolations must be carried out carefully and the uncertainty given by the fits must be taken into consideration. With this aim we fit standard relaxation times, which are usually accessible over four orders of magnitude with respect to the location of the onset ( $\tau_\alpha/\tau_o \approx 10^4$ ). Here we recall that in experiments, the accessible regime is 8 orders of magnitude broader, the experimental glass transition happens at  $\tau_\alpha/\tau_o \approx 10^{12}$ . To quantify how close our simulation scheme can equilibrate with respect to the laboratory transition we fit the standard dynamics using three different laws: VFT, parabolic and Arrhenius function, described respectively by Eqs. (3.18), (3.19), (3.20). These three functional forms have different theoretical foundations and a different behaviour. The first predicts a divergence of relaxation time at finite temperature, whereas the last two diverge at  $T = 0$ . The three different fits allow us to extrapolate three different laboratory glass transition temperatures. We use the one from the VFT functional form  $T_g^{VFT}$  as an upper limit and the one from the Arrhenius equation  $T_g^{Arrhenius}$  as a lower limit for the real glass transition of the system to happen. The extrapolated value from the parabolic law  $T_g^{parabolic}$  is in between them.

We illustrate our procedure for one system in Fig. 3.14a, where relaxation times are shown as a function of the inverse temperature. The three vertical lines indicate the location of the glass transition temperature from the three different extrapolations. As can be noticed the model can be equilibrated at extremely low temperatures, even beyond  $T_g$  extrapolated using the Arrhenius law. Fig. 3.14b illustrates the results for many different models. Interestingly, the difference of the three different extrapolated temperature remains under control in all the systems under investigation, with a typical interval:

$$\frac{\Delta T_g}{T_g} = \frac{T_g^{VFT} - T_g^{Arrhenius}}{2T_g^{parabolic}} \approx 12\%. \quad (3.26)$$

This value is small enough to give significance to the extrapolation.  $\alpha$ -relaxation times at the glass transition remain always finite and small, of the order of  $\tau_\alpha/\tau_o \approx 10^2 - 10^3$ , the most important problem in equilibration being the appearance of ordered phase in the system. The analysis carried out here has three consequences:

- The speed up at the glass transition is about  $10(\pm 1)$  orders of magnitude, allowing simulations to perform equilibrium studies of the laboratory glass transition.
- The maximal speed up for certain models is even larger than this and the quantification is a delicate matter relying on extrapolations.
- Swap Monte Carlo allows to produce configurations equilibrated at lower temperature than their experimental analogs.



(a) Relaxation times for the non-additive model with  $n = 12$  and  $\epsilon = 0.2$  for standard and swap Monte Carlo dynamics. The standard dynamics is fitted with the VFT, parabolic and Arrhenius laws, as shown with lines, which are used to estimate the location of the experimental glass temperature  $T_g$ , as shown with vertical dashed lines. For this system, the swap dynamics is able to provide stable and thermalized configurations at temperature below  $T_g$ .

(b) Relaxation times obtained from standard (open symbols) and swap (filled symbols) dynamics for various size polydisperse models of various softness ( $n$ ) and non-additivity ( $\epsilon$ ) are shown in an Arrhenius form with rescaled temperature  $T_g/T$ , where  $T_g$  is estimated as in (a). For all models the thermalization speedup near  $T_g$  is of about 10 orders of magnitude, some models being structurally stable down to temperatures below  $T_g$ .

The analysis performed in this subsection shows that we are now able to close the gap of equilibration between simulations and experiments. This represents an important improvement of simulations of supercooled liquids and it could give answers and clarifications about many aspects of the glass transition.

### 3.7.4 Hard spheres

*Simulations and analysis reported in this paragraph were performed by L. Berthier and D. Coslovich*

Hard spheres have a high density behaviour in many respects similar to the low temperature one of thermal systems [10]. The natural control parameters for this system are the packing fraction  $\phi = \frac{\pi}{6L} \langle \sigma^3 \rangle$  and the reduced pressure  $Z = \frac{P}{\rho k_B T}$ . Note that this last quantity directly relates the pressure and the temperature of the system. In a monodisperse system, by increasing the packing fraction  $\phi$  the system slows down and a melting point is reached above which particles start to crystallize. By further compression, a maximal packing fraction is reached  $\phi \approx 0.74$  with the system in a FCC packing. This is the highest possible packing and the system is in a pure crystalline state [155]. If polydispersity is introduced, the increase of density does not coincide

with crystallization and the system may remain disordered up to the point where it does not relax anymore and it goes out of equilibrium. A kinetic slowing down can be also observed in hard spheres by increasing density or pressure [6] and one can find the following analogy between the glassiness of hard sphere systems and thermal glasses [10]

$$T \leftrightarrow \frac{1}{Z}, e \leftrightarrow \frac{1}{\phi}. \quad (3.27)$$

Analogously to the soft-sphere systems, standard simulations can usually equilibrate hard spheres at packing fractions comparable to the Mode Coupling crossover [10, 42].

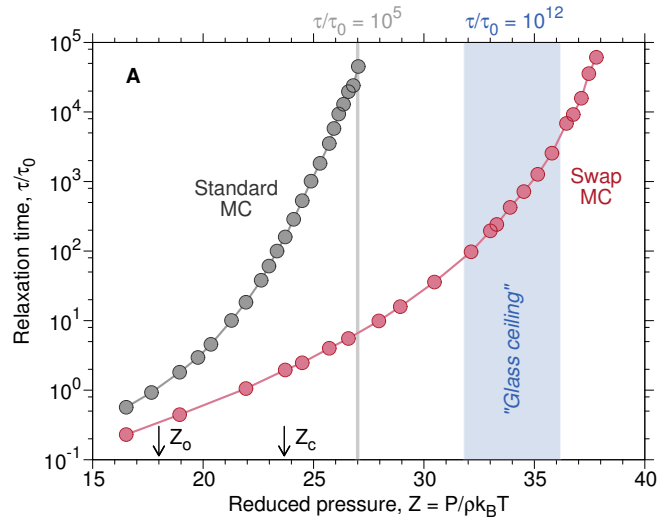


**Figure 3.15** – Relaxation time  $\tau_\alpha$  normalized by its value at the onset as a function of the reduced pressure  $P$ . Results are both for standard simulations in grey and swap simulations in red. The blue box indicates the location of the glass transition defined extrapolating the standard relaxation time (see Sec. 3.7.3).  $Z_0$  and  $Z_c$  indicate respectively the onset and the Mode-Coupling pressures.

For this reason, one of the first model we investigate using swap simulations was made of hard spheres. We will show that a huge dynamical gain can be obtained also for this model. In order to do this, we use a hard sphere version of the model introduced in Sec. 3.7.2. The two particle interaction potential is described by (3.9) and (3.10) with  $\epsilon = 0$  which corresponds to an additive model. We perform constant volume standard Monte Carlo simulations in which only standard displacements are allowed. Pressure can be measured using the contact value of the pair correlation function [156]. Measuring  $\alpha$ -relaxation times as a function of the pressure allows one to locate the *in silico* dynamical transition,  $\tau_\alpha/\tau_0 \sim 10^5$ . Next we introduce swap moves in the simulation, using the same procedure as before. By doing this we allow thermalization of the system at remarkably higher density compared to the standard dynamical transition. The situation is reported in Fig. 3.15, where relaxation times are plotted as function of the reduced pressure  $Z$ . Grey points indicate results from standard simulations and red point are for swap simulations. The blue box indicates possible location of the glass transition as defined in the previous paragraph. We observe that thermalization is achieved for pressures

beyond the experimental glass transition. The model is very stable compared to the other additive cases studied and the dynamical gain can be estimated in more than 12 orders of magnitude.

### 3.8 Microscopic insight into the swap dynamics

So far we have shown how swap simulations could dramatically accelerate the dynamics. Yet the physical reason behind this dynamical speed up remains unclear. Some years ago it was proposed that swap simulations were able to break the particle cages characteristic of supercooled liquids [69], however this has a vague meaning, since the concept of cage is itself ambiguous as discussed in the introduction. To clarify this point and make some quantitative statements, here we study the microscopic dynamics during swap simulations. First we follow the displacement  $\Delta r(t)$  and the diameter  $\sigma(t)$  of the same particle as a function of time. Fig. 3.16 shows the results for two chosen particles. The system is the non-additive model of Sec. 3.7.2 with  $\epsilon = 0.2$  at  $T = 0.0555$ . It can be

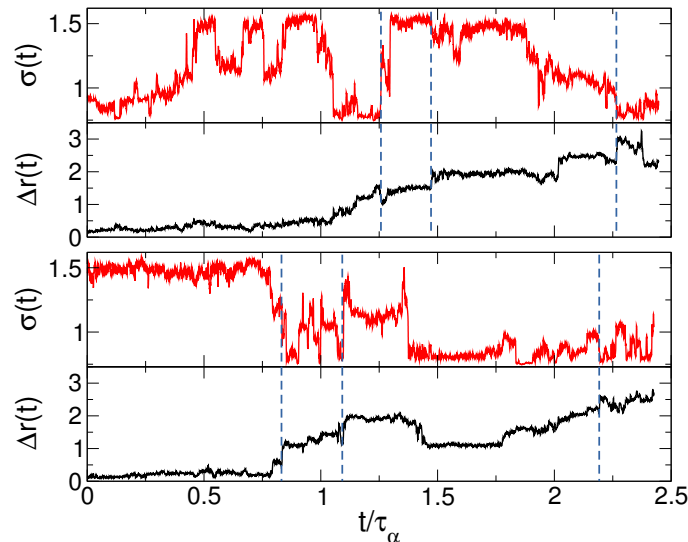


**Figure 3.16** – Time-series of individual displacement  $\Delta r(t)$  and diameter value  $\sigma(t)$  for two tagged particles in the non-additive model of Sec. 3.7.2 with  $\epsilon = 0.2$  at  $T = 0.0555$ . Intermittent diffusion in real and diameter space is observed, with strong correlations between  $\Delta r(t)$  and  $\sigma(t)$  highlighted with dashed lines, but we also observe many events in one observable that have no counterpart in the other indicating that the correlation between the two observables is non-local.

seen that the mean squared displacements follow the usual behaviour in supercooled liquids simulations already shown in Ref. [157]. Particles first vibrate around their initial position and then they suddenly perform a jump in real space changing position markedly and starting to vibrate around another position. The behaviour of particle diameters is surprisingly similar. They first assume values around the starting diameter and then they suddenly decorrelate and change their size by a significant value. One can notice that, sometimes, relaxation in diameters coincides with relaxation in position.

Besides, many changes in diameter or position do not happen concurrently on the same particle indicating that all these phenomena should be considered as collective. Namely, a diameter relaxation could also induce relaxation of position or diameter of neighbouring particles. This is why an analysis based on the caging idea is not enough to explain the reason for relaxation in the system. However these qualitative observations led us to introduce a diameter self-correlation function:

$$C_\sigma(t) = \langle c_\sigma(t) \rangle = \left\langle \frac{\sum_i \delta\sigma_i(t)\delta\sigma_i(0)}{\sum_i \delta\sigma_i^2(0)} \right\rangle. \quad (3.28)$$

This quantity is normalized to one at time  $t = 0$  and becomes zero when the diameters of all the particles are decorrelated with respect to their initial value.

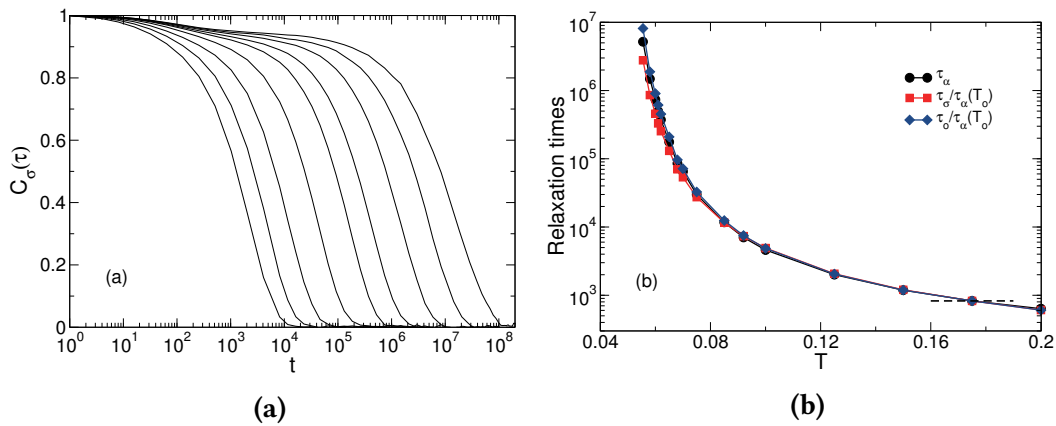


**Figure 3.17** – Non-additive model of Sec. 3.7.2 with  $\epsilon = 0.2$ . (a) Time auto-correlation of particle diameters  $C_\sigma(t)$  measured during the swap dynamics for temperatures as in Fig. 1.3. (b) Relaxation times  $\tau_\alpha$ ,  $\tau_\sigma$  and  $\tau_o$  as a function of temperature, with  $\tau_\sigma$  and  $\tau_o$  rescaled to coincide with  $\tau_\alpha$  at  $T = 0.175$  (shown with horizontal bar). The three timescales obviously have the same temperature dependence.

The result is shown in Fig. 3.17a, where we plot  $C_\sigma(t)$  for different temperatures. While at high temperature decorrelations are exponentially fast, by lowering the temperature  $C_\sigma(t)$  develops a plateau. This is a consequence of the jump dynamics observed in the diameter time series and is related to the average amplitude of fluctuations around the starting diameters. At longer time, it decorrelates to zero indicating that diameters have lost memory of the starting values. From this correlation function one can extract a relaxation time  $\tau_\sigma$  defined through the relation  $C_\sigma(\tau_\sigma) = e^{-1}$ . Interestingly this relaxation happens on a time scale comparable to the  $\alpha$ -relaxation. In Fig. 3.17b we compare relaxation times from the self-intermediate scattering function, the collective overlap function and the diameter self-correlation function. All the values are rescaled by  $\tau_\alpha$  at  $T = 0.175$  in order to compare these quantities with each other. It can be seen that all the relaxation times have the same behaviour as a function of  $T$  and can be rescaled on a single curve. This shows quantitatively that positional and diameter correlations are profoundly interconnected in swap simulations.

To further inspect the swap dynamics we also quantify dynamical heterogeneities both in real and in diameter space. Dynamical heterogeneity is one of the most remarkable features of supercooled dynamics and a huge amount of work has been dedicated to elucidate this property [157]. The main observation is that by lowering the temperature and entering the supercooled regime, the system presents fast and slow regions which relax over different timescales. From this behaviour it is possible to extract a dynamical lengthscale  $\xi_{dyn}$  whose definition and the computation was deeply discussed in the last decade [25, 142] and it was found to increase by lowering the temperature. The role of this lengthscale is clear from a dynamical viewpoint, since it gives the size of the dynamical correlated regions.

One way to quantify dynamical heterogeneities is the use of a dynamical susceptibility, which is a time-dependent four point quantity defined as [128]

$$\chi_4^O(t) = N [\langle O^2(t) \rangle - \langle O(t) \rangle^2] \quad (3.29)$$

where  $O(t)$  is a generic observable. This susceptibility quantifies the amount of spatial correlations associated to the observable  $O(t)$  at a given time  $t$ . It starts from zero, the correlation being zero at initial time, then it increases to a maximal value, at a time comparable with the relaxation time of the two point correlation function of observable  $O(t)$  and finally it decreases and reaches a constant value. The peak value at intermediate times quantifies the volume of the dynamically correlated regions. In particular, in three dimensional  $NVT$  simulations, the cube root of the peak value was found to be a lower bound for the dynamical correlation length  $\xi_{dyn}$  [25]. We measure susceptibilities associated to self density fluctuations,  $\chi_4^d(t)$  with  $O(t) = f_s(k, t)$  (see Eq. (3.16)), and to diameter fluctuations,  $\chi_4^\sigma(t)$  with  $O(t) = c_\sigma(t)$  (see Eq. (3.28)).

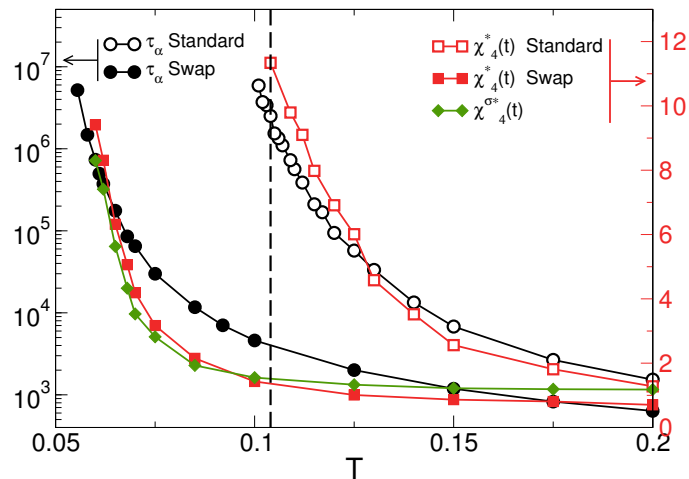


**Figure 3.18** – Temperature evolution of dynamic susceptibilities (right axis) and relaxation times (left axis), the vertical dashed line is  $T_{MCT} = 0.104$ . Whereas  $\chi_4^d(t)$  grows together with  $\tau_\alpha$  in standard simulations,  $\chi_4^d(t)$  and  $\chi_4^\sigma(t)$  behave similarly and have a very different temperature dependence which mirrors instead the evolution of the swap relaxation time.

In Fig. 3.18 we report the peak value of this dynamical susceptibilities for standard and swap simulations. In the same figure we also plot relaxation times for comparison. The peak values are for positional  $\chi_4^{d*}$  and diameter  $\chi_4^{\sigma*}$  degrees of freedom, these are lower bound for the dynamical correlation lengths in real and diameter space. The standard simulations present the usual behaviour. The extent of dynamically correlated regions increases by lowering the temperature in a regime corresponding to the dynamical slowdown. In swap simulations, the value remains low across the  $T_{MCT}$  regime and it increases in the temperature regime corresponding to the dynamical slowdown. Also the extent of dynamical correlations in diameter space increases of the same amount and at the same temperatures. Two pieces of information can be extracted from this figure. First, we confirm that in swap simulations position and size relax on the same timescales. Second, in swap simulations dynamical heterogeneity is suppressed as compared to standard simulations at the same temperature and it can be re-established at lower temperatures.

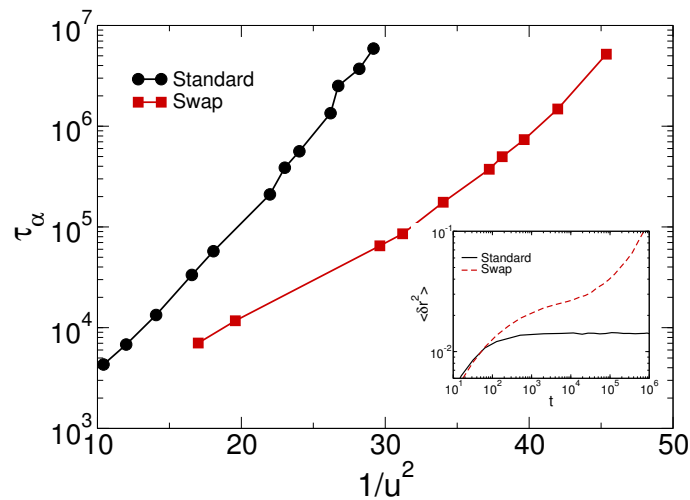


**Figure 3.19** – Relaxation time evolution in function of the inverse average cage size  $u^2$  both for standard (black point) and swap (red squares) simulations. At equal times swap simulations always present smaller cages.

Still, two questions remain unanswered: how does swap simulations *kill* dynamical correlations? And why is there another dynamical arrest at lower temperature which is so similar to the one of standard simulations? One possible way to understand better the swap dynamics is to look at the relation between short time vibrations and long time  $\alpha$  relaxations. There is a theoretical scheme, proposed by Dyre [158, 159, 160] that goes under the name of *shoving model*, in which the non-Arrhenius behaviour of relaxation times is ascribed to the changes in  $T$  of the high frequency shear modulus  $G_{\infty}$ . On the other hand thermal fluctuations can also be understood in terms of shear properties. In particular the shear modulus can be directly related to the average size of the cage  $u^2$  in

the supercooled regime and the following relation can be obtained

$$\ln \frac{\tau_\alpha}{\tau_0} = A \frac{a^2}{u^2} \quad (3.30)$$

Here  $\tau_\alpha$  is the self relaxation time,  $\tau_0$  is a macroscopic time (see Eq. 1.4),  $A$  is a temperature independent constant and  $a$  is the average interatomic distance. One way to measure  $u^2$  is through the value of the plateau in the mean squared displacement  $\langle \delta r^2 \rangle$  which is related to the presence of a caging effect. We define  $u^2$  as the value of the mean squared displacement at the center of the flatten region enclosed by the diffusive behaviour at short and long times (see inset of Fig. 3.19). Having in mind this model, we compared  $\langle \delta r^2 \rangle$  both in standard and in swap simulations finding that at a given temperature the plateau is always higher in swap simulations. An example for a single temperature is shown in the inset of Fig. 3.19 and similar curves can be found at other temperatures as well. Bearing in mind the shoving model, we can interpret the huge dynamical acceleration of swap simulations in terms of larger cages and the relation between the two features has been found also in other glass forming liquids [161, 162, 163].

However this reasoning does not completely explain the relation between vibrations and relaxation in swap simulations. In main panel of Fig. 3.19 we report  $\tau_\alpha$  versus the inverse of  $u^2$ . Interestingly, comparing the value of  $u^2$  at the same relaxation time, we notice that this is always smaller in swap simulations, indicating that there are vibrational degrees of freedom which are not taken into account by the mean square displacement and that are related to fluctuations of the diameters. Our analysis, at this point cannot explain or quantify exactly these *additional* vibrations. Overall we believe that a deeper understanding of swap simulations and of the enhanced thermalization could add some useful information to the glass puzzle [164].

## 3.9 Designing new models for swap Monte Carlo simulations

### 3.9.1 Binary mixtures, polydispersity and attractive forces

Many computational models of glass-forming liquids are made of two component mixtures [40, 48]. However we saw before that in swap simulations pure mixtures have two big drawbacks, they both have a small acceptance and they easily present crystal nuclei or compositional fluctuations. Of course trying to increase the acceptance by lowering the size ratio would enhance ordering and, on the contrary, increasing size ratio would reduce swap benefits. On the other hand, we observe that in continuously polydisperse systems acceptance increases by orders of magnitude and this can be explained by the fact that particles can slowly change their size by assuming many intermediate values. In the following we introduce a class of systems that includes both the main features of binary mixtures and the presence of continuous polydispersity.

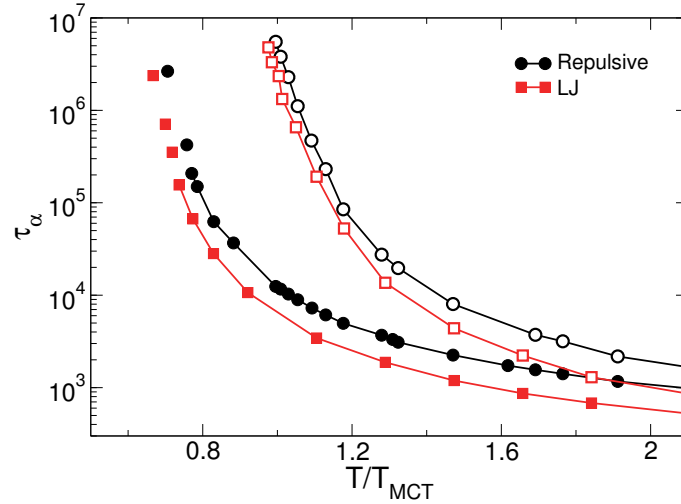


**Figure 3.20** – Relaxation times for repulsive and Lennard-Jones potentials with a hybrid particle size distribution. Temperatures are scaled by  $T_{MCT}$  to allow direct comparison between models, with  $T_{MCT} = 0.680$  and  $0.543$  for repulsive and LJ potentials, respectively. Open symbols represent the standard Monte Carlo dynamics, closed symbols the swap algorithm, for which unconnected symbols represent structurally unstable state points where only a rough estimate of  $\tau_\alpha$  is obtained in short simulations.

The starting point is made of two groups of particles ( $A, B$ ) presenting a continuous flat polydispersity around two average value whose size ratio is  $\frac{\sigma_B}{\sigma_A} = 1.6$  and each of them having the same number of particles. Then we introduce another flat polydisperse species  $C$  with particles having diameter values in between the species ( $A, B$ ). The idea here is to create a *channel* in diameter space to allow particles to tunnel between species  $A$  and  $B$ . The situation is well represented in the top right panel of Fig. 3.1. The system can be described by the size dispersion of Eq.3.4 with parameters  $\gamma_A = 0.33$ ,  $\gamma_B = 0.34$ ,  $\gamma_C = 0.33$ ,  $\sigma_A = 0.76$ ,  $\sigma_B = 1.23$ ,  $\sigma_C = 1.00$ ,  $b_A = 0.04$ ,  $b_B = 0.04$ ,  $b_C = 0.26$ , the resulting polydispersity is  $\delta \approx 20\%$ . We perform simulations of  $N = 1000$  particles at  $\rho = 1.3$ . The two particle interaction potential is given by Eqs. (3.6) and (3.7) with  $n = 12$  and a cut-off distance of  $r_{cut} = 1.3\sigma_{ij}$ . Results for the relaxation times are reported in Fig. 3.20 both for standard and swap simulations. The acceptance here is  $a \approx 20\%$ . In the figure disconnected points represent temperatures at which relaxation times are computed on simulations shorter than  $200\tau_\alpha$ , as long as the system remains an equilibrium fluid. The main ordering danger in this system is again represented by long wavelength fluctuations, which can be observed by looking at the low- $q$  values of the partial structure factor as already done for the other continuously polydisperse systems. When compared to the binary mixture, we see that the dynamical gain here is high, since the lower temperature at which the system can be equilibrated is  $T \approx 0.075$  corresponding to  $0.6T_{MCT}$ .

Until now we always dealt with purely repulsive interactions. To better understand the role of attractive forces in swap simulations we modify this last model by introducing

another form of two particle interactions. In this new model, we leave everything unchanged with respect to the previous one, apart for the potential form that is now described by Eqs. (3.8) and (3.10), where  $\epsilon_{ij} = 1/4$  and  $\epsilon = 0.0$ . We find an acceptance comparable to the previous one,  $a \approx 20\%$ , and also the dynamical properties of this system do not change dramatically. In Fig. 3.20 we report relaxation times for this system. As one can notice the introduction of attractive interactions has the main effect of modifying the temperature scale whereas many properties are similar, such as the shape and location of the dynamical arrest both in standard and swap simulations and also the main ordering processes which is characterized by phase separation. In the traditional view [1], the physical properties of simple liquids are to a large extent determined by the repulsive forces. This was challenged recently by Berthier and Tarjus in Ref. [165] where they show that adding attractive interactions would leave the statics almost unmodified while the dynamical properties may change a lot. The issue was also further inspected in Ref. [166] where it was claimed that the most important role in determining physical properties of liquids is given by the first coordination shell. Here we do not perform a detailed study of this issue, yet our results tends to reconcile with the traditional view in which repulsion makes the most of the work in simple liquids. For this model we observe that swap simulations are able to equilibrate down to a very low temperature  $T \approx 0.7T_{MCT}$  telling us that this Monte Carlo method can be used also in presence of attraction. This opens up the possibility to use swap simulations for more complex systems such as models of metallic glasses [137]. The results shown in this subsection bring about the following questions: can swap simulations be used in other historical glass-forming liquids presenting attractive interaction? How much would it be the dynamical gain? How low could we go in temperature? In the next subsection these questions will be systematically addressed for a well known glass-forming liquid.

### 3.9.2 Extending the Kob-Andersen Lennard-Jones model

In this section we introduce an extension of the Kob-Andersen Lennard-Jones (KA) system with the aim of creating a model for which swap simulations are effective and lead to considerable dynamical acceleration. The original system was first introduced in 1994 [48], it was inspired by the metallic glass  $Ni_{80}P_{20}$  and in the last decades has been an archetype for simulations of supercooled liquids. In the traditional version of the system, there are two species of particles ( $A, B$ ) that interact via a potential given by Eq. (3.8) where  $\epsilon_{AA} = 1.0$ ,  $\epsilon_{AB} = 1.5$ ,  $\epsilon_{BB} = 0.5$ ,  $\sigma_{AA} = 1.0$ ,  $\sigma_{AB} = 0.8$ ,  $\sigma_{BB} = 0.88$ . This non additivity, both in energy and size, gives to the system a prominent resistance to ordering even though, in recent years, the increasing performances of computational resources led to the observation of ordering effects [167, 168]. Given the relative larger size ratio, performing swap of this system is highly inefficient and the speed up would be essentially inexistent. We then decided to exploit the idea of allowing the tunneling of particles between species  $A$  and  $B$  by adding few particles in between them. This

is very similar to the procedure introduced in the previous section, however, here we always employ a small number of additional particles, in order to consider them as a perturbation to the original system. To this aim we introduce  $N_\omega$  additional particles in the traditional mixture interacting with the other through Eq. (3.8) in which interaction energy and cross-diameter are described by (3.11) where  $\omega_i = \frac{i}{N_\omega+1}$  assumes discrete values between zero and one ( $i \in [1, N_\omega]$ ). We start by performing standard Monte Carlo simulations of a system with  $N = 1000$  and  $\rho = 1.2$  at various temperatures and we compare results for potential energy and relaxation times with previous literature. We then simulate three different systems by adding  $N_\omega = 10, 50, 100$  particles to the original mixture and keeping the number density constant. In the following we call them respectively  $KA1, KA2, KA3$ . For these systems we both perform standard and swap simulations. We detect an acceptance of the swap moves between 5% and 10%. We then compared the relaxation times for the standard and swap simulations. We notice that the introduction of additional particles causes a shift of the dynamic slowing down at lower temperatures. However by multiplying the temperature with a constant value, the relaxation times as a function of the temperature for standard simulations can be rescaled in a single curve. The results are shown in Fig. 3.21. We will discuss the physical meaning of the temperature rescaling in the following.

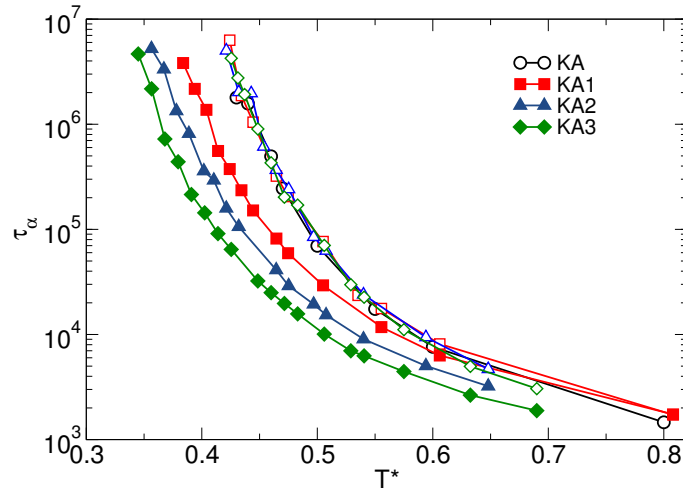


**Figure 3.21** – Relaxation times for the modified Kob-Andersen model. Empty and full symbols indicate respectively standard and swap simulations. Circles are for the original KA model. The modified models are indicated with squares (KA1), triangle (KA2), diamond (KA3). Temperatures of the modified models are rescaled by a factor  $\lambda = 1.01, 1.08, 1.15$  such that  $T^* = T/\lambda$  in order to collapse the curves for standard simulations in the curve for the original KA.

Fig. 3.21 also shows that by increasing the number of  $\omega$  particles the dynamical gain increases significantly. For the system with 100 additional  $\omega$  particles we are able to equilibrate down to a rescaled temperature  $T^* \approx 0.35$ , which is much lower compared to the Mode-Coupling temperature that for this system is located at  $T_{MCT} \approx 0.435$  [125].

The validity of our temperature rescaling can be interpreted in the context of a

framework developed some years ago indicating the presence of *isomorphs* for strongly correlated liquids [169, 170, 171]. It was found that liquids presenting strong correlations between potential energy  $e$  and virial  $w$  equilibrium fluctuations obey specific rescaling relations. In particular changing the density or the temperature of the system, static and dynamic properties such as radial distribution functions or the intermediate scattering function remains unchanged if the ratio  $\frac{\rho^\gamma}{T}$  is kept constant. The exponent  $\langle w \rangle \approx \gamma \langle e \rangle$  can be measured using energy and virial fluctuations. Here we measure  $\gamma$  for our systems finding  $\gamma = 5.115, 5.154, 5.218$  respectively for the  $KA1, KA2, KA3$  which are very similar to  $\gamma = 0.493$  found previously for the KA system at the same density [169]. We conclude that the introduction of the additional particles, keeping the number density constant, can be mostly thought as a change in the density and consequently by a temperature rescaling we bring back the system to its initial state point following the isomorph.

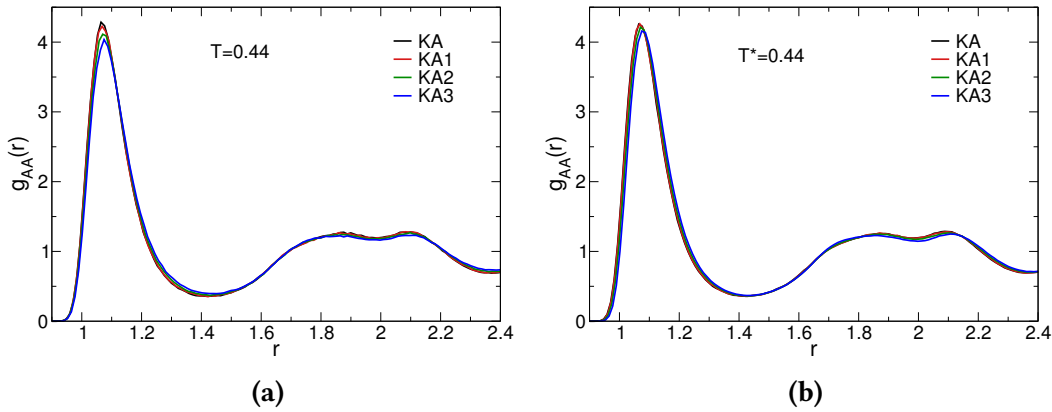


**Figure 3.22** – The radial distribution function for the particles in the species A in four models. KA indicates the original binary mixture. KA1, KA2, KA3 indicate the three modified systems. (a) results are given for temperature  $T = 0.44$ . (b) results are given for the rescaled temperature  $T^* = 0.44$ .

As for the other changes, they could have a structural nature. To better understand to which extent the perturbation introduced by the tunneling particles modifies the statics of the original system, we compare a structural quantity, the radial distribution function. As we already said, changes in two point static functions do not drastically depend on the degree of supercooling or on the density. In a typical glass-forming liquid [125] reducing the temperature produces an increase of the first peak of the  $g(r)$ , while reducing the density leads to a horizontal shift. We also detect similar shifts comparing systems with different amount of additional  $\alpha$ -particles. The results for the  $g(r)$  computed only on particles in the species A are reported in Fig. 3.22. Here we compare this quantity for the four different realization of the system at the same bare temperature  $T = 0.44$  (Fig. 3.22a) and at the same rescaled temperature  $T^* = 0.44$  (Fig. 3.22b). We observe that in both cases changes with respect to the original system are minimal. In Fig. 3.22a we observe a reduced intensity of the first peak for measurements at the same bare temperature.

This could be again explained, within the isomorph framework, as a change to lower effective temperatures that leads to a reduced packing of the first shell of neighbours. The comparison made at the same rescaled temperature  $T^*$  as in Fig. 3.22b gives a better information on the changes introduced by the new particles. In this case we observe a small shift of the first peak to bigger values of  $r$  which is the typical consequence of reducing the density. Then we are prone to think that the main modification given by the  $\omega$ -particles is a change in the effective density.

In recent years the increased computational power made feasible longer simulations such that the Kob-Andersen model has shown crystal nucleation [167, 168]. Since we perform long simulations at low temperature and having experienced that swap enhances phase space exploration, we decided to monitor ordering in this system as well. However, previous literature findings [167, 168] revealed that crystal nucleation in this system can unlikely be observed looking only at potential energy, radial distribution functions, structure factors or bond-orientational order. It was also found that in this system the best tool to detect ordering is the common neighbour analysis parameter CNA-142 [172], which measures the concentration of two neighbouring particles having four mutual neighbours such that these last share two bonds each other. When all the neighbouring particles are involved in such a structure, this observable assumes values close to one, while when none is involved it is equal to zero. Essentially, it measures the concentration of crystalline structures and it increases in presence of high fcc and hpc crystalline order [172, 168].

The definition of the neighbour is given by a cut-off value  $c_{\alpha\alpha}$  which depends on the species and can be defined by looking at the first minimum in the  $g_{AA}(r)$ . Following previous literature [168] we use  $c_{AA} = 1.41$ ,  $c_{AB} = 1.30$ ,  $c_{BB} = 1.09$ . We do not include the  $\omega$ -particles in our analysis, to better compare with the results for the original system. We set up a CNA analysis tool that first detects couple of neighbouring particles, then counts the number of mutual neighbours and finally counts how many bonds these last particles share each other. In the supercooled regime, usual values for the CNA-142 give concentrations around 9 – 10% for the original binary mixture [167, 168].

We confirm this value in our simulation of  $KA$  and we detect a roughly constant behaviour in temperature which is a good marker of the fact that the system structure does not change drastically reducing the temperature. We recall here that previous simulations [167] found that values around 14% are already indicating the presence of crystal nuclei. Then we compute the same quantity using the modified system. We found that increasing the number of tunneling particles the system present systematically larger values of crystalline structures, with values ranging around  $\sim 10\%$  for the  $KA1$  system to  $\sim 12.5\%$  for the  $KA3$  system. This effect could be explained by the fact that we count less mutual neighbours between original particles in the modified system. Nonetheless we observe comparable values for this quantity at different temperatures. This indicates that the system structure does not change noticeably with changing temperature and crystal nucleation cannot be observed. This could be due to the fact that our simulations, which

last for up to  $300\tau_\alpha$ , are not long enough to induce ordering in the system. Interestingly the modified system does not present structural anomalies and its glass-forming ability is comparable with the original system. However longer simulations and a more systematic study would be needed to understand the consequences for ordering processes given by additional  $\omega$ -particles and swap simulations.

Overall this model represents a huge improvement in terms of equilibration regime compared to the original binary mixture. Since this last was largely employed in simulations of supercooled liquids and many physically relevant results were obtained using this system, it is now possible to investigate the conclusions previously obtained in a new temperature regime.

### 3.10 Swap Monte Carlo in 2D

It is well known that the formation of ordered solids in two and three dimensions is fundamentally different. First it was theoretically understood that the presence of fluctuations determines the absence of the breaking of continuous symmetries for dimensions equal or lower than two [173, 106]. These fluctuations, named after Mermin and Wagner, rule out the presence of a single crystal at finite temperature. Yet, the presence of a solid phase is still possible. This is characterized by positional correlation decaying to zero as a power law, and orientational correlations that are long-ranged. Between these two phases, the presence of a hexatic phase was detected in hard spheres [56], distinguished by quasi-long-range orientational order, thus confirming the existence of the predicted Kosterlitz and Thouless scenario [174].

As discussed in Sec. 1.3.5 of the introduction, the situation for two dimensional amorphous solids is much less clear than crystal. For a long time it was believed that the two and three dimensional glass transitions have no substantial difference [102]. However results from the last three years have shaken up this popular view. Nowadays, thanks to computational [103, 105] and experimental [107, 108] investigations, it is clear that two dimensional glass forming liquids present dynamical features absent in their three dimensional analogous. Using large enough computational systems or colloidal particles, it was shown that long wavelength fluctuations are present in amorphous solids as well [107, 108]. Their main observed consequence has a dynamical nature: on the one hand caging is absent in the translational degrees of freedom, on the other hand relaxations of the local environment present a timescale separation between short time vibrations and long time relaxations. This can be explained by the fact that the size of single particle density fluctuations increases with system size and particles can travel a long path together with their neighbours.

The main aim of this paragraph is to have an insight on the two dimensional glass formation both with standard and swap Monte Carlo. We study the nature of fluctuations and their size dependence for one glass-forming liquid. We decided to employ one of the most successful systems in three dimensions: a non-additive continuous polydisperse

system. The size dispersion is described by Eq. (3.2). This expression, with a cube of the diameter at denominator, was set up for three dimensional systems. Here we leave it unchanged in order to better compare these results with the previous three dimensional version. The two particles interaction is given by Eqs. (3.6) and (3.10) with  $n = 12$  and  $\epsilon = 0.2$ . We perform simulations of  $N = 300, 1000, 20000$  particles at  $\rho = 1.0131$ . As was shown in Ref. [103] the dynamics of two dimensional glass-forming liquids changes with varying the system size. In particular, for small system of few hundreds of particles, a caging effect is present characterized by the existence of a plateau in the self-incoherent scattering function which disappears by increasing the system size to some thousands of particles. For this reason we decided to simulate different system sizes in two dimensions.

We perform both standard and swap simulations as previously. We carefully check structural quantities such as radial distribution function and structure factor to detect possible deviations from the metastable equilibrium and we find a non pathological behaviour at all temperatures, with results that are qualitatively similar to the 3D realization of the system. Also in two dimensions we perform simulations of hundreds of relaxation times and we do not find indications of phase separation and crystallization, meaning that in 2D the system becomes even a more robust supercooled liquid as compared to the three dimensional version. Particular attention is needed in two dimensional systems to the formation of orientational order [104, 141]. In previous works it was shown that both monodisperse [56] and polydisperse [175, 116] hard disks are prone to form hexagonal order. For this reason we compute the bond-orientational order parameter given by Eq. 3.15 as main indicator of ordering. This quantity measures average hexagonal order, being one for perfect triangular lattice. We found very small values ( $|\Psi| \sim 0.02$ ) indicating the amorphous nature of the system. To compute this quantity we defined the neighbour shell including all the particles up to a cut-off value  $r_{ij}/\sigma_{ij} = 1.33$ , corresponding to the first minimum in the rescaled radial distribution function  $g(r_{ij}/\sigma_{ij})$ .

The dynamical behaviour presents similar features as the previous two dimensional simulations concerning the presence of cages. We report results for the self-intermediate scattering function in Figs. 3.23a and 3.23b respectively for  $N = 300$  and  $N = 20000$ . For  $N = 300$  we detect the presence of a well defined plateau. Increasing the system size to  $N = 20000$  this plateau disappears and relaxation happens with stretched exponentials. It is likely that the effect could be magnified by using larger systems, as in Ref. [103] size dependencies have been found for systems up to four millions of particles, while our biggest system are two orders of magnitude smaller. As the slow degrees of freedom in two dimension are expected to be orientational, we measure the time correlation function of the bond-orientational parameter defined as

$$C_{\Psi}(t) = \frac{\langle \sum_i \psi_6^i(t) [\psi_6^i(0)]^* \rangle}{\langle \sum_i |\psi_6^i(0)|^2 \rangle} \quad (3.31)$$

Where  $\psi_6^i$  is defined in Eq. (3.15). This time correlation function is normalized to one at zero time and it does not quantify the degree of hexagonal order in the system. Instead it

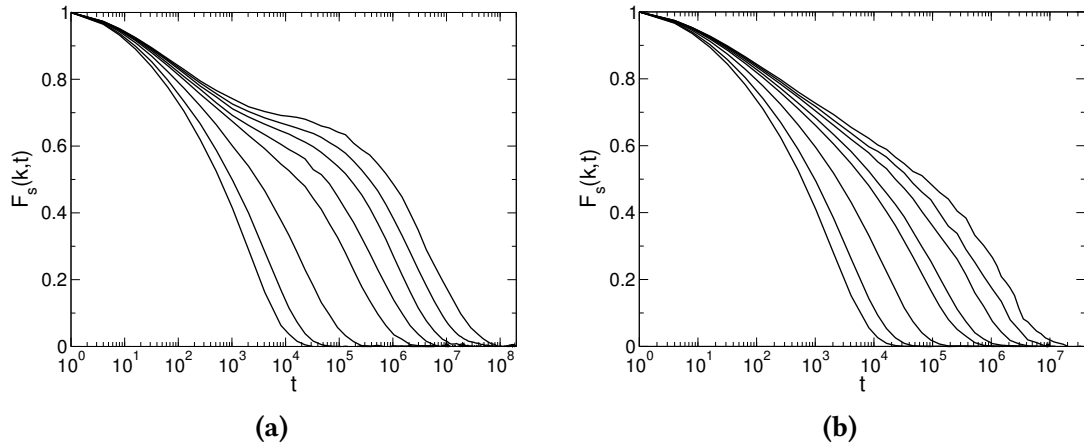
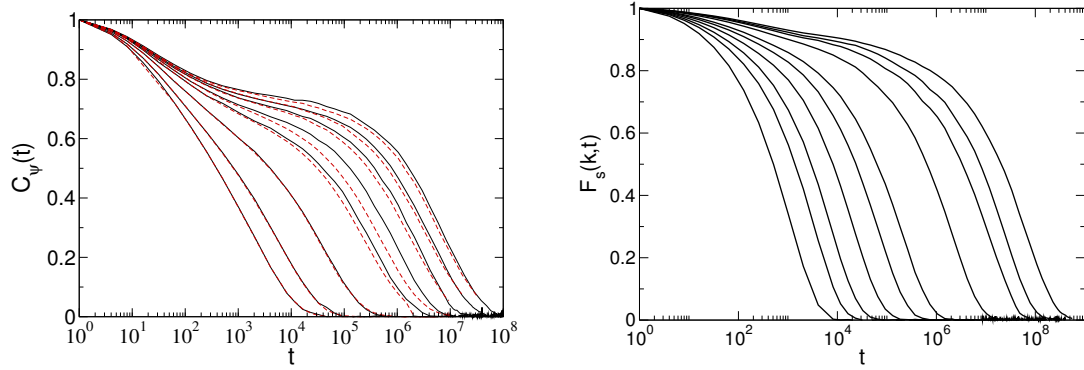


**Figure 3.23** – Self-density relaxation times for standard Monte Carlo simulations in two dimensions for a system of  $N=300$  (a) and  $N=20000$  (b) particles. We notice the absence of well defined plateau increasing the system size. The results are obtained at  $T=0.300, 0.250, 0.200, 0.170, 0.160, 0.150, 0.145, 0.140$ .

detects changes in time of the position of the particles in the nearest neighbour shell. This allows to define a bond-orientational relaxation time as  $C_\Psi(\tau_\Psi) = e^{-1}$  that corresponds to the timescale for relaxation of the local environment. We report the result in Fig. 3.24a both for  $N = 300$  with full black lines and for  $N = 20000$  with red dashed lines. Here we observe that a two step decay is present for both system sizes, confirming previous literature results [103]. Relaxation are slightly faster in the bigger system and this might be an effect caused by long wavelength fluctuations.

Next we introduce swap moves using the same setting as before. For this system swap acceptance is high ( $a \sim 20\%$ ). We notice that the nature of density fluctuations in presence of swap dynamics changes remarkably. At temperature above and close to  $T_{MCT}$  the glassy dynamics disappears and density relaxations happens exponentially without caging. This was already observed in three dimensional system (see Fig. 3.2a). However, in that case, by lowering the temperature in swap Monte Carlo simulations,  $F_s(k, t)$  developed a plateau reminiscent of the standard supercooled dynamics. In the two dimensional system the situation deeply changes. By cooling, the vibrational dynamics is always localized and short-ranged, while timescales for relaxation grow. However the decay of density correlation function remains purely exponential. This can be observed in Fig. 3.24b where  $F_s(k, t)$  is shown as a function of time for the big system ( $N = 20000$ ).

Finally, we extract relaxation times from correlation functions for both translational and orientational degrees of freedom in standard and swap simulations. We report the result in Fig. 3.25. As usual we show with empty (full) symbols results from standard (swap) simulations. The standard kinetic arrest presents features already accounted for by the previous discussion. Density relaxations show system size dependence, the small systems being slower to relax due to the presence of transient localization. The decoupling



(a) Bond-orientational time correlation function for standard simulations. Black full lines are for  $N=300$ , red dashed lines are for  $N=20000$ . Small system size dependency are detected. Results are for the same temperatures as in Fig. 3.23.

(b) Self-intermediate scattering function for swap simulations of the  $N=3000$  system. No short time relaxation is present and the decrease of temperature has the main effect of stretch times for short ranged vibrations. Results are  $T=0.200, 0.120, 0.092, 0.070, 0.0555, 0.047, 0.035, 0.030, 0.028, 0.026$ .

Figure 3.24 –

between relaxation time of the smaller ( $N = 300$ ) and the biggest ( $N = 20000$ ) system can be quantified with a maximum factor of 50. On the other hand relaxation times from orientational degrees of freedom  $\tau_\Psi$  superimpose on the same curve using different sizes. Performing a power law fit (see Eq. 1.9) on  $\tau_\alpha$  for the small system we found  $T_{MCT} = 0.140$ . As for swap simulations, in Fig. 3.25 we observe that the system can be equilibrated at extremely low temperatures, well below  $T_{MCT}$ , with a maximal speed up observed around  $T_{MCT}$  of almost four orders of magnitude. We detect small system size dependency for translational relaxations, with an  $\alpha$ -relaxation time slightly smaller increasing the system size. This may be due to the fact that reducing the temperature the effect given by long wavelength fluctuation becomes weaker [105]. Interestingly, we found that swap relaxation times at low temperatures are well described by an Arrhenius law. At this point we are not able to give an exact interpretation of this behaviour, which adds a tile in the 2D puzzle. Although this suggests that swap dynamics influences deeply the elastic behaviour of the system. Overall we confirm the fact that standard Monte Carlo dynamics reproduces, at least qualitatively, results found with Brownian dynamics [103]. Moreover the nature of glass transition in swap Monte Carlo simulations is fundamentally different from the three dimensional analogous, with the disappearance of caging, exponential decays and Arrhenius relaxation times. The results presented in this section suggest that the glass formation in two dimensions could be fundamentally different from the three dimensional case, although an investigation of thermodynamic properties would be needed to better elucidate this point. This problem will be addressed in the next chapter.

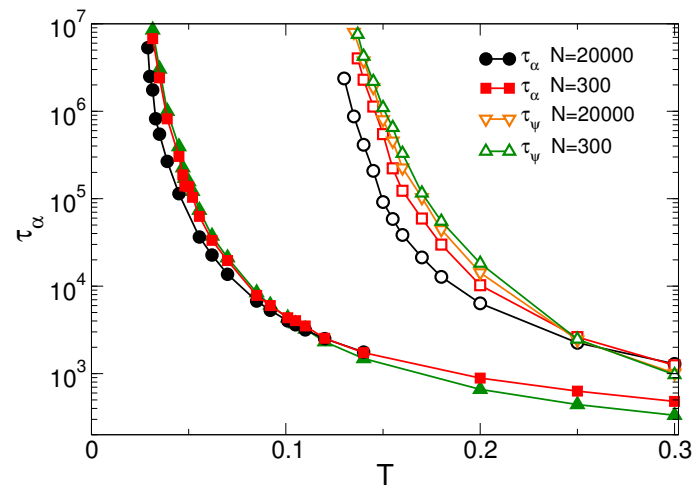


**Figure 3.25** – Relaxation time as a function of the temperature for standard (empty symbols) and swap (full symbols) simulations for two system sizes  $N=300$ ,  $N=20000$ . In standard simulations density relaxations decouples for different system sizes whereas orientational degrees of freedom have same relaxation timescales. In swap simulations orientational and translational relaxation have the same timescales to happen and smaller size effects are observed.

# Chapter 4

## Thermodynamic properties at deep supercooling

Supercooled liquids show a sudden dynamical arrest decreasing the temperature [133]. The reason for this behaviour has no universally accepted theoretical explanation and some competing theories have been proposed through the years [6]. Some of them present arguments that rely on thermodynamics and static observables to explain the change in the dynamical properties, such as the Adam-Gibbs theory (AG) [14], Random First Order Transition (RFOT) theory [17] and Frustration Limited Domain theory [19]. On the other hand, there are theories that explain the glass formation using purely kinetic concepts such as Dynamical Facilitation theory [176]. All these theories have never been tested in a real glass-forming systems beyond the kinetic glass transition, the slowness of the system being the main obstacle for conclusive statement on the glass transition. In the previous chapter we show that using specific models and techniques it is possible to equilibrate beyond both the computational and the experimental kinetic slowing down. This allows measuring static and thermodynamic quantities in a regime unattainable so far in standard simulations and even in experiments. This chapter will be dedicated to revisit some open problems of the glass transition in this novel region and in the next five sections we address five different open problems.

In Sec. 4.1 we discuss the relation between the jamming and the glass transition. Thanks to extremely well equilibrated hard spheres we are able to show that the equilibrium fluid phase can be found at, and even beyond, the jamming density, and we will discuss the implications that this result has for the theoretical explanations of jamming.

Sec. 4.2 is dedicated to study the existence of a Kauzmann transition lowering the temperature and its dependence on dimensionality. The new temperature regime allows us to understand that the thermodynamic point of view of the glass transition is relevant and must be taken into consideration in a theory of the glass formation. Moreover, performing simulations in two and three dimensions, we find out that the glass formation and the existence of a finite Kauzmann temperature  $T_K$  may strongly depend on the dimensionality of the system.

In Sec. 4.3 we investigate the growth of amorphous order and of a static correlation length throughout the cooling process. We find that a point-to-set correlation length increases monotonically both in two and in three dimensional systems beyond the experimental glass transition. At the same time we measure the configurational entropy using four different possible definitions for this quantity.

The connection between the dynamical slowing down and the thermodynamic properties is investigated in Sec. 4.4. Here we explicitly test the dependence of relaxation times on configurational entropy and on the static correlation lengthscale in this new simulation range, and we will see how simulation timescales can affect the link between statics and dynamics.

The last section (Sec. 4.5) is dedicated to the relation between the topology of the potential energy landscape and the dynamics. Here we show the absence of a geometric transition across the Mode-Coupling crossover.

## 4.1 Equilibration of a hard sphere fluid at and beyond the jamming density

*Simulations and analysis of this section were performed by L. Berthier, D. Coslovich and M. Ozawa. Results are published in Ref. [111].*

We discussed before (Sec. 3.7.4) the analogy between glassy behaviour of soft and hard spheres. We saw that a polydisperse hard sphere liquid can enter a supercooled regime by compression up to the point where a kinetic transition steps in at  $\phi_g$ . By further compression the system reaches the packing fraction  $\phi_J$  at which it is said to be *jammed* [177]. This *jamming transition* is characterized by isostaticity, which means that every particle has on average  $2D$  contacts with the neighbours. The reason for this is given by the Maxwell argument [178]. In recent years a huge research effort has been devoted to the investigation of the relation between the glass and the jamming transition. The debate became particularly intense after Liu and Nagel proposed to reunify the two phenomena in a single phase diagram using as state variables the temperature, the external loading and the volume fraction [179]. In the following years two possible theoretical scenarios were proposed. One [180, 181] predicts that increasing the density the system would first encounter a dynamical glass transition point characterized by a dynamical arrest. Then, by further compression, it would arrive at the end point of the equilibrium fluid branch which would correspond to the jamming transition point. Another scenario [182, 183] predicts the existence of a thermodynamic glass transition point by increasing the density above the dynamical glass transition regime. The Kauzmann point would coincide with the end point of the fluid branch and the jamming transition would appear for larger densities.

On the computational side, giving an answer to this problem is not easy. This is mainly due to the intervention of the glassy slowing down around  $\phi \sim \phi_{MCT}$ , at which the system stops to be an equilibrium fluid, happening for densities well below the jamming densities. Consequently, the only way to relate glass and jamming phases is relying on extrapolation from the accessible equilibrium regime and compare with jamming densities. However, this procedure give inconclusive results.

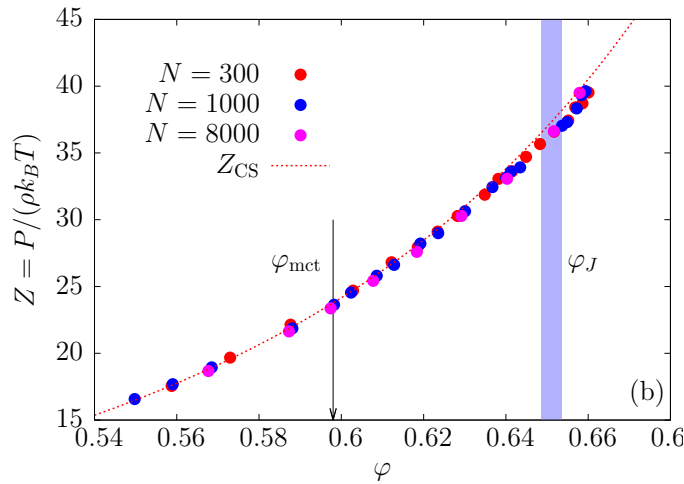


**Figure 4.1** – Equilibrium equation of state obtained with swap simulations of continuously polydisperse hard spheres for different system sizes. Our equilibrium data go beyond the shaded area, which represents the determined range of jamming densities. The dashed line is the Carnahan-Stirling empirical expression [184].

For this reason we want to exploit the huge dynamical gain obtained in swap simulations (Sec. 3.7.4) to address the problem in a completely new density region. Details of the system were explained before, and we recall here that we have been able to thermalize this system at extremely high packing fractions, beyond the experimental glass transition. The equilibration issue has then been partially resolved. The next step is to locate the jamming density. To this end we start from dilute hard spheres, and we follow two methods. In the first one uses constant pressure simulations, imposes a very high pressure, and measures the long time limit of the volume fraction [10]. The second approach starts from low packing fraction, converts the hard spheres into harmonic spheres and compress and expand the system iteratively until isostaticity has been reached [185]. These two protocols give similar values of the volume fraction and allow the definition of  $\phi_J$ , a range of density at which jamming is happening.

It turns out that equilibration of the hard sphere fluid is possible at the jamming transition densities and even beyond. This is shown in Fig. 4.1 where the equation of state is reported as a function of the inverse pressure  $Z$  and the packing fraction  $\phi$ . Standard simulations fall out of equilibrium around  $\phi_{MCT}$ . On the contrary, swap simulations can obtain equilibrium values at higher packing fractions even beyond the shaded area that indicates jamming densities measured through independent protocols.

This result questions both the theoretical predictions discussed before and asks for a third theoretical explanation. The first hypothesis that jamming would occur at the end of the fluid equilibrium line becomes impossible, since jammed state and equilibrium can coexist at the same densities. On the other hand, the second theoretical prediction, that jamming would occur for densities above a Kauzmann transition density is not completely ruled out, since jamming and thermodynamic glass transition could be disconnected phenomena, the first happening out of equilibrium and the second at equilibrium. Further details about simulations and result can be found in Ref. [111]. This result represents the first case in which we use swap simulations to provide elucidations of longstanding problems, those being possible since a totally new regime is now accessible.

## 4.2 Configurational entropy in extremely supercooled liquids: assessing the role of dimensionality

*Results of this section were produced in collaboration with M. Ozawa*

### 4.2.1 Why measuring configurational entropy?

One of their key features of liquids is a larger specific heat as compared to the crystal that implies a faster entropy decrease as compared to the crystalline entropy [133, 2]. For this reason Kauzmann introduced the configurational entropy which is experimentally defined as the total liquid entropy minus the crystalline entropy and accounts for the number of allowed states that the system can assume at a given temperature [3]. Extrapolating linearly its behaviour at temperature below the experimental transition, this quantity becomes zero at a finite temperature  $T_K$ , for which the crystal and the supercooled liquid have the same entropy: this is called a *Kauzmann transition*. The existence of a finite  $T_K$  is a longstanding problem of the glass transition studies and, as anticipated in the introduction, this debate assumed the status of one of the most interesting open problems of condensed matter physics. Thereupon two theoretical positions exist. In one case the presence of a finite transition temperature is rejected and thermodynamics does not play any role in the glass formation. In the other case the transition is believed to exist and the dynamical slowing down is explained using a thermodynamic point of view.

Equilibration of supercooled liquids at low temperatures represents an improvement in the solution of this problem, getting closer to the putative transition point and, in the best case scenario, allowing a conclusive statement on the transition. For instance, computational studies clarified the fate of the Kauzmann transition in silica [87]. Equilibrating a computational model of silica at very low temperatures it was found a fragile

to strong crossover through the bending of the configurational entropy corresponding in a peak in the specific heat. This allowed to better understand the *strong* behaviour of silica usually observed in experiments and to confirm computationally the absence of a Kauzmann transition for finite temperatures. The situation for many others fragile glass formers remains unclear. The main problem is that these systems cannot be equilibrated at temperatures low enough that something remarkable can be said regarding the existence of a finite  $T_K$ .

Configurational entropy has been measured in many fragile glass formers such as hard spheres [89], repulsive soft spheres [88] or binary mixtures of Lennard-Jones particles [86, 84]. All these literature results showed a decreasing configurational entropy with lowering the temperature. However, these simulations were not able to access very low temperatures (or high density for hard spheres) and they fell out of equilibrium 8 orders of magnitude of relaxation times far from the laboratory glass transition. Most of the studies were performed for three dimensional glass formers, but evidences of a decreasing configurational entropy were also found in two and four dimensions [186, 187]. The dependence on dimensionality should not be underestimated since the mean field theory of glasses has been developed at infinite dimension [18] and all the thermodynamic transitions and properties found in that framework have an unknown fate when varying the dimension.

The first method to compute configurational entropy in a simulation was introduced more than a decade ago [86]. It relies on potential energy landscape (PEL) calculations and thermodynamic integration. Namely, one computes the total liquid entropy accessible at a certain temperature and then subtracts the vibrational entropy. This technique was largely used in many glass-forming liquids over the last 15 years.

In this section we address two problems at the same time. First, thank to the thermalization technique developed in chapter 3 we are now able to compute the configurational entropy in a regime comparable with experiments, going much further than previous simulations and closing the gap with laboratory results. Secondly, we test the dimensional dependence of the entropy, employing both a two and a three dimensional systems.

Our models are the non-additive continuous polydisperse model of Secs. 3.7 and 3.10 with  $n = 12$  and  $\epsilon = 0.2$ . We use systems of  $N = 1000$  and  $N = 1500$  particles respectively for the  $2D$  and  $3D$  case. Here  $D$  is the dimension. In the following we will always report first results for the two dimensional case and then for the three dimensional case. Equilibrium configurations are produced with swap Monte Carlo simulations by quenches to the target temperature. The equilibrium and the absence of ordering in the system is ensured by using the protocol and the analysis detailed in chapter 3. We obtained equilibrium configurations across  $T_{MCT}$  and below the experimental glass transition temperature  $T_g$ , defined through the method discussed in Sec.3.7.3.

### 4.2.2 Total entropy

Following a largely employed procedure [16], we first obtain the total entropy through thermodynamic integration. We use the inverse of the temperature  $\beta$  and we integrate the total entropy  $s_{\text{tot}}(\beta)$  in  $D$  dimensions from the ideal gas limit  $1/T = \beta' = 0$  to the target temperature:

$$s_{\text{tot}}(\beta) = s_{\text{tot}}(0) + \int_0^\beta d\beta' \frac{\partial s_{\text{tot}}}{\partial \beta'} = \frac{1}{N} \left[ (\beta \langle H \rangle)_{\beta=0} - (\beta F)_{\beta=0} + \int_0^\beta d\beta' \beta' \frac{\partial \langle H \rangle}{\partial \beta'} \right] \quad (4.1)$$

$$= \frac{D}{2} + 1 - \ln \rho - D \ln \Lambda + \beta e(\beta) - \int_0^\beta d\beta' e(\beta') + s_{\text{mix}}. \quad (4.2)$$

In the first line,  $F(\beta)$  is the free energy,  $H$  is the Hamiltonian and the angle brackets indicate the average on the canonical ensemble. In the second line,  $e(\beta)$  is the potential energy,  $s_{\text{mix}}$  the mixing entropy, and  $\Lambda = \sqrt{2\pi\beta\hbar^2/m}$  the De Broglie thermal wave.

We notice that the integral in expression (4.2) diverges in the high temperature limit. To compute it, we divided the integration interval in two parts: a high temperature regime  $\beta' \in [0, \beta_0]$  and an intermediate to low temperature regime  $\beta' \in (\beta_0, \beta]$ , so that the last integral in Eq. 4.2 can be decomposed as

$$I = \int_0^\beta d\beta' e(\beta') = \int_0^{\beta_0} d\beta' e(\beta') + \int_{\beta_0}^\beta d\beta' e(\beta') = I_F + I_N. \quad (4.3)$$

We set  $\beta_0 = 6.65 \times 10^{-5}$  and  $\beta_0 = 1.68 \times 10^{-3}$ . The integral  $I_N$  can be obtained by straightforward numerical integration.

For the integral  $I_F$ , instead, we perform a polynomial fit on the high temperature values of the potential energy, and we obtain an analytic expression that we employ instead of using the numerical integration of  $e(\beta \rightarrow 0)$ , which is divergent. In a general  $D$  dimensional system of particle interacting through a potential  $v(r_{ij}) \propto r_{ij}^{-n}$  one can obtain the high temperature expansion of the potential energy using Mayer cluster expansion [1]

$$e(\beta) = A\beta^{(D/n)-1} + B\beta^{(2D/n)-1} + C\beta^{(3D/n)-1} + \dots, \quad (4.4)$$

where  $A$ ,  $B$  and  $C$  are constant that can be obtained by polynomial fit. Then the integral  $I_F$  can be rewritten as

$$I_F = \frac{n}{D} A \beta_0^{D/n} + \frac{n}{2D} B \beta_0^{2D/n} + \frac{n}{3D} C \beta_0^{3D/n} + \dots. \quad (4.5)$$

We use up to the second order of the expansion to perform the fit in both two and three dimensions.

The result for  $s_{\text{tot}} - s_{\text{mix}}$  from the integration are reported in Fig. 4.2. Points are for the measured data and curves are low temperature extrapolations. This latter is possible using the Rosenfeld-Tarazona expression that is based on density functional theory and

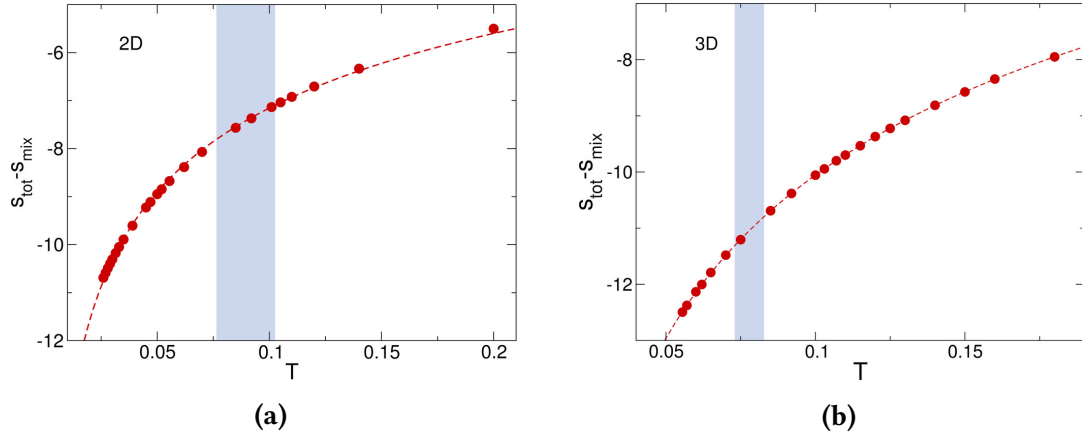


**Figure 4.2** –  $s_{\text{tot}} - s_{\text{mix}}$  as a function of  $T$ . The dashed curve is the Rosenfeld-Tarazona expression: (a)  $s_{\text{tot}} - s_{\text{mix}} + 2 \ln \Lambda \propto T^{-2/7}$ , (b)  $s_{\text{tot}} - s_{\text{mix}} + 3 \ln \Lambda \propto T^{-2/5}$ . Shaded areas indicate the location of the laboratory glass transition.

the free energy expansion [188] and gives an expression for the potential energy at low  $T$  in general dimension:

$$e(T) \propto T^{\frac{2}{3D+1}}. \quad (4.6)$$

We confirm the reliability of this extrapolation in our range of simulations.

### 4.2.3 Mixing entropy

To compute the mixing entropy  $s_{\text{mix}}$  special care should be used. The usual expression of the mixing entropy of a general system of  $N$  particles grouped in  $M$  different species each containing  $N_i$  particles goes as [189]

$$s_{\text{mix}}(M) = -N \sum_{i=1}^M \frac{N_i}{N} \ln \frac{N_i}{N}. \quad (4.7)$$

This expression is well defined in case of mixtures of particles for which it gives a finite value. On the other hand in the case of continuously polydisperse system, when  $M = N$ , the expression gives an infinite value in the thermodynamic limit. This problem was tackled in Ref. [146] where it is shown how the mixing entropy can be computed by mapping the system onto an effective description in term of a mixture of  $M^*$ -component for which a finite mixing entropy can be computed. The details for computing the value of  $M^*$  are reported in Ref. [146].

Here we only show the final result for the mixing entropy in the two and three dimensional cases in Fig. 4.3. We perform fits to a polynomial of order three (Fig. 4.3a) and to a straight line (Fig. 4.3b) of the raw data, and we find an analytical expression for  $s_{\text{mix}}$ .

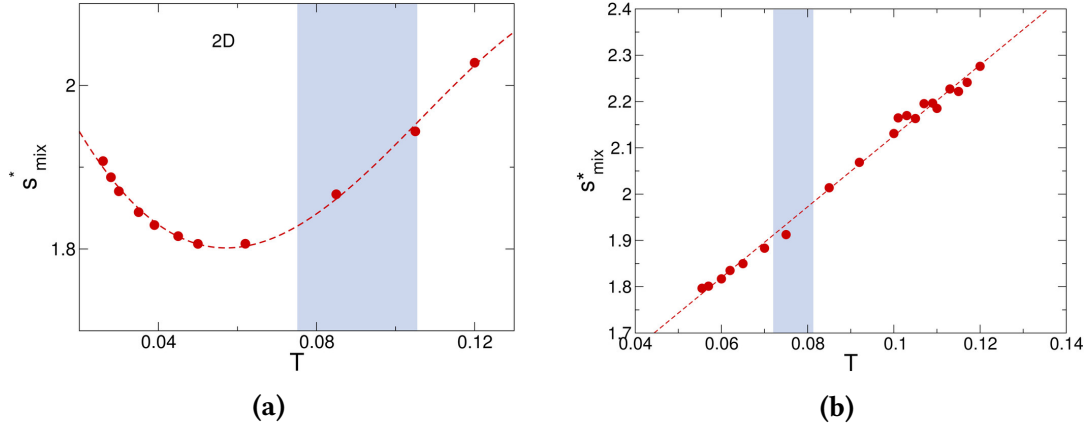


**Figure 4.3** – The effective mixing entropy  $s_{\text{mix}}^*$ . The dashed line is an empirical fit (a) to a polynomial of order three and (b) to straight line. Shaded areas indicate the location of the laboratory glass transition.

#### 4.2.4 Vibrational entropy

To compute the configurational entropy, we need to compute the vibrational entropy. Experimentally this quantity is usually identified as the vibrational entropy of the crystalline state [133]. In simulations, it can be directly measured by looking at vibrations around an amorphous configuration in the PEL framework, where it represents the average volume in configurational space of vibrational contribution to the partition function. The free energy per particle in the PEL formalism can be written as:

$$f(T, V) = T s_c + f_{\text{basin}}. \quad (4.8)$$

Here the  $f_{\text{basin}}$  is the free energy of a system constrained to be in one basin and  $T s_c$ , where  $s_c$  is the configurational entropy, counts the number of basin explored at temperature  $T$ . To compute the vibrational entropy inside a basin one can start from an inherent structure and measures vibrations around the lowest energy point. Close to a local minimum of the PEL, the total potential energy in the inherent structure can be expanded such that:

$$V(\{r\}) = e_{IS} + \sum_{i,j,\alpha,\beta} \left. \frac{\partial^2 V(r)}{\partial r_i^\alpha \partial r_j^\beta} \right|_{IS} \delta r_i^\alpha \delta r_j^\beta + \dots \quad (4.9)$$

$$= e_{IS} + \sum_{i,j,\alpha,\beta} (\text{Hess } V(r))_{i,j,\alpha,\beta} \delta r_i^\alpha \delta r_j^\beta + \dots \quad (4.10)$$

where the first part accounts for the energy of the inherent structure and the second is a second order expansion of the potential. Here  $\text{Hess } V\{r\}$  is the  $ND \times ND$  Hessian of the potential, with  $D$  the dimension and  $N$  the number of particles. The corresponding expression for the basin free energy becomes:

$$f_{\text{basin}}(e_{IS}, T, V) = e_{IS} + \frac{T}{N} \left\langle \sum_{a=1}^{DN} \ln \beta \hbar \omega_a \right\rangle. \quad (4.11)$$

Here the Hessian has been diagonalized and the  $\omega_\alpha$  represents its  $DN$  eigenvalues. This equation leads to the following expression for the vibrational entropy

$$s_{\text{harm}}(\beta) = \frac{1}{N} \left\langle \sum_{a=1}^{DN} \{1 - \ln(\beta \hbar \omega_a)\} \right\rangle_{\text{IS}}, \quad (4.12)$$

that represents the harmonic contribution to the vibrational entropy in the PEL formalism. In order to compute this quantity, we start from equilibrium configurations at a finite temperature, and we minimize them at  $T = 0$  through a conjugate gradient algorithm [190]. This brings the system from a generic point in the configurational space to the underlying minimum of the basin of attraction, that is, the inherent structure. Then in order to obtain the  $ND$  eigenvalues we perform a direct diagonalization of the hessian matrix  $\text{Hess } V\{r\}$  using a parallel version of the *LAPACK* package implemented in the *Intel MKL* library [191]. The result for  $s_{\text{harm}}$  are reported in Fig. 4.4

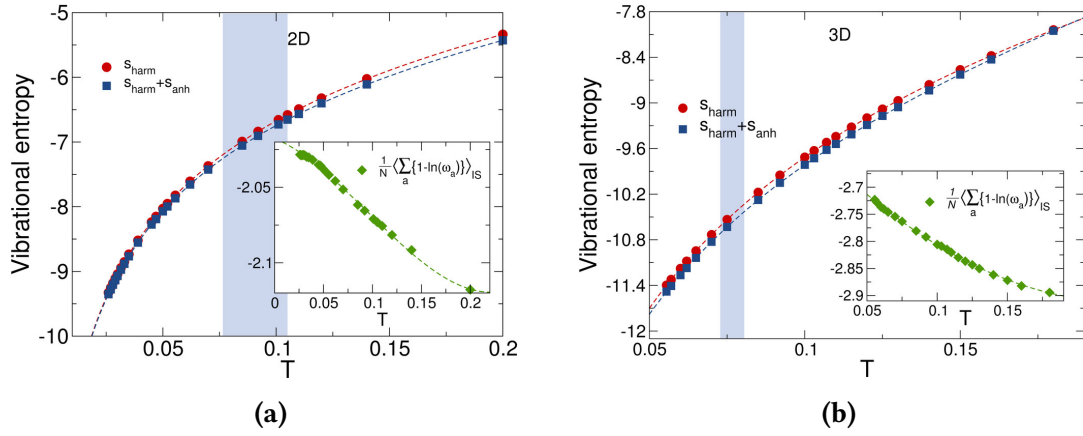


**Figure 4.4** – The harmonic vibrational entropy  $s_{\text{harm}}$  and anharmonic correction  $s_{\text{anh}}$ . The dashed curves are obtained by a quadratic fit for  $(1/N) \sum_{a=1}^{3N} \{1 - \ln(\omega_a)\}$ . (a) 2D system, (b) 3D system. Shaded areas indicate the location of the laboratory glass transition.

where we also show the result of an empirical quadratic fit that allows extrapolation to lower temperature. We notice that this quantity increases with annealing temperature, which corresponds to the physical situation in which by increasing the temperature vibrations start to be large and the harmonic approximation gives a worse description of the vibrational entropy since some anharmonic effects take place. This is why we also take into consideration the anharmonic component to the vibrational entropy.

The anharmonic energy  $e_{\text{anh}}(T)$  can be quantified as [16]

$$e_{\text{anh}}(T) = e(T) - e_{\text{IS}}(T) - \frac{D}{2}T, \quad (4.13)$$

using the equipartition theorem. Assuming both that the anharmonicity is independent on the basin depth and that it does not contribute to the specific heat at  $T = 0$  then Eq. 4.13 can be written as a polynomial expansion in temperature of order  $i \geq 2$ :

$$e_{\text{anh}}(T) = \sum_{k=2} a_k T^k, \quad (4.14)$$

where  $a_k$  are temperature independent coefficients. Then we can obtain the anharmonic entropy by thermodynamic integration of this quantity

$$s_{\text{anh}}(T) = \sum_{k=2} \frac{k}{k-1} a_k T^{k-1} \quad (4.15)$$

Values of the anharmonic entropy in this system are very small and represent a small correction to the total vibrational entropy  $s_{\text{vib}} = s_{\text{harm}} + s_{\text{anh}}$  that is shown in Fig. 4.4.

#### 4.2.5 Configurational entropy

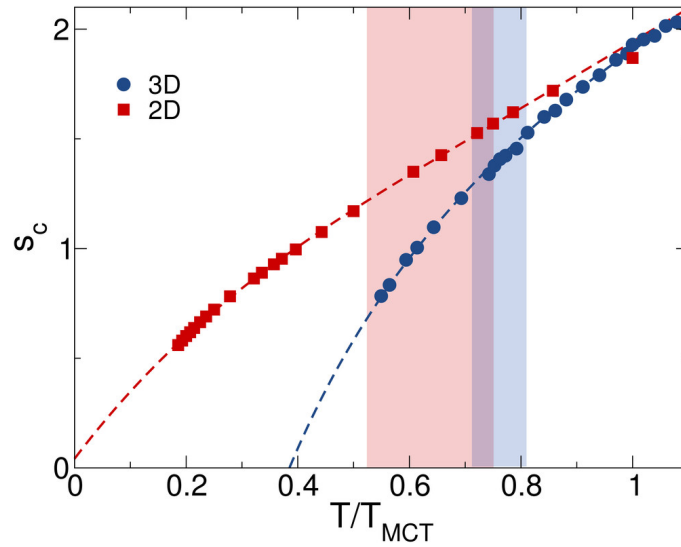


**Figure 4.5** – The configurational entropy of the soft spheres,  $s_c = s_{\text{tot}} - s_{\text{vib}}$ , in two and three dimensions as a function of temperature rescaled by  $T_{MCT}$ . The location of the laboratory glass transition is indicated with shaded regions,  $T/T_{MCT} = 0.539 - 0.748$  (red) and  $T/T_{MCT} = 0.71287 - 0.80891$  (blue) respectively in 2D and in 3D, obtained with the method discussed in Sec.3.7.3. The dashed curve is an extrapolation based on fits of the individual terms.

Putting the various pieces together we obtain the configurational entropy reported in Fig. 4.5. Overall this quantity shows a decrease with temperature, however two different behaviours are observed changing the dimensionality. In three dimensions, it has a strong decrease and it can be extrapolated using a Rosenfeld-Tarazona expression [188] to a finite temperature  $T \approx 0.038$ . In two dimensions, instead, the decrease is less evident and the extrapolation by a polynomial fit leads to  $T = 0$ . In this case we prefer a polynomial fit since the Rosenfeld-Tarazona expression is unable to describe the potential energy for a vanishing temperature. We observe that, in both cases, the lowest accessible temperature, thanks to the technique developed in Ch. 3, has now decreased from  $T_{MCT}$  to a temperature that is below the laboratory glass transition. This establishes an important methodological improvement in the measurement of the configurational entropy and this result can be directly compared with experiments.

The two dimensional behaviour is difficult to compare with previous results, since, to our knowledge, the only previous measurements of configurational entropy in low dimensions were performed for temperature  $T > T_{MCT}$  in Refs. [186, 187], where  $s_c$  as a function of temperature does not show remarkable differences changing the dimension. Interestingly, in that case, the authors found a deviation from the Adam Gibbs relation in the two dimensional system [186]. Whether this deviation is related to our results, it cannot be clarified here. Our extrapolation suggests that the Kauzmann transition does not exist or that it is pushed to  $T = 0$  in this two dimensional system. We will be discussing in the next section this result and its possible consequences.

Comparing the three dimensional case with previous literature results, we notice a clear decrease, by a factor 2.5, of the entropy compared to its value at  $T_{MCT}$ . Previous computational results have also found decreasing configurational entropy, as for instance in Ref. [89] where a decreasing of a factor 2 – 2.5 was found in a hard sphere system. However, this was in a simulation region between the onset temperature  $T_0$  and  $T_{MCT}$ , which is very different from our case. Moreover, in that case, the measured configurational entropy at the Mode-Coupling temperature  $s_c(T_{MCT}) \approx 1$  while in our case  $s_c(T_{MCT}) \approx 2$ . This difference in absolute values can be explained by the fact that the literature model was a binary mixture of hard spheres, whereas in our case we use soft particles which are polydisperse. This polydisperse nature of the system increases the mixing entropy, and results in a different value of the configurational entropy. Overall, direct comparison with previous computational findings is difficult because of the difference in model and in simulation ranges. As for experiments, a decreasing configurational entropy in three dimensional glass-forming liquids is known since a long time. As shown in Fig. 1.2 the relative decrease of configurational entropy strongly depends on the system and our 2.5 factor is comparable with the results for glycerol [133]. Our findings for the three dimensional systems agrees with the existence of a finite Kauzmann transition temperature  $T_K = 0.38T_{MCT}$ .

The results shown in these section suggest that a thermodynamic perspective of the glass formation process is needed. However, a decrease of configurational entropy alone is not enough to validate or disprove theoretical viewpoint of the glass transition, not completely explaining the mechanism, both energetical and microscopical, behind the glass formation. Many questions are left unanswered: Is the decrease of configurational entropy accompanied by the growth of a static correlation length? How is the configurational entropy measured by thermodynamic integration related to the complexity of the mean field theory of glasses? How are these thermodynamic properties related to the dynamical slowdown? We try to partially answer some of these questions in the next sections.

### 4.3 A static correlation length grows throughout the glass formation

*This section presents results obtained in collaboration with L. Berthier, P. Charbonneau, D. Coslovich, M. Ozawa, S. Yaida. Point-to-set length was measured by P. Charbonneau and S. Yaida. Configurational entropy in the Franz-Parisi framework was measured by L. Berthier and D. Coslovich.*

#### 4.3.1 Counting metastable states: 4 different methods

A debated problem about configurational entropy concerns its definition. Within the replica theory configurational entropy is defined as an entropic contribution to the total entropy that counts the number of accessible metastable states [192]. This idea is very far from the experimental definition of configurational entropy that relies on subtraction of the crystalline entropy to the total liquid entropy [3, 133]. This is a practice that cannot be completely justified from a theoretical point of view, since one would really compute a quantity that gives the number of accessible states in the liquid phase rather than comparing the liquid phase with the crystalline one. However, this is an experimental limitation that cannot be overcome for the moment.

The commonly used method to compute configurational entropy in simulations is based on the Potential Energy Landscape (PEL) and it relies on an identification between inherent structure, i.e. minima of the PEL, and thermodynamic states that we employed in the previous section. However, this is not the only way to estimate the number of accessible states in a supercooled liquid. In the following we will introduce three other possible definitions of configurational entropy, more directly related to the mean field complexity.

The thermodynamic integration method was recently questioned in Ref. [38] since it relies on the identification of *inherent structures* with *thermodynamic states*, which is unsafe from a theoretical point of view. In the same article another method was proposed to compute configurational entropy in supercooled liquids that is closer to the mean-field theoretical tools and is based on the Franz-Parisi theoretical construction [193]. In this case the configurational entropy can be directly related to a first-order phase transition happening in liquids coupled through a field  $\epsilon$ . The situation is computationally very similar to the one discussed in chapter 2. First an overlap  $Q$  is defined to quantify the degree of similarity between two configurations as in Eq. 2.2. The equilibrium probability of the overlap can be defined as  $P_\epsilon(Q) = \langle \delta(Q - Q_{12}) \rangle$  from which the free energy can be rewritten in a constrained equilibrium form as  $V_\epsilon(Q) = -\frac{T}{N} \ln P(Q)$ . In unconstrained system this function is convex as a consequence of the gaussianity of the overlap. By introducing a coupling field  $\epsilon$  conjugated variable of the overlap  $Q$  one can induce a first order phase transition between a low overlap phase  $Q_{\text{low}}$  and a high

overlap phase  $Q_{\text{high}}$  for temperature lower than a critical temperature  $T_c$  which is close to  $T_{MCT}$ . The presence of these two phases changes the shape of the free energy  $V_\epsilon(Q)$  which develops a secondary minimum. The behaviour for the unconstrained system can be obtained by performing biased simulations with a coupling field  $\epsilon$  and then get back to unbiased simulation through a histogram reweighting technique, resulting in the appearance of linear tails in  $V_{\epsilon \rightarrow 0}(Q)$ . The configurational entropy can be defined as the free energy price that the system has to pay to remain localized in configuration space, consequently it is equal to the difference in free-energy in the high- $Q$  phase and the low- $Q$  phases in the zero field case:

$$s_c = \lim_{\epsilon \rightarrow 0} (V_\epsilon(Q_{\text{high}}) - V_\epsilon(Q_{\text{low}})) = V(Q_{\text{high}}) - V(Q_{\text{low}}). \quad (4.16)$$

Using the reweighting method one could also find the value of the field  $\epsilon^*$  corresponding to a phase coexistence between a high and a low  $Q$  [63]. This is characterized by an overlap probability distribution  $P(Q, \epsilon^*)$  presenting two peaks with equal amplitude. This  $\epsilon^*$  value must be interpreted as the field value needed to *tilt* the potential  $V_{\epsilon^*}(Q)$  towards coexistence. Since the relation  $V_{\epsilon^*}(Q) \approx \epsilon^* Q$  holds to a good approximation, one can measure  $s_c$  by using

$$s_c = \epsilon^* (Q_{\text{high}} - Q_{\text{low}}) \quad (4.17)$$

In previous simulations the configurational entropy measured by Eq. (4.16) was found to decrease with decreasing temperature and to be smaller than the configurational entropy computed by thermodynamic integration. This is consistent with the fact that it is more closely related to the number of metastable states of the system rather than to the number of energy minima.

Even though of relevant in characterizing the thermodynamic properties of glass-forming liquids, any measure of the configurational entropy will always leave unanswered the question about the microscopic mechanism of glass formation. Some theories as the Adam Gibbs or the Random First Order Transition theory (RFOT) try to explain glass formation using the notion of correlated regions in the system. This correlation has mainly an entropic nature and the system can be thought of as a mosaic made of tiles in different thermodynamic state whose size increases with decreasing temperature. In the RFOT theory [17] the typical size of correlated tiles is given by a correlation length  $\xi_{PTS}$  that has been introduced more than ten years ago in [34]. In computations,  $\xi_{PTS}$  can be studied by first pinning the particle in an equilibrium configuration. Then only the particles inside a cavity of radius  $R$  are left able to explore the phase space in presence of the constraint given by particles outside the cavity [72, 116]. Once the phase space has been properly sampled, the new configurations can be compared with the starting one and a degree of similarity can be defined through an overlap function integrated in a small region around the center of the cavity. From the behaviour of this overlap function at different cavity sizes  $R$  a point-to-set length can be extracted at a given temperature. Repeating the measurement at different temperatures allow to measure

$\xi_{PTS}(T)$ . Nowadays the presence of an increasing correlation length is well established in literature [72, 116, 194]. However, the amount of increase measured has always been small, less than a factor 2 with respect to onset temperature value, and correlations have always involved a few particles. In addition to a measurement for the size of correlated regions, also an estimate of the configurational entropy can be directly made by using the point-to-set length. Within RFOT the connection between  $s_c$  and  $\xi_{PTS}$  is given by  $s_c \propto \xi_{PTS}^{-(D-\theta)}$  where the exponent is  $\theta \leq D - 1$ . The minimal assumption is  $\theta = D - 1$  that was also found in mean field computations [193], then configurational entropy can be simply extracted using  $s_c \propto \xi_{PTS}^{-1}$ .

So far we discussed four possible definitions of the configurational entropy. The aim of this section is to test all these different definitions in the completely new regime reached with swap simulations. We do this by performing measurement of configurational entropy using overlap fluctuations and static correlation length  $\xi_{PTS}$ . Whether the different definitions are comparable to each other and their behaviour at very low temperature have never being investigated. This will give useful and compelling information about the Kauzmann transition from observables that have a mean field origin and, at the same time, allow to make a direct comparison with the thermodynamic integration method. As a byproduct we also want to observe the behaviour of  $\xi_{PTS}$  in this totally new regime to observe whether it keeps increasing and quantify the size of correlated regions reducing the temperature. This will give precise indication of the presence of a local growing amorphous order lowering the temperature. As in the previous section we analyze the differences induced by changing dimensionality, comparing the two and the three dimensions case. Following the presentation order used in the previous section, we first discuss results in two dimension and later we introduce the three dimensional case.

### 4.3.2 The two dimensional case

For the two dimensional case we employ the same system as in Sec.3.10 and 4.2, made of continuously polydisperse soft spheres with a polydispersity  $\delta = 0.2$ . For this system we already measured  $s_c$  by thermodynamic integration finding a mild decrease with lowering the temperature, consistent with a  $T_K = 0$ . Here we measure point-to-set correlation length using the cavity technique discussed previously. Fig. 4.6 reports the result for both configurational entropy and the inverse of the static point-to-set length as a function of temperature normalized by its value at the onset temperature  $\xi_{MCT} = \xi_{PTS}(T_{MCT})$ . We observe that the two quantities are consistently decreasing with decreasing temperature. However, they both seem to vanish for temperature  $T = 0$ , discarding the possibility of an entropy crisis at a finite temperature. Measurements have been obtained beyond the laboratory glass transition at temperatures extremely low as compared to equilibrium regime of standard simulations. This result raises many questions on the nature of glass formation depending on the dimension. We think that there are two important issues. First, in the mean field infinite dimension theory the

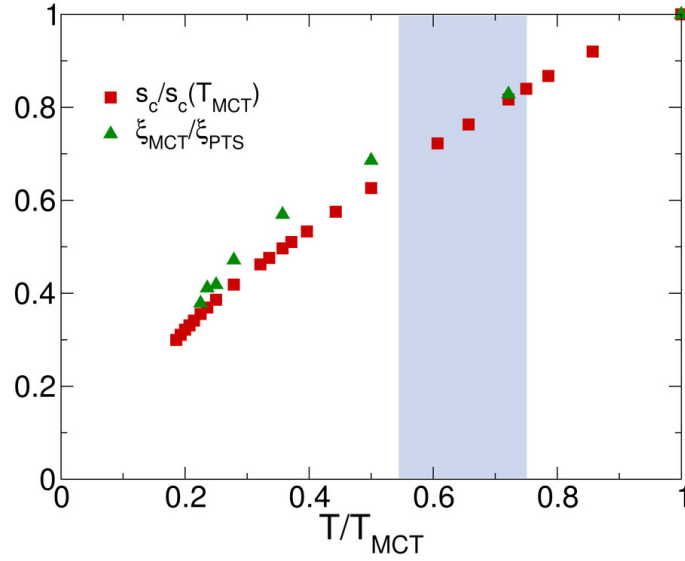


**Figure 4.6** – Red squares indicate configurational entropy by thermodynamic integration. Green triangles indicate the inverse of the point-to-set length normalized by its value at the Mode-Coupling temperature  $\xi_{MCT} = 2.57$ . The shaded area indicate the location of the laboratory glass transition.

existence of a Kauzmann transition was confirmed. However, the presence of fluctuations at finite dimensions could completely change this result [18]. What is then the fate of the Kauzmann transition varying the dimension? Is it possible that it exists in three dimensional systems and it is not present in two dimensional systems? Secondly, as we discussed 1.3.5, the dynamical anomalies in two dimensions with respect to three dimensional case are now established [103]. Here we claim that also a thermodynamic difference is present between two and three dimensions. What is then the relation between dynamics and thermodynamics in two dimensions? To our knowledge, this question has never been asked in real models of glass-forming liquids, with the only exception of Refs. [186, 187].

Generally, in statistical physics, thermodynamic transition can be suppressed varying the dimensionality. In renormalization group analysis of phase transitions, two critical dimensions can be defined as the dimension at which the nature of the phase transition in the system changes [195]. Below the lower critical dimension  $D_c$  there is no phase transition and above the upper critical dimension the critical exponents of the theory can be identified with the one of the mean field theory. In case of some spin systems the lower critical dimensions have been computed. For instance in the Ising model the system has a discrete symmetry breaking depending on the temperature for dimensions above  $D_c = 1$  [196]. Another well established result is given by the Mermin-Wagner theorem that states that no continuous symmetry can be spontaneously broken for dimension equal or lower than  $D_c = 2$  [106]. This also led to the suppression of single crystalline states in two dimensional systems.

More related to disordered systems, there is a theoretical proposal to describe the

behaviour of supercooled liquids and structural glasses in term of the Random Field Ising Model [197, 122], a spin system presenting disorder and exposed to a field. For this model the lower critical dimension is  $D_c = 2$  below which there is no replica-symmetry breaking. For this reason the dimension two could be criticality-free also in real space systems and the self-induced disorder of the spin system could have an equivalent in the Mermim-Wagner fluctuations discussed in Sec. 3.10 and Ref. [103, 198, 107, 108]. Overall, there are few theoretical predictions in two dimensions and it is unclear what one should expect.

Another piece of information useful to understand these two dimensional peculiarities was recently discussed in Ref. [199]. In this article by analyzing vibrational spectra of amorphous solids it was discovered that the nature of low frequency vibrations is different between two and three dimensions. In  $3D$  are both present modes which can be explained using the continuum approximation within the Debye model and modes related to the amorphous nature of the system. These last disappear in two dimension where the low frequency behaviour of the density of state can be completely explained using the Debye theory. Putting all this information together we believe that there is a fundamental difference between glass formation in two or three dimensions and that many questions have still to find an answer.

### 4.3.3 The three dimensional case

*Results shown in this subsection have been included in Ref. [113]*

For the three dimensional case we perform a complete analysis using the four definitions of the configuration entropy. We recall that the first one use thermodynamic integration, the second and the third ones are based on the Franz-Parisi theoretical construction and the fourth is realized computing the point-to-set lengthscale  $\xi_{PTS}$ . We both compare these four independent methods to each other, and we do this in a totally new regime beyond standard simulations. The system employed in this case is the hard sphere model already used in Secs. 3.7.4 and 4.1 and it is made of continuously polydisperse and additive hard spheres. We both employ systems of  $N = 300$  and  $N = 8000$  particles. The large systems were used within the first and the fourth method to compute configurational entropy. The small systems are needed to perform the measurement of overlap fluctuations, since large systems give prohibitive computational times.

Also for this model we measured the configurational entropy by thermodynamic integration. The various pieces are as before: the total entropy, the vibrational entropy and mixing entropy. Total entropy can be integrated in a similar way as reported previously, with the main difference that now the integration must be performed using the packing fraction  $\phi$  as a variable instead of the temperature  $T$ . In a hard sphere system it is not possible to define a hessian matrix without divergences, consequently vibrational

entropy cannot be measured with the method discussed previously. In exchange, one can use a thermodynamic integration known as Frenkel-Ladd method based on performing dynamical simulations of a constrained system [200]. Mixing entropy can be computed in a totally equivalent way as discussed before and reported in Ref. [146]. All the pieces together gives a configurational entropy by thermodynamic integration  $s_c = s_{tot} - s_{vib}$  reported in Fig. 4.7. This plot shows the configurational entropy in  $y$ -axis as a function

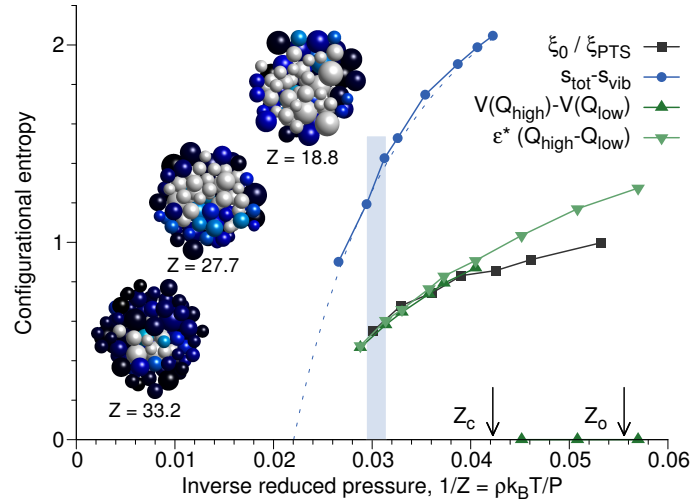


**Figure 4.7** – Four different measurements of configurational entropy as a function of the inverse pressure. The four curves are consistent with an extrapolation to the same pressure  $Z_k \approx 45$ . The blue region locates experimental glass transition pressures.  $Z_c$  and  $Z_o$  are respectively the Mode-Coupling crossover and the onset pressures. The inset shows the typical overlap profiles inside a cavity for three different pressures. The colour code indicates the overlap value from low(white) to high(blue).

of the inverse pressure in the  $x$ -axis. In hard spheres one can map the usual temperature driven glass transition in a reduced pressure driven phenomenon, as discussed in Sec. 4.1. The result is an equivalent representation to the one used before for soft spheres where the pressure of the onset of glassy behaviour is indicated with  $Z_o$  and the pressure of the Mode-Coupling dynamical transition is  $Z_c$ . We observe that the behaviour of the configurational entropy is equivalent to the one previously found in soft spheres. It decreases by more than a factor 2 as compared to its value at  $Z_c$ . Also in this case we are able to obtain a measurement of the configurational entropy in a regime previously unattained neither with experiments or simulations, equilibrating the system across the experimental glass transition that is indicated with a blue box. This temperature regime is defined through a fitting procedure similar to the one of Sec. 3.7.3 and it was found to be in the pressure interval  $Z_g = (32 - 34)$ . The second and the third methods to compute configurational entropy rely on measurements of overlap fluctuations as discussed before. We both measured differences in the high and low- $Q$  value of the free-energy (Eq. 4.16) and the critical field value to induce the phase transition (Eq. 4.17). Results are reported in Fig. 4.7. The two methods give a similar value for the configurational entropy, and they

both can be used in the high pressure regime  $Z > Z_c$ . At low pressures only the third method can be defined, since  $P(Q)$  does not develop evident tails. We observe that the value of the configurational entropy measured with this two methods is similar, however they both show lower values as compared to the one measured by thermodynamic integration. This discrepancy was already observed in Ref. [38], and it is mainly due to the fact that the thermodynamic integration method overcounts the states by identifying inherent structures with states, whereas the Franz-Parisi method is a computational implementation of a replica theory tool and gives a better estimation of the real number of the metastable states.

Finally, for the fourth method, we first compute  $\xi_{PTS}$  at different pressures, and then we estimate the configurational entropy using the fact that the latter is inversely proportional to the increase of amorphous order in the system. We measured an increase of  $\xi_{PTS}$  of more than a factor two with respect to the onset value, this means an amorphous order involving around 200 particles. The result is reported in Fig. 4.7 that shows the inverse of point-to-set length  $\xi_{PTS}$  normalized for its value at the onset pressure  $\xi_o$  as a function of the inverse pressure. This is consistent with the method used in the previous subsection in the two dimensional case.

Interestingly, the four methods result in a similar behaviour for the configurational entropy that decreases with increasing pressure and can be extrapolated by eye at a similar finite value of the pressure  $Z_k \approx 45$ . This three dimensional result solves two open questions. First different methods of measuring the configurational entropy give similar and consistent values. This is very good news for the definition of this quantity. In simulations, as well as in experiments, it is not possible to introduce a quantity completely equal to the one introduced in replica theories. All the methods presented here, as well as the experimental methodology, represent approximations with a different degree of similarity to the theoretical observable. Despite these differences, they all have the same behaviour meaning that the problem of a rarefaction of metastable states increasing the degree of supercooling is well defined. Secondly these measurements have been made in a supercooling regime completely unknown to previous simulations, closing the gap between experimental and computational observations. Although we are still far from the definitive solution of the existence of a Kauzmann transition, the methodological improvement discussed here represents a huge step forward. Overall we observe that the four definitions of configurational entropy follow the same behaviour across many orders of magnitude of relaxation time of the dynamics, and the importance of a thermodynamic perspective of the glass transition is undeniable.

Yet, so far we have not discussed of the explicit relation between relaxation times and thermodynamic observables. This problem will be addressed in the next section.

## 4.4 Critical exponents of RFOT theory close to the ideal glass transition

*This work has been done in collaboration with M. Ozawa*

### 4.4.1 Relating relaxation times and configurational entropy

In the previous section we made a point about the role of thermodynamics in glass formation. However the observation of a decreasing configurational entropy accompanying the increase of the relaxation time is not enough to explain the slowing down.

What would be needed is a theory that gives a quantitative evaluation of the relation between the thermodynamic quantities and the dynamical ones. At the moment there are two theories available that explicitly relate the relaxation times and the configurational entropy, the Adam-Gibbs-Di Marzio theory (AGD) and the Random First Order Transition theory (RFOT). We both discussed them in the introduction (Secs. 1.2.2 and 1.2.4).

The AGD theory has been the first theoretical step to connect dynamics and thermodynamics. This theory relies on the existence of a Kauzmann transition at a finite temperature  $T_K$  and in the original formulation it was predicted a second order nature for this transition. Using the notion of Cooperative Rearranging Regions one can directly relate relaxation times with a decreasing configurational entropy (see Eq. 1.8). The transition would then correspond to a divergence of relaxation times with a vanishing configurational entropy. On the other hand it is a common practice [201] to assume that relaxation times from experiments can be described using a VFT law (see Eq. 3.18). In this case their divergence happens for a finite temperature  $T_0$ . One then is apt to identify the two temperatures  $T_0 \simeq T_K$  as it was empirically established in [201]. This argument allows to merge Eqs. 1.8 and 3.18 in

$$\tau_\alpha = \tau_0 \exp\left(\frac{A}{T - T_0}\right) = \tau_0 \exp\left(\frac{B}{T s_c(T)}\right). \quad (4.18)$$

More recently, this relation was criticized in Ref. [202], where systematic deviations of the ratio  $T_k/T_0$  from unity were found in many experimental glass-forming liquids. This also questioned the existence of a Kauzmann transition at finite temperature and whether the thermodynamic singularity is the cause of the dynamical arrest. Moreover, reinforcing this objection, relaxation times were shown to equally well obey functional forms that do not provide for a dynamical criticality [143, 144].

A deeper explanation of the dynamical arrest was given in the context of RFOT where the presence of a surface tension term and a non trivial relation between a growing static correlation length  $\xi$  and the configurational entropy were introduced. The fundamental

equation of the theory is given by Eq. 1.13. We write it here again since it will be discussed in more details in the following

$$\tau_\alpha = \tau_0 \exp\left(\frac{\Delta_0(T)\xi^\psi}{T}\right) = \tau_0 \exp\left[\frac{\Delta_0(T)}{T} \left(\frac{\Upsilon(T)}{S_c(T)}\right)^{\frac{\psi}{d-\theta}}\right]. \quad (4.19)$$

This equation presents two critical exponents  $(\theta, \psi)$  and three unknown terms  $(\Upsilon(T), \Delta_0(T), \tau_0)$ . We recall here that in the current formulation of RFOT the barriers to overcome for the rearrangement of a region of size  $R$  are given by  $\Delta_0 R^\psi$  whereas a surface tension  $\Upsilon(T)TR^\theta$  quantifies the degree of energy that must be paid to allow the mismatch between regions [17]. Critical exponents could not be directly measured in experiments so far, the static correlation  $\xi$  being inaccessible, and estimations of growing spatial correlations relied on dynamical measurements [203, 204]. In simulations, on the other hand, a static point-to-set correlation can be measured using cavity geometry, although accessible timescales have been limited by the computational glass transition. The need of such a complete theory is not universally accepted and many experimental works make use exclusively of AGD concepts [133]. Finally, different mechanism may contribute to the dynamical arrest, each being the relevant one in a different temperature regime. Some studies proposed that the first three or four orders of magnitude are controlled by dynamical equations of Mode-Coupling theory, whereas, at lower temperatures, activation processes sets in [205]. However, standard simulations fall out of equilibrium close to this putative crossover.

The introduction of models and algorithms that allows equilibration at temperature below  $T_g$  have boosted computer simulations to explore previously unattained regimes. In this section we tackle some of the open questions discussed before in light of the results presented in previous paragraphs. We concentrate on the three dimensional case.

First we show that AGD theory fails to describe consistently computational results in all temperature regimes and consequently we interpret the dynamical results within the RFOT framework. Then we use computational results to extract RFOT critical exponents and to compare with previous findings. Finally we support our results with an analysis of experimental data.

#### 4.4.2 Failure of the Adam-Gibbs equation

RFOT theory predicts a criticality at a very low temperature, the Kauzmann temperature, with a divergence of relaxation times and of a static length. However both in experiments and in simulations, the system falls out of equilibrium well before the critical point. The improvements given by swap Monte Carlo simulations of polydisperse systems definitely help in getting closer to the putative transition point, although the critical point, with a vanishing configurational entropy, could not be reached. In this subsection we show that the newly accessed regime allows for reconsidering the relation between relaxation times and configurational entropy under a new light. We use both

results for the soft and the hard sphere systems in 3D that have been reported in Secs. 4.2 and 4.3.3.

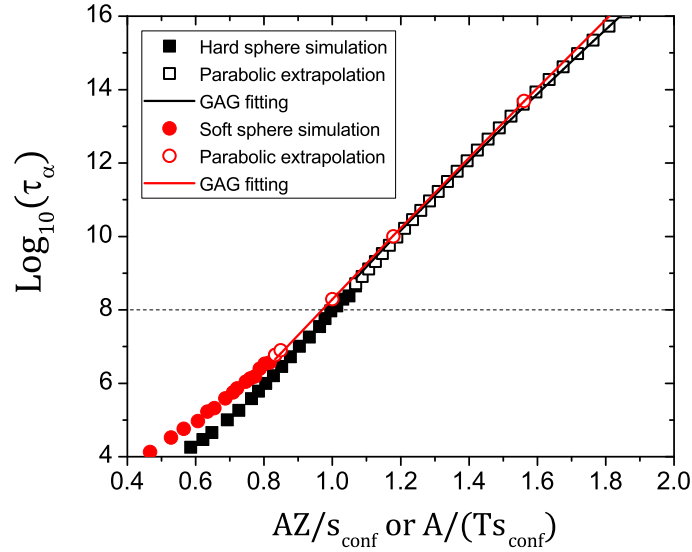


**Figure 4.8** – Adam-Gibbs plot of the logarithm of relaxation times as a function of the inverse configurational entropy  $s_c$  for a hard (squares) and a soft (circles) sphere system over 12 orders of magnitude. Configurational entropy is either divided by reduced pressure in hard spheres or multiplied to temperature in soft spheres. Full points are simulation results. Empty points are extrapolations (see text for more details). Full lines indicate the fit to the GAG equation ((4.20)) in experimental timescale, with  $\alpha = 0.8, 0.75$  for soft and hard spheres respectively. The x-axis is rescaled by a constant.

We recall that swap Monte Carlo simulations do not allow to measure relaxation dynamics at temperature lower than  $T_{MCT}$ . Then, to extract values of  $\tau_\alpha$  at experimental timescales, we have to rely on extrapolations of values obtained at higher temperature. In Sec. 3.7.3 we found that the most reasonable extrapolation of relaxation times at low temperature is given by a parabolic fit of Eq. (3.19), this was also shown in Ref. [144] where relaxation times of many experimental glass-forming liquids were found to be correctly described by this equation. Moreover we observe that other common functional forms, as VFT of Eq. 3.18, strongly depends on the fitting regime and are not good predictor of relaxation times at experimental timescales if fitted on computational timescales. The configurational entropy, on the other hand, can be directly measured using the thermodynamic integration method and we also showed previously that extrapolation curves describe very well data in the interval of measurement. For this reason we use the fitting curves of Figs. 4.5 and 4.7 to obtain a continuous expression of configurational entropy as a function of temperature or pressure. Moreover we notice that values of the configurational entropy using other techniques reported in Fig. 4.3.3 can be obtained by a trivial rescaling by a constant factor, such that our conclusion holds generally.

Combining this last expression with the parabolic extrapolation in a parametric figure we obtain the Adam-Gibbs plot for soft and hard spheres that is shown in Fig. 4.8.

We notice that the overall agreement with a linear behaviour is poor. This failure of AGD theory in describing experimental data lead us to introduce a Generalized Adam Gibbs (GAG) relation of the form

$$\tau = \tau_0 \exp \left[ \frac{A}{T s_c^\alpha} \right]. \quad (4.20)$$

Here the factor  $\alpha$  accounts for the observed deviations from a linear behaviour and in the case of  $\alpha = 1$  we obtain the Adam Gibbs relation. To fit this function we define two different ranges of relaxation times: *experimental* timescale ( $\tau_\alpha = 10^8 - 10^{16}$ ) and a *simulation* timescale ( $\tau_\alpha = 10^4 - 10^8$ ), which correspond respectively to the timescales only accessible in experiments and timescale usually accessed by simulations. In Fig. 4.8 we report the fitting result for experimental timescales and we observe a good agreement between data and the fitting curve. We do not show the fits on simulations timescales since they present large deviation from the fitted curve, in particular in the deep supercooling region. In case of both soft and hard spheres we found values of the exponent  $\alpha \leq 1$  for experimental and  $\alpha \sim 2$  for simulation timescale. These results give two pieces of information. On the one hand the prediction for exponents does strongly depend on the fitting range and standard simulations, because limited in timescale and very far from the putative criticality, should not be used to extract exponents. On the other hand  $\alpha$  values at experimental regimes are in general smaller than one. This supports the need of introducing a more detailed theory than AGD.

### 4.4.3 A RFOT theory interpretation

In the previous subsection we found values of  $\alpha < 1$  fitting relaxation times in the experimental regime. We also observe a temperature dependence of the exponents. Both these ideas can be explained within RFOT.

The difference observed between exponents using long and short timescale suggests the presence of a Mode-Coupling regime at mild supercooling and of an activated regime closer to the glass transition. Let us now consider again Eq. 4.19 and disregard the effect of the unknown terms such as activation barrier  $\Delta_0$  or surface tension  $\Upsilon(T)$ . We obtain two equations, one is connecting the relaxation times and the static length:

$$\log \left( \frac{\tau_\alpha}{\tau_0} \right) \propto \left( \frac{\xi^\psi}{T} \right). \quad (4.21)$$

The other relates the static length and the configurational entropy:

$$\xi \propto \left( \frac{1}{s_c} \right)^{\frac{1}{D-\theta}}. \quad (4.22)$$

Merging these two equations we end up with a simplified relation connecting the relaxation times with the configurational entropy:

$$\log \left( \frac{\tau_\alpha}{\tau_0} \right) \propto \frac{1}{T s_c^{\frac{\psi}{D-\theta}}}. \quad (4.23)$$

Interestingly this equation has the same form as the GAG equation introduced previously (see Eq. 4.20) and consequently we are allowed to identify the exponents:

$$\alpha = \frac{\psi}{D - \theta}. \quad (4.24)$$

Here we see that the previous findings on experimental data can be interpreted using RFOT where the presence of an exponent  $\alpha$  less than one can derive from various combinations of exponents  $\psi$  and  $\theta$ .

The original AGD argument predicts  $\psi = D$  and  $\theta = 0$  by construction, since the correlated regions are compact and their volume is inversely proportional to the configurational entropy. Moreover the role of the effective surface tension and the energy barrier were not directly taken into account. This leads to the value  $\alpha = 1$  that has been extensively used. However other combinations of exponents can lead to the same results.

Within the framework of RFOT theory there are various predictions of the unknown terms in Eq. 4.19. In the following we will try to sum up previous literature findings in theory, computer simulations and experiments. On the basis of spin glass theory, one could expect that the barrier to overcome should be bigger or equal than barrier equal to excess energy of final state  $\psi \geq \theta$  or  $\psi = \theta$  and  $\Delta_0 \geq \Gamma_0$  [206]. We will see however that this is not the case for many theoretical and computational findings. In the first formulation of RFOT, scaling arguments gives  $\psi = \theta = d/2$  [27]. In the same articles the authors also proposed  $\Delta_0 = \Upsilon_0 = \kappa T$  where  $\kappa$  is a constant mildly dependent on molecular details. This last equality comes from a nucleation argument in which the droplet of another state nucleates inside the original state. Another prediction comes from the Kac limit:  $\theta = D - 1$  [193]. Some other theoretical consideration may lead to think that  $\Delta_0$  should be increasing for lower free-energy state, that is, increasing with temperature [17]. This energy barrier could also be thought as directly related to the high frequency shear modulus  $G_\infty$  and be explained as the energy necessary to create a void in the bulk system to make space for some particle to rearrange. This point could offer a connection between the RFOT theory and the shoving model briefly discussed before (see Sec. 3.9.2 and Refs. [169, 170, 171]).

On the computational side, measurements of RFOT exponents were given in Refs. [147, 207]. Here, based on a computational method for the study of amorphous excitations, it was found  $\psi = 1$ ,  $\theta = 2$ , and a surface temperature increasing with decreasing temperature. In other simulation based on point-to-set measurements was also found  $\psi = 1$  [208]. Random pinning studies found  $\psi = 1$  and  $\theta = 2$  as well [120]. Using dynamical correlation it was found  $\psi \approx 1.3$  and  $\theta = 0.3$  to  $0.7$  in models of glass forming polymer melt assuming  $\Upsilon(T) \propto T$  [209].

As far as experiments were involved, dynamical correlation have been used to determine the exponents, since static lengths are not directly observable in real glass-formers. In particular Capaccioli et al. found  $\psi = 0.3 - 1.5$  assuming  $\Upsilon_0 = \text{const.}$  [203] and Brun et al. found  $\psi = 1$  with  $\Delta_0 = \text{const.}$  and  $\psi = 1.5$  with  $\Delta_0 = \kappa T$  [210].

Overall both the computational and the experimental results were found by measuring observables very far from the RFOT theoretical formulation, such as dynamical quantities [203, 210, 209], short time excitations [147, 207] or static length in pinning geometry [208, 120]. We notice that some of these results are coherent or not with our determination of  $\alpha$ . However, a little can be said by using our  $\alpha$  value without knowing individually the exponents of RFOT ( $\theta$ ,  $\psi$ ). The aim of the next subsection is to determine the  $\theta$  exponents using the computational results obtained in Secs. 4.3.

#### 4.4.4 Measuring $\theta$

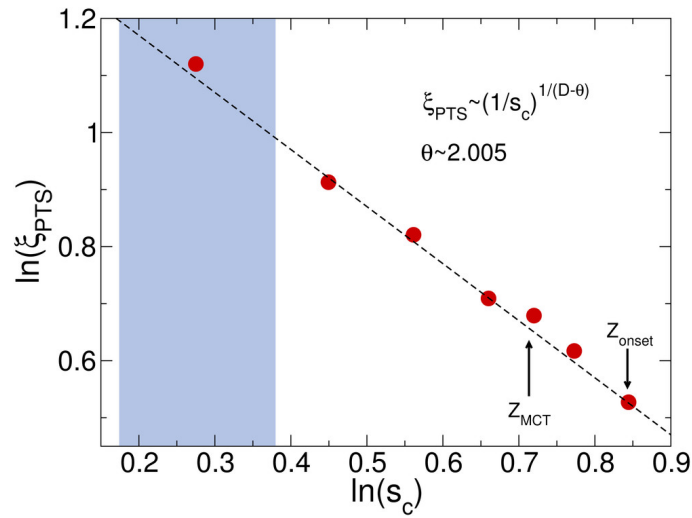


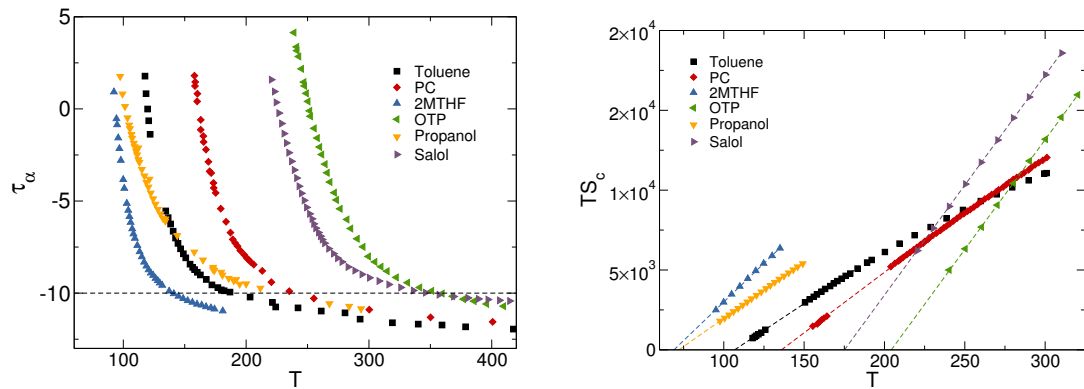
**Figure 4.9** – Point-to-set length  $\xi_{PTS}$  as a function of the configurational entropy in a log-log scale. The predicted RFOT behaviour is fitted and we found a value of  $\theta = 2.005$ . The grey box indicates the location of the laboratory glass transition.  $Z_{MCT}$  and  $Z_{onset}$  are respectively the Mode-Coupling pressure and the onset pressure.

We are now in the position to give a realistic estimation of the value of exponents in RFOT, that would reduce the number of free parameters in Eq. (4.24). To do so one has to directly analyze the relation between growing static length and configurational entropy, so as to retrieve the exponent  $\theta$ . In Sec. 4.3.3 we showed results for  $s_c$  and  $\xi_{PTS}$  independently obtained for the hard sphere system. Our aim here is to use this result to fit Eq. (4.22) and get the  $\theta$  exponent. For this reason we plot  $\xi_{PTS}$  versus  $s_c$  in log-log scale in Fig. 4.9 with red points. We both indicate the onset pressure with  $Z_{onset}$  and the Mode-Coupling crossover with  $Z_{MCT}$ . Here the laboratory glass transition is denoted by a blue shaded region. The black dashed line indicates a fit to Eq. (4.22) that give the value  $\theta = 2.005$  in three dimension. This result is consistent with the theoretical prediction of Ref. [193] ( $\theta = D - 1$ ) and with computational findings of Ref. [147, 207]. Moreover it strongly disagrees with the AGD prediction of  $\theta = 0$  confirming once again that this theory is not enough to explain the behaviour of glass-formers.

### 4.4.5 Agreement with experimental data

So far we have dealt with computer simulations and in some case we employed extrapolations. Our aim now is to use experimental data to validate our previous findings. For this reason we directly test the validity of Adam-Gibbs relation between relaxation times and configurational entropy using experimental data.

First we extract data from for six glass forming liquids: 2MTHF, OPT, PC, Propanol, Salol, Toluene. Relaxation times measured by dielectric spectroscopy and dynamic light scattering are taken from Refs. [133, 211]. Configurational entropy from calorimetric measurements is taken from Refs. [133, 212].



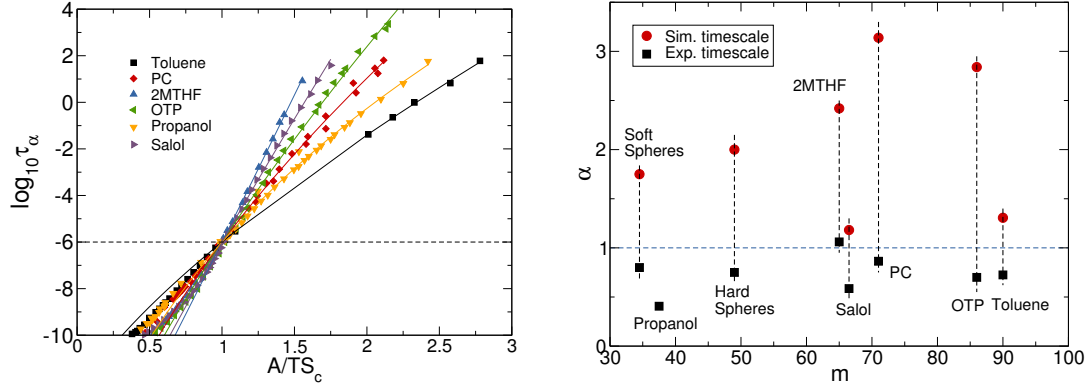
(a) Relaxation times from dielectric spectroscopy and dynamic light scattering for six molecular glass formers. Data for Toluene, PC, OTP, Salol are taken from Ref. [211], for Propanol and 2MTHF are from Ref. [133].

(b) Configurational entropy times temperature plotted as a function of temperature from calorimetric measurements. Data for Toluene and PC are from Ref. [212], for Propanol, 2MTHF, OTP, Salol are from Ref. [133].

Figure 4.10 –

Raw data are shown in Fig. 4.10. Relaxation times as a function of temperature are shown in Fig. 4.10a, the horizontal dotted line indicates the onset of supercooled behaviour set up to be  $\tau_\alpha = 10^{-10}s$ . Configurational entropy times temperature is shown as a function of temperature in Fig. 4.10b. This plot was done to reveal the linear behaviour of this quantity at low temperature. We perform a linear fit indicated by dashed lines.

Raw data of relaxation times and linear fit of configurational entropy were used to build an Adam Gibbs like plot reported in Fig. 4.11a. Temperatures are rescaled by a constant factor such that the data collapse on a single point at  $\tau_\alpha = 10^{-6}$ . We notice that the agreement with an Adam Gibbs relation is very poor for five out of six molecular liquids. Only 2MTHF shows a linear behavior, whereas the other systems show a bending both at low and at high temperatures. As before we define simulation and experiment timescales and we fit with a GAG expression both using experimental ( $\tau_\alpha = 10^{-6} - 10^2$ ) and simulation ( $\tau_\alpha = 10^{-10} - 10^{-6}s$ ) timescales. Here we assume that time in Monte Carlo steps can be compared to time in seconds using  $1\text{step} \approx 10^{-14}s$ .



(a) Adam-Gibbs plot of common logarithm of relaxation times as a function of inverse configurational entropy times temperatures for experimental data. Only 2MTHF shows a linear agreement with the Standard Adam Gibbs relation. Lines are from fit of the Generalized Adam Gibbs performed at experimental timescales.

(b) Value of the coefficient  $\alpha$  from the GAG equation (Eq. 4.20) for six experimental and two computational glass-forming liquids as a function of the fragility parameter  $m$  both in experimental and computational timescales.

Figure 4.11 –

The resulting  $\alpha$  obtained by fitting in these two different regions is shown in Fig. 4.11b as a function of the fragility index:

$$m = \left. \frac{\partial \log_{10} \tau_\alpha(T)}{\partial (T_g/T)} \right|_{T=T_g}. \quad (4.25)$$

We notice that experimental timescales give similar values for  $\alpha$  in most of the cases, which is less than unity,  $\alpha \sim 0.5 - 1.1$ . Contrary to Ref. [202] we do not find any systematic behaviour as a function of the fragility. On the other hand, values given by fitting simulations time scales are always larger than one and strongly scattered between  $1.25 < \alpha < 3.5$ . The dependency on the fitting region may be due to the presence of more compact correlated regions with lowering the temperature. These results are consistent with the finding on computational glass formers (also reported in Fig. 4.11b). Going back to Eq. (4.24) and using our estimation of  $\theta \sim 2$ , we are now able to state  $\psi \approx \alpha$ . Therefore, we found  $0.45 < \psi < 1.1$  and on average  $\psi \simeq 0.7$ . Remarkably, these values are consistent with previous experimental finding using dynamic correlation of Ref. [203]  $0.3 < \psi < 1.5$ .

In conclusion, we study the Adam-Gibbs relation for experimental and computational glass-forming liquids over 12 orders of magnitude finding systematic deviation from the prediction of AGD theory and calling for its generalization to a more complete form that includes physical effects predicted within RFOT theory. We use computational measurements of the configurational entropy and of static correlations obtained at extremely low temperatures using swap Monte Carlo simulations to determine values of the expo-

nents of RFOT and we found consistent values for the exponents with previous results obtained in simulations of mildly supercooled liquids and using dynamical correlation from experiments.

The temperature of divergence of relaxation times using a VFT equation  $T_0$  and the temperature of a vanishing configurational entropy  $T_K$  were found to be different for many glass-formers and a trend with fragility was observed as well [202]. These facts, together with a better description of the kinetic arrest given by singularity-free functional forms, has been used to challenge the existence of an ideal glass transition [143, 144].

Here we show that the original versions of VFT and Adam-Gibbs relations are insufficient to describe glass formation and the difference between  $T_0$  and  $T_K$  could be an artifact of the employed functional forms. Using more carefully theoretical indication from RFOT theory one finds that an ideal glass transition is not ruled out by the current knowledge we have about glass-forming liquids. On the other hand there are very few available information about activation energy  $\Delta_0$  and surface tension  $\Upsilon(T)$ . Additional work to estimate these terms would be needed to obtain more conclusive results.

## 4.5 Absence of a geometric transition across the Mode-Coupling crossover

### 4.5.1 Transition points in mean field and structural glasses

So far we have made a large use of the PEL and we mainly referred to the properties of the inherent structures. However the rough energy landscape distinctive of supercooled liquids possesses many other features, generically called topological features, that depend on the energy level of the exploration. These properties, even though independent of temperature, may have an influence on the dynamical slowdown of the system. Indeed, changing the temperature, the system probes different regions of the landscape at different energetic levels.

One of these topological features was first predicted in mean field models of spin glasses and goes under the name of geometric transition [91, 92, 90, 93, 94]. This consists in a change in the properties of the landscape at a given energy. At low temperature  $T < T_d$  the system is constrained in a minimum and its dynamics is mainly vibrational. This also means that time correlation functions do not relax to zero and have a finite non zero value at infinite time. In other words, the system remains in a single thermodynamic state. In this condition of broken ergodicity one could study in an exact way the topological properties of the minimum.

In particular one can compute its height in the landscape, given by the *bare* energy  $e_m$ , without the contribution of kinetic energy. Moreover, the spectrum of the Hessian matrix can be computed and it consists in the eigenvalues  $\lambda$ , which are positive being in a minimum, and corresponding eigenvectors  $\mathbf{e}_\lambda$ . Each eigenvalue  $\lambda$  describes the curvature of the minimum along the direction of the corresponding eigenvector  $\mathbf{e}_\lambda$ . This

means that a positive amount of energy is needed for a system in a minimum to displace in the landscape in any direction. Since the properties of the landscape vary if tested at different heights, we can define a density of state as a function of the energy level of the minima  $e_m$ :

$$\rho(\lambda, e_m) = \frac{1}{N} \sum_{i=1}^N \delta(\lambda - \lambda_i). \quad (4.26)$$

Let us now imagine to start from a very low energy at which the minima are stable, eigenvalues have a large value and basins are very steep. If we increase the sampling energy other minima will be explored characterized by some smaller eigenvalues as well as more gradual slopes around the basins. It exists a given energy  $e_{TH}$  at which some of the eigenvalues become zero. These states are called marginal and are characterized by the fact that the system can move in the direction of the corresponding eigenvector without paying an energetical price. Going at higher energy some eigenvalues become negative. These points are called *saddles* and are topologically different from minima since the system has some preferential directions in which relaxations are enhanced. The transition between a region at high energy  $e > e_{TH}$  and a region at low energy  $e < e_{TH}$  was named *geometric transition* [92]. Even though the properties of the landscape do not change by changing the temperature, the system explores very different zones at different temperatures. Indeed the threshold energy  $e_{TH}$  is sampled at the threshold temperature  $T_{TH}$ . Specifically, at temperature above  $T > T_{TH}$  the system explores landscape regions having a bare energy  $e > e_{TH}$  and the dynamics is a nonactivated *MCT* like. Moreover it was also shown that in this region the closest stationary point of the landscape is a saddle and not a minimum [93]. Whereas for  $T < T_{TH}$  a dynamical transition sets in and the system remains confined in a minimum of the landscape. These results allowed the identification between the dynamical transition temperature  $T_d$  and the geometrical transition temperature  $T_{TH}$ .

Some years ago there has been a proposal to employ all this information from mean field theory to explain the relaxation behaviour of glass-forming liquids [90]. In the original formulation of the problem for structural glasses, two mechanism for relaxation were assumed to exist above  $T_{TH}$  [90]. *Mechanism A*: the system starts from a minimum, converts some kinetic energy into potential energy, climbs up a potential energy barrier, passes through a saddle point of the potential and falls again in a minimum. *Mechanism B*: the system starts from a saddle point, finds a direction downhill converting some potential energy into kinetic energy, goes through a minimum and finally it climbs again to a saddle. These arguments were used to explain the different behaviour observed in fragile and strong glass-formers. At the geometrical transition the system stops visiting saddles and consequently Mechanism B is suppressed and only activation process of Mechanism A are allowed. Strong glass formers already use activation processes at high temperatures such that the suppression of the B channel does not change dramatically their dynamics. On the contrary, the main relaxation channel for fragile glasses is B, therefore at temperature lower than  $T_{TH} \sim T_{MCT}$  the dynamics slows down remarkably

and the activation processes are rare or completely suppressed.

### 4.5.2 Statistical properties of saddles in simulations

The possible existence of a geometric transition in structural glasses was extensively investigated some years ago [96, 97, 98, 99, 100, 101, 95]. In supercooled liquids starting from an equilibrium configuration at a certain temperature one would like to find the closest stationary point. However this is not as easy as finding minima of the PEL. Indeed for each configuration it is possible to associate a given minimum using an algorithm that descends along the curvature of the basin, and this is a well defined object with a well defined region of attraction.

The situation for saddles is different and the point found numerically depends on the path followed in the landscape, more specifically, on the algorithm employed. Mainly two different algorithms were proposed able to associate a saddle to a starting equilibrium configuration. The first method was employed in Ref.[97]. It relies on the idea of using a minimization algorithm of the force, by defining a pseudo-potential:

$$W = |\nabla V|^2, \quad (4.27)$$

where  $V$  is the total potential energy of the system. This defines a secondary landscape characterized by minima corresponding to stationary points in the original potential energy landscape of the system. Saddles can be classified on the basis of the number of the negative eigenvalues  $N_{\lambda < 0}$  defining a saddle index:

$$n_s = \frac{N_{\lambda < 0}}{3N}. \quad (4.28)$$

This method was questioned in Ref [98] where Doye and Wales argued that the algorithm does not find only true saddles in the PEL, that is, absolute minima of  $W$ , instead it also finds relative minima of  $W$  which correspond to inflection points of  $V$ . The frequency of this last possibility was quantified to be the 95% on the cases [100]. Consequently the stationary point revealed with this technique were called *quasi saddles*. Interestingly, it was shown in Ref. [100] that the properties of quasi saddles are consistent to the true saddles and the number of inflection directions remains small, confirming the relevance of the minima of  $W$  to analyze the topological properties of the PEL. In Ref. [98] Doye and Wales also introduced another method, which establishes an alternative to the previous one. This is called eigenvector following technique and consists in starting from an equilibrium configuration and dividing the spectrum of the eigenvalues in two groups. The first group is made of the  $N_\lambda$  smaller eigenvalues together with their corresponding eigenvectors where  $N_\lambda \ll N$  and the second group is made of the remaining  $3N - N_\lambda$  modes. The algorithm consists in a Newton method that maximizes the potential energy  $V$  along the  $N_\lambda$  smallest eigenvectors and minimizes along the remaining directions. This algorithm has the advantage to converge exactly to a saddle point of chosen order  $n_s$ , however this comes with a high computational cost and an exploration of the landscape

somehow unnatural, the distance between the original configuration and the final one being large [77]. By direct comparison of the two algorithms, it was found that they give consistent results, confirming the validity of the previous studies [77].

The presence of a geometric transition was investigated in several glass forming systems, presenting purely repulsive or Lennard-Jones interactions, various softness of the potential, and monodisperse or bidisperse in size [97, 95]. The main finding was that a large number of models have properties consistent with the presence of geometric transition. Two questions were asked, both inspired by the mean field findings. First, whether exploration of the saddle stops at a given temperature  $e_{TH}$ , and second, whether this temperature coincides with the Mode Coupling temperature  $T_{MCT}$ . There have been an overall agreement amongst many researcher that the two questions have a positive answer. Moreover it was claimed for a universality of topological landscape properties of glass-forming liquids [95]. This results supported the presence of a geometric transition also in structural glasses, elucidating an important point regarding the thermodynamic properties underlying the dynamical properties. However it has to be noted that this topological analysis was always confined to temperature  $T \leq T_{MCT}$ , and the detection of the geometric transition relied on extrapolation strategies. What happens at temperature lower than  $T_{MCT}$ , however, remained unclear.

### 4.5.3 The geometric crossover

With the aim of investigate the presence of a geometric transition across the Mode-Coupling temperature, we decided to perform an analysis of the topology of the landscape of some of the systems that we are able to equilibrate below the Mode-Coupling temperature. To do so we analyze two continuously polydisperse systems of repulsive soft spheres, the additive  $n = 18$  and  $\epsilon = 0$  and the non-additive  $n = 12$  and  $\epsilon = 0.2$  both introduced in Sec.3.7. We employ, 50 and 200 configurations of  $N = 250$  and  $N = 500$  particles respectively for the two models. Here we decided to use a gradient descent algorithm and minimize the force  $W$  following [97]. The reasons behind this choice are mainly historical, since we want to directly compare to previous literature results. Moreover this method, as discussed before, gives results in agreement with the eigenvector following technique [77]. Finally it is computationally lighter and can be easily applied to large systems to verify the presence of finite size effects.

In order to compare with previous results we also employ two other models. One of the two is a 80:20 binary mixture of soft particles interacting with the potential

$$v(r_{ij}) = 4\epsilon_{ij} \left( \frac{\sigma_{ij}}{r_{ij}} \right)^{12} + c_{LJ}, \quad (4.29)$$

where  $\epsilon_{AA} = 1.0$ ,  $\epsilon_{AB} = 1.5$ ,  $\epsilon_{BB} = 0.5$ ,  $\sigma_{AA} = 1.0$ ,  $\sigma_{AB} = 0.8$ ,  $\sigma_{BB} = 0.88$ . Here we cutoff and shift the pair potential at the cutoff distance  $r_{cut} = 2.5\sigma_{ij}$ . Here we employ a system with  $N = 1000$  particles. This potential is the same as the historical Kob Andersen mixture already employed in Ch. 2 and Sec. 3.9.2 without the attractive

part, it was employed, using different softnesses, in Ref. [151] to study the dynamics and in Ref. [95] to detect topological properties. We performed standard Monte Carlo simulations for this system, comparing both statical and dynamical quantities with the previous literature, as a consistency check. We obtained 20 equilibrated configurations at the same temperatures as in Refs. [151, 95]. We also want to understand how the fragility of the system influences the presence of saddles in its landscape to compare with the theoretical conjectures discussed before (Sec. 4.5.1) and in Ref. [90]. For this reason we employ data of the landscape analysis of a tetrahedral network glass-former from Ref. [213]. The fragility index defined by Eq. (4.25) of the various model are:  $m = 83$  for the polydisperse  $n = 12$  system,  $m = 78$  for the polydisperse  $n = 18$  system and  $m = 108$  for the binary mixture.

Starting from an equilibrium configuration we perform a minimization of the pseudo-potential  $W$  using a conjugate gradient algorithm [190]. Once the minimization of the force is performed and the stationary points are found, there are two possible approaches to represent the data and reveal the geometric transition. In some cases [96, 100, 101, 95] the saddle index  $n_s$  was represented as a function of sampling temperature and it was observed a vanishing power law behaviour at a finite temperature identified with the Mode Coupling temperature  $T_{MCT}$ . Another possibility exists for representing the data, more related to the topological features of the landscape. Following [97, 99] one can plot the average saddle energy  $e_{SP}$  as a function of the saddle index  $n_s$ . This gives a parametric plot in which points are placed on a curve determined only from the landscape topology. The usual analysis performed on this curve is a linear extrapolation of the form:

$$e_{SP} = An_s + e_{TH}, \quad (4.30)$$

where  $A$  is a constant. This allows to define the threshold energy  $e_{TH}$  as the energy at which the saddle order  $n_s$  goes to zero and all the eigenvalues becomes positive, that is an energy at which the landscape do not present saddles anymore, but only minima.

The procedure is illustrated in Fig. 4.12 where  $e_{TH}$  is measured for the four models. The fitting procedure varies depending on the model. For models only accessible with standard simulations (Figs. 4.12c and 4.12d), we fit on the entire range of data, as in previous works. For models that can be equilibrated below the Mode Coupling temperature (Figs. 4.12a and 4.12b), we only fit in regions accessible to standard simulations, which corresponds to  $T > T_{MCT}$ . For all the curves we observe that a linear behaviour correctly describes the data at high  $n_s$  while deviations are systematically found at low  $n_s$ . In the case of previous studied models these deviations are small and involve few points close to  $n_s = 0$ , larger deviations were found in presence of constraints such as in pinning geometries [64].

The new systems sampled at extremely low temperatures, on the other hand, present large deviations from a linear behavior and a strong bending to low energy getting closer to  $n_s = 0$ . It was claimed that this bending, already mildly observed in previous literature, could be a consequence of the fact that the algorithm at low  $n_s$  finds mainly

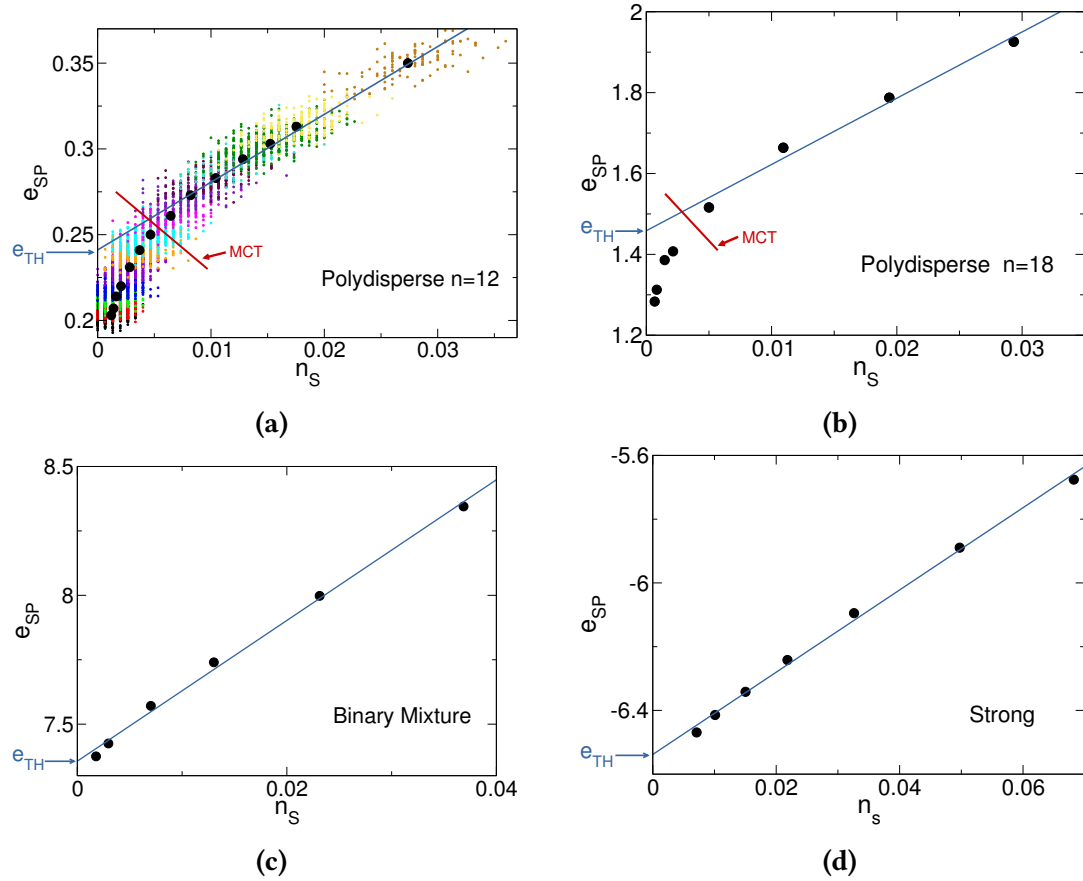


**Figure 4.12** – Saddle energy  $e_{SP}$  as a function of saddle index  $n_S$  for four different supercooled liquids: (a) polydisperse non-additive model with  $n=12$ , (b) polydisperse additive model with  $n=18$ , (c) binary mixture, (d) strong glass-former. Straight lines are fits on the standard simulations region, arrows roughly indicate the correspondent location of the Mode-Coupling. Figure (a) include also the scatter plot of the data, different colors are for different sampling temperatures.

minima and the averaging operation, depending on the sampling temperature, would bias the data towards lower values of the energy [214]. For this reason we report a scatter plot of the raw data in Fig. 4.12a. Different colors correspond to different sampling temperatures. We observe that also at very small  $n_s$  the raw data go continuously to lower energies and there is no evidence of a jump between values of the energy of the minima  $n_s = 0$  and values of the energy of saddles. To be sure of this point we also performed an average grouping raw data with respect to the saddle index regardless of the sampling temperature and we confirm that deviations of the linear behaviour are a robust properties of the topology of the landscape.

The extrapolated energy  $e_{TH}$  can be used to locate a corresponding temperature  $T_{TH}$ . This procedure comes from the mean field theoretical approach and consists in using the curve of the energy of the inherent structure as a function of temperature setting the condition:

$$e_{IS}(T_{TH}) = e_{TH}. \quad (4.31)$$

	Polydisperse n=12	Polydisperse n=18	Binary Mixture	Strong
$T_{TH}$	0.100	0.493	0.829	0.328
$T_{MCT}$	0.101	0.468	0.747	0.318
$\frac{T_{TH}}{T_{MCT}}$	0.99	1.05	1.11	1.03

**Table 4.1** – Threshold temperature, Mode-Coupling temperature, and their ratio. Values for this last are always around 1.

In table 4.1 we compare the crossover temperature  $T_{MCT}$  obtained by directly fitting the relaxation times with Eq.1.9 and the threshold temperature defined using the notion of geometric transition  $T_{TH}$ . We observe a good agreement between the two temperatures. However, this finding conflicts with the bending detected before, meaning that the description is incomplete at lower temperatures. The bending do not rule out other interpretation of the behaviour of saddles with varying temperature, such as the ones discussed in the context of kinetically constrained models [215].

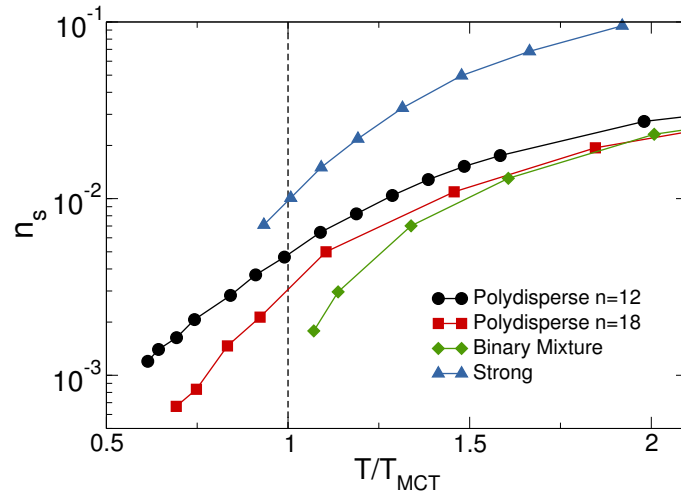


**Figure 4.13** – Saddle index  $n_S$  as a function of the temperature rescaled by  $T_{MCT}$  for four models. The behaviour is non-universal and models able to be equilibrated below  $T_{MCT}$  present a non-vanishing number of saddle.

To understand the behaviour of the four models close and below  $T_{MCT}$  we report the saddle index  $n_S$  as a function of the sampling temperature in Fig. 4.13. We notice that this plot is algorithm dependent since it contains explicitly the temperature. First we observe that, for the literature binary mixture, results are consistent with previous finding, with a curve that could vanish at a finite temperature. The strong glass-former presents overall values of the saddle index higher as compared to other models. Our result is in contrast with the prediction of Ref. [90] where it was claimed that saddles should be less important in the relaxation process in systems with low fragility.

Finally, for the two systems equilibrated beyond  $T_{MCT}$ , we observe that the saddle index decreases monotonously and it does not vanish for temperature well beyond

the standard regime. Interestingly the Mode-Coupling crossover is not captured by the saddle index and this quantity is insensitive to the kinetic slowing down. In other words, the expected geometrical transition, in these systems is at best a *crossover*, from a high to a low index regime. However these results show that the relation between topology and Mode-Coupling crossover is rather weak.

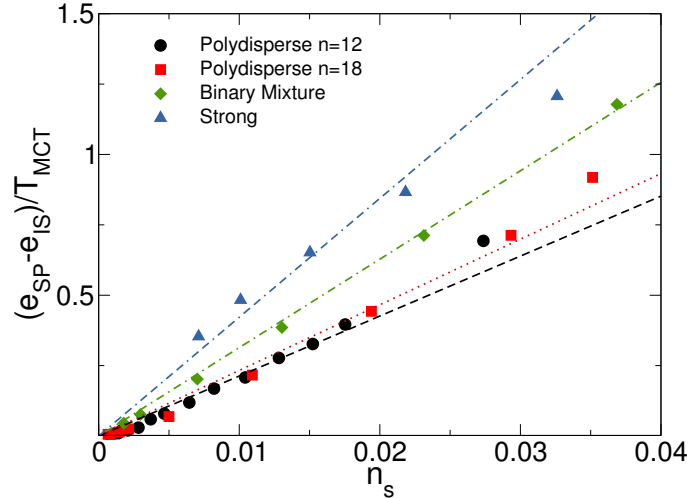


**Figure 4.14** – Difference in energy between saddles and corresponding minima as a function of the saddle index for four different models. The  $y$ -axis is rescaled by  $T_{MCT}$  to compare. Linear fits are performed in regions accessible by standard simulations.

The next aim is to quantify the height of the saddles with respect to minima, this will give an indication of the energetical price to pay to perform a relaxation. For this reason we report in Fig. 4.14 the energy of the saddles  $e_{SP}$  minus the energy of minima  $e_{IS}$  as a function of the saddle index  $n_s$ . Since we are interested in barrier height at the dynamical crossover we divide the  $y$ -axis by  $T_{MCT}$ . We employ the average inherent structure energy and saddle energy sampled at the corresponding temperature. Another possibility would be to subtract the raw values of inherent structure energy to the saddle energy for each configuration and then compute the average. We confirmed that the two approaches are equivalent.

Previous simulation results claimed to find a linear functional form for many different glass-forming liquids [99, 95]. This result was explained in terms of a fixed amount of energy needed to increase the saddles order of 1. This also implies an independence between processes that are responsible for this increase. Our results show that a linear regime exists between  $0.05 \leq n_s \leq 0.25$ , which corresponds to mildly supercooled liquids. However, going at very small saddles orders the curve bends towards 0, suggesting that at low saddle index relaxation processes may be correlated. We fit the intermediate regime with a linear functional form

$$\frac{e_{SP} - e_{IS}}{T_{MCT}} = A'n_s + B'. \quad (4.32)$$

in order to extract the height of the energy barrier at the Mode-Coupling transition  $\Delta e_{MCT}$ . One can show that the slope  $A'$  can be related to  $\Delta e_{MCT}$  using the relation  $A'/3 = \Delta e_{MCT}$ , where the factor three is given by normalization in Eq.(4.28). In previous literature, it was found a system independent values  $\Delta e_{MCT} \sim 10k_B T_{MCT}$ , a result that we confirm for the Binary Mixture. However other model present a very different behaviour. The polydisperse systems, for instance, have lower barriers  $\Delta e_{MCT} \sim 7 - 7.5k_B T_{MCT}$  and in the case of the strong glass former we find  $\Delta e_{MCT} \sim 14k_B T_{MCT}$ .

These results are in disagreement with previous findings. On the one hand, different fragile glass forming liquids have different energy barriers, contrary to the idea that the topology is system independent [99, 100, 95]. On the other hand the height of the barriers follows a nonmonotonous trend with fragility.

The largest barrier value is the one of the strong system. Then, the barrier of the most fragile system, the binary mixture, assumes intermediate value. Finally the barrier for the polydisperse models are the smallest. This is contrary to the prediction of Ref. [90]. Finally at low  $n_s$ , in systems sampled beyond the dynamical transition, we found deviations from a linearity of the behaviour of the energy barriers, with values of the barrier very small  $e_{SP} - e_{IS} \sim 0.01$ . This result gives further information about the regions of the landscape sampled at very low temperature. indicating that the energy needed to increase the saddle order of 1 is not constant in this regime. This means that structural rearrangements in real space correspondent to a given saddle may not be independent. However, a more detailed analysis of the real space behaviour is needed to clarify this point.

In conclusion, in this section we observed that the mean-field geometric transition may survive at best as a crossover in finite dimensional glass-forming liquids. Moreover the topology of the landscape varies significantly in different models, contrary to the expectation of universality of previous works.



# Chapter 5

## Summary of the work

This chapter is dedicated to a summary of the thesis work presented in the previous three chapters.

Chapter 2 presents a study of coupled liquids. Taking two copies of a three dimensional glass-forming liquid, we define an overlap between them that quantifies their degree of similarity, and we define a coupling field as a conjugate variable of the overlap. The situation is similar to the theoretical one described in Sec. 1.2.5. In the mean field theory the system is supposed to undergo a first order transition between a low overlap and high overlap regime by decreasing the temperature or increasing the coupling. The first order critical line in the  $(\epsilon, T)$  phase diagram culminates in a second order critical point. We have been able to systematically describe the high temperature behaviour above the second order critical point revealing the existence of a Widom line, which support the presence of a thermodynamic transition at lower temperatures. We study statical and dynamical properties of the system. In the high coupling regime we detect the presence of a jump dynamics, dynamical heterogeneities and the violation of the Stokes Einstein relation that appears in an exotic form as compared to the original system. These results are not conclusive about the existence of a thermodynamic transition, and they mainly suffer from the intervention of the slowing down.

Results from this chapter led to the publication of one article, Ref. [110].

Chapter 3 represents the bulk of our study. In this chapter we address the problem of equilibrating supercooled liquids below the computational glass transition  $T \approx T_{MCT}$ . To this aim we employ Monte Carlo simulations based on the swap algorithm discussed in Sec. 1.3.3. We simulate both systems already previously employed in the literature and systems introduced on purpose. For many systems we have been able to reach thermalization beyond the computational glass transition and for some of them

we produce equilibrium configurations at temperatures comparable to the laboratory systems. There are two main drawbacks in performing swap simulations. The first is the fact that, since it allows the equilibration at prohibitive temperatures for standard simulations, one needs to be certain of equilibration. The second issue is the fact that an enhanced exploration of phase diagram also boosts ordering, the ground state of supercooled liquids being the crystalline state. For many of our systems we observe ordering effects during the simulations that either lead to crystals or to phase separation. To solve these issues we set up a protocol that carefully deals both with equilibration and ordering. We quantify the orders of magnitude of speed up obtained in swap simulations using an extrapolation technique that is able to locate the laboratory glass transition  $T_g$ . We detect the presence of a kinetic slowing down in swap simulations at lower temperature as compared to standard dynamics, the nature of which is still unclear. We perform an analysis of the physical mechanism behind swap simulations finding that the three dimensional dynamics is characterized by two time correlation functions that decay in two-steps both for translational and for diameter degrees of freedom. Moreover, we observe that dynamical heterogeneity disappears across the Mode-Coupling regime and it is re-established for lower temperatures, concurrently with the kinetic slowing down.

In the following we sum up results found for each system under investigation.

We simulate a binary mixture and a ternary mixture that were previously employed in swap Monte Carlo simulations. The binary mixture was largely used in the literature, however, we find a very poor stability reducing the temperature, and the system cannot be equilibrated below  $T_{MCT}$ . The ternary mixture was introduced two years ago in Ref. [80]. We repeat and extend previous simulations, and we find that the accessible temperature regime using swap simulations is considerably narrower compared to the one previously claimed since the system easily presents phase separation. This model, however, can be equilibrated slightly below  $T_{MCT}$ .

We introduce a class of polydisperse models in which particle diameters vary continuously from a lower to an upper bound. We tune polydispersity in order to suppress ordering in the system, and we perform simulations varying potential softness and using both additive and non additive interactions. We conclude that both reducing the softness and introducing non additivity suppress ordering and enhance the ability to equilibrate at very low temperatures. For this class of systems we also test a two dimensional realization obtaining equilibration at extremely low temperatures also in this case. For many of these systems we are able to equilibrate below  $T_{MCT}$  and for some of them we get an equilibrium fluid below  $T_g$ .

We introduce two classes of systems to be considered polydisperse extensions of binary mixtures. The strategy is to introduce some additional particles in between the two original species to allow particles to progressively change their diameter and improve swap performances. In one case, we modify the binary mixture of soft spheres,

we both tested a purely repulsive case and a system with Lennard-Jones interactions. We find comparable results in the two cases, equilibration the systems at extremely low temperatures. We introduce an extension of the well known Kob-Andersen Lennard Jones mixture in which few particles interpolates between the two species. We tested different realizations of the system in which the number of additional particles introduced is between 1% and 10%, such that they can be considered as a perturbation to the original system. We notice that efficiency of swap simulations depends continuously on the number of additional particles introduced and in the best case we have been able to equilibrate the modified system at a temperature remarkably below the one reached by using any other computational method.

Results presented in this chapter led to one publication [112]. Another paper is in preparation concerning the extension of the Kob-Andersen binary mixture.

In chapter 4 we employ the ability developed to equilibrate glass-forming liquids at previously unattained temperature to address four open problems of the glass transition.

The first study involves the relation between the glass and the jammed state. Since the introduction of a unified phase diagram for the glass and the jamming transitions [179], different theoretical scenarios have been proposed to clarify the relation between these two phenomena. One of them predicts that the jamming transition represents the endpoint of the equilibrium fluid line in the phase diagram [180]. In another possible scenario, by compression at equilibrium, the system first enters an ideal glass state  $\phi_K$  and subsequently it goes out of equilibrium and hits a jamming point [182]. We employ a system of continuously polydisperse hard spheres that can be equilibrated at packing fractions higher than the laboratory glass transition  $\phi_g$ . We independently locate the jamming packing fraction compressing the system out-of-equilibrium. We find that the system can be found at some high packing fractions both in equilibrium and in the jammed phase. Showing that the jamming transition cannot be the endpoint of the fluid branch, our result rules out the first theoretical scenario and demands a modification of the second scenario. Moreover, it adds some novel information about the relation between the glass and the jammed states, showing that they might be less related than what has been suggested for a long time.

This work led to one publication [111].

The second open problem regards the thermodynamic behaviour of supercooled liquids reducing the temperature. Some theories explain the slowing down through a rarefaction of the metastable states that can be directly quantified by measuring the configurational entropy. Some other theories do not assign any role to thermodynamics in the explanation of the glass formation and rely on purely dynamical considerations. The debate is hard to be settled since liquids fall out of equilibrium at the dynamical

glass transition. In fragile systems a monotonic decrease of configurational entropy was found both in experimental and in computational glass-forming liquids. However computational results were confined to the standard simulation regime. Moreover, little information is available about the dependence of this feature on dimensionality of the system. We employ a model of polydisperse soft sphere both in two and three dimensions to compute configurational entropy by thermodynamic integration for temperatures below the laboratory glass transition  $T_g$ . We found a monotonic decrease of this quantity over the whole range of temperature. The three dimensional results are consistent with the presence of a Kauzmann transition at a finite temperature, extending experimental findings in a deep supercooled regime. In two dimensions the situation is remarkably different and the result is more consistent with a vanishing Kauzmann temperature. Theoretical interpretation of this result is missing in the current state of glass theory. Also, it is unclear the relation of this thermodynamic behaviour with the recent observation of long wavelength fluctuations in two dimensional amorphous solids, both in experiments and simulations. Overall these results indicate the prominent role of the thermodynamic point of view in explaining the glass formation. We also feature a measurement of a point-to-set length that directly tests the extent of amorphous order accompanying a rarefaction of metastable states, finding coherent results with the ones obtained for the configurational entropy.

Results for the three dimensional model are included in Ref. [113], and another publication is in preparation concerning the findings in two dimensions.

The third question we address concerns the relation between relaxation times and the configurational entropy. Different theoretical predictions within the Adam-Gibbs-DiMarzio (AGD) theory and the Random First Order Transition (RFOT) theory connects these two quantities in order to quantitatively explain the glassy slowdown, and they also require the presence of growing amorphous order in the system.

Using thermodynamic and dynamic observables one can extract two critical temperatures, that coincide in AGD and RFOT frameworks, and represent temperature of divergence of relaxation times. It has been proposed a counterargument to the validity of critical theories based on the fact that extrapolated values of these two temperature were found to be different in some experimental systems and the increase of relaxation times could also be described with divergence-free functional forms. We employ the measurements previously obtained of configurational entropy, point-to-set length and relaxation times to test theoretical predictions in a novel regime. We found that the AGD framework makes poor predictions of data, and we introduce an empirical functional form that can be directly connected to the scaling prediction of the RFOT theory. We measure two critical exponents characteristic of RFOT, the first,  $\theta$ , relating the typical size of correlated amorphous regions to configurational entropy, and the second,  $\psi$ , linking thermodynamic and dynamic properties. For the estimation of  $\theta$ , we use purely thermodynamic quantities in a bare system and compare with result previously obtained either using dynamical correlation or constrained systems. Finally, we employ exper-

imental data to provide strong basis to our claim, finding a good agreement with our predictions. We found that the introduction of a surface tension term, provided in RFOT, is a necessary ingredient to a correct description of the slowing down and thanks to this additional refinement the observed deviations between thermodynamic and dynamical critical temperatures can be explained also within RFOT theory.

A paper featuring these results is in preparation.

Finally, we want to inspect the topological properties of the Potential Energy Landscape(PEL) beyond the Mode-Coupling crossover temperature  $T_{MCT}$ . Some years ago it was found, both in mean-field theory and in computational glass formers, a so-called geometric transition. This is a topology change of the landscape between a saddle-dominated region at high energy and a minima-dominated region at low energy that has consequences for the system dynamics. Namely, at high temperature  $T > T_{MCT}$  the system explores zone of the landscape dominated by the presence of the saddle points, and complete relaxations are allowed, whereas at low temperatures  $T < T_{MCT}$  the system do not relax and it remains confined in minima of the landscape. It was also claimed that the PEL presents some universal characteristic in structural glass-forming liquids concerning saddle points. We compare the topological properties of four different supercooled liquids. Two of them, a fragile and strong glass-former, were previously employed in the literature. Two other, made of polydisperse soft particles, were introduced in this thesis and equilibrated below  $T_{MCT}$ . We found that the previous conclusion about the presence of a geometric transition in computational glass models does not hold for our systems. Measuring topological properties in regions explored at temperatures below  $T_{MCT}$  we found the presence of saddle points together with minima. Therefore, the transition should be regarded at best as a crossover in our systems. We detect differences in landscape properties among the models under investigation that represent deviations from the claimed universality.

A paper featuring these results is in preparation.



# Chapter 6

## Discussion and Perspectives

The main result of this thesis is the equilibration of supercooled liquids in a completely novel temperature regime. This opens up a huge number of perspectives and the limited time of a doctoral thesis does not allow to cover all of them. In the following we will be dealing with perspectives and ongoing works. Some of these works involved us in person and some other involved other researchers and other groups.

One of the main questions that is left unanswered by this thesis is the reason of the remarkable dynamical speed up. Recently [164] this acceleration was motivated by enhanced relaxation at local scale. The rationale for this goes as follows. The starting point is the assumption that the glassy slowing down has two main sources. One is due to the local environment, for instance to growing energy barrier for local rearrangements. The other involves collective degrees of freedom and can be quantified with a static length. Since efficiency of the swap algorithm does not change whether exchanges moves are performed locally or on the whole system scale, the authors conclude that swap simulations are able to relax local degrees of freedom. Consequently, the kinetic slowdown should be ascribed to the presence of increasing local stiffness. The presence of a growing static length is not completely ruled out, although, in this reasoning, it would explain only 2-3 orders of magnitude of the 13 decades that characterize the slowing down. This argument is in good agreement with theoretical explanations for the glass transition that involve the shear modulus [160, 216]. However, it does not completely explain the role of the RFOT theoretical approach, where both an increasing shear modulus and static correlation length participate in the kinetic slowing down (see [17] Sec.VI). The situation may be settled by performing quantitative analysis of the role that local and collective phenomena play in the standard and swap dynamics, although so far it is unclear to us what precise quantity should be measured.

Related to the previous question is the nature of the observed slowing down in the swap Monte Carlo dynamics at lower temperature. We think that there are many possible

explanations for this to happen. It may be exclusively driven by growing static amorphous order, as suggested in [164]. Or it could have a Mode-Coupling like nature where the diameters are considered as dynamical variables. Finally, it can be a combination of the two framework or even something else. Theoretical work is in progress in this sense. Using the Mari-Kurchan model, a dynamical model able to interpolate between the infinite dimension mean-field limit and a finite dimension  $D$ , it was found that swap dynamics presents a Mode-Coupling like transition at lower temperatures [217]. This does not disagree with our results in three dimensional systems. Yet the two dimensional swap dynamics is very different, presenting relaxation times that are well described by an Arrhenius growth. The reason for this is currently under investigation.

Some criticism was address about our results, especially in oral discussions at conferences and meetings. The stronger argument is based on the fact that we created a model which is intentionally designed to work with swap simulations although it might not well describe the glass formation in general. The results presented in this thesis address this concern in many aspects. Throughout the whole manuscript we describe glassy properties of our systems featuring static, dynamical and thermodynamic properties, and we find numerous analogies with previous computational glass-forming models. Our next aim, is to dispel any doubt left by using the extension of the Kob-Andersen mixture introduced in chapter 3. By performing a further inspection of this model, continuously varying the amount of additional polydisperse particles from zero to a large value, we will show that high polydispersity do not invalidate our results and the good glass-forming ability of our models.

Another perspective for our work concerns the study of transition points in the Potential Energy Landscape. In the last chapter we describe the topological nature across  $T_{MCT}$  for two of our models. We plan to complete this investigation looking more carefully at the saddle points found below the standard simulation regime to understand whether they present a local or collective nature. This will be carried out using standard tools employed in the study of the low frequency vibrations of amorphous solids such as participation ratio and soft modes analysis.

Recently the possibility to create glasses presenting high kinetic stability was introduced by using a vapor deposition technique [218]. This *ultrastable glasses* represent a huge step forward in equilibration ability of experimental glassy material. The computational study of the properties of these material is however very limited if one uses standard simulations. Using swap simulations it was possible to recreate similar performances in equilibration in Ref. [219]. This helped in understanding the role of an enhanced surface diffusion in the creation of ultrastable glasses. Moreover, as a byprod-

uct, this also gave a hint of the extremely high stability of glassy samples produced using swap simulations. Work to quantify this stability is currently in progress [220].

Very low temperature in silico configurations, presenting high stability, can also be employed to study short time relaxations using Newtonian dynamics. Anomalies in low temperature glasses are a well established experimental property. Recently the presence of a Gardner transition in glasses was found in the mean field theory of hard spheres. This transition, happening inside the glass state, is characterized by growing timescales and lengthscales in vibrational properties. Interestingly, it was suggested that this may explain the low temperature anomalous behaviour of glasses [18]. There have been an increasing experimental and computational interest around this transition. Some evidence of a critical behaviour of vibrations was found in hard spheres using configuration prepared with a swap protocol [221]. On the contrary, results suggesting the absence of a Gardner transition have been found in one of the soft sphere system introduced in this thesis [222]. For this model no growing lengthscale and timescale was detected observing the low temperature vibrational properties.

In recent years a debated question about the glass behaviour concerned its response to mechanical deformation. In amorphous solids the stress increases as a function of an applied strain until the point at which a mechanical breakdown exhibits. This is called the yielding point. A theoretical scenario, together with some computational confirmation, was proposed in which the first order nature of this transition is revealed using as order parameter an overlap function between two glassy replicas [223]. In this framework the yielding transition is considered a spinodal with disorder [224]. Another approach, both computational and experimental, is keen on assigning a percolative nature to the transition [225]. The possibility to create very well annealed glasses offers a direct opportunity to study the nature of this transition with a high level of accuracy. Work is in progress in this direction [226].



# Chapter 7

## Acknowledgements

A PhD thesis is theater piece that lasts for years, any person I met played a role. I would like to thank them all, I feel having learned something from everyone of them.

In particular, I would like to express my gratitude to my supervisor, Ludovic Berthier, that constantly encouraged me to improve and supported me during this three years. His insight has been invaluable to my work. I would like, as well, to show my appreciation to my co-supervisor, Daniele Coslovich, and to its precious advice. I feel lucky to have had them supervising my work. I am in debit to Misaki Ozawa for all the discussions, the help, and the exchanges, scientific or not, we had during the last two years. I will repay with some special pasta.

The scientific advice coming from the professor participating to my annual *comité de thèse* has been a fundamental guidance to my work. For this I thank Jean-Louis Barrat, Giulio Biroli, Luca Cippelletti, Francesco Sciortino, and Gilles Tarjus.

Matthieu Wyart and Florent Krzakala kindly accepted to be referees of my thesis. I am grateful to them and I am sure this thesis work will deeply benefit from their contribution. I thank the professors that accepted to be part of my thesis committee: Jeppe Dyre and Chantal Valeriani. I am glad they found some time to evaluate my work.

Since science is collaboration before being competition, I am grateful to all the people that I have been, or I am, collaborating with: Patrick Charbonneau, Elijah Flenner, Grzegorz Szamel, and Sho Yaida.

People I have talked to in conferences, meetings, during short visits, or by email exchanges made a great contribution to my thesis work. Thanks to Jörg Baschnagel, Matthias Fuchs, Nicoletta Gnan, Atsushi Ikeda, Harukuni Ikeda, Robert Jack, Edan Lerner, Giorgio Parisi, Itamar Procaccia, Corrado Rainone, Riccardo Ravasio, Pierre Ronceray, Emanuela Zaccarelli, and Francesco Zamponi, for helpful discussions and comments.

The life in the lab would have not been so pleasant without all the people with which I shared the same corridor or room, and with some of them I also shared dinners, running sessions or scientific discussions. For this I thank Silvia Bonfanti, Luca Ciandrini, Supravat Dey, Christopher Fullerton, Simona Ispas, Takeshi Kawasaki, Dimitrios Kylimis, Valentin Raban, Camille Scalliet, Elsen Tjhung, Daniel Vågberg, and Zhang Zhen. Thanks

to Walter Kob, that gave me constructive comments and warm encouragement. Valerio Sorichetti introduced me to the art of climbing, thanks, I really appreciate that. Discussions and support also came from the soft matter group of Bat.11, for this I thank Stefano Aime, Dafne Musino, Angelo Pommella, and Domenico Truzzolillo.

# Chapter 8

## Résumé en français

### 8.1 Motivations

Dans le chapitre d'introduction, nous traitons de nombreux sujets liés à la formation de verre qui fournissent le contexte de recherche de cette thèse. Dans cette section, nous nous concentrons brièvement sur certains d'entre eux qui ont été la principale source de motivation de ce travail.

Dans la Sec. 1.2.5, nous avons discuté des systèmes couplés dans la théorie des champs moyens. Nous avons vu que l'introduction d'un champ de couplage entre deux répliques du système conduisait à l'émergence d'une transition de premier ordre dont le paramètre d'ordre est donné par un chevauchement qui mesure la similitude entre les deux répliques. La distribution de probabilité de cette quantité est directement liée au potentiel de Franz-Parisi et à l'entropie configurationnelle. Au cours des premiers mois de cette thèse, nous avons utilisé des simulations numériques pour étudier les propriétés statiques et dynamiques des liquides couplés, en particulier concernant le comportement du chevauchement avec la réduction de la température.

Nous avons discuté dans la Sec. 1.3.1 qu'un problème fondamental dans les études numériques des liquides surfondus provient du fait que seulement quatre ou cinq ordres de grandeur des temps de relaxation sont accessibles en équilibre, par rapport aux 13 ordres de grandeur que les expériences peuvent examiner à l'équilibre. Certaines techniques ont été introduites pour équilibrer les liquides surfondus à une température plus basse. Dans l'ensemble, ils ont été prouvés pour accélérer l'équilibration d'environ deux ordres de grandeur (Sec. 1.3.2). Seul dans le cas de Ref. [80], il a été affirmé que une accélération de plus de dix ordres de grandeur est possible en utilisant l'algorithme swap Monte Carlo (Sec. 1.3.3). L'un des principaux objectifs de cette thèse est de concevoir et mettre en œuvre des modèles et des méthodes pour accélérer la thermalisation et étendre le régime de simulation à des échelles de temps comparables à celles accessibles expérimentalement. Nous veillons particulièrement à ce que notre système atteigne une bonne équilibration et reste un fluide désordonné. Ce résultat ouvre la voie à l'étude des liquides surfondus et des verres dans des régimes inexplorés.

La troisième partie de la thèse est consacrée à l'étude des liquides surfondus dans ce nouveau régime. Parmi les questions ouvertes traitées précédemment (Ch. 1), nous abordons les éléments suivants.

Des mesures de l'entropie configurationnelle dans le cadre du paysage énergétique potentiel, ont été discutées dans les sections 1.2.1 et 1.3.4. Ils révèlent une diminution de cette quantité avec une température décroissante dans des nombreux liquides surfondus. Cependant, ces résultats ont toujours été obtenus pour de température supérieure au ralentissement dynamique des simulations. La grande majorité des résultats ont été obtenus en trois dimensions et on connaît peu du comportement thermodynamique des systèmes bidimensionnels, bien que du point de vue dynamique, la transition vitreuse s'est avéré différente en deux et trois dimensions (Sec. 1.3.5). Dans cette thèse, nous abordons deux problèmes en même temps. D'une part, nous mesurons l'entropie configurationnelle dans un régime complètement inexploré et, d'autre part, nous comparons directement entre une réalisation bidimensionnelle et une réalisation tridimensionnelle d'un système.

Dans les liquides surfondus, il n'est toujours pas clair quelle est la relation entre la thermodynamique et la dynamique, à savoir, entre les temps de relaxation et l'entropie configurationnelle. Des approches théoriques, telle que ces données par Adam-Gibbs (Sec.1.2.2) ou RFOT (Sec.1.2.4), soutiennent une relation directe entre ces deux quantités. Nous employons des résultats de simulation obtenus à une température extrêmement basse pour tester ces théories et mesurer l'exposant critique de la théorie RFOT.

Il y a quelques années, on prétendait l'existence d'une transition géométrique dans le paysage énergétique des liquides formateurs de verre (Sec. 1.3.4). Le résultat numérique, cependant, a été obtenu pour une température supérieure à la transition putative. Nous étudions la présence de cette transition effectuant des études du paysage énergétique dans le nouveau régime accessible avec des simulations de swap.

Le travail de la thèse a mené à quatre publications [110, 111, 112, 113]. Deux d'entre eux sont une production directe de cette thèse [110, 112]. Les deux autres résultent d'une plus large collaboration et incluent des résultats et des analyses développés dans cette thèse [111, 113]. Trois autres publications sont en préparation. L'un concerne les résultats sur l'entropie configurationnelle et la longueur point-to-set dans un système bidimensionnel et l'absence d'une transition de verre idéale à une température finie. Une autre caractéristique de la relation entre les temps de relaxation et l'entropie configurationnelle et la mesure de l'exposant critique de la RFOT proche de la transition. Le dernier considère l'absence de transition géométrique dans les modèles numériques des liquides formateurs de verre.

## 8.2 Résultats

Cette section est dédiée à un résumé du travail de thèse présenté dans le chapitre précédent.

Le chapitre 2 présente une étude des liquides couplés. Prenant deux copies d'un liquide formateur un verre tridimensionnel, nous définissons un chevauchement entre eux qui quantifie leur degré de similarité et nous définissons un champ de couplage comme variable conjuguée du chevauchement. La situation est similaire à celle théorique décrite dans la Sec. 1.2.5. Dans la théorie du champ moyen, le système subit une transition de premier ordre entre un régime de chevauchement faible et un de chevauchement élevé en diminuant la température ou en augmentant le couplage. La ligne critique de premier ordre dans le diagramme de phase  $(\epsilon, T)$  culmine dans un point critique de deuxième ordre. Nous avons pu décrire systématiquement le comportement à haute température au-dessus du point critique du second ordre révélant l'existence d'une ligne de Widom, qui soutiennent la présence d'une transition thermodynamique à des températures plus basses. Nous étudions les propriétés statiques et dynamiques du système. Dans le régime de couplage élevé, nous détectons la présence d'une dynamique de saut, d'hétérogénéités dynamiques et de violation de la relation de Stokes Einstein Apparatus sous une forme exotique par rapport au système d'origine. Ces résultats ne sont pas concluants quant à l'existence d'une transition thermodynamique et ils souffrent principalement de l'intervention du ralentissement.

Les résultats de ce chapitre ont conduit à la publication d'un article, Ref. [110].

Le chapitre 3 représente la majeure partie de notre étude. Dans ce chapitre, nous abordons le problème de l'équilibration des liquides surfondus en dessous de la transition vitreuse numérique  $T \approx T_{MCT}$ . Dans ce but, nous utilisons des simulations Monte Carlo basées sur l'algorithme de swap décrit dans Sec. 1.3.3. Nous simulons les deux systèmes précédemment employés dans la littérature et introduisons d'autres nouveaux systèmes. Pour des nombreux systèmes, nous avons pu atteindre la thermisation au-delà de la transition vitreuse numérique et pour certains d'entre eux nous avons produit des configurations d'équilibre à des températures comparables aux systèmes expérimentales. Il existe deux inconvénients principaux dans l'exécution de simulations de swap. Le premier est le fait que, puisqu'il permet l'équilibration à des températures prohibitives pour les simulations standard, il faut s'assurer d'être vraiment à l'équilibre. Le deuxième problème est le fait que l'amélioration de l'exploration du diagramme de phase augmente également la possibilité de présence d'ordre, étant donné que l'état fondamental des liquides surfondus est l'état cristallin. Pour beaucoup de nos systèmes, nous observons des effets d'ordre pendant les simulations qui conduisent soit à des cristaux, soit à des phases séparées. Pour résoudre ces problèmes, nous avons mis en place un protocole qui traite soigneusement l'équilibration et l'ordre. Nous quantifions les ordres de grandeur d'accélération obtenus dans les simulations de swap à l'aide d'une technique d'extrapolation qui est capable de localiser la transition vitreuse expérimentale  $T_g$ . Nous détectons la présence d'un ralentissement cinétique dans les simulations de swap à basse

température par rapport à la dynamique standard dont la nature est encore incertaine. Nous effectuons une analyse du mécanisme physique derrière les simulations de swap constatant que la dynamique est caractérisée par des relaxations qui se décomposent en deux étapes: d'abord une partie vibrationnelle et ensuite une partie structurelle, à la fois pour des degrés de libération et pour des degrés de liberté de diamètre. De plus nous observons que l'hétérogénéité dynamique disparaît à travers le régime de crossover de la théorie de couplage de mode et est rétablie pour des températures plus basses, en même temps que le ralentissement cinétique.

Dans ce qui suit, nous résumons les résultats obtenus pour chaque système.

Nous simulons un mélange binaire et un mélange ternaire qui ont déjà été employés dans des simulations Monte Carlo. Le mélange binaire a été largement utilisé dans la littérature, mais nous avons trouvé une très mauvaise stabilité en réduisant la température et le système ne peut être équilibré en dessous de  $T_{MCT}$ . Le mélange ternaire a été introduit il y a deux ans dans la Ref. [80]. Nous répétons et étendons les simulations précédentes et nous avons constaté que le régime de température accessible utilisant des simulations de swap est considérablement plus étroit par rapport à celui revendiqué précédemment puisque le système présente facilement une séparation de phase. Ce modèle, cependant, peut être équilibré légèrement en dessous de  $T_{MCT}$ .

Nous présentons une classe de modèles polydispersés dans lesquels les diamètres des particules varient continuellement entre une limite inférieure à une limite supérieure. Nous réglons la polydispersité afin de supprimer l'ordre dans le système et nous effectuons des simulations variant la souplesse du potentiel et en utilisant à la fois des interactions additive et non additive. Nous concluons que la réduction de la souplesse et l'introduction de la non-additivité supprime l'ordre et améliore la capacité à équilibrer à des températures très basses, le meilleur cas donné par un fluide de sphère dure. Pour cette classe de systèmes, nous testons également une réalisation bidimensionnelle obtenant l'équilibre à des températures extrêmement basses dans ce cas également. Pour beaucoup de ces systèmes, nous pouvons équilibrer dessous  $T_{MCT}$  et pour certains d'entre eux, dessous  $T_g$ .

Nous présentons deux classes de systèmes que peuvent être considérés comme des extensions polydisperses de mélanges binaires. La stratégie consiste à introduire des particules entre les deux espèces pour permettre aux particules de changer progressivement leur diamètre et d'améliorer les performances de swap. Dans un cas, nous modifions la mélange binaire de sphères molles, nous avons testé à la fois un cas purement répulsif ainsi que un système avec des interactions Lennard-Jones. Nous avons trouvé des résultats comparables dans les deux cas, ce qui a permis d'équilibrer également ce système à des températures extrêmement basses. Nous introduisons une extension du mélange de Kob-Andersen Lennard Jones dans lequel un petit nombre de particules inter-pole entre les deux espèces. Nous avons testé différentes réalisations du système dans lequel le nombre de particules introduites est entre 1% et 10% tel qu'ils peuvent être con-

sidérés comme une perturbation du système original. Nous constatons que l'efficacité des simulations de swap dépend continuellement du nombre de particules supplémentaires introduites et dans le meilleur des cas nous avons été capable d'équilibrer le système à une température remarquablement inférieure à celle atteinte en utilisant des autres méthodes numériques.

Les résultats présentés dans ce chapitre ont conduit à une publication [112]. Un autre article est en préparation concernant l'extension du mélange binaire Kob-Andersen.

Dans le chapitre 4, nous employons la capacité développée pour équilibrer les liquides formateurs de verre à une température précédemment non atteinte pour résoudre quatre problèmes ouverts de la transition vitreuse.

La première étude implique la relation entre la transition vitreuse et le jamming. Depuis l'introduction d'un diagramme de phase unifié pour le verre et la transition de jamming [179], des différents scénarios théoriques ont été proposés pour clarifier la relation entre ces deux phénomènes. L'un d'entre eux prédit que la transition de jamming se produit comme point final de la ligne de fluide d'équilibre dans le diagramme de phase [180]. Dans un autre scénario possible, par compression depuis l'équilibre, le système entre d'abord dans un état de verre idéal  $\phi_k$  et par la suite il sort de l'équilibre et frappe un point de jamming [182]. Nous employons un système à polydispersité continu de sphère dure qui peut être équilibré aux fractions d'emballage plus haut que celle de la transition vitreuse expérimentale  $\phi_g$ . Nous localisons de manière indépendante la fraction d'emballage de jamming en comprimant le système hors d'équilibre. Nous trouvons que le système peut être trouvé à des fractions d'emballage élevées à la fois en équilibre et en phase bloquée. Ce résultat exclut le premier scénario théorique et plaide pour une modification de la deuxième possibilité, montrant que la transition de jamming ne peut pas être le point final de la branche de fluide. En outre, il ajoute des informations nouvelles sur la relation entre le verre et les états bloqués, montrant qu'ils pourraient être moins liés par rapport à ce qui a été suggéré depuis longtemps.

Ces résultats ont mené à une publication [111].

Le deuxième problème ouvert concerne le comportement thermodynamique des liquides surfondus réduisant la température. Certaines théories expliquent le ralentissement par une raréfaction des états métastables qui peut être quantifié directement en mesurant l'entropie configurationnelle. Certaines autres théories n'attribuent aucun rôle à la thermodynamique dans l'explication de la formation du verre et reposent sur des considérations purement dynamiques. Le débat est difficile à régler, car les liquides tombent hors d'équilibre lors de la transition vitreuse dynamique. Dans les systèmes fragiles, une diminution monotone de l'entropie configurationnelle a été trouvée à la fois dans les expériences et dans les simulations des liquides formateurs de verre. Cepen-

dant, les résultats numériques ont été confinés au régime de simulation standard. En outre, peu d'informations sont disponibles sur la dépendance de cette fonction de la dimensionnalité du système. Nous employons un modèle de sphère molle polydispersée à la fois en deux et trois dimensions pour calculer l'entropie configurationnelle par intégration thermodynamique pour des températures inférieures à la transition vitreuse expérimentale  $T_g$ . Nous avons constaté une diminution monotone de cette quantité sur toute la gamme de température atteinte. Les résultats tridimensionnels sont compatibles avec la présence d'une transition de Kauzmann à une température finie. Dans deux dimensions, la situation est remarquablement différente et le résultat est plus conforme à une température de Kauzmann qui disparaît. L'interprétation théorique de ces résultats est manquante dans l'état actuel de la théorie du verre. En outre, il n'est pas clair la relation de ce comportement thermodynamique avec l'observation récente de fluctuations à grande longueur d'onde dans les solides amorphes, à la fois dans des expériences et des simulations. Dans l'ensemble, ces résultats indiquent le rôle prépondérant du point de vue thermodynamique en expliquant la formation du verre. Nous disposons également d'une mesure d'une longueur ponctuelle qui teste directement l'extension de l'ordre amorphe accompagnant une raréfaction d'états métastables, en trouvant un scénario cohérent avec l'entropie configurationnelle.

Les résultats pour le modèle tridimensionnel sont inclus dans Ref. [113] et une autre publication est en préparation concernant les résultats en deux dimensions.

La troisième question à l'examen concerne la relation entre les temps de relaxation et l'entropie configurationnelle. Différentes prédictions théoriques, au sein de la théorie Adam-Gibbs-DiMarzio (AGD) et de la théorie Random First Order Transition (RFOT), utilisent ces deux quantités afin d'expliquer quantitativement l'arrestation cinétique et ils exigent également la présence d'un ordre amorphe croissant dans le système. En réalisant indépendamment des ajustements dans la région accessible des données thermodynamiques et dynamiques, on peut extraire deux températures critiques pour la divergence des temps de relaxation, qui coïncident dans certains cadres théoriques. Il a été proposé un contre-argument à la validité des théories critiques en fonction du fait que ces extrapolations ont été trouvées différentes dans certains systèmes expérimentaux et l'augmentation des temps de relaxation pourrait également être décrite avec des formes fonctionnelles sans divergences. Nous employons les mesures précédemment obtenues d'entropie configurationnelle, de longueur point-to-set et de temps de relaxation pour mettre à l'épreuve les prédictions théoriques dans un nouveau régime. Nous avons constaté que le cadre AGD fait de mauvaises prédictions des données et nous introduisons une fonction qui peut être directement reliée aux prédictions de la théorie RFOT. Suivant cette analogie, nous mesurons deux exposants critiques de la théorie, le premier reliant la taille typique des régions amorphes corrélées à l'entropie configurationnelle et la deuxième reliant les propriétés thermodynamiques et dynamiques. Dans le premier cas, nous faisons cela en utilisant des quantités purement thermodynamiques dans un système non contraint et on compare avec les précédents obtenus soit en utilisant une

corrélation dynamique si bien que des systèmes contraints. Enfin, nous utilisons des données expérimentales pour fournir une base solide à notre résultat, en trouvant un bon accord avec nos prévisions. Nous avons constaté que le traitement du terme de tension de surface donné par RFOT est un ingrédient nécessaire à une description correcte du ralentissement et grâce à ce raffinement supplémentaire, les écarts observés entre les facteurs thermodynamiques et des températures de transition dynamiques peuvent être expliqués.

Un article présentant ces résultats est en préparation.

Enfin, nous voulons inspecter les propriétés topologiques du paysage énergétique potentiel au-delà de la température de crossover de la théorie de couplages de modes  $T_{MCT}$ . Il y a quelques années, il a été trouvé une transition dite géométrique, tant dans la théorie des champs moyens que dans les formateurs de verre numériques. Il s'agit d'un changement de topologie du paysage entre une région dominée par les selles à haute énergie et une région dominée par les minima à faible énergie qui se reflète dans la dynamique du système et on prétendait être universel dans les liquides formateurs de verre numériques. À savoir, à haute température  $T > T_{MCT}$  le système explore la zone du paysage dominée par la présence des points de selle, et les relaxations complètes sont autorisées, alors qu'à basse température  $T < T_{MCT}$  le système ne décorrèle pas et il reste confiné dans les minima du paysage. Nous comparons les propriétés topologiques de quatre liquides surfondus différents. Deux d'entre eux, un verre fragile et un verre fort, étaient précédemment employés dans la littérature. Deux autres, constitués de particules molles polydispersées, ont été introduits dans cette thèse et équilibrés au-dessous de  $T_{MCT}$ . Nous avons constaté que la conclusion précédente concernant la présence d'une transition géométrique dans les modèles numériques ne se tiennent pas pour nos systèmes. En mesurant les propriétés topologiques dans les régions explorées à des températures inférieures à  $T_{MCT}$  nous avons trouvé toujours la présence de points de selle. Par conséquent, la transition devrait être considérée au mieux comme un crossover dans nos systèmes. Nous détectons aussi des différences dans les propriétés du paysage énergétique parmi les modèles qui représentent des écarts par rapport à l'universalité revendiquée précédemment.

Un article présentant ces résultats est en préparation.

### 8.3 Discussion et Perspectives

Le résultat principal de cette thèse est l'équilibration des liquides surfondus dans un régime de température complètement nouveau. Cela ouvre un grand nombre de perspectives et le temps limité d'une thèse de doctorat ne permet pas de couvrir tous ceux-ci. Dans ce qui suit, nous aborderons les perspectives et les travaux en cours. Certains de ces travaux nous ont impliqué en personne et d'autres ont été réalisés par d'autres chercheurs et d'autres groupes.

L'une des principales questions qui restent sans réponse dans par cette thèse est la raison de vitesse dynamique remarquable. Récemment [164], cette accélération a été motivée par une relaxation accrue à l'échelle locale. La raison d'être est la suivante. Le point de départ est l'hypothèse que le ralentissement vitreux comporte deux sources principales. L'un est dû à l'environnement local, par exemple à la barrière énergétique croissante pour les réarrangements locaux. L'autre implique des degrés de liberté collectifs et peut être quantifié avec une longueur statique. Puisque l'efficacité de l'algorithme de swap ne change pas si les mouvements d'échanges sont effectués localement ou sur l'ensemble de l'échelle du système, les auteurs concluent que les simulations de swap permettent de relcher les degrés de liberté locaux. Par conséquent, le ralentissement cinétique devrait être attribué à la présence d'une rigidité locale croissante. La présence d'une longueur statique croissante n'est pas complètement exclue, bien que, dans ce raisonnement, il explique seulement 2-3 ordres de grandeur des 13 ordres qui caractérisent le ralentissement. Cet argument est en accord avec les explications théoriques de la transition vitreuse qu'implique le module de cisaillement [160, 216]. Cependant, il n'explique pas complètement le rôle de l'approche théorique RFOT, où un module de cisaillement croissant et la longueur de corrélation statique participe ensemble au ralentissement cinétique (voir [17] Sec.VI). La situation peut être réglée en effectuant une analyse quantitative du rôle que jouent les phénomènes locaux et collectifs jouer dans la dynamique standard et de swap, bien qu'il ne nous soit pas clair jusqu'ici quelle quantité précise doit être mesurée.

Une autre question, aussi reliée à la question précédente, regarde la nature du ralentissement observé dans la dynamique swap Monte Carlo à basse température. Nous pensons qu'il existe de nombreuses explications possibles pour que cela se produise. Il peut être exclusivement conduit par un ordre amorphe statique croissant, comme suggéré dans [164]. Ou il pourrait être expliqué par une théorie de couplages de modes où les diamètres sont considérés comme des variables dynamiques. Enfin, il peut s'agir d'une combinaison des deux frameworks ou même d'une autre chose. Le travail théorique est en cours dans ce sens [217]. En utilisant le modèle Mari-Kurchan, un modèle dynamique capable d'interpoler entre La limite de champ moyen de dimension infinie et une dimension finie  $D$ , on a constaté que la dynamique de swap présente une transition de théorie de couplages de modes à températures plus basses par rapport au system où les swap sont interdits. Ceci n'est pas en désaccord avec nos résultats dans les systèmes tridimensionnels. Pourtant, la dynamique bidimensionnelle des échanges est très différents, présentant des temps de relaxation bien décrits par une croissance d'Arrhenius la raison pour cela est actuellement à l'étude.

Certaines critiques ont été portés sur nos résultats, en particulier dans les discussions orales lors de conférences et réunions. L'argument le plus fort est basé sur le fait que

nous avons créé un modèle qui est intentionnellement réalisé pour fonctionner avec des simulations de swap bien que cela ne décrit pas bien la formation de verre en général. Les résultats présentés dans cette thèse abordent cette préoccupation dans de nombreux aspects. Tout au long du manuscrit, nous décrivons les propriétés vitreuses de nos systèmes présentant des caractéristiques statiques, dynamiques et thermodynamiques et nous trouvons de nombreuses analogies avec les précédents modèles de formation de verre. Notre prochain objectif sur ce front est de dissiper tout doute en utilisant l'extension du mélange Kob-Andersen introduit dans Chapitre 3. En effectuant une inspection supplémentaire de ce modèle, en variant en manière continu la quantité de particules polydisperses supplémentaires de zéro à une grande valeur, nous montrerons que la haute polydispersité n'invalide pas nos résultats et la bonne capacité de formation du verre de nos modèles.

Une autre perspective pour notre travail concerne l'étude des points de transition dans le paysage énergétique potentiel. Dans le dernier chapitre, nous décrivons la topologie du paysage énergétique à travers  $T_{MCT}$  pour deux de nos modèles. Nous prévoyons compléter cette enquête en examinant plus attentivement les points de selle trouvés dessous du régime de simulation standard pour comprendre s'ils présentent une nature locale ou collective. Cela sera réalisé à l'aide d'outils standard utilisés dans l'étude des vibrations à basse fréquence des solides amorphes tels que le taux de participation et l'analyse des modes doux.

Récemment, la possibilité de créer des verres présentant une grande stabilité cinétique a été introduite en utilisant une technique de dépôt en phase vapeur [218]. Ces *verres ultra-stables* représentent un énorme pas en avant dans la capacité d'équilibration du matériau vitreux expérimental. L'étude de calcul des propriétés de ces matériaux est toutefois très limitée si l'on utilise des simulations standard. En utilisant des simulations de swap, il a été possible de recréer des performances similaires en équilibration dans Ref. [219]. Cela a permis de comprendre le rôle de la diffusion de surface dans la création de verres ultra-stables. En outre, en tant que sous-produit, cela a également donné un soupçon de la stabilité extrêmement élevée des échantillons vitreux produits en utilisant des simulations de swap. Des études pour quantifier cette stabilité sont actuellement en cours [220].

Des configurations numérique à très basse température, présentant une stabilité élevée, peuvent également être utilisées pour étudier des relaxations à court terme à l'aide de la dynamique newtonienne. Les anomalies dans les verres à basse température sont une propriété expérimentale bien établie. Récemment, la présence d'une transition de Gardner a été trouvée dans la théorie de champ moyen des sphères dures. Cette transition,

se produisant à l'intérieur de l'état du verre, se caractérise par l'augmentation du temps et des longueurs des vibrations. Fait intéressant, il a été suggéré que cela pourrait expliquer le comportement anormal des verres [18]. Il y a eu un intérêt expérimental et numérique croissant autour de cette transition. Quelques preuves d'un comportement critique des vibrations ont été trouvées dans la sphère dure en utilisant des configurations préparées avec un protocole de swap [221]. Au contraire, des résultats suggérant l'absence d'une transition de Gardner ont été trouvés dans Ref. [222] où aucune croissance de la longueur de corrélation ou des échelles de temps n'a été détectée en observant les propriétés vibrationnelles de sphère molles à basse température.

Au cours des dernières années, une question débattue à l'égard du comportement du verre a concerné sa réponse à la déformation mécanique. Dans les solides amorphes, la déformation augmente en fonction du contrainte appliqué jusqu'au point de déformation plastique. C'est ce qu'on appelle la limite d'élasticité. Un scénario théorique, accompagné d'une confirmation numérique, a été proposé dans lequel la nature du premier ordre de cette transition est révélée en utilisant comme paramètre d'ordre une fonction de chevauchement entre deux répliques cristallines [223]. Dans ce cadre, la transition est considérée comme une spinodale avec désordre [224]. Une autre approche, à la fois computationnelle et expérimentale, est désireuse d'affecter un caractère percolatif à la transition [225]. La possibilité de créer des verres très bien recuit offre une opportunité directe d'étudier la nature de cette transition avec un haut niveau de précision. Des travaux sont en cours dans cette direction [226].

# Bibliography

- [1] J. P. Hansen and I. R. McDonald, *Theory of simple liquids : with applications to soft matter*. Amsterdam Boston: Academic Press, 2013.
- [2] C. Angell, “Structural instability and relaxation in liquid and glassy phases near the fragile liquid limit,” *Journal of Non-Crystalline Solids*, vol. 102, pp. 205–221, jun 1988.
- [3] W. Kauzmann, “The nature of the glassy state and the behavior of liquids at low temperatures.,” *Chemical Reviews*, vol. 43, pp. 219–256, oct 1948.
- [4] M. D. Ediger, C. A. Angell, and S. R. Nagel, “Supercooled liquids and glasses,” *J. Phys. Chem.*, vol. 100, p. 13200, 1996.
- [5] J. Wuttke, W. Petry, and S. Pouget, “Structural relaxation in viscous glycerol: Coherent neutron scattering,” *The Journal of Chemical Physics*, vol. 105, pp. 5177–5182, sep 1996.
- [6] L. Berthier and G. Biroli, “Theoretical perspective on the glass transition and amorphous materials,” *Rev. Mod. Phys.*, vol. 83, pp. 587–645, Jun 2011.
- [7] J. P. Boon and S. Yip, *Molecular hydrodynamics*. New York: Dover Publications, 1991.
- [8] M. E. Cates, *Course 3: Structural Relaxation and Rheology of Soft Condensed Matter*, pp. 75–129. Berlin, Heidelberg: Springer Berlin Heidelberg, 2003.
- [9] G. L. Hunter and E. R. Weeks, “The physics of the colloidal glass transition,” *Reports on Progress in Physics*, vol. 75, p. 066501, may 2012.
- [10] L. Berthier and T. A. Witten, “Glass transition of dense fluids of hard and compressible spheres,” *Physical Review E*, vol. 80, aug 2009.
- [11] P. W. Anderson, “Through the glass lightly,” *Science*, vol. 267, no. 5204, pp. 1615–1616, 1995.
- [12] J. H. Gibbs, “Nature of the glass transition in polymers,” *The Journal of Chemical Physics*, vol. 25, pp. 185–186, jul 1956.
- [13] J. H. Gibbs and E. A. DiMarzio, “Nature of the glass transition and the glassy state,” *The Journal of Chemical Physics*, vol. 28, pp. 373–383, mar 1958.
- [14] G. Adam and J. H. Gibbs, “On the temperature dependence of cooperative relaxation properties in glass-forming liquids,” *The Journal of Chemical Physics*, vol. 43, no. 1, pp. 139–146, 1965.
- [15] W. Götze, *Complex Dynamics of Glass-Forming Liquids: A Mode-Coupling Theory (International Series of Monographs on Physics)*. Oxford University Press, 2009.
- [16] F. Sciortino, “Potential energy landscape description of supercooled liquids and glasses,” *Journal of Statistical Mechanics: Theory and Experiment*, vol. 2005, p. P05015, may 2005.

- [17] G. Biroli and J.-P. Bouchaud, *The Random First-Order Transition Theory of Glasses: A Critical Assessment*, pp. 31–113. John Wiley and Sons, Inc., 2012.
- [18] P. Charbonneau, J. Kurchan, G. Parisi, P. Urbani, and F. Zamponi, “Glass and jamming transitions: From exact results to finite-dimensional descriptions,” *Annual Review of Condensed Matter Physics*, vol. 8, pp. 265–288, mar 2017.
- [19] G. Tarjus, S. A. Kivelson, Z. Nussinov, and P. Viot, “The frustration-based approach of supercooled liquids and the glass transition: a review and critical assessment,” *Journal of Physics: Condensed Matter*, vol. 17, pp. R1143–R1182, dec 2005.
- [20] J. P. Garrahan and D. Chandler, “Coarse-grained microscopic model of glass formers,” *Proceedings of the National Academy of Sciences*, vol. 100, pp. 9710–9714, aug 2003.
- [21] M. Goldstein, “Viscous liquids and the glass transition: A potential energy barrier picture,” *The Journal of Chemical Physics*, vol. 51, pp. 3728–3739, nov 1969.
- [22] F. H. Stillinger and T. A. Weber, “Hidden structure in liquids,” *Phys. Rev. A*, vol. 25, pp. 978–989, Feb. 1982.
- [23] F. H. Stillinger and T. A. Weber, “Packing structures and transitions in liquids and solids,” *Science*, vol. 225, pp. 983–989, sep 1984.
- [24] F. H. Stillinger, “A topographic view of supercooled liquids and glass formation,” *Science*, vol. 267, no. 5206, pp. 1935–1939, 1995.
- [25] L. Berthier, G. Biroli, J.-P. Bouchaud, L. Cipelletti, D. E. Masri, D. L’Hôte, F. Ladieu, and M. Pierno, “Direct experimental evidence of a growing length scale accompanying the glass transition,” *Science*, vol. 310, no. 5755, pp. 1797–1800, 2005.
- [26] T. R. Kirkpatrick and D. Thirumalai, “Dynamics of the structural glass transition and the p-spin–interaction spin-glass model,” *Physical Review Letters*, vol. 58, pp. 2091–2094, may 1987.
- [27] T. R. Kirkpatrick, D. Thirumalai, and P. G. Wolynes, “Scaling concepts for the dynamics of viscous liquids near an ideal glassy state,” *Phys. Rev. A*, vol. 40, p. 1045, 1989.
- [28] T. R. Kirkpatrick and D. Thirumalai, “Random solutions from a regular density functional hamiltonian: a static and dynamical theory for the structural glass transition,” *Journal of Physics A: Mathematical and General*, vol. 22, no. 5, p. L149, 1989.
- [29] M. Mezard and G. Parisi, *Glasses and Replicas in ‘Structural Glasses and Supercooled Liquids: Theory, Experiment, and Applications’*. New Jersey: Wiley, 2012.
- [30] J. Kurchan, G. Parisi, and F. Zamponi, “Exact theory of dense amorphous hard spheres in high dimension i. the free energy,” *Journal of Statistical Mechanics: Theory and Experiment*, vol. 2012, p. P10012, oct 2012.
- [31] J. Kurchan, G. Parisi, P. Urbani, and F. Zamponi, “Exact theory of dense amorphous hard spheres in high dimension. II. the high density regime and the gardner transition,” *The Journal of Physical Chemistry B*, vol. 117, pp. 12979–12994, oct 2013.
- [32] P. Charbonneau, J. Kurchan, G. Parisi, P. Urbani, and F. Zamponi, “Exact theory of dense amorphous hard spheres in high dimension. III. the full replica symmetry breaking solution,” *Journal of Statistical Mechanics: Theory and Experiment*, vol. 2014, p. P10009, oct 2014.

- [33] A. Montanari and G. Semerjian, "Rigorous inequalities between length and time scales in glassy systems," *Journal of Statistical Physics*, vol. 125, pp. 23–54, oct 2006.
- [34] J.-P. Bouchaud and G. Biroli, "On the adam-gibbs-kirkpatrick-thirumalai-wolynes scenario for the viscosity increase in glasses," *J. Chem. Phys.*, vol. 121, no. 15, pp. 7347–7354, 2004.
- [35] L. Berthier and M. D. Ediger, "Facets of glass physics," *Physics Today*, vol. 69, pp. 40–46, jan 2016.
- [36] S. Franz and G. Parisi, "Phase diagram of coupled glassy systems: A mean-field study," *Phys. Rev. Lett.*, vol. 79, p. 13, 1997.
- [37] S. Franz and G. Parisi, "Effective potential in glassy systems: theory and simulations," *Physica A*, vol. 261, pp. 317–339, 1998.
- [38] L. Berthier and D. Coslovich, "A novel approach to numerical measurements of the configurational entropy in supercooled liquids," *Proc. Natl. Acad. USA*, vol. 111, p. 11668, 2014.
- [39] L. Berthier, "Overlap fluctuations in glass-forming liquids," *Phys. Rev. E*, vol. 88, p. 022313, 2013.
- [40] J.-L. Barrat, J.-N. Roux, and J.-P. Hansen, "Diffusion, viscosity and structural slowing down in soft sphere alloys near the kinetic glass transition," *Chem. Phys.*, vol. 149, p. 197, dec 1990.
- [41] W. Kob and H. C. Andersen, "Testing mode-coupling theory for a supercooled binary Lennard-Jones mixture. II. Intermediate scattering function and dynamic susceptibility," *Phys. Rev. E*, vol. 52, pp. 4134–4153, oct 1995.
- [42] G. Brambilla, D. E. Masri, M. Pierno, L. Berthier, L. Cipelletti, G. Petekidis, and A. B. Schofield, "Probing the equilibrium dynamics of colloidal hard spheres above the mode-coupling glass transition," *Phys. Rev. Lett.*, vol. 102, p. 085703, feb 2009.
- [43] M. P. Allen and D. J. Tildesley, *Computer simulation of liquids*. Oxford England New York: Clarendon Press Oxford University Press, 1989.
- [44] D. Frenkel and B. Smit, *Understanding Molecular Simulation*. London: Academic Press, 2002.
- [45] W. Kob, "Computer simulations of supercooled liquids and glasses," *Journal of Physics: Condensed Matter*, vol. 11, no. 10, p. R85, 1999.
- [46] N. Metropolis, A. W. Rosenbluth, M. N. Rosenbluth, A. H. Teller, and E. Teller, "Equation of state calculations by fast computing machines," *The Journal of Chemical Physics*, vol. 21, pp. 1087–1092, jun 1953.
- [47] L. Berthier and W. Kob, "The Monte Carlo dynamics of a binary Lennard-Jones glass-forming mixture," *J. Phys.: Condens. Matter*, vol. 19, p. 205130, apr 2007.
- [48] W. Kob and H. C. Andersen, "Scaling behavior in the beta-relaxation regime of a supercooled lennard-jones mixture," *Phys. Rev. Lett.*, vol. 73, p. 1376, sep 1994.
- [49] N. P. Bailey, T. S. Ingebrigtsen, J. S. Hansen, A. A. Veldhorst, L. Bhling, C. A. Lemarchand, A. E. Olsen, A. K. Bacher, H. Larsen, J. C. Dyre, and et al., "RUMD: A general purpose molecular dynamics package optimized to utilize GPU hardware down to a few thousand particles," *arXiv:1506.05094*, Jun 2015.

- [50] R. H. Swendsen and J.-S. Wang, "Nonuniversal critical dynamics in Monte Carlo simulations," *Phys. Rev. Lett.*, vol. 58, p. 86, Jan 1987.
- [51] K. Binder, *The Monte-Carlo Methods in Condensed Matter Physics*. Springer, Heidelberg, 1992.
- [52] W. Krauth, *Statistical Physics: algorithms and computations*. Oxford: Oxford University Press, 2011.
- [53] W. Krauth and L. Santen, "Absence of thermodynamic phase transition in a model glass former," *Nature*, vol. 405, pp. 550–551, Jun 2000.
- [54] E. P. Bernard, W. Krauth, and D. B. Wilson, "Event-chain Monte Carlo algorithms for hard-sphere systems," *Phys. Rev. E*, vol. 80, p. 056704, Nov 2009.
- [55] M. Michel, S. C. Kapfer, and W. Krauth, "Generalized event-chain monte carlo: Constructing rejection-free global-balance algorithms from infinitesimal steps," *The Journal of Chemical Physics*, vol. 140, p. 054116, Feb 2014.
- [56] E. P. Bernard and W. Krauth, "Two-step melting in two dimensions: First-order liquid-hexatic transition," *Phys. Rev. Lett.*, vol. 107, p. 155704, Oct 2011.
- [57] M. Isobe and W. Krauth, "Hard-sphere melting and crystallization with event-chain Monte Carlo," *J. Chem. Phys.*, vol. 143, p. 084509, Aug 2015.
- [58] K. Hukushima and K. Nemoto, "Exchange Monte Carlo Method and Application to Spin Glass Simulations," *J. Phys. Soc. Jap.*, vol. 65, p. 1604, Jun 1996.
- [59] K. Hukushima, H. Takayama, and H. Yoshino, "Exchange Monte Carlo Dynamics in the SK Model," *J. Phys. Soc. Jap.*, vol. 67, p. 12, Jan 1998.
- [60] R. Yamamoto and W. Kob, "Replica-exchange molecular dynamics simulation for supercooled liquids," *Phys. Rev. E*, vol. 61, p. 5473, May 2000.
- [61] G. Odriozola and L. Berthier, "Equilibrium equation of state of a hard sphere binary mixture at very large densities using replica exchange Monte Carlo simulations," *J. Chem. Phys.*, vol. 134, p. 054504, Feb 2011.
- [62] W. Kob and L. Berthier, "Probing a Liquid to Glass Transition in Equilibrium," *Phys. Rev. Lett.*, vol. 110, p. 245702, 2013.
- [63] L. Berthier and R. L. Jack, "Evidence for a disordered critical point in a glass-forming liquid," *Phys. Rev. Lett.*, vol. 114, no. 20, p. 205701, 2015.
- [64] M. Ozawa, W. Kob, A. Ikeda, and K. Miyazaki, "Equilibrium phase diagram of a randomly pinned glass-former," *Proc. Nat. Acad. Sci.*, vol. 112, no. 22, p. 6914, 2015.
- [65] J. Callahan and J. Machta, "Population annealing simulations of a binary hard sphere mixture," *arXiv:1701.00263*, 2017.
- [66] P. Sindzingre, G. Ciccotti, C. Massobrio, and D. Frenkel, "Partial enthalpies and related quantities in mixtures from computer simulation," *Chemical Physics Letters*, vol. 136, pp. 35–41, Apr 1987.
- [67] P. Sindzingre, C. Massobrio, G. Ciccotti, and D. Frenkel, "Calculation of partial enthalpies of an argon-krypton mixture by NPT molecular dynamics," *Chemical Physics*, vol. 129, pp. 213–224, Jan 1989.

- [68] D. Gazzillo and G. Pastore, "Equation of state for symmetric non-additive hard-sphere fluids: An approximate analytic expression and new Monte Carlo results," *Chem. Phys. Lett.*, vol. 159, p. 388, Jul 1989.
- [69] T. S. Grigera and G. Parisi, "Fast Monte Carlo algorithm for supercooled soft spheres," *Phys. Rev. E*, vol. 63, p. 045102, 2001.
- [70] Y. Brumer and D. R. Reichman, "Numerical Investigation of the Entropy Crisis in Model Glass Formers," *J. Phys. Chem. B*, vol. 108, p. 6832, may 2004.
- [71] T. S. Grigera, V. Martín-Mayor, G. Parisi, and P. Verrocchio, "Phonon interpretation of the 'boson peak' in supercooled liquids," *Nature*, vol. 422, pp. 289–292, mar 2003.
- [72] G. Biroli, J.-P. Bouchaud, A. Cavagna, T. S. Grigera, and P. Verrocchio, "Thermodynamic signature of growing amorphous order in glass-forming liquids," *Nat. Phys.*, vol. 4, no. 10, pp. 771–775, 2008.
- [73] A. Cavagna, T. S. Grigera, and P. Verrocchio, "Numerical simulations of liquids with amorphous boundary conditions," *Journal of Statistical Mechanics: Theory and Experiment*, vol. 2010, p. P10001, oct 2010.
- [74] G. Gradenigo, R. Trozzo, A. Cavagna, T. S. Grigera, and P. Verrocchio, "Static correlations functions and domain walls in glass-forming liquids: The case of a sandwich geometry," *The Journal of Chemical Physics*, vol. 138, p. 12A509, mar 2013.
- [75] L. A. Fernández, V. Martín-Mayor, and P. Verrocchio, "Critical behavior of the specific heat in glass formers," *Phys. Rev. E*, vol. 73, p. 020501, Feb 2006.
- [76] D. A. Martín, A. Cavagna, and T. S. Grigera, "Specific Heat Anomaly in a Supercooled Liquid with Amorphous Boundary Conditions," *Phys. Rev. Lett.*, vol. 114, p. 225901, Jun 2015.
- [77] T. S. Grigera, "Geometrical properties of the potential energy of the soft-sphere binary mixture," *The Journal of Chemical Physics*, vol. 124, p. 064502, feb 2006.
- [78] L. Santen and W. Krauth, "Liquid, Glass and Crystal in Two-dimensional Hard disks," *arxiv:0107459*, jul 2001.
- [79] L. A. Fernández, V. Martín-Mayor, and P. Verrocchio, "Phase Diagram of a Polydisperse Soft-Spheres Model for Liquids and Colloids," *Phys. Rev. Lett.*, vol. 98, p. 085702, Feb 2007.
- [80] R. Gutiérrez, S. Karmakar, Y. G. Pollack, and I. Procaccia, "The static lengthscale characterizing the glass transition at lower temperatures," *EPL (Europhysics Letters)*, vol. 111, no. 5, p. 56009, 2015.
- [81] S. Karmakar, E. Lerner, and I. Procaccia, "Direct estimate of the static length-scale accompanying the glass transition," *Physica A: Statistical Mechanics and its Applications*, vol. 391, pp. 1001–1008, feb 2012.
- [82] G. Biroli, S. Karmakar, and I. Procaccia, "Comparison of static length scales characterizing the glass transition," *Physical Review Letters*, vol. 111, oct 2013.
- [83] S. Sastry, P. G. Debenedetti, and F. H. Stillinger, "Signatures of distinct dynamical regimes in the energy landscape of a glass-forming liquid," *Nature*, vol. 393, no. 6685, pp. 554–557, 1998.

- [84] S. Sastry, "The relationship between fragility, configurational entropy and the potential energy landscape of glass-forming liquids," *Nature*, vol. 409, no. 6817, pp. 164–167, 2001.
- [85] W. Kob, F. Sciortino, and P. Tartaglia, "Aging as dynamics in configuration space," *Europhysics Letters (EPL)*, vol. 49, pp. 590–596, mar 2000.
- [86] F. Sciortino, W. Kob, and P. Tartaglia, "Inherent structure entropy of supercooled liquids," *Phys. Rev. Lett.*, vol. 83, no. 16, p. 3214, 1999.
- [87] I. Saika-Voivod, P. H. Poole, and F. Sciortino, "Fragile-to-strong transition and polyamorphism in the energy landscape of liquid silica," *Nature*, vol. 412, pp. 514–517, aug 2001.
- [88] B. Coluzzi, G. Parisi, and P. Verrocchio, "Thermodynamical liquid-glass transition in a lennard-jones binary mixture," *Phys. Rev. Lett.*, vol. 84, pp. 306–309, Jan 2000.
- [89] L. Angelani and G. Foffi, "Configurational entropy of hard spheres," *J. Phys. Cond. Matter*, vol. 19, no. 25, p. 256207, 2007.
- [90] A. Cavagna, "Fragile vs. strong liquids: A saddles-ruled scenario," *Europhysics Letters (EPL)*, vol. 53, pp. 490–496, feb 2001.
- [91] A. Cavagna, I. Giardina, and G. Parisi, "Barriers between metastable states in the p-spin spherical model," *arXiv:cond-mat/9702069*, 1997.
- [92] A. Cavagna, I. Giardina, and G. Parisi, "Stationary points of the thouless-anderson-palmer free energy," *Physical Review B*, vol. 57, pp. 11251–11257, may 1998.
- [93] A. Cavagna, I. Giardina, and G. Parisi, "Role of saddles in mean-field dynamics above the glass transition," *Journal of Physics A: Mathematical and General*, vol. 34, pp. 5317–5326, jun 2001.
- [94] T. Castellani and A. Cavagna, "Spin-glass theory for pedestrians," *Journal of Statistical Mechanics: Theory and Experiment*, vol. 2005, p. P05012, may 2005.
- [95] L. Angelani, C. D. Michele, G. Ruocco, and F. Sciortino, "Saddles and softness in simple model liquids," *The Journal of Chemical Physics*, vol. 121, pp. 7533–7534, oct 2004.
- [96] L. Angelani, R. D. Leonardo, G. Ruocco, A. Scala, and F. Sciortino, "Saddles in the energy landscape probed by supercooled liquids," *Physical Review Letters*, vol. 85, pp. 5356–5359, dec 2000.
- [97] K. Broderix, K. K. Bhattacharya, A. Cavagna, A. Zippelius, and I. Giardina, "Energy landscape of a lennard-jones liquid: Statistics of stationary points," *Physical Review Letters*, vol. 85, pp. 5360–5363, dec 2000.
- [98] J. P. K. Doye and D. J. Wales, "Saddle points and dynamics of lennard-jones clusters, solids, and supercooled liquids," *The Journal of Chemical Physics*, vol. 116, pp. 3777–3788, mar 2002.
- [99] T. S. Grigera, A. Cavagna, I. Giardina, and G. Parisi, "Geometric approach to the dynamic glass transition," *Physical Review Letters*, vol. 88, jan 2002.
- [100] L. Angelani, R. D. Leonardo, G. Ruocco, A. Scala, and F. Sciortino, "Quasisaddles as relevant points of the potential energy surface in the dynamics of supercooled liquids," *The Journal of Chemical Physics*, vol. 116, pp. 10297–10306, jun 2002.

- [101] M. Sampoli, P. Benassi, R. Eramo, L. Angelani, and G. Ruocco, “The potential energy landscape in the lennard-jones binary mixture model,” *Journal of Physics: Condensed Matter*, vol. 15, no. 11, p. S1227, 2003.
- [102] P. Harrowell, “Nonlinear physics: Glass transitions in plane view,” *Nature Physics*, vol. 2, pp. 157–158, mar 2006.
- [103] E. Flenner and G. Szamel, “Fundamental differences between glassy dynamics in two and three dimensions,” *Nature Communications*, vol. 6, p. 7392, jun 2015.
- [104] H. Tanaka, “Bond orientational order in liquids: Towards a unified description of water-like anomalies, liquid-liquid transition, glass transition, and crystallization,” *Eur. Phys. J. E*, vol. 35, oct 2012.
- [105] H. Shiba, Y. Yamada, T. Kawasaki, and K. Kim, “Unveiling dimensionality dependence of glassy dynamics: 2d infinite fluctuation eclipses inherent structural relaxation,” *Phys. Rev. Lett.*, vol. 117, p. 245701, Dec 2016.
- [106] N. D. Mermin and H. Wagner, “Absence of ferromagnetism or antiferromagnetism in one- or two-dimensional isotropic heisenberg models,” *Phys. Rev. Lett.*, vol. 17, pp. 1133–1136, Nov 1966.
- [107] B. Illing, S. Fritschi, H. Kaiser, C. L. Klix, G. Maret, and P. Keim, “Mermin–wagner fluctuations in 2d amorphous solids,” *Proceedings of the National Academy of Sciences*, vol. 114, pp. 1856–1861, jan 2017.
- [108] S. Vivek, C. P. Kelleher, P. M. Chaikin, and E. R. Weeks, “Long-wavelength fluctuations and the glass transition in two dimensions and three dimensions,” *Proceedings of the National Academy of Sciences*, vol. 114, pp. 1850–1855, jan 2017.
- [109] G. Tarjus, “Glass transitions may be similar in two and three dimensions, after all,” *Proceedings of the National Academy of Sciences*, vol. 114, pp. 2440–2442, feb 2017.
- [110] A. Ninarello, L. Berthier, and D. Coslovich, “Structure and dynamics of coupled viscous liquids,” *Molecular Physics*, vol. 113, pp. 2707–2715, apr 2015.
- [111] L. Berthier, D. Coslovich, A. Ninarello, and M. Ozawa, “Equilibrium sampling of hard spheres up to the jamming density and beyond,” *Phys. Rev. Lett.*, vol. 116, p. 238002, Jun 2016.
- [112] A. Ninarello, L. Berthier, and D. Coslovich, “Models and algorithms for the next generation of glass transition studies,” *Physical Review X*, vol. 7, jun 2017.
- [113] L. Berthier, P. Charbonneau, D. Coslovich, A. Ninarello, M. Ozawa, and S. Yaida, “Breaking the glass ceiling: Configurational entropy measurements in extremely supercooled liquids,” *arXiv:1704.08257*, 2017.
- [114] M. Mézard, G. Parisi, and M. A. Virasoro, *Spin Glass Theory And Beyond: An Introduction To The Replica Method And Its Applications*. Singapore: World Scientific, 1986.
- [115] A. P. Young, *Spin Glasses and Random Fields*. Singapore: World Scientific, 1998.
- [116] S. Yaida, L. Berthier, P. Charbonneau, and G. Tarjus, “Point-to-set lengths, local structure, and glassiness,” *Physical Review E*, vol. 94, sep 2016.
- [117] W. Kob, S. Roldán-Vargas, and L. Berthier, “Non-monotonic temperature evolution of dynamic correlations in glass-forming liquids,” *Nature Physics*, vol. 8, pp. 164–167, oct 2011.

- [118] G. M. Hocky, L. Berthier, W. Kob, and D. R. Reichman, "Crossovers in the dynamics of supercooled liquids probed by an amorphous wall," *Phys. Rev. E*, vol. 89, p. 052311, 2014.
- [119] C. Cammarota and G. Biroli, "Ideal glass transitions by random pinning," *Proc. Natl. Acad. Sci.*, vol. 109, p. 8850, 2012.
- [120] S. Chakrabarty, R. Das, S. Karmakar, and C. Dasgupta, "Understanding the dynamics of glass-forming liquids with random pinning within the random first order transition theory," *The Journal of Chemical Physics*, vol. 145, p. 034507, jul 2016.
- [121] S. Franz and G. Parisi, "Universality classes of critical points in constrained glasses," *Journal of Statistical Mechanics: Theory and Experiment*, vol. 2013, no. 11, p. P11012, 2013.
- [122] G. Biroli, C. Cammarota, G. Tarjus, and M. Tarzia, "Random-field-like criticality in glass-forming liquids," *Physical Review Letters*, vol. 112, apr 2014.
- [123] L. Foini, F. Krzakala, and F. Zamponi, "On the relation between kinetically constrained models of glass dynamics and the random first-order transition theory," *Journal of Statistical Mechanics: Theory and Experiment*, vol. 2012, p. P06013, jun 2012.
- [124] R. L. Jack and J. P. Garrahan, "Phase transition for quenched coupled replicas in a plaquette spin model of glasses," *Physical Review Letters*, vol. 116, feb 2016.
- [125] W. Kob and H. C. Andersen, "Testing mode-coupling theory for a supercooled binary lennard-jones mixture i: The van hove correlation function," *Phys. Rev. E*, vol. 51, pp. 4626–4641, may 1995.
- [126] M. D. Ediger, "Spatially heterogeneous dynamics in supercooled liquids," *Annual Review of Physical Chemistry*, vol. 51, pp. 99–128, oct 2000.
- [127] B. Charbonneau, P. Charbonneau, Y. Jin, G. Parisi, and F. Zamponi, "Dimensional dependence of the stokes–einstein relation and its violation," *The Journal of Chemical Physics*, vol. 139, p. 164502, oct 2013.
- [128] C. Toninelli, M. Wyart, L. Berthier, G. Biroli, and J.-P. Bouchaud, "Dynamical susceptibility of glass formers: Contrasting the predictions of theoretical scenarios," *Phys. Rev. E*, vol. 71, p. 041505, Apr 2005.
- [129] L. Berthier, G. Biroli, J.-P. Bouchaud, W. Kob, K. Miyazaki, and D. R. Reichman, "Spontaneous and induced dynamic correlations in glass formers. II. Model calculations and comparison to numerical simulations," *J. Chem. Phys.*, vol. 126, p. 184504, 2007.
- [130] L. Berthier, G. Biroli, J.-P. Bouchaud, W. Kob, K. Miyazaki, and D. R. Reichman, "Spontaneous and induced dynamic fluctuations in glass formers. I. General results and dependence on ensemble and dynamics," *J. Chem. Phys.*, vol. 126, p. 184503, 2007.
- [131] L. Berthier, D. Chandler, and J. P. Garrahan, "Length scale for the onset of fickian diffusion in supercooled liquids," *Europhysics Letters (EPL)*, vol. 69, pp. 320–326, feb 2005.
- [132] C. Domb and M. S. Green, *Phase Transitions and Critical Phenomena. Vol. 2*. London: Academic Press, 1972.
- [133] R. Richert and C. A. Angell, "Dynamics of glass-forming liquids. v. on the link between molecular dynamics and configurational entropy," *The Journal of Chemical Physics*, vol. 108, pp. 9016–9026, jun 1998.

- [134] L. O. Hedges, R. L. Jack, J. P. Garrahan, and D. Chandler, “Dynamic order-disorder in atomistic models of structural glass formers,” *Science*, vol. 323, pp. 1309–1313, mar 2009.
- [135] D. Coslovich and R. L. Jack, “Structure of inactive states of a binary lennard-jones mixture,” *Journal of Statistical Mechanics: Theory and Experiment*, vol. 2016, no. 7, p. 074012, 2016.
- [136] M. Chen, “A brief overview of bulk metallic glasses,” *NPG Asia Materials*, vol. 3, pp. 82–90, sep 2011.
- [137] K. Zhang, B. Dice, Y. Liu, J. Schroers, M. D. Shattuck, and C. S. O’Hern, “On the origin of multi-component bulk metallic glasses: Atomic size mismatches and de-mixing,” *J. Chem. Phys.*, vol. 143, p. 054501, aug 2015.
- [138] G. S. Grest, S. R. Nagel, and A. Rahman, “Longitudinal and transverse excitations in a glass,” *Phys. Rev. Lett.*, vol. 49, pp. 1271–1274, Oct 1982.
- [139] C. E. Maloney and A. Lemaître, “Amorphous systems in athermal, quasistatic shear,” *Physical Review E*, vol. 74, jul 2006.
- [140] L. Berthier, P. Chaudhuri, C. Coulais, O. Dauchot, and P. Sollich, “Suppressed Compressibility at Large Scale in Jammed Packings of Size-Disperse Spheres,” *Phys. Rev. Lett.*, vol. 106, p. 120601, Mar 2011.
- [141] C. P. Royall and S. R. Williams, “The role of local structure in dynamical arrest,” *Physics Reports*, vol. 560, pp. 1–75, feb 2015.
- [142] E. Flenner and G. Szamel, “Dynamic heterogeneity in a glass forming fluid: Susceptibility, structure factor, and correlation length,” *Physical Review Letters*, vol. 105, nov 2010.
- [143] T. Hecksher, A. I. Nielsen, N. B. Olsen, and J. C. Dyre, “Little evidence for dynamic divergences in ultraviscous molecular liquids,” *Nature Physics*, vol. 4, pp. 737–741, jul 2008.
- [144] Y. S. Elmatad, D. Chandler, and J. P. Garrahan, “Corresponding states of structural glass formers,” *J. Phys. Chem. B*, vol. 113, pp. 5563–5567, apr 2009.
- [145] N. Newman and G. Barkema, *Monte Carlo Methods in Statistical Physics*. Oxford: Clarendon Press, 2011.
- [146] M. Ozawa and L. Berthier, “Does the configurational entropy of polydisperse particles exist?,” *The Journal of Chemical Physics*, vol. 146, p. 014502, jan 2017.
- [147] C. Cammarota, A. Cavagna, G. Gradenigo, T. S. Grigera, and P. Verrocchio, “Numerical determination of the exponents controlling the relationship between time, length, and temperature in glass-forming liquids,” *J. Chem. Phys.*, vol. 131, no. 19, p. 194901, 2009.
- [148] P. Sollich, “Weakly polydisperse systems: Perturbative phase diagrams that include the critical region,” *Physical Review Letters*, vol. 100, jan 2008.
- [149] P. Sollich and N. B. Wilding, “Crystalline Phases of Polydisperse Spheres,” *Phys. Rev. Lett.*, vol. 104, p. 118302, Mar 2010.
- [150] P. Sollich and N. B. Wilding, “Phase behaviour of polydisperse spheres: simulation strategies and an application to the freezing transition,” *J. Chem. Phys.*, vol. 133, p. 224102, 2010.
- [151] C. D. Michele, F. Sciortino, and A. Coniglio, “Scaling in soft spheres: fragility invariance on the repulsive potential softness,” *J. Phys.: Condens. Matter*, vol. 16, p. L489, oct 2004.
- [152] J. Mattsson, H. M. Wyss, A. Fernandez-Nieves, K. Miyazaki, Z. Hu, D. R. Reichman, and D. A. Weitz, “Soft colloids make strong glasses,” *Nature*, vol. 462, pp. 83–86, nov 2009.

- [153] D. Gazzillo, G. Pastore, and S. Enzo, "Chemical short-range order in amorphous Ni-Ti alloys: an integral equation approach with a non-additive hard-sphere model," *J. Phys.: Condens. Matter*, vol. 1, no. 22, p. 3469, 1989.
- [154] D. Gazzillo, G. Pastore, and R. Frattini, "The role of excluded volume effects on the structure and chemical short-range order of Ni<sub>33</sub>Y<sub>67</sub> metallic glass," *J. Phys.: Condens. Matter*, vol. 2, no. 42, p. 8463, 1990.
- [155] S. Torquato and F. H. Stillinger, "Jammed hard-particle packings: From kepler to bernal and beyond," *Reviews of Modern Physics*, vol. 82, pp. 2633–2672, sep 2010.
- [156] A. Santos, S. B. Yuste, and M. L. de Haro, "Contact values of the particle-particle and wall-particle correlation functions in a hard-sphere polydisperse fluid," *The Journal of Chemical Physics*, vol. 123, p. 234512, dec 2005.
- [157] L. Berthier, G. Biroli, J.-P. Bouchaud, L. Cipelletti, and W. van Saarloos, eds., *Dynamical Heterogeneities in Glasses, Colloids, and Granular Media*. Oxford University Press, jul 2011.
- [158] J. C. Dyre, N. B. Olsen, and T. Christensen, "Local elastic expansion model for viscous-flow activation energies of glass-forming molecular liquids," *Physical Review B*, vol. 53, pp. 2171–2174, feb 1996.
- [159] J. C. Dyre, "Source of non-arrhenius average relaxation time in glass-forming liquids," *Journal of Non-Crystalline Solids*, vol. 235-237, pp. 142–149, aug 1998.
- [160] J. C. Dyre, "Colloquium," *Rev. Mod. Phys.*, vol. 78, pp. 953–972, Sep 2006.
- [161] H. W. Hansen, B. Frick, T. Hecksher, J. C. Dyre, and K. Niss, "Connection between fragility, mean-squared displacement, and shear modulus in two van der waals bonded glass-forming liquids," *Physical Review B*, vol. 95, mar 2017.
- [162] T. Hecksher, N. B. Olsen, and J. C. Dyre, "Model for the alpha and beta shear-mechanical properties of supercooled liquids and its comparison to squalane data," *arXiv:1701.05086*, 2017.
- [163] R. Pastore, G. Pesce, A. Sasso, and M. P. Ciamarra, "Cage size and jump precursors in glass-forming liquids: Experiment and simulations," *arXiv:1705.04852*, 2017.
- [164] M. Wyart and M. E. Cates, "Does a growing static length scale control the glass transition?" *arXiv:1705.06588*, 2017.
- [165] L. Berthier and G. Tarjus, "The role of attractive forces in viscous liquids," *The Journal of Chemical Physics*, vol. 134, p. 214503, jun 2011.
- [166] S. Toxvaerd and J. C. Dyre, "Role of the first coordination shell in determining the equilibrium structure and dynamics of simple liquids," *The Journal of Chemical Physics*, vol. 135, p. 134501, oct 2011.
- [167] L. O. Hedges, R. L. Jack, J. P. Garrahan, and D. Chandler, "Dynamic order-disorder in atomistic models of structural glass formers," *Science*, vol. 323, pp. 1309–1313, mar 2009.
- [168] D. Coslovich and R. L. Jack, "Structure of inactive states of a binary lennard-jones mixture," *Journal of Statistical Mechanics: Theory and Experiment*, vol. 2016, p. 074012, jul 2016.
- [169] U. R. Pedersen, N. Gnan, N. P. Bailey, T. B. Schröder, and J. C. Dyre, "Strongly correlating liquids and their isomorphs," *Journal of Non-Crystalline Solids*, vol. 357, pp. 320–328, jan 2011.

- [170] N. Gnan, T. B. Schröder, U. R. Pedersen, N. P. Bailey, and J. C. Dyre, “Pressure-energy correlations in liquids. IV. “isomorphs” in liquid phase diagrams,” *The Journal of Chemical Physics*, vol. 131, p. 234504, dec 2009.
- [171] T. B. Schröder, N. Gnan, U. R. Pedersen, N. P. Bailey, and J. C. Dyre, “Pressure-energy correlations in liquids. v. isomorphs in generalized lennard-jones systems,” *The Journal of Chemical Physics*, vol. 134, p. 164505, apr 2011.
- [172] J. D. Honeycutt and H. C. Andersen, “Molecular dynamics study of melting and freezing of small lennard-jones clusters,” *The Journal of Physical Chemistry*, vol. 91, pp. 4950–4963, sep 1987.
- [173] R. Peierls, “Bemerkungen uber umwandlungstemperaturen,” *Helv. Phys. Acta*, vol. 7, p. 81, 1934.
- [174] J. M. Kosterlitz and D. J. Thouless, “Ordering, metastability and phase transitions in two-dimensional systems,” *Journal of Physics C: Solid State Physics*, vol. 6, no. 7, p. 1181, 1973.
- [175] J. Russo and H. Tanaka, “Assessing the role of static length scales behind glassy dynamics in polydisperse hard disks,” *Proceedings of the National Academy of Sciences*, vol. 112, pp. 6920–6924, may 2015.
- [176] D. Chandler and J. P. Garrahan, “Dynamics on the way to forming glass: Bubbles in space-time,” *Annual Review of Physical Chemistry*, vol. 61, pp. 191–217, mar 2010.
- [177] C. S. O’Hern, L. E. Silbert, A. J. Liu, and S. R. Nagel, “Jamming at zero temperature and zero applied stress: The epitome of disorder,” *Physical Review E*, vol. 68, jul 2003.
- [178] J. C. M. F.R.S., “L. on the calculation of the equilibrium and stiffness of frames,” *Philosophical Magazine Series 4*, vol. 27, no. 182, pp. 294–299, 1864.
- [179] A. J. Liu and S. R. Nagel, “Jamming is not just cool any more,” *Nature*, vol. 396, pp. 21–22, nov 1998.
- [180] T. Aste and A. Coniglio, “Cell theory for liquid solids and glasses: From local packing configurations to global complex behaviors,” *Europhysics Letters (EPL)*, vol. 67, pp. 165–171, jul 2004.
- [181] R. D. Kamien and A. J. Liu, “Why is random close packing reproducible?,” *Physical Review Letters*, vol. 99, oct 2007.
- [182] G. Parisi and F. Zamponi, “Mean-field theory of hard sphere glasses and jamming,” *Reviews of Modern Physics*, vol. 82, pp. 789–845, mar 2010.
- [183] R. Mari, F. Krzakala, and J. Kurchan, “Jamming versus glass transitions,” *Physical Review Letters*, vol. 103, jul 2009.
- [184] G. A. Mansoori, N. F. Carnahan, K. E. Starling, and T. W. Leland, “Equilibrium thermodynamic properties of the mixture of hard spheres,” *The Journal of Chemical Physics*, vol. 54, pp. 1523–1525, feb 1971.
- [185] C. S. O’Hern, S. A. Langer, A. J. Liu, and S. R. Nagel, “Random packings of frictionless particles,” *Physical Review Letters*, vol. 88, jan 2002.
- [186] S. Sengupta, S. Karmakar, C. Dasgupta, and S. Sastry, “Adam-gibbs relation for glass-forming liquids in two, three, and four dimensions,” *Physical Review Letters*, vol. 109, aug 2012.

- [187] S. Sengupta, S. Karmakar, C. Dasgupta, and S. Sastry, "Breakdown of the stokes-einstein relation in two, three, and four dimensions," *The Journal of Chemical Physics*, vol. 138, p. 12A548, mar 2013.
- [188] Y. Rosenfeld and P. Tarazona, "Density functional theory and the asymptotic high density expansion of the free energy of classical solids and fluids," *Mol. Phys.*, vol. 95, no. 2, pp. 141–150, 1998.
- [189] D. Frenkel, "Why colloidal systems can be described by statistical mechanics: some not very original comments on the gibbs paradox," *Molecular Physics*, vol. 112, pp. 2325–2329, apr 2014.
- [190] W. Press, *Numerical recipes : the art of scientific computing*. Cambridge, UK New York: Cambridge University Press, 2007.
- [191] Intel, "Math kernel library,"
- [192] G. Biroli and R. Monasson, "From inherent structures to pure states: Some simple remarks and examples," *EPL (Europhysics Letters)*, vol. 50, no. 2, p. 155, 2000.
- [193] S. Franz and A. Montanari, "Analytic determination of dynamical and mosaic length scales in a kac glass model," *Journal of Physics A: Mathematical and Theoretical*, vol. 40, pp. F251–F257, feb 2007.
- [194] L. Berthier, P. Charbonneau, and S. Yaida, "Efficient measurement of point-to-set correlations and overlap fluctuations in glass-forming liquids," *J. Chem. Phys.*, vol. 144, no. 2, p. 024501, 2016.
- [195] J. Justin, *Quantum field theory and critical phenomena*. Oxford New York: Clarendon Press Oxford University Press, 1996.
- [196] K. Huang, *Statistical mechanics*. New York: Wiley, 1987.
- [197] S. Franz, G. Parisi, F. Ricci-Tersenghi, and T. Rizzo, "Field theory of fluctuations in glasses," *The European Physical Journal E*, vol. 34, sep 2011.
- [198] R. Miyazaki, T. Kawasaki, and K. Miyazaki, "Cluster glass transition of ultrasoft-potential fluids at high density," *Physical Review Letters*, vol. 117, oct 2016.
- [199] H. Mizuno, H. Shiba, and A. Ikeda, "Continuum limit of the vibrational properties of amorphous solids," *arXiv:1703.10004*, 2017.
- [200] D. Frenkel and A. J. C. Ladd, "New monte carlo method to compute the free energy of arbitrary solids. application to the fcc and hcp phases of hard spheres," *The Journal of Chemical Physics*, vol. 81, pp. 3188–3193, oct 1984.
- [201] C. Angell, "Entropy and fragility in supercooling liquids," *Journal of Research of the National Institute of Standards and Technology*, vol. 102, p. 171, mar 1997.
- [202] H. Tanaka, "Relation between thermodynamics and kinetics of glass-forming liquids," *Physical Review Letters*, vol. 90, feb 2003.
- [203] S. Capaccioli, G. Ruocco, and F. Zamponi, "Dynamically correlated regions and configurational entropy in supercooled liquids," *The Journal of Physical Chemistry B*, vol. 112, pp. 10652–10658, aug 2008.

- [204] S. Albert, T. Bauer, M. Michl, G. Biroli, J.-P. Bouchaud, A. Loidl, P. Lunkenheimer, R. Tourbot, C. Wiertel-Gasquet, and F. Ladieu, “Fifth-order susceptibility unveils growth of thermodynamic amorphous order in glass-formers,” *Science*, vol. 352, no. 6291, pp. 1308–1311, 2016.
- [205] G. Szamel, “Colloidal glass transition: Beyond mode-coupling theory,” *Physical Review Letters*, vol. 90, jun 2003.
- [206] D. S. Fisher and D. A. Huse, “Nonequilibrium dynamics of spin glasses,” *Phys. Rev. B*, vol. 38, pp. 373–385, Jul 1988.
- [207] C. Cammarota, A. Cavagna, G. Gradenigo, T. S. Grigera, and P. Verrocchio, “Evidence for a spinodal limit of amorphous excitations in glassy systems,” *Journal of Statistical Mechanics: Theory and Experiment*, vol. 2009, p. L12002, dec 2009.
- [208] G. M. Hocky, T. E. Markland, and D. R. Reichman, “Growing point-to-set length scale correlates with growing relaxation times in model supercooled liquids,” *Physical Review Letters*, vol. 108, jun 2012.
- [209] F. W. Starr, J. F. Douglas, and S. Sastry, “The relationship of dynamical heterogeneity to the adam-gibbs and random first-order transition theories of glass formation,” *The Journal of Chemical Physics*, vol. 138, p. 12A541, mar 2013.
- [210] C. Brun, F. Ladieu, D. L’Hôte, G. Biroli, and J.-P. Bouchaud, “Evidence of growing spatial correlations during the aging of glassy glycerol,” *Physical Review Letters*, vol. 109, oct 2012.
- [211] B. Schmidtke, N. Petzold, R. Kahlau, M. Hofmann, and E. A. Rössler, “From boiling point to glass transition temperature: Transport coefficients in molecular liquids follow three-parameter scaling,” *Physical Review E*, vol. 86, oct 2012.
- [212] S. Tatsumi, S. Aso, and O. Yamamuro, “Thermodynamic study of simple molecular glasses: Universal features in their heat capacity and the size of the cooperatively rearranging regions,” *Physical Review Letters*, vol. 109, jul 2012.
- [213] D. Coslovich and G. Pastore, “Dynamics and energy landscape in a tetrahedral network glass-former: direct comparison with models of fragile liquids,” *Journal of Physics: Condensed Matter*, vol. 21, p. 285107, jun 2009.
- [214] A. Cavagna, “Supercooled liquids for pedestrians,” *Physics Reports*, vol. 476, pp. 51–124, jun 2009.
- [215] L. Berthier and J. P. Garrahan, “Real space origin of temperature crossovers in supercooled liquids,” *Physical Review E*, vol. 68, oct 2003.
- [216] S. Saw and P. Harrowell, “Rigidity in condensed matter and its origin in configurational constraint,” *Physical Review Letters*, vol. 116, mar 2016.
- [217] H. Ikeda and F. Zamponi *private communication*, 2017.
- [218] S. F. Swallen, K. L. Kearns, M. K. Mapes, Y. S. Kim, R. McMahon, M. D. Ediger, T. Wu, L. Yu, and S. Satija, “Organic glasses with exceptional thermodynamic and kinetic stability,” *Science*, 2006.
- [219] L. Berthier, P. Charbonneau, E. Flenner, and F. Zamponi, “How to create equilibrium vapor-deposited glasses,” *arXiv:1706.02738*, 2017.
- [220] C. Fullerton and L. Berthier, “in preparation,” 2017.

- [221] L. Berthier, P. Charbonneau, Y. Jin, G. Parisi, B. Seoane, and F. Zamponi, “Growing timescales and lengthscales characterizing vibrations of amorphous solids,” *Proceedings of the National Academy of Sciences*, vol. 113, pp. 8397–8401, jul 2016.
- [222] C. Scalliet, L. Berthier, and F. Zamponi, “Absence of marginal stability in structural glasses,” *arXiv:1706.04112*, 2017.
- [223] G. Parisi, I. Procaccia, C. Rainone, and M. Singh, “Shear bands as manifestation of a criticality in yielding amorphous solids,” *Proceedings of the National Academy of Sciences*, vol. 114, pp. 5577–5582, may 2017.
- [224] P. Urbani and F. Zamponi, “Shear yielding and shear jamming of dense hard sphere glasses,” *Physical Review Letters*, vol. 118, jan 2017.
- [225] A. Ghosh, Z. Budrikis, V. Chikkadi, A. L. Sellerio, S. Zapperi, and P. Schall, “Direct observation of percolation in the yielding transition of colloidal glasses,” *Physical Review Letters*, vol. 118, apr 2017.
- [226] M. Ozawa, “in preparation,” 2017.



## Abstract

Understanding the mechanisms that lead to glass formation is one of the open problems for the condensed matter research. Numerous questions remain unanswered, because the tremendous increase of relaxation times during the cooling process prevents the exploration of equilibrium properties of supercooled liquids at very low temperature. Computer simulations of glass-forming liquids are nowadays able to reach equilibrium at temperatures comparable to the Mode-Coupling crossover temperature, which is well above the experimental glass transition temperature. As a consequence, simulations lag eight orders of magnitude behind experiments in terms of equilibration times. Progress to close this gap has been slow, and stems mostly from hardware improvements.

In this thesis we make an important step to close this gap. We combine the use of a Monte Carlo algorithm, known as the swap algorithm, with the design of novel glass-forming models. We systematically test numerous models using both discrete mixtures and polydisperse systems. We discuss the role that polydispersity and particle softness play in avoiding crystallization and in efficiently reaching previously unexplored regimes. We study the dynamical processes taking place during swap Monte Carlo simulations. We demonstrate that in some cases our technique is able to produce thermalized configurations at temperatures inaccessible even by experiments.

In this newly accessible regime, we investigate some open questions concerning the glass transition. We show that a hard sphere fluid can be equilibrated at, and even beyond, the jamming packing fraction. We measure the configurational entropy in extremely supercooled liquid, finding a strong dimensional dependence that supports, on the one hand, the existence of an ideal glass transition at a finite temperature in three dimensions and, on the other hand, its absence in two dimensions. We detect the increase of amorphous order quantified through a static point-to-set length throughout the glass formation. We measure the critical exponents introduced in the mean-field theory of glasses much closer to the supposed ideal glass transition. Finally, we reveal the absence of a sharp geometric transition in the potential energy landscape across the Mode-Coupling crossover.

The models and the algorithms developed in this thesis shift the computational studies of glass-forming liquids to an entirely new territory, which should help to close the gap between theory and experiments, and get us closer to solve the long-standing problem of the glass transition.

## Résumé

La compréhension du mécanisme de la formation du verre est l'un des importants problèmes ouverts en recherche sur la matière condensée. De nombreuses questions restent sans réponse, en raison d'une énorme augmentation des temps de relaxation pendant le processus de refroidissement qui ne permet pas l'exploration des propriétés d'équilibre des liquides surfondus à très basses températures. Les simulations numériques des liquides surfondus sont actuellement en mesure d'atteindre l'équilibre à des températures comparables à la température du crossover de la théorie de couplages de modes, qui est bien supérieure à la température de transition vitreuse expérimentale. En conséquence, les simulations plus lentes que les expériences pour équilibrer un liquide surfondu par un facteur d'environ huit ordres de grandeur. Les progrès réalisés pour combler cet écart ont été lents et résultent essentiellement d'améliorations de l'architecture des ordinateurs.

Dans cette thèse, nous résolvons en partie le problème de la thermalisation à basse température de liquides surfondus dans des simulations numériques. Nous combinons l'utilisation d'un algorithme Monte Carlo, connu sous le nom d'algorithme de swap, avec la conception de nouveaux modèles de formateurs de verre. Nous examinons systématiquement des nombreux systèmes, à la fois des mélanges discrets de particules, ainsi que des systèmes à polydispersité continue. Nous discutons le rôle que la polydispersité et la forme du potentiel entre particules jouent pour éviter la cristallisation et parvenir efficacement à des régimes de température inexplorés. De plus, nous étudions les processus dynamiques à l'œuvre pendant une simulation de swap Monte Carlo. Nous démontrons que, dans certains cas, notre technique permet de produire des configurations équilibrées à des températures inaccessibles même dans des expériences.

Dans ce régime de température complètement nouveau, nous examinons plusieurs questions ouvertes concernant la physique de la transition vitreuse. Nous montrons qu'un fluide de sphères dures peut être équilibré jusqu'à la densité critique du jamming, et même au-delà. Nous mesurons l'entropie configurationnelle dans un liquide refroidi à très basse température. Nous mettons en évidence une forte dépendance dimensionnelle, qui suggère l'existence d'une transition vitreuse idéale à une température finie en trois dimensions et à son absence en deux dimensions. Nous détectons l'augmentation de l'ordre amorphe quantifié par une longueur statique point-to-set pendant la formation du verre. Nous mesurons les exposants critiques introduits dans la théorie de champ moyen des verres beaucoup plus proche de la température critique prédite dans la théorie. Enfin, nous révélons l'absence de transition géométrique caractérisant le paysage d'énergie potentiel au travers de la température du crossover de la théorie de couplages de modes.

Les modèles et les algorithmes développés dans cette thèse déplacent les études des liquides surfondus vers un territoire entièrement nouveau, en réduisant l'écart entre la théorie et les expériences, ce qui nous amène plus proche de la solution du problème de la transition vitreuse.